Developments in Road Vehicle Crush Analysis for Forensic Collision Investigation

Ph.D. Thesis

Joseph George Jonathan Neades

Faculty of Technology

De Montfort University, March 2011

A thesis submitted in partial fulfilment of the requirements for the degree of Doctor of Philosophy

Declaration

I declare that the work described in this thesis was originally carried out by me during the period of registration for the degree of Doctor of Philosophy at the De Montfort University, United Kingdom, from January 2006 to March 2011. It is submitted for the degree of Doctor of Philosophy at the De Montfort University. Apart from the degree that this thesis is currently applying for, no other academic degreee or award was applied for by me based on this work.

Acknowledgements

Firstly I would like to acknowledge the support of my company, Ai Training Services Ltd (AiTS) who provided financial support and more importantly provided me with sufficient time where necessary to complete this research.

I also would like to thank my colleagues at AiTS, especially Rod Shephard who was a willing and helpful 'sounding board' for some ideas. Particular thanks are also due to my business partner, Ric Ward who has ever been supportive of my studies and encouraging throughout this research.

My thanks are also due to my supervisory team, Bob John when he stepped in to replace Marouan Nazha and my first supervisor, Roy Smith. Both Bob and Marouan helped tremendously with the bureaucratic processes and I am grateful for their advice.

My deepest gratitude is due to Roy, who managed on several occasions to pull off the neat trick of simultaneously being both my most vociferous critic and staunchest ally. His patience when explaining some particular concepts has been an inspiration which I can only hope to emulate, thank you.

Thanks are also due to Peter Jennings who many years ago inadvertently provided the inspiration for part of this research.

I would also like to thank the many students and software users of AiTS who have patiently listened to my explanations of the background theory as it developed. Explaining it to them has furthered my understanding tremendously and in no small part is responsible for this thesis. Particular thanks in this respect must go to the CCIS / OTS research teams at Loughborough University, the University of Birmingham and TRL.

Finally, I am particularly grateful to my partner, Tracey and to my children, Sam and Ali for their love and support over the years. They gave me the strength of deal with the low and the high points and the space to pursue my work. I dedicate this thesis to them.

Abstract

The change of a vehicle's velocity due to an impact, DeltaV (Δv) is often calculated and used in the scientific investigation of road traffic collisions. Two types of model are in common use to achieve this purpose, those based on the conservation of linear and angular momentum and the CRASH model which also considers the conservation of energy. It is shown that CRASH and major implementations of the momentum models are equivalent provided certain conditions are satisfied. Explicit conversions between the main variants of the models are presented. A method is also presented which describes a new formula for determining the total work performed in causing crush to a particular vehicle. This has the advantage of incorporating restitution effects and yields identical results to the momentum only models.

Although the CRASH model has received adverse criticism due to perceived inaccuracies in the results, little work has been performed to determine the theoretical limitations on accuracy. This thesis rectifies that shortcoming. A Monte Carlo simulation and analytical model are developed here to provide two independent methods for determining the overall accuracy of the CRASH method. The principal direction of force was found to be the most likely to introduce error based on the CRASH assessment. It is shown how this and other sources of error in the CRASH model can be quantified for a particular collision suggesting priorities for minimising the overall uncertainty. The data from a series of well known crash tests are used with each of the models to provide comparison and validation data.

It is recognised that without additional data velocity change is of limited use for forensic investigation. However DeltaV can be used as a proxy for acceleration and is particularly useful in studies involving injury causation. A method is also presented here which uses the change in velocity sustained by a vehicle in a planar collision to estimate the velocities of a vehicle before and after a collision. This method relies solely on conservation laws and is also applicable to situations where the coefficient of restitution is non-zero. An extension to the method is also described which allows an initial estimate to be modified to generate more realistic directions of force. This extension has the desirable effect of reducing uncertainty in the estimation of the direction of force which significantly improves the overall accuracy.

Publications

Neades, J. and Shephard, R. *Review of Measurement Protocols Applicable to Speed from Damage Programs*, (2009) Impact 17 (1) 4-12

Neades, J. and Smith, R. *The Determination of Vehicle Speeds from Delta-V in Two Vehicle Planar Collisions*, (2011) Journal of Automobile Engineering, Proc IMechE Part D 225 (1)

Table of Contents

Notation

A,B	stiffness coefficients
A,B,C	coefficients used in Brach's impact model
d	distance of point of action from centre of mass
e	coefficient of restitution
E	energy absorbed by each vehicle
h	perpendicular distance from the vehicle's centre of mass to $\boldsymbol{P}$
I	yaw moment of inertia
k	radius of gyration for each vehicle
m	mass of each vehicle
$\boldsymbol{p}$	unit vector in the direction of $\boldsymbol{P}_1$
$\boldsymbol{P}$	impulse due to the collision
$\boldsymbol{u}$	linear velocity of the centre of mass of each vehicle before impact
U	component of the velocity of the point of action before impact
$\boldsymbol{v}$	linear velocity of the centre of mass of each vehicle after impact
V	component of the velocity of the point of action after impact
α	angle of impulse $\boldsymbol{p}$ to face of vehicle
β	angle between $\boldsymbol{p}$ and closing velocity vector
ζ	difference between α and β i.e. $\zeta = \alpha - \beta$
η, κ	coefficients used in determining crush energy in Singh's method
γ	scalar factor $k^2/(k^2+h^2)$
δ	scalar factor $1+h^2/k^2$ i.e. $1/\gamma$

λ	angle between closing velocity vector and direction of travel of vehicle
μ	tangential impulse coefficient such that $\boldsymbol{P_t} = \mu \boldsymbol{P_n}$
θ	principal direction of force
φ	angle of point of action relative to vehicle heading
$\Delta\boldsymbol{v}$	velocity change at centre of mass due to impact, $\boldsymbol{v} - \boldsymbol{u}$
ΔV	component of the velocity change at the point of action, $V - U$
Ψ	impact angle between the vehicles
$\Delta\omega$	change in angular velocity due to the impact, $\Omega - \omega$
ω	angular velocity of the vehicle before impact
Ω	angular velocity of the vehicle after impact

Subscripts

m,n,0	mass subscripts used in solution to Ishikawa's impact model
n	motion normal to the impact plane
p	motion along the line of action of $\boldsymbol{P}$
t	motion perpendicular or tangential to the line of action of $\boldsymbol{P}$
1	vehicle 1
2	vehicle 2
R	relative value at the point of action of the impulse $\boldsymbol{P}$

List of Key Abbreviations

ABS	Anti-lock Braking System
AiTS	Ai Training Services Ltd.
BEV	Barrier Equivalent Velocity. Also known as EBS.
CCIS	Cooperative Crash Investigation Study. UK Government funded vehicle safety programme.
CDC	Collision Deformation Classification. Older method of describing pattern of damage sustained by a vehicle in a collision.
CRASH	Calspan Reconstruction of Accident Speeds on the Highway. Algorithm to determine change in velocity of vehicles in a collision.
DeltaV	Change in velocity sustained by a vehicle. Often abbreviated to Δv
DOT	United States Department of Transportation.
EBS	Equivalent Barrier Speed. Also known as BEV.
FTF	Front To Front. Type of vehicle collision.
FTR	Front To Rear. Type of vehicle collision.
FTS	Front To Side. Type of vehicle collision.
ITAI	Institute of Traffic Accident Investigators. UK professional body.
NCAP	New Car Assessment Programme.
NHTSA	National Highway Traffic Administration. US Government organisation.
OTS	On The Spot. UK Government funded road safety programme.
PDF	Principal Direction of Force. Also known as PDOF, PDoF.
PDOD	Principal Direction of Deformation.
PDOF	Principal Direction Of Force. Also known as PDF, PDoF.
PIM	Planar Impact Model.
RICSAC	Research Input for Computer Simulation of Automobile Collisions. Series of vehicle to vehicle crash tests.
SMAC	Simulation Model for Automobile Collisions. Computer algorithm to model vehicle collisions.
TRL	Transport Research Laboratory.
VTB	Vehicle To Barrier. Type of vehicle collision.
VTV	Vehicle To Vehicle. Type of vehicle collision.

List of Figures

List of Tables

List of Tables in Appendices

Chapter 1

Introduction

1.1 Objectives

In this Chapter the motivation behind this research is explained. The scope and limits of the research are also described. The original contribution made by this research is summarised and criteria are defined by which this work can be evaluated.

1.2 Scope of the thesis

Two main models are currently used to forensically analyse road vehicle collisions. The first type of model is based on the conservation of linear and angular momentum and is exemplified by the models by Brach [**11**], Ishikawa [**43**] and Steffan [**111**]. The second type is the CRASH algorithm as described by McHenry [**65**] and Smith [**105**]. Solution of the momentum models requires the post-impact trajectories and velocities of each vehicle. Such data is frequently obtained from ephemeral evidence at the scene, usually tyre marks from which the post-impact trajectories and velocities can be determined. In the absence of such scene data solutions using the momentum models become impractical. CRASH takes as input the vehicle crush damage from which an estimate of the change in velocity (DeltaV or Δv) of each vehicle can be obtained. The increased use of ABS braking systems has led to an increase in the number of collisions where insufficient scene data exists to perform momentum based calculations. This leads to an increased reliance on the CRASH calculations.

Criticism has been levelled by Brach [**11**] and others [**132**] concerning the overall accuracy of CRASH and its dependence on user estimated values, primarily the principal direction of force (PDOF). Brach [**9**] also expresses doubt over the inclusion of an energy adjustment factor which he claims does not have a sound theoretical basis and may be somewhat arbitrary. It is important to explore these criticisms and to quantify how these factors affect the results of calculations.

At present CRASH does not provide an estimate of the actual velocities, just the DeltaV. A substantial extension to the CRASH model will be to derive a new method whereby the actual velocities of the vehicles can be determined. This innovation will increase the application of CRASH to real-world collisions and will represent a significant advancement within this field.

The main aims of this research are then threefold and can be summarised as follows

- To quantify factors affecting accuracy of DeltaV and predicted speeds
- To determine the relevance and accuracy of energy adjustment factors in CRASH calculations
- To develop a method to determine actual vehicle velocities from DeltaV values

1.3 Research Objectives

The main aims of this thesis can be subdivided into a series of objectives. For evaluation purposes these objectives are listed below

- Determine how the various impact phase models are interrelated.
- So that consistency can be achieved, describe a systematic method to determine crush damage profiles.
- Determine whether the energy adjustment factor commonly used by CRASH accurately models reality.
- If not, determine whether there an alternative adjustment factor which can be utilised or developed.
- Determine the overall accuracy that can be expected from CRASH analyses.
- Determine the most significant factors affecting the accuracy of CRASH.
- Ascertain whether it is possible to determine the actual velocities of vehicles from DeltaV values.
- Describe techniques which can be used or developed to reduce uncertainty in the most significant factors affecting accuracy.

1.4 Limitations

This research considers only the impact phase of a collision; the pre and post impact phases are well documented elsewhere. Since the majority of impact phase models in use are planar, only planar models are considered in this work. In practice this is not unduly limiting since the majority of road vehicle collisions are essentially planar in nature.

1.5 Original contributions

The original contributions provided by this research are as follows

1. It is shown that the momentum based models of Brach [**11**] and Ishikawa [**43**] are equivalent. It is shown that the CRASH algorithm can be separated into two distinct parts. The first determines the amount of work done in causing crush. The result of the first part is then used as input into the second part which determines the change in velocity of each vehicle. Significantly it is shown that provided that certain criteria are met, namely that the impact plane is orientated perpendicular to the impulse, the second part of the CRASH model is also equivalent to the momentum models and yield identical results. Explicit methods of converting between the various models are described.

2. The measurement protocols used to systematically determine crush energy are summarised and consolidated. A new technique is demonstrated to cater for collisions where one or other vehicle is significantly bowed.

3. It is shown that the standard energy adjustment factor used by the first part of CRASH and described by McHenry [**65**] does not generate the same energy values as predicted by the models of Brach [**11**] or Ishikawa [**43**]. An alternative energy adjustment factor is developed which does produce energy values which match those predicted by the momentum models.

4. The accuracy of CRASH is explored in detail and the major factors affecting accuracy are identified. Two methods of analysing accuracy are considered, a purely analytical method and a Monte Carlo simulation. It is found that both

methods yield similar results. The overall accuracy of certain types of collisions are found to be inherently less accurate than other types of collisions.

5. A method to determine actual vehicle velocities from DeltaV values is developed and validated against a well-known series of test collisions. The new method does not rely solely on CRASH generated DeltaV values, but can be used with DeltaV values derived from any other technique. This new method provides a significant enhancement to the overall knowledge in this area.

6. It is also shown that the method to determine actual vehicle speeds can be utilised to provide a better estimate of the PDOF values applicable to each vehicle. This substantially improves the overall accuracy of CRASH.

7. The final contribution of this work is to provide a significant theoretical basis upon which further research can be built in the area of road vehicle collisions.

1.6 Organisation of the thesis

The remainder of this thesis is organised as follows

- Chapter 2 provides an overview of the existing research in this area and shows the equivalence of the models considered by this research.
- Chapter 3 provides a description of the measurement protocols designed to obtain crush measurements. This Chapter aims to consolidate the existing protocols from a wide variety of sources and discuss differences between them. An extension to the protocols is described resulting in a new protocol to consistently and accurately measure significantly bowed vehicles.
- Chapter 4 describes existing energy adjustment factors and shows how they can be related to results obtained using the momentum models. It is shown that the existing adjustment factors do not match the results obtained from momentum models. A new adjustment factor is developed which does match the results from momentum models. The results of applying this adjustment factor to real-world collisions is explored in brief in this Chapter with a more complete analysis in Chapter 7.

- Chapter 5 provides an analysis of the accuracy that can be expected from the CRASH algorithm using analytical techniques. A model is developed using Mathcad and applied to a series of well-known test collisions.
- Chapter 6 describes a Monte Carlo simulation of the CRASH algorithm. A Mathcad model is developed to perform the simulation. The results from a well-known test series are analysed using the simulation model and compared with the analytical model presented in Chapter 5.
- Chapter 7 shows how changes in velocity data can be used to determine the actual velocities of vehicles in a collision. For validation the method is applied to a series of test collisions using both the standard energy adjustment factor and the new energy adjustment factor developed in Chapter 4
- Chapter 8 summarises the conclusions reached by this research. The research is evaluated and suggestions are made for further work in this area.
- The appendices contain much of the data obtained as a result of this research and listings of the Mathcad models used in Chapters 5 and 6.

1.7 Summary

This Chapter has explained the motivation and scope for this research. A summary of the contributions to knowledge are described together with an outline of the thesis and the criteria by which this work can be evaluated. In the next Chapter a summary of the existing research in this field is presented.

Chapter 2

Crash Phase Models

2.1 Objectives

In this Chapter the scope of the current research is outlined to provide a description of the main crash phase models in current use. The strengths and weaknesses of each model are highlighted and it is demonstrated how the models are interrelated.

2.2 Introduction

The forensic investigation of collisions between vehicles is a relatively recent pursuit although the theory underlying such investigations has a much longer history. One of the earliest references to collision theory is Thomas Harriot's manuscript on the Theory of Impacts which is dated to 1619 [**86**]. In 1687 Newton published his *Philosophiae Naturalis Principia Mathematica* which forms the basis of impact theory and also modern crash investigation. A useful reference describing the current theory is provided by Stronge [**113**]

From the perspective of a forensic investigator a collision can be considered as comprising three main phases. There is an initial pre-impact phase where the vehicles move towards impact, the collision phase itself where the vehicles interact with each other and finally a post-impact phase where the motion of the vehicles from impact towards rest is considered.

The pre and post impact phases are concerned mainly with the analysis of tyre and other marks on the road surface. Techniques to establish the speeds of vehicles from these marks are well established. Simple examples are described in [**104**] or [**102**] Such techniques yield considerable information about the behaviour of vehicles during the pre and post impact phases. With the increased use of anti-lock braking systems (ABS), tyre marks are becoming less common. The presence of water on a road surface also decreases the chance of suitable tyre marks being found on the road surface. In situations where there are no tyre marks, any model based on the analysis of those marks cannot succeed and the determination of pre-impact speeds in particular becomes more problematic. There are a variety of methods that provide information on vehicle speeds in the absence of tyre marks. One such method involves the use of the pedestrian throw distance discussed, for example, by Evans and Smith [**106**]

Where there are no tyre marks, an analysis of the impact phase of the collision becomes more relevant to forensic investigators and is often the only source of information concerning the behaviour of the vehicles. This research considers the modelling of the impact phase of a collision. It examines the existing impact phase models and considers their various strengths, weaknesses and accuracy. It also seeks to develop a new model to generate more relevant results and to quantify the accuracy of these innovations.

Crash phase models tend to fall into two broad categories, those based solely on the conservation of linear and/or angular momentum and the CRASH model which also considers the conservation of energy. Three main crash models are used to describe the crash phase of a collision. Two are momentum based models as defined by Ishikawa [**42**] and Brach [**9**]. The third model is the CRASH algorithm developed during the 1970's and described by McHenry [**65**].

Although several other models also exist, such as those by Woolley [**130**] and that used in PC-CRASH [**111**], these are similar in many respects to the momentum based models considered in detail by this research. An overview of the basic assumptions made by the three main crash phase models is provided in the next section together with a summary of the salient features for each of the models.

2.3 Description of the existing models

2.3.1 Common theory and assumptions

In this research planar collisions only are considered. In a planar collision each vehicle has three degrees of freedom, two parameters describing the motion of the centre of mass and a third parameter describing the rotation of the vehicle. The three crash phase models examined in this research make a number of common assumptions,

1. Tyre and other external forces are assumed to be negligible during the impact, so that momentum is conserved.

2. The vehicle masses and moments of inertia are maintained throughout the collision. That is the deformations caused by the collision do not significantly change the moments of inertia and the masses of the vehicles are not significantly changed, for example, by parts of a vehicle becoming detached as a result of the collision.

3. The time dependent impulse can be modelled as one force, its resultant (***P***) which acts at some point in or on the vehicle.

The conservation of linear momentum is based on the linear form of Newton's Second and Third laws and leads to the equations

$$m_1(\boldsymbol{v}_1 - \boldsymbol{u}_1) = m_1\Delta\boldsymbol{v}_1 = \boldsymbol{P}, \tag{2.1}$$

$$m_2(\boldsymbol{v}_2 - \boldsymbol{u}_2) = m_2\Delta\boldsymbol{v}_2 = -\boldsymbol{P} \tag{2.2}$$

where m is the mass of each vehicle, ***P*** is the impulse and ***u*** and ***v*** are the initial and final velocities and $\Delta\boldsymbol{v}$ is defined as the change in velocity ***v*** - ***u***. Subscripts 1 and 2 refer throughout to vehicles 1 and 2 respectively. In collinear collisions, the line of action of the impulse ***P*** passes through the centres of mass of the vehicles and there is no change in the rotational velocity of either vehicle. If ***P*** does not act through the centres of mass it produces a change not only in the motion of the centres of mass, but also a rotation of each vehicle about the centre of mass given by

$$m_1k_1^2(\Omega_1 - \omega_1) = m_1k_1^2\Delta\omega_1 = h_1P, \tag{2.3}$$

$$m_2k_2^2(\Omega_2 - \omega_2) = m_2k_2^2\Delta\omega_2 = -h_2P \tag{2.4}$$

where k is the radius of gyration, h the moment arm of the impulse about the centre of mass, ω and Ω are the pre and post-impact rotational velocities of each vehicle and $\Delta\omega$ represents the change in rotational velocity $\Omega - \omega$. In a vehicle to vehicle collision it is not unreasonable to assume that the masses, radii of gyration and moment arms for each vehicle are known or can be obtained easily. Equations (2.1) - (2.4) then form a system of four equations with eight unknown velocity variables. Provided that four velocity variables can be established then complete solutions for the remaining four variables can be determined. The momentum based models utilise equations (2.1) - (2.4) and attempt to provide methods to establish solutions for the unknown velocities. Particular solutions using momentum alone are exemplified by the models proposed by Brach [**9**] and Ishikawa [**42**] and these are examined in more detail.

Figure 2.1 shows the vehicle based reference frame and notation used by this research. The position of the point of application relative to the centre of mass of a vehicle can be described using the distance d and angle ϕ. The parameter h is the length of the moment arm of the impulse about the centre of mass. In this research the length of the moment arm tangential to the impulse h_t is also relevant and is utilised in Chapter 7.

Figure 2.1: Vehicle based reference frame

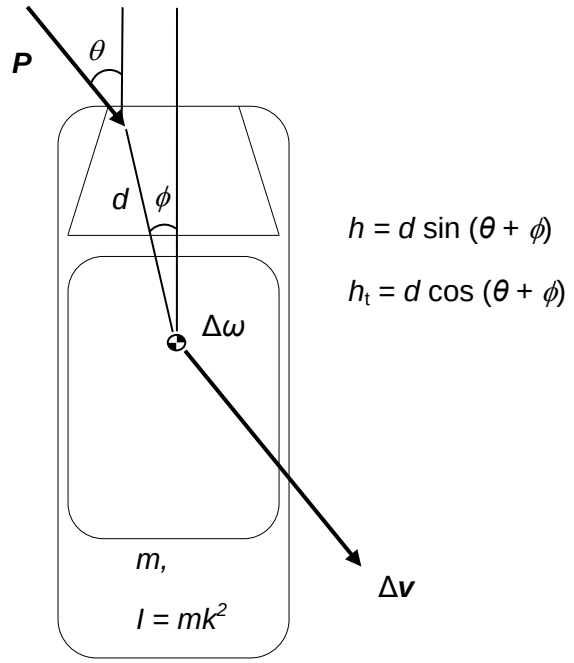

The First Law of Thermodynamics leads to the conclusion that in a closed system, the total energy is also conserved. The assumption that an impact between two vehicles may be modelled as a closed system allows the development of an equation describing the energy transfer as a result of that collision,

$$m_1u_1^2 + m_2u_2^2 + m_1k_1^2\omega_1^2 + m_2k_2^2\omega_2^2 = m_1v_1^2 + m_2v_2^2 + m_1k_1^2\Omega_1^2 + m_2k_2^2\Omega_2^2 + 2E \qquad (2.5)$$

where *E* denotes the work done in deforming the vehicles.

Equation (2.5) provides another equation and another relevant unknown variable, the total work performed. This forms a system of five equations with nine unknowns. In general, if five values can be estimated by some method, then a complete solution can be obtained for the remaining variables. This forms the basis for the CRASH model which is also examined in more detail.

2.3.2 Brach's Model

Brach has published several descriptions of his Planar Impact Mechanics (PIM) model since 1983 and his model is described extensively in the literature and compared with existing crash test data. A comprehensive explanation of his PIM model is contained in [**7**], [**8**] and [**11**]. Figure 2.2 shows a diagram illustrating the coordinate systems used in the PIM model.

Figure 2.2: Coordinate Systems used in Planar Impact Mechanics

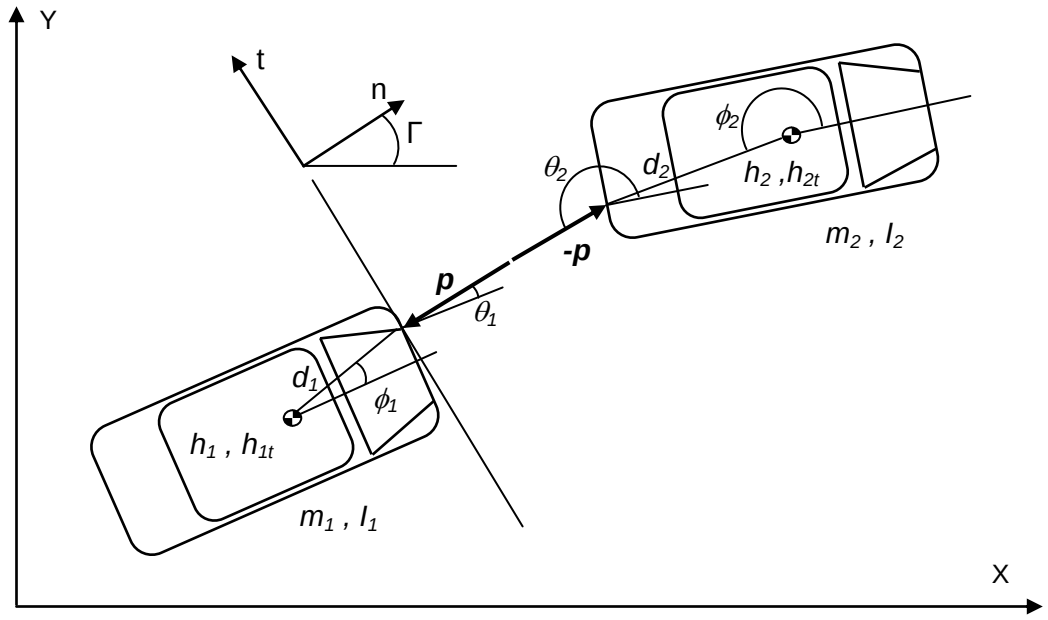

In essence Brach's PIM model considers the conservation of linear and angular momentum in a orthonormal coordinate system oriented to an impact plane which is established parallel to a hypothetical contact surface common to both vehicles. The impact plane is related to the x-y coordinate system by the angle *Γ*.

The impulse due to impact is resolved into two components, normal and tangential to the impact plane. The resulting six equations and eight unknowns are supplemented with two coefficients to provide additional constraints and thereby generate a solution.

Brach defines a coefficient of restitution normal to the impact plane (e_n) which is defined as the ratio of the relative normal velocity post impact to the relative normal velocity pre impact. Brach also introduces another coefficient, the impulse ratio μ. This is effectively a coefficient of friction and is defined as the ratio of the normal and tangential impulse components. Brach's solution to equations (2.1) - (2.4) is a series of equations which are shown in Appendix A and summarised below

$$\begin{aligned}
v_{1n} &= u_{1n} + \overline{m}(1+e_n)U_{Rn}q/m_1,\\
v_{1t} &= u_{1t} + \mu\overline{m}(1+e_n)U_{Rn}q/m_1,\\
v_{2n} &= u_{2n} - \overline{m}(1+e_n)U_{Rn}q/m_2,\\
v_{2t} &= u_{2t} - \mu\overline{m}(1+e_n)U_{Rn}q/m_2,\\
\Omega_1 &= \omega_1 + \overline{m}(1+e_n)U_{Rn}(h_1-\mu h_{1t})q/(m_1k_1^2),\\
\Omega_2 &= \omega_2 + \overline{m}(1+e_n)U_{Rn}(h_2-\mu h_{2t})q/(m_2k_2^2)
\end{aligned} \tag{2.6}$$

where

$$\begin{aligned}
\overline{m} &= m_1m_2/(m_1+m_2),\\
e_n &= -(V_{Rn}/U_{Rn}),\\
\mu &= P_t/P_n,\\
U_{Rn} &= u_{2n} - h_2\omega_2 - u_{1n} + h_1\omega_1,\\
\frac{1}{q} &= 1 + \frac{\overline{m}h_1^2}{m_1k_1^2} + \frac{\overline{m}h_2^2}{m_2k_2^2} - \mu\left(\frac{\overline{m}h_1h_{1t}}{m_1k_1^2} + \frac{\overline{m}h_2h_{2t}}{m_2k_2^2}\right).
\end{aligned} \tag{2.7}$$

The subscripts *n* and *t* represent component variables normal and tangential to the impact plane. From equation (2.6) it is relatively straightforward to determine the total change in velocity (Δ*v*) of each vehicle. This is discussed further in section 2.5.3

Brach [**11**] shows that an important quantity in the PIM model is the value μ_0 which is the impulse ratio μ that provides a common post-impact velocity tangential to the impact plane, i.e. where

$$V_{1t} = V_{2t}\,. \tag{2.8}$$

For vehicle to vehicle collisions the point of application of the impulse on each of the vehicles frequently reach a common velocity. In the PIM model this condition is satisfied when

$$e_n = 0\,, \tag{2.9}$$

$$\mu = \mu_0 \tag{2.10}$$

The parameter μ_0 is described by Brach as the critical impulse ratio

$$\mu_0 = \frac{rA + B(1+e_n)}{(1+e_n)(1+C) + rB} \tag{2.11}$$

where

$$\begin{aligned} r &= U_{Rt} / U_{Rn}, \\ A &= 1 + \frac{\bar{m}h_1^2}{m_1 k_1^2} + \frac{\bar{m}h_2^2}{m_2 k_2^2}, \\ B &= \frac{\bar{m}h_1 h_{1t}}{m_1 k_1^2} + \frac{\bar{m}h_2 h_{2t}}{m_2 k_2^2}, \\ C &= \frac{\bar{m}h_{1t}^2}{m_1 k_1^2} + \frac{\bar{m}h_{2t}^2}{m_2 k_2^2}. \end{aligned} \tag{2.12}$$

This terminology allows the value of the parameter *q* in the PIM model to be expressed using

$$\frac{1}{q} = A - \mu B \tag{2.13}$$

Brach's model takes as input the initial velocities and provides the final velocities as solutions. In collision reconstruction, the desired output is normally the initial velocities and this limits the utility of PIM. Using an iterative process the initial velocities can be

adjusted until the desired output is obtained and Brach [**11**] provides several hints as to how that process may be performed.

As a side effect to this model, Brach outlines how the principal direction of force (PDOF) can be determined from the ratio of the normal and tangential impulses. He also outlines a method for determining the total energy loss. In their later work Brach *et al.* [**13**] extend this technique and partition the total energy loss into normal and tangential components. This aspect is discussed in more detail in Chapter 4.

2.3.3 Ishikawa's Model

Ishikawa's model [**42**] is similar in many respects to planar impact mechanics proposed by Brach. Ishikawa also defines an impact plane to resolve the impulse into normal and tangential components. Where Ishikawa's model differs from Brach is that he proposes the utilisation of two coefficients of restitution, one normal to the impact plane (e_n) and the other tangential to the impact plane (e_t). These are defined such that the relative velocities of the point of application before (*U)* and after (*V*) impact are given by

$$V_{Rn} = -e_n U_{Rn}, \qquad V_{Rt} = -e_t U_{Rt} \tag{2.14}$$

where

$$\begin{aligned} U_{Rn} &= u_{2n} - h_2\omega_2 - u_{1n} + h_1\omega_1, \qquad V_{Rn} = v_{2n} - h_2\Omega_2 - v_{1n} + h_1\Omega_1 \\ U_{Rt} &= u_{2t} + h_{2t}\omega_2 - u_{1t} - h_{1t}\omega_1, \qquad V_{Rt} = v_{2t} + h_{2t}\Omega_2 - v_{1t} - h_{1t}\Omega_1 \end{aligned} \tag{2.15}$$

Ishikawa does not attempt to solve the equations directly for either the pre or post impact velocities, but instead provides a solution for the impulse components, P_n and P_t using the relative closing speeds and relative separation speeds at impact. Ishikawa's solution makes extensive use of a factor gamma (γ) which is defined as

$$\gamma = \frac{k^2}{k^2 + h^2} \tag{2.16}$$

where *k* is the radius of gyration and *h* the length of the moment arm. This factor implicitly takes account of the rotational effects caused by the application of an impulse at a distance *h* from the centre of mass of a vehicle.

Ishikawa's solutions are shown in Appendix B and summarised below

$$\begin{aligned} P_n &= \frac{1}{(1-m_n m_t m_0^2)}\left[m_n U_{Rn}(1+e_n) + m_n m_t m_0 U_{Rt}(1+e_t)\right], \\ P_t &= \frac{1}{(1-m_n m_t m_0^2)}\left[m_t U_{Rt}(1+e_t) + m_n m_t m_0 U_{Rn}(1+e_n)\right] \end{aligned} \tag{2.17}$$

where

$$\begin{aligned} m_n &= \frac{\gamma_{1n} m_1 \gamma_{2n} m_2}{\gamma_{1n} m_1 + \gamma_{2n} m_2}, \\ m_t &= \frac{\gamma_{1t} m_1 \gamma_{2t} m_2}{\gamma_{1t} m_1 + \gamma_{2t} m_2}, \\ m_0 &= \frac{h_1 h_{1t}}{m_1 k_1^2} + \frac{h_2 h_{2t}}{m_2 k_2^2}, \end{aligned} \tag{2.18}$$

and

$$\begin{aligned} \gamma_{1n} &= \frac{k_1^2}{k_1^2 + h_1^2}, \qquad \gamma_{2n} = \frac{k_2^2}{k_2^2 + h_2^2}, \\ \gamma_{1t} &= \frac{k_1^2}{k_1^2 + h_{1t}^2}, \qquad \gamma_{2t} = \frac{k_2^2}{k_2^2 + h_{2t}^2}. \end{aligned} \tag{2.19}$$

From the impulse components, P_n and P_t it is straightforward to use equation (2.1) to determine the change in velocity sustained by each vehicle. If either the post-impact or pre-impact velocities are known, then it is then possible to determine the remaining linear velocities.

Ishikawa does not provide explicit solutions to determine the change in rotation of each vehicle. However the change in rotation can be derived from equations (2.1) - (2.4) as it can be shown that

$$\Delta\omega_1 = \frac{h_1}{k_1^2}\Delta v_1, \qquad \Delta\omega_2 = \frac{h_2}{k_2^2}\Delta v_2. \tag{2.20}$$

Ishikawa uses the ratio of the two impulse components obtained when there is a common post-impact velocity, i.e. $e_n = e_t = 0$ to establish a method for indexing collisions. This particular aspect is not relevant to this research and is not discussed

further. Ishikawa also discusses the relationship between the energy loss as a result of the collision and the two coefficients of restitution. He shows that the two coefficients of restitution e_n and e_t are related to the impulse ratio μ by the equation

$$e_t = \frac{m_n U_{Rn}(1+e_n)(\mu - m_t m_0)}{m_t U_{Rt}(1-\mu m_n m_0)} - 1 \quad (2.21)$$

.

Provided the same orientation of the impact plane is used in both Ishikawa's and Brach's models and that provided there is a common value for e_n, equation (2.21) provides a useful way of converting Brach's impulse ratio μ into Ishikawa's tangential coefficient of restitution e_t. In the reverse scenario, the normal and tangential components determined from Ishikawa's model can be used to define Brach's impulse ratio.

2.3.4 The CRASH Model

From earlier work by Mason and Whitcomb [**63**], Campbell [**16**] derived a method to estimate the energy involved in causing vehicle crush. With the assumption that the work done in causing crush was the only factor causing a loss of kinetic energy in the system, an estimate could then be made of the Equivalent Barrier Speed (EBS). This concept was extended by McHenry [**65**] on behalf of the Cornell Aeronautical Laboratory (later Calspan Corporation) during the late 1970s and eventually developed into the CRASH algorithm. The name itself is an acronym for Calspan Reconstruction of Accident Speeds on the Highway. Various variations of the algorithms were developed, CRASH in February 1976 through to CRASH3 in February 1981. All variants share the same underlying principles and for the purposes of this research can be considered equivalent. CRASH was initially designed to run on a mainframe computer however these algorithms were adopted by a variety of manufacturers for use on personal computers. In the UK the most common derivatives in use are probably AiDamage [**74**], EDCRASH [**26**], and WinCrash [**124**]

Although originally intended as a tool for assessing accident severity, CRASH has been widely adopted by the crash investigation community. This is probably because where there is insufficient information as to the desired output velocities, methods based on the conservation of momentum alone cannot succeed e.g. Brach's PIM. Information about the collision severity and changes in velocity can still be obtained

from an analysis of the damage sustained by each of the vehicles and this is the basis for CRASH.

CRASH comprises a series of modules to estimate the change in velocity (Δv) of a vehicle from the damage sustained by each vehicle (E_1 and E_2). Post-impact trajectory simulation modules are also included to establish post impact speeds. The damage only part of CRASH utilises the conservation laws of momentum and energy to establish the change in velocity of vehicles involved in a collision. The assumption is made that the points of application of the impulse reach a common velocity during the approach phase of the collision. This is known as the common velocity condition. With this assumption, Tsongas [**117**] shows that the CRASH equation can be expressed as

$$\Delta v_1 = \sqrt{\frac{2\gamma_1\gamma_2 m_2(E_1+E_2)}{m_1(\gamma_1 m_1+\gamma_2 m_2)}} = \sqrt{\frac{2\gamma_1(E_1+E_2)}{m_1\left(1+\frac{\gamma_1 m_1}{\gamma_2 m_2}\right)}} \quad . \tag{2.22}$$

Equations (2.1) and (2.2) lead to an expression relating the two changes in velocity from which the change in velocity of vehicle 2 can be derived

$$\Delta \boldsymbol{v}_1 = -\Delta \boldsymbol{v}_2 \frac{m_2}{m_1} \tag{2.23}$$

The change in velocity calculated by this method is the change in velocity of the centre of mass of each vehicle along the line of action of the impulse. From Newton's Second Law it follows that there can be no change in velocity at the centre of mass tangential to the impulse so CRASH implicitly defines the total change in velocity.

The incorporation of a coefficient of restitution allows the changes in velocity to change beyond that required simply to reach a common velocity. As Brach [**11**] indicates this requires that a common velocity is achieved both parallel to and tangentially to the impulse. Smith [**105**] shows that some relaxation to the common velocity condition can be achieved by incorporating a coefficient of restitution parallel to the impulse e_p. His derivation provides an expression for the change in velocity

$$\Delta v_1 = \sqrt{\frac{2\gamma_1\gamma_2 m_2(E_1+E_2)(1+e_p)}{m_1(\gamma_1 m_1+\gamma_2 m_2)(1-e_p)}} = \sqrt{\frac{2m_2(E_1+E_2)(1+e_p)}{m_1(m_1\delta_2+m_2\delta_1)(1-e_p)}} \tag{2.24}$$

where $\delta = 1/\gamma$. Smith's derivation is utilised in Chapter 7 where it is shown that it is possible to relax the common velocity condition still further to model collisions where a common velocity is not achieved either along the line of action or tangentially to the impulse.

A variety of methods can be utilised to determine the crush energy, the damage analysis part of the CRASH algorithm can therefore be viewed as two separate techniques although they are commonly quoted as one technique. The first technique is to establish an estimate of the work done in causing deformation and the second is to calculate the change in speed.

The second part of the CRASH algorithm takes as input the work done in causing deformation to each vehicle and outputs the change in speed for each vehicle. Rose *et al* [**95**] describe the CRASH algorithm as a quasi-one-dimensional model. They argue that although rotational changes is implicitly incorporated into the model (through their description of γ as an 'effective mass' factor) any change in velocity is implicitly assumed to take place along the line of action of the impulse. In practice this means that the user needs to define the line of action of the impulse or principal direction of force (PDOF).

The requirement to estimate a PDOF is a regarded as a major weakness by several commentators (e.g. Brach [**11**], Woolley [**132**]) since it is difficult to estimate this quantity reliably or consistently. Smith and Noga [**108**] for example suggest that the PDOF for each vehicle may be subject to a range of ±20° for different investigators.

CRASH has received a considerable amount of criticism since its release mainly concerning some possible inadequacies and overall accuracy of the model e.g. Woolley [**132**]. It is worth noting that the introduction to the CRASH3 User's Manual states [**117**]

> *CRASH3 is not, nor was it intended, to be a high fidelity collision simulation program. In most accidents, only a minimum amount of data are available, and even these data are only available second hand. CRASH3 is intended primarily as a tool for making a standardized assessment of an accident's severity.*

Despite these comments CRASH remains a popular algorithm within the forensic investigation community. The potential accuracy of CRASH is discussed in detail in

Chapter 5 and Chapter 6. In the next section the CRASH technique to determine the work done in causing crush is discussed.

2.4 Determining the work done in causing crush

In order to generate a solution some method must be applied to determine the work done in causing deformation to the vehicles and thereby the values of E_1 and E_2. The derivation by Smith [**105**] shows that a solution is not dependent upon any particular energy loss model to determine the crush energy so that any suitable model may be used. It was found in early studies of frontal rigid barrier tests e.g. Campbell [**16**] that for impact speeds above about 20 mph (9 ms^{-1}) a near linear relationship between the impact speed and crush depth was obtained as shown in Figure 2.3

Figure 2.3: Campbell's Results

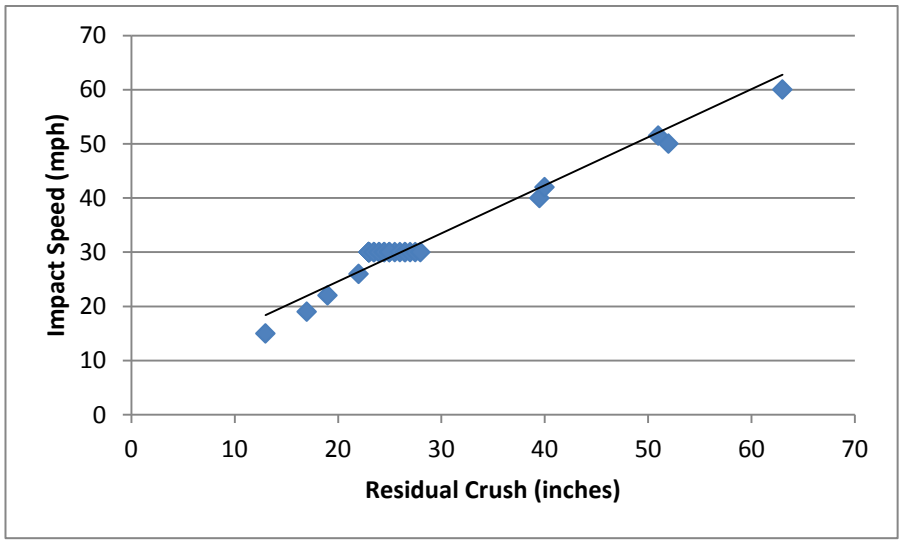

Campbell described the linear relationship as

$$v = b_0 + b_1 C \tag{2.25}$$

where

$$\begin{aligned} V &= \text{Impact speed (mph)} \\ b_0 &= \text{y-intercept (mph)} \\ b_1 &= \text{gradient (mph/inch)} \\ C &= \text{Average crush (inch)} \end{aligned} \tag{2.26}$$

Campbell showed that this is equivalent to a linear force / crush model to describe the force per unit width and has the form shown in Figure 2.4

Figure 2.4: Force per Unit Width

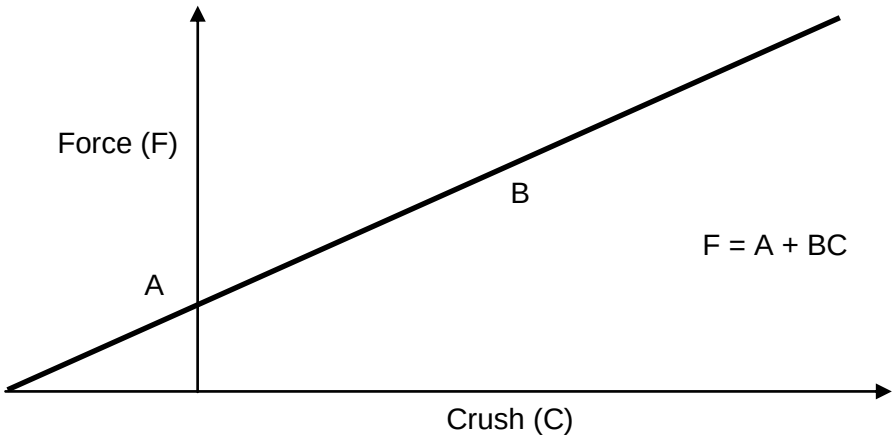

The equation of the graph in Figure 2.4 is

$$F = A + BC\,. \tag{2.27}$$

Campbell made the assumption that in a barrier impact, all the kinetic energy of the vehicle at impact is converted into residual crush, i.e.

$$E = \frac{1}{2} m(b_0 + b_1 C)^2\,. \tag{2.28}$$

The work done in deforming the vehicle can be determined by integrating equation (2.27) with respect to the distance crushed (C) and the damage width (*L*) i.e.

$$E = \int_0^L \int_0^C (A + BC)\; dC\; dL. \tag{2.29}$$

If it is assumed that the crush is uniform over the entire damage width (as is likely with frontal barrier impacts), equation (2.28) can be substituted into equation (2.29) and solved to produce expressions for *A* and *B* and a constant of integration *G* in terms of b_0 and b_1 i.e.

$$A = \frac{m}{L} b_0 b_1, \qquad B = \frac{m}{L} b_1^2, \qquad G = \frac{A^2}{2B}. \tag{2.30}$$

The constant of integration *G* corresponds to an expression for the work done on the vehicle which is performed with no residual crush. Campbell's methods were

developed by McHenry [**65**] who derived a similar model using Emori's [**27**] earlier assumption that the crush to vehicles can be modelled as a linear spring. McHenry devised a practical method which divided the crush area into a number of discrete crush zones defined by a series of crush measurements as shown in Figure 2.5

Figure 2.5: Crush zone measurements

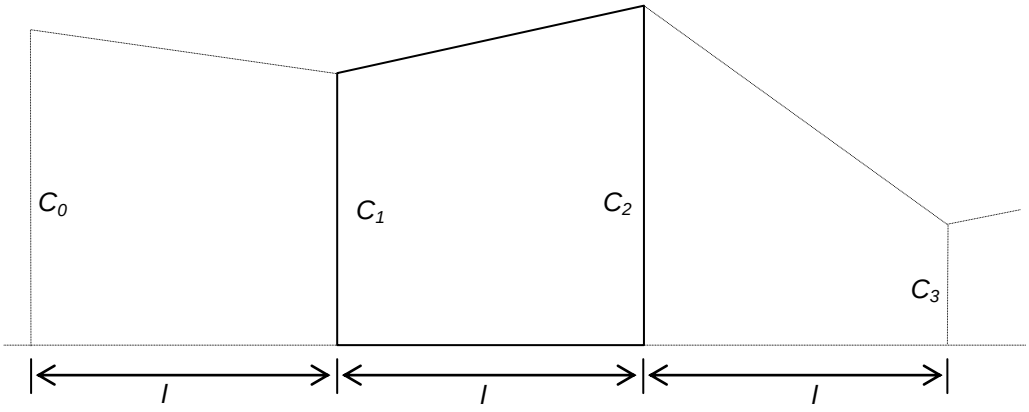

Each crush zone is thereby defined by two crush measurements and the width of the zone *l*. The work done in causing crush to each zone can then be described by the equation

$$E = \frac{A^2}{2B} l + A(area) + B\bar{x}(area) \tag{2.31}$$

where $\bar{x}$ is the displacement of the centre of mass of the zone perpendicular to the original surface and *area* is the area of the each crush zone, i.e.

$$\bar{x} = \frac{C_1^2 + C_1 C_2 + C_2^2}{3(C_1 + C_2)}, \tag{2.32}$$

$$area = l(C_1 + C_2)/2. \tag{2.33}$$

Typically 2, 4 or 6 crush measurements are used to define a complete damage profile and McHenry provided explicit solutions to cater for each of these numbers of measurements. McHenry also used the geometric properties of crushed area to define the point of application of the impulse. The CRASH model he describes uses the geometric centre of the damaged area, the damage centroid, as the point of application

of the impulse. Again, McHenry provides explicit solutions for 2, 4 or 6 crush measurements to define the position of the damage centroid. Neades [**74**] extended McHenry's work in the implementation of AiDamage to allow an unlimited number of crush zones to be defined. Singh [**100**] also shows that with a arbitrary number of equally spaced crush measurements, C_1 to C_n and by assuming a constant stiffness for all crush zones, the total force F and work done in causing crush E can be determined by

$$F = \sum_{i=1}^{n-1} F_i = L\left(A + \frac{B}{2(n-1)}.\eta \right), \tag{2.34}$$

$$E = \frac{L}{(n-1)}\left(\frac{A\eta}{2} + \frac{B\kappa}{6} + \frac{(n-1)A^2}{2B} \right) \tag{2.35}$$

where

$$\begin{aligned} \eta &= \sum_{i=1}^{n-1} [C_i + C_{i+1}] \\ \kappa &= \sum_{i=1}^{n-1} \left[C_i^2 + C_i C_{i+1} + C_{i+1}^2 \right]. \end{aligned} \tag{2.36}$$

If it is assumed that the initial kinetic energy of a vehicle is converted into crush, as is the case for a car to barrier collision, then the initial speed of the vehicle is known as the equivalent barrier speed (EBS) or barrier equivalent velocity (BEV). With this assumption, equation (2.35) can be equated to the initial kinetic energy of the vehicle. Substitution of equation (2.30) then produces

$$(n-1)EBS^2 = \left(b_0 b_1 \eta + b_1^2 \kappa + b_1^2 (n-1) \right). \tag{2.37}$$

Singh [**100**] shows that for non-uniform crush profiles the quadratic b_1 in equation (2.37) can be determined as

$$b_1 = \frac{-b_0\eta + \sqrt{(b_0\eta)^2 - 4\kappa(n-1)(b_0^2 - EBS^2)/3}}{2\kappa/3}. \tag{2.38}$$

Similar derivations can be made to determine stiffness coefficients from angled collisions and collisions with moveable barriers. Singh [**99**] extended this model to determine analytically the value of b_0 which is helpful in providing an estimate of this

parameter. His derivation however requires knowledge of the time over which a common velocity was achieved during the impact. This effectively means that it can only be used for test collisions where a suitable acceleration-time history of the test impact exists. It also makes the additional assumption that the peak force reached during the impact is equal to twice the average force.

Prasad [**90**], [**88**], [**89**] noticed that in an extensive series of crash tests the vehicles tested were found to be linear in $\sqrt{2E/L}$ against residual crush. He reasoned that since the change in velocity equation (equation (2.22)) required energy as an input, then it made more sense to determine stiffness coefficients which provided energy directly. As a result he reformulated the crush damage equation to give

$$\sqrt{\frac{2E}{L}} = d_0 + d_1 C \tag{2.39}$$

where the coefficients d_0 and d_1 in equation (2.39) are related to the A and B coefficients as follows

$$d_0 = \frac{A}{\sqrt{B}}, \qquad d_1 = \sqrt{B}. \tag{2.40}$$

Prasad showed that the linear impact speed / crush relationship described by Campbell continued to hold for more modern vehicles (up to 1990). *A* and *B* coefficients for real vehicles can be calculated from the results of existing crash tests using the methods described by Prasad, Neptune [**80**], or Jean [**46**].

A comprehensive summary of the stiffness coefficients obtained for a variety of vehicle categories is given by Siddall and Day [**98**]. Their work forms the basis for the coefficients used in a number of commercially available CRASH based programs e.g. AiDamage [**74**]. Hague [**39**] updated the frontal coefficients again in 2005 and showed that there was a general trend relating vehicle stiffness and model year. He found that more modern vehicles tended to be stiffer and therefore have higher coefficients than older models.

Techniques for measuring vehicles to obtain the input values required to determine the work done in causing crush are described by Neades and Shephard [**75**] and are discussed in Chapter 3. Kerkhoff *et al*. [**54**] noted that at high impact speeds vehicle

the linear response of crush and impact speed at lower speeds may not be valid at higher speeds as shown in Figure 2.6

Figure 2.6: Speed / Crush Graph for US Ford Escorts

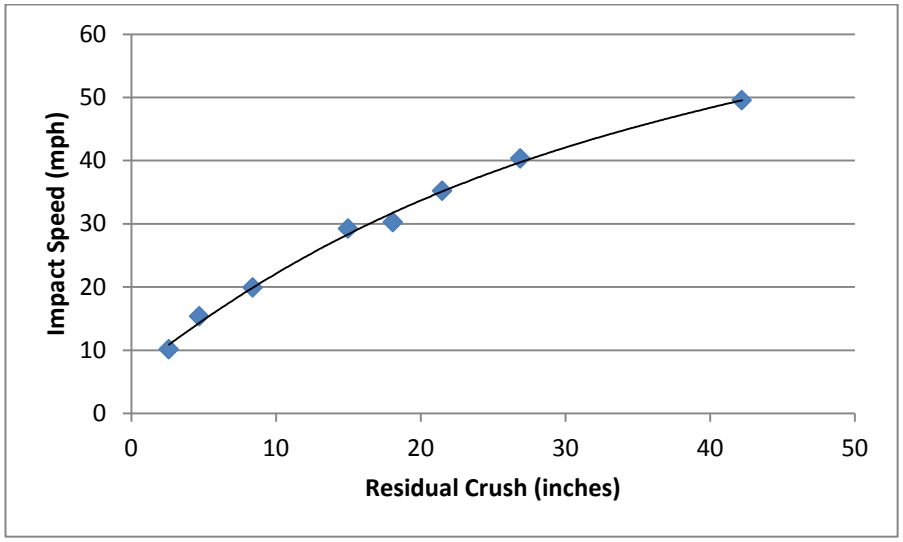

In effect there is a softening of the vehicle at higher impact speeds. Hague [**39**] suggests that this may be due to the energy absorbing structures at the front of the vehicle becoming saturated and the occupant compartment beginning to collapse. From a series of similar tests, Varat *et al.* [**121**] noted that a quadratic model provided a good fit to the data. They proposed a bi-linear approximation to determine the relationship between impact speed and crush with a change in slope at an impact speed of 30 mph. Additional techniques are also proposed for example Wood [**126**] where a power law is described to show the relationship between energy absorbed and residual crush. Other methods also exist for estimating the work done in causing deformation. One such technique involves a visual comparison of the damage sustained with vehicles crashed at known speeds.

All these models are essentially based on the response of the vehicle to head-on crash tests at various speeds. This is not the case in the majority of real-world collisions. An enhancement proposed by McHenry in the CRASH User's Manual [**117**] is to correct the work done as calculated by the standard CRASH analysis technique by a factor to allow for impulses which do not act perpendicularly to the measured surface. This energy adjustment factor is defined in the CRASH User's Manual as,

$$E = E_c(1+\tan^2\alpha) \tag{2.41}$$

where E_c is the calculated work, E is the corrected work performed and α is the angle formed between the direction of the impulse and the undamaged surface of the vehicle. Brach [**11**] criticises the calculation of crush energy calculations and in particular the energy adjustment factor described above. He asserts that there is no physical basis for this adjustment and instead proposes a method whereby the work done can be partitioned in normal and tangential components [**13**]. A more detailed description of how the work performed is calculated by CRASH is provided in Chapter 4 together with a discussion of the validity of the energy adjustment factor in equation (2.41).

2.5 Relationships between the models – similarities and differences

Since all the models are planar models, then any impact which has a substantial vertical force component cannot be modelled. These include rollovers and falls. The momentum based models such as those exemplified here by Brach and Ishikawa have the advantage of being able to potentially model a wide variety of impacts and can be considered to be more general in their application than CRASH. CRASH, at least in its traditional form, cannot be used unless a common velocity is achieved at the point of contact between the vehicles during the approach phase. This effectively excludes sideswipe impacts from being modelled in CRASH.

The requirement to estimate the total amount of energy lost as a result of the collision also means that CRASH will calculate an underestimate whenever a significant amount of energy cannot be estimated. For example, CRASH will underestimate the velocity change for impacts with pedestrians, animals and other objects which do absorb some energy. It is possible to model a collision with a motorcycle or truck as a collision with a barrier [**74**]. Barriers are defined in CRASH as objects which do not themselves absorb energy. Unless some alternative method is available to estimate the energy lost in causing crush, then CRASH will underestimate the change in velocity. Collisions between vehicles where there is significant override or underride of the main structural members tend too to render the estimation of the crush energy unreliable [**65**].

All the models make the assumption that the resultant impulse (the impact centre) acts at a single fixed point. Ishikawa [**42**] demonstrates that this point is not fixed during an impact, but moves to a certain extent. The location of the impact centre is defined by McHenry [**65**] in CRASH as the geometric centre of the damage profile. Inevitably this definition positions the point of application away from the physical line forming the

damage profile. Both Brach and Ishikawa suggest that the location of the point of application should be chosen so as to lie on the damage profile. Ishikawa [**42**] proposes a method to determine the position of this point. However this method requires prior knowledge of the impulse components and angular velocity which are to some extent determined by the choice of impact centre. As such, the utility of this method in practical forensic investigation is questionable. In any event the choice of the location of the impact centre is one that requires estimation by the user and is thus subject to error

2.5.1 Equivalence of Brach's and Ishikawa's models

The similarity between the two momentum based models has already been mentioned and provided the same impact plane is used for the PIM and Ishikawa's models, identical results can be obtained. The equivalence of the two models can also be shown. Ishikawa [**43**] defines impulse components as outlined in equations (2.17). From these equations Ishikawa shows that the ratio of the impulse components (μ) is

$$\mu = \frac{P_t}{P_n} = \frac{m_n m_t m_0 U_{Rn}(1+e_n) + m_t U_{Rt}(1+e_t)}{m_n m_t m_0 U_{Rt}(1+e_t) + m_n U_{Rn}(1+e_n)}. \tag{2.42}$$

This can be solved for the normal coefficient of restitution e_n in terms of the tangential coefficient e_t and the ratio of the impulse components μ to give equation (2.21). Equation (2.42) can also be solved to give an expression relating the two coefficients of restitution i.e.

$$\frac{1+e_t}{1+e_n} = \frac{m_n U_{Rn}(\mu - m_t m_0)}{m_t U_{Rt}(1-\mu m_n m_0)}. \tag{2.43}$$

There are obvious similarities between the coefficients *A*, *B* and *C* used in Brach's model [equations (2.12)] and the coefficients m_n, m_t and m_0 [equations (2.18)] in Ishikawa's model. Further analysis shows that the coefficients are related by the expressions

$$\overline{m} = \frac{m_1 m_2}{(m_1 + m_2)}, \qquad m_n = \frac{\overline{m}}{A}, \qquad m_t = \frac{\overline{m}}{(1+C)}, \qquad m_0 = \frac{B}{\overline{m}}. \tag{2.44}$$

Appendix C shows these relationships and derived products which facilitate conversion between Brach's model and that of Ishikawa. Substitution of equations (2.44) into equation (2.43) and solving for μ produces

$$\mu = \frac{(1+e_t)rA + B(1+e_n)}{(1+e_n)(1+C) + rB(1+e_t)}. \tag{2.45}$$

Brach defines the critical impulse ratio μ_0 as the impulse ratio μ which gives a common post-impact velocity tangential to the impact plane, i.e. $e_t = 0$. When e_t is zero then equation (2.45) simplifies to become identical to Brach's critical impulse ratio shown in equation (2.11).

2.5.2 Coefficients of restitution

In both momentum models two coefficients are required to generate solutions. In the PIM model these are a coefficient of restitution normal to the impact plane e_n and μ which is the ratio of the normal and tangential impulse components. Ishikawa's model utilises two coefficients of restitution, e_n which is defined in the same way as Brach's coefficient of restitution and e_t which is a tangential coefficient of restitution. Conversion between the two models can be achieved through equations (2.21) and (2.44). As shown by Smith [**105**] CRASH can also utilise a coefficient of restitution e_p acting along the line of action of the impulse.

Brach [**13**] states that in the majority of collisions involving light vehicles, relative tangential motion at the impact centre ceases prior to separation of the vehicles. In his PIM model a common tangential post-impact velocity is achieved when $\mu = \mu_0$ Similarly in Ishikawa's model this will be achieved when $e_t = 0$. In the standard form of CRASH, a common tangential velocity is assumed. Considerable research has been directed towards establishing estimates for a coefficient of restitution along the line of action of the impulse, or normally to an impact plane. Smith and Tsongas [**110**] reported a series of staged collisions where they found that the coefficient of restitution was between 0 and 0.26. They concluded that in general lower values of restitution tend to be found as the closing speed increases. Little information is available to indicate their methodology but it seems likely that these collisions were central and that restitution was calculated along the line of action of the impulse. Wood [**125**] also suggests a similar relationship based on a series of full scale crash tests with a maximum

restitution of about 0.3 Rose, Fenton and Beauchamp [**94**] investigated the effects of restitution for a single type of vehicle (a Chevrolet Astro van) in head-on collisions with a barrier. They found that the coefficient of restitution varied from 0.11 to 0.19 for impact speeds around 47 – 57 kmh^{-1}. Cipriani *et al.* [**21**] studied a series of vehicle to vehicle collinear impacts with low speeds up to 7 ms^{-1} and discovered that restitution varied from about 0.2 to 0.6 with the lower values found for higher impact speeds. Brach [**13**] suggests that restitution ranges from 0 to 0.3 for light vehicle collisions with the majority of values at the lower end of that range. At lower closing speeds it is apparent that restitution effects can be significant.

Both the PIM and Ishikawa models are forward iterative models. In use they require the pre-impact velocities to be defined from which it is then possible to determine the post-impact velocities. The input data is adjusted until the output data matches some desired post-impact scenario. For forensic collision investigation, in practice this means that without knowledge of the post-impact velocities, such as those obtained using traditional methods, it is difficult to obtain reliable solutions and this is a disadvantage. Brach [**11**] does attempt to address this issue by using a technique he describes as LESCOR (Least Squares Collision Reconstruction). In this technique a spreadsheet is used to iterate through suitable ranges of input data to determine the best fit to some known quantity. Examples he uses include matching the post-impact speeds to known speeds and matching the energy loss calculated by PIM to that determined from CRASH measurements.

As previously mentioned, CRASH requires an estimate of the PDOF. This is required to determine the line of action of the impulse and also to determine the magnitude of the energy adjustment factor described by McHenry [**65**]. It is recognised that this parameter is difficult to estimate and this has been used to indicate the unreliability of CRASH [**108**], [**132**], [**3**]. However it should be noted that the models of Brach and Ishikawa also require an estimate to determine the orientation of the impact plane. Ishikawa [**42**] suggests that the impact plane is formed by the common surface forming the damage profile of each vehicle. Brach [**13**] identified that where there was a common post-impact velocity ($e_n = 0$ and $\mu = \mu_0$) the choice of impact plane is immaterial as identical results are obtained for all orientations of the impact plane. In other types of collision, the choice of the impact plane affects the specific values of e_n and μ required to obtain a particular solution (e_n and e_t in Ishikawa's model). Brach also provides guidelines for choosing the orientation of the impact plane. His

suggestion is to nominally define the impact plane to the mean angle between the attitude of the vehicles at impact and use a range of values to examine the uncertainty associated by this choice.

2.5.3 Equivalence of CRASH and momentum models

Through the explicit incorporation of the conservation of total energy in the system as described by Smith [**105**], the CRASH solution as shown in equation (2.24) takes as input the masses of the vehicles, the lengths of the moment arms and the work done in causing crush. This part of the CRASH algorithm is entirely separate from any model describing how the crush energy value may be obtained. The conservation laws are common to all three models, thus it should be possible to use common data in each model and obtain identical results. For example it should be possible to use the total kinetic energy lost derived from Brach or Ishikawa's models and use this as input to CRASH. Although the energy calculated from Brach or Ishikawa's models can be used directly, to obtain identical results in each of the models a common impact plane is required. If not then coefficients of restitution are not common between the models. This requirement is relaxed somewhat in Chapter 4 where a technique is described to transform coefficients of restitution between differing impact planes. An explanation as to how impact planes can be aligned follows.

Brach [**9**] and [**10**] shows how the momentum change in each vehicle can be written using his model as

$$m_i \Delta v_i = \sqrt{\frac{2\bar{m}(1+\mu^2)qE_L(1+e_n)}{(1-e_n)+2\mu r-\dfrac{\mu r^2}{\mu_c}}} \tag{2.46}$$

where

$$\mu_c = r/(1+e_t)\,. \tag{2.47}$$

(Note that in Brach [**10**] equation (2.46) appears to have been misprinted so that the $(1+\mu^2)$ term appears incorrectly as $(1+\mu)$ and the numerator in the final term reads incorrectly as $\mu^2 r$ instead of μr^2.) When μ is zero then by definition Brach's (or Ishikawa's) tangential impulse component must also be zero. When the tangential

impulse component is zero, this corresponds to an impact plane perpendicular to the total impulse ***P***. Where μ is zero, equation (2.46) reduces to

$$m_i \Delta v_i = \sqrt{\frac{2\bar{m}qE_L(1+e_n)}{(1-e_n)}} \tag{2.48}$$

and since μ is zero, q in equation (2.48) can also be simplified and can be found from

$$\frac{1}{q} = 1 + \frac{\bar{m}h_1^2}{m_1 k_1^2} + \frac{\bar{m}h_2^2}{m_2 k_2^2} \tag{2.49}$$

Equation (2.49) can be expanded and solved for q to give

$$q = \frac{(m_1 + m_2)k_1^2 k_2^2}{m_1 k_1^2 (k_2^2 + h_2^2) + m_2 k_2^2 (k_1^2 + h_1^2)} \tag{2.50}$$

Equation (2.48) can therefore be expressed as

$$m_i \Delta v_i = \sqrt{\frac{2m_1 m_2 E_L (1+e_n)}{\left[m_1 k_1^2 (k_2^2 + h_2^2) + m_2 k_2^2 (k_1^2 + h_1^2)\right](1-e_n)}} \tag{2.51}$$

The CRASH solution as shown in equation (2.24) can also be written in a similar manner to equation (2.48) to show the change in momentum of each vehicle

$$m_i \Delta v_i = \sqrt{\frac{2\gamma_1 \gamma_2 m_1 m_2 (E_1 + E_2)(1+e_p)}{(\gamma_1 m_1 + \gamma_2 m_2)(1-e_p)}} \tag{2.52}$$

From the definition of γ in equation (2.16), equation (2.52) can be expanded to produce

$$m_i \Delta v_i = \sqrt{\frac{2m_1 m_2 (E_1 + E_2)(1+e_p)}{\left[m_1 k_1^2 (k_2^2 + h_2^2) + m_2 k_2^2 (k_1^2 + h_1^2)\right](1-e_p)}} \tag{2.53}$$

Equation (2.53) is therefore shown to be equivalent to equation (2.51) with $e_p = e_n$ and $E_L = E_1 + E_2$. This demonstrates that the part of the CRASH algorithm to determine velocity change from the energy loss (equation (2.24)) can be regarded as a special case of the more general Brach or Ishikawa models. Specifically the special case of CRASH will be achieved when the impact plane in Brach's or Ishikawa's models is orientated so as to be perpendicular to the total impulse ***P***. It can also be seen that

CRASH therefore implicitly defines an impact plane; one which is perpendicular to the total impulse.

A further condition implicit in the discussion above, is that a common tangential velocity is achieved at the point of application of the impulse. In Ishikawa's model this will be achieved when $e_t = 0$. In Brach's PIM model a common tangential velocity is achieved when $\mu = \mu_0$. Since μ is zero, this implies that the numerator in the equation to determine μ_0 in Brach's PIM model (equation (2.11)) must also be zero, so that

$$0 = rA + B(1 + e_n) \tag{2.54}$$

The implications of this relationship are discussed further in Chapter 7.

2.6 Crash test data

The National Highway Traffic Safety Administration (NHTSA) was established in 1970 as an agency of the US Department of Transportation (DOT). Their mandate is to carry out safety programs concerning road vehicles. As part of their road safety program they maintain and publish a comprehensive database of a series of crash tests [**83**]. The database contains details of over 6800 crash tests dating back to 1978. A variety of tests are recorded such as those for the New Car Assessment Program (NCAP), barrier tests and car to car impacts. This crash test database is the main source of data for determining stiffness coefficients for use in CRASH analyses. Similar data is not published from the Euro NCAP tests and without detailed crush measurements this series of tests is not suitable for determining stiffness coefficients or for validation purposes.

A series of 12 vehicle to vehicle crash tests were performed during the late 1970s to provide validation data for the Simulation Model for Automobile Collisions (SMAC) and CRASH. The results were published by Jones and Baum in 1978 [**51**] and the test series has since become known by an acronym derived from the title of their paper, Research Input for Computer Simulation of Automobile Collisions (RICSAC). Several authors have analysed the RICSAC tests in detail and a number of discrepancies between those analyses are apparent e.g. Smith and Noga [**109**] and Brach [**6**]. It is also apparent that in several of the tests there are significant discrepancies between the recorded damage profiles and the photographs of the damage. Nevertheless, the series of tests are useful for validation purposes.

Several other vehicle to vehicle crash test series also exist such as those performed by ITAI for their crash test days at Leyland [**29**] and Lotus [**45**]. These tend to be more ad-hoc but again provide useful validation data. Woolley and Kinney [**131**] provided data for 45 reference cases involving two vehicle collisions. This data set was generated using the SMAC model rather than from actual crash testing so its utility for validation is questionable.

2.7 Accuracy

A key aspect to forensic collision investigation is an ability to quantify the likely errors and sources of errors in any particular case. Most of the research relating to the accuracy of the various impact models tends to be empirical in nature comparing the correlation between a particular model and crash tests. For example, Brach and Brach [**10**] provide an analysis of how his PIM and CRASH models compare with the RICSAC test data. Lenard *et al.* [**56**], [**57**] consider the accuracy of CRASH compared with a series of collisions. There is little information available however concerning the theoretical accuracy of each of the models with variation in the input parameters.

Bartlett *et al*. [**3**] discuss the uncertainly in collision investigation measurements in a general way. This discussion is continued by Fonda [**32**] who considers in more detail the uncertainty in the collision phase. An early (1982) paper by Smith and Noga [**108**] provided an analysis of the confidence limits applicable to measurements for CRASH. They concluded that for low DeltaV collisions (10-15 mph) the mean sensitivity was ±17.8% For high DeltaV collisions (25-30 mph) the mean sensitivity was ±13.7%.

More recently (2004) Singh [**100**] performed a detailed statistical analysis to determine the confidence limits applicable to the stiffness coefficients A, B and G as used in equation (2.30). This work is extended in Chapter 5 where the theoretical confidence applicable to impact phase models is considered in detail. In Chapter 6 a Monte Carlo simulation for the CRASH model is presented to further analyse confidence levels.

2.8 Summary

In this Chapter the three main impact phase models were discussed in some detail. Similarities between the models were highlighted which show that the momentum based models of Brach and Ishikawa are essentially different representations of the same model. In addition it was shown that the CRASH model is equivalent to the momentum models. CRASH implicitly defines an impact plane which is orientated perpendicular to the impulse and provided a common impact plane is used in each of the models identical results can be achieved.

In the next chapter a series of measuring protocols are described. These enable investigators to determine the work done in causing crush to each vehicle and thereby establish the input parameters E_1 and E_2 to use in the CRASH model as described in equation (2.24)

Chapter 3

Measurement of Crush Damage

3.1 Objectives

In this Chapter a series of techniques are described to enable investigators to measure vehicles and thereby obtain an estimate of the work done in causing crush to each vehicle. The damage profile is an important factor in determining the total work done, as too are the direction of the impulse and location of the point of application of that impulse. A comprehensive description of the measuring process as applied in the UK is not available elsewhere and is crucial to overall accuracy so is included in this Chapter. The overall objective is to describe measuring protocols so that investigators are able to produce consistent and reproducible results. A new technique is also described for measuring severely bowed vehicles.

3.2 Introduction

The CRASH algorithm as described earlier has lead to the development of computer programs to estimate the changes in velocity (DeltaV) sustained by a vehicle in a collision. In essence the CRASH algorithm estimates the work done in causing crush from a series of crush damage measurements. The work done in causing crush is then used to determine the change in velocity of individual vehicles. Commonly used implementations in the UK are AiDamage [**74**], EDCRASH [**26**], and WinCrash [**124**].

Although such programs are often capable of using scene data for simulations and momentum analysis, it is the damage-only option which is of particular interest since

the techniques can often be used when there is insufficient information to perform more traditional analyses. A variety of information exists in the literature which describes the algorithms used and their derivation, as discussed previously, but little is available which describes exactly what measurements should be taken. A notable exception is that by Tumbas and Smith [**118**]. There remains a considerable amount of confusion as to which methods of measuring produce the most realistic results. The purpose of this chapter is to provide an overview of a series of simple measurement protocols which have been developed in the UK to overcome some of the traditional measurement difficulties. Substantial parts of this Chapter were published in *Impact* 17 (1) in 2009, pp 4 – 12.

3.3 Background

Alongside the development of the original CRASH program came the descriptive Collision Deformation Classification (CDC) [**1**]. This was developed from an earlier coding known as the Vehicle Deformation Index [**112**]. Using the CDC it is possible to concisely define a description of the damage caused to a vehicle using a seven character alphanumeric code. The code is limited in that it can only describe uniform perpendicular crush, as only one character is allowed to specify the maximum extent of the damage. More complicated damage profiles cannot therefore be defined. An estimation of the CDC is still required in some programs e.g. EDCRASH [**26**], but the maximum extent is ignored if additional data is supplied in the form of actual measurements describing the damage profile. One part of the CDC which is not ignored is the user estimation of the principal direction of force (PDOF) which is arguably the most difficult factor to estimate. Those programs which do not use the CDC still require an estimate of this parameter and this is discussed in more detail later.

The theory underlying the determination of the change in velocity from an analysis of the crush damage sustained was discussed in Chapter 2. Following work by Campbell [**16**] , McHenry [**65**] , Prasad [**89**] , Smith [**105**] and others it was shown that the change in velocity can be determined from the equations

$$\Delta v_1 = \sqrt{\frac{2m_2(E_1 + E_2)(1+e_p)}{m_1(m_1\delta_2 + m_2\delta_1)(1-e_p)}} \tag{3.1}$$

$$\Delta v_1 = -\Delta v_2 \frac{m_2}{m_1}. \tag{3.2}$$

The two energy parameters in equation (3.1) E_1 and E_2 represent the amount of work done in causing crush to each vehicle. These are of particular interest since if it is possible to estimate these values to a reasonable degree of accuracy then it follows that a realistic solution can be obtained. One technique to obtain an estimate of these values was described by Campbell [**16**] who showed that the amount of crush is approximately linear with respect to the impact speed with a damage threshold speed (intercept) b_0 and gradient b_1.

Methods described by Neptune [**80**], Prasad [**88**] and Jean [**46**] show how Campbell's linear relationship can be used in practice to derive two stiffness coefficients (*A* and *B*) which describe how the depth of crush is related to the work done in crushing the vehicle. These techniques are based on head-on collisions between vehicles and solid immovable barriers. In a head-on collision with a barrier, the crush sustained by the vehicle will be approximately uniform. As described in Chapter 2 it can be shown that the two stiffness coefficients *A* and *B* are related to b_0 and b_1 as follows

$$A = \frac{m}{L} b_0 b_1, \qquad B = \frac{m}{L} b_1^2. \tag{3.3}$$

To determine the two coefficients, suitable values for b_0 and b_1 are required. The most commonly used and comprehensive database from which stiffness coefficients can be obtained is the NHTSA crash test database [**83**]. This database contains detailed descriptions of a variety of tests defined mainly by the US Government to meet various safety criteria such as the New Car Assessment Programme (NCAP). As safety requirements have changed over the years, these criteria have altered to match. As a result of these criteria therefore the majority of collisions involve moderate speed impacts of around 30 – 35 mph. Lower speed impacts are rare. This has a consequent effect on the ability to estimate the threshold speed b_0 since all the data tends to be clustered around 30 – 35 mph.

The clustering of data at around 30 – 35 mph means that there are few if any data points from which to determine a realistic best-fit line using linear regression. As a result, the value of b_0 is very often estimated when determining *A* and *B* coefficients. Both Neptune [**80**] and Strother *et al.* [**114**] suggest a reasonable value is about 5 mph.

Varat *et al.* [**121**] in a comprehensive study of crash tests suggest that for vehicles manufactured during the 1970s and 1980s a suitable value for b_0 is 7.5 mph.

McHenry [**65**] provides explicit solutions to determine the values of E_1 and E_2 for either two, four or six crush measurements. Neades [**74**] extended this model to cater for an unlimited number of crush measurements and Singh [**99**] provides a mathematical description of a model which permits an unlimited number of uniformly spaced measurements.

Inherent in this method generally is the assumption that the vehicle is of uniform stiffness. Since the sides and rear of a vehicle may well behave differently to the front, separate stiffness coefficients are normally defined for front, rear and side impacts. All the CRASH derivative programs make extensive use of generic stiffness coefficients which are used when specific coefficients for a particular vehicle are not available. These are derived from the NHTSA database. The generic coefficients partition the vehicle data set into a number of categories or classes of vehicle dependent on the wheelbase. Hague [**39**] suggests that a better classification may be to partition the database by model year rather than wheelbase. Hague cautions that although vehicle specific stiffness coefficients should in theory lead to more accurate representations of the stiffness coefficients, incomplete or inaccurate data in the NHTSA database can lead to erroneous results.

3.4 Crush Measurements

3.4.1 General

Other input data for damage measurement takes the form of a series of crush measurements (C_1 – C_n) from the vehicles involved together with the width of the damaged area (L) and an offset (d) describing the displacement of the centre of the damaged area with the centre of mass of the vehicle. Usually the crush measurements are obtained by measuring a damaged vehicle and then comparing these with similar measurements taken from an undamaged vehicle. The crush sustained by the damaged vehicle can then be determined by simple subtraction and entered into the program.

Figure 3.1 summarises the basic measurements required by CRASH derivative programs which are discussed in more detail in subsequent sections.

Figure 3.1: Measurements Required by CRASH programs

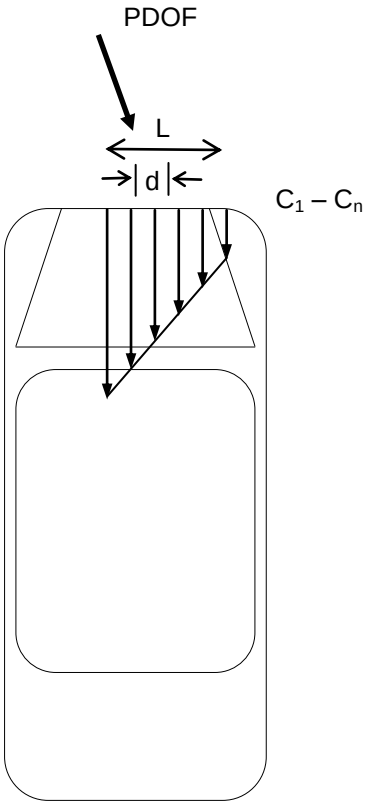

$C_1 - C_n$ Crush measurements

L Width of damage

d Offset

PDOF Principle direction of force

Several assumptions are inherent in the measurement process. First it is assumed that the front of the vehicle is a straight line and that the vehicle can be represented as a rectangle. In essence a real three dimensional vehicle ends up being represented by a two dimensional rectangle. Crush damage to a vehicle can take the form of direct contact damage between the vehicles or induced damage. Direct damage and induced damage which is contiguous to the direct contact damage should both be included in crush measurements.

Since real-world collisions frequently result in a non-uniform vertical crush, the level at which the measurements are taken is of great importance. As noted by Tumbas and Smith [**118**] crush measurements generally should be taken at frame height around the vehicle. For front and rear impacts this will be at bumper height. Where there is a distinct difference between the level of maximum intrusion and frame level (which often occurs in side impacts due to override by the impacting vehicle) measuring at sill or bumper level tends to generate an underestimate of the total energy absorbed. However if measured at the level of maximum intrusion the energy absorbed tends to be overestimated. A better estimate of the true value therefore probably lies

somewhere between these two extremes. It is therefore suggested that for side impacts in particular, the height at which the crush measurements are obtained is the mid-point between frame level and maximum intrusion. A similar process is also suggested by Tumbas and Smith. Otubushin and Galer [**84**] indicated that for completeness a series of crush measurements is taken, at the level of maximum crush, at mid-level and at sill/bumper level. When estimating DeltaV values however, for frontal impacts they utilise the bumper level of crush and for side impacts the mid-level crush.

In any event the process required is to establish a baseline parallel to the undamaged face of the vehicle under investigation either parallel to the longitudinal or lateral axes of the vehicle as appropriate. Crush measurements are then taken at intervals from the baseline to the along the length of the damaged area to form a description of the damage profile.

One problem for an investigator is to determine the length of the damaged area *L*. The process as described in the CRASH Manuals is to split up the baseline into equally spaced segments and take the crush measurements. A similar process is described by Struble [**115**]. The baseline width *L* as shown in Figure 3.1 then forms the measurement *L* which can be entered into the program. Note that this can result in a smaller value for the damage width *L* than the true width of the vehicle.

A smaller value for *L* reduces the area of damage which in turn results in an underestimate of the energy absorbed in crush and therefore an underestimate in the value of DeltaV. This problem was recognised by Smith and Tumbas [**118**]. Their recommended solution was to measure the *L* parameter in the field as described above, so that an appropriate spacing could be determined but subsequently enter the actual length into the program.

Although the Smith and Tumbas [**118**] solution works well for regular damage profiles, it does not work so well for those damage profiles where only part of the vehicle width is damaged, or where the profile is irregular. This is because the crush depths measured in this way do not necessarily correlate when irregular damage profiles are encountered. A more appropriate solution is that developed by Jennings [**47**]. This method assumes that the damage profile retains a consistent length compared with an undamaged vehicle, although it will be twisted into a different shape. A similar

assumption was made by Wood *et al*. [**127**] although their calculation of crush energy was somewhat different.

In this method the damage length *L* is determined by measuring directly along the face of the damage. The spacing between the crush zones can then be determined and crush measurements taken from the baseline to the relevant points. The measured value of *L* is inserted into the program and removes the use of arbitrary adjustments suggested by Smith and Tumbas [**118**]. A secondary beneficial effect is that corresponding points on damaged and undamaged vehicles are compared directly.

The standard CRASH algorithm defines a maximum of six crush measurements which does not always permit a realistic representation of the damage profile to be obtained. This was noted by Struble [**115**] who recognised that six equally spaced crush measurements can mask or omit details of the profile. He suggested moving one or more of the measurements to capture such detail where necessary. Such an adjustment will introduce additional errors. An alternative is to use a greater number of measurements to capture the profile as is described by Neades [**74**] or Singh [**99**].

3.4.2 Determining the damage offset measurement *d*

The damage sustained by a vehicle does not always extend over the whole side of the vehicle, particularly for those collisions involving side impacts. Some collisions result in damage which not only causes crush to the vehicle but also distorts the original to such an extent that it moves outside the bounding rectangle. Some method to locate the damage profile in relation to the original vehicle is required. This is achieved by the use of a damage offset measurement *d*. Note that this parameter, together with the direction of the impulse (PDOF), affects the length *h* of the impulse about the centre of mass which in turn affects the calculation of the value for δ used in equation (3.1).

The EDCRASH Training Manual [**28**] follows CRASH [**65**] and states that *the offset measurement d is the difference between the centre of the damaged area and the centre of mass of the vehicle*. This is a reasonable definition although it does presuppose that the location of the centre of mass is readily identifiable. Since the centre of mass of a vehicle is not readily identifiable in the field this can be problematic. In practice a field measurement to the centre of the vehicle may be desirable from which the actual offset can be determined.

3.4.3 Side impacts

Side impacts between the wheels of a vehicle can cause a vehicle to bow. Bowing is defined as a vehicle which distorts during the impact so that the ends of the vehicle curl round towards each other. A similar effect is noticed in end-wise collisions where the wings fold inwards due to a pole impact. This effect is shown in Figure 3.2

Figure 3.2: Bowing of a vehicle due to side impact

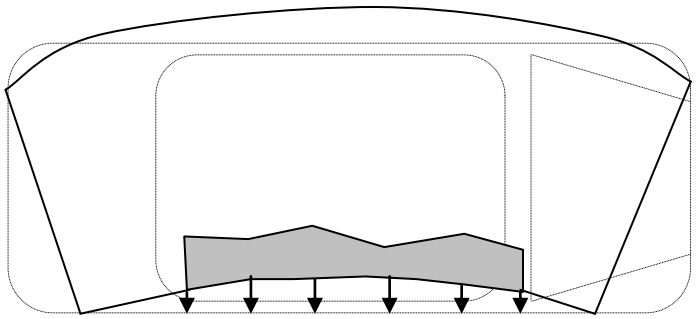

Vehicles which are not bowed can be measured in much the same way as described previously. A vehicle which is significantly bowed however would result in the investigator recording higher crush measurements, since the bowing contributes to the net depth as illustrated in Figure 3.2. It is possible to quantify the amount of bowing present by measuring the lateral displacement of the non-struck ends of the vehicles using a process described by Tumbas and Smith [**118**], but this does not lead to a simple method for recording the true crush of the vehicle. It can be argued that since the bowing of the vehicle must itself be caused by a force acting through a distance, then any apparent additional crush ought properly to be included in the measuring process. However this *may* lead to an overestimate of the crush damage. In the absence of empirical data to support this argument, it is suggested that any apparent crush due to bowing is removed.

An alternative protocol is proposed which negates the effect of any bowing and generates a more accurate representation of the true crush sustained by the vehicle. This method requires the construction of a reference frame around both the damaged vehicle and its undamaged counterpart. Measurements are taken at the same equal

spacing along either side of the vehicle together with the distance measured along the datum lines. It is important to start the measurements at a readily identifiable point on the vehicle so that measurements from an undamaged vehicle generate a one-to-one correspondence with the damaged widths. The method proposed here allows the calculation of the width of the vehicle at various points along the damage profile as shown by the dashed lines in Figure 3.3. For clarity only the first damaged measurement (*W*) is shown on the diagram. The same method when applied to all the points allows the true width of the vehicle to be determined at each point.

Figure 3.3: Measurement protocol for bowed vehicles

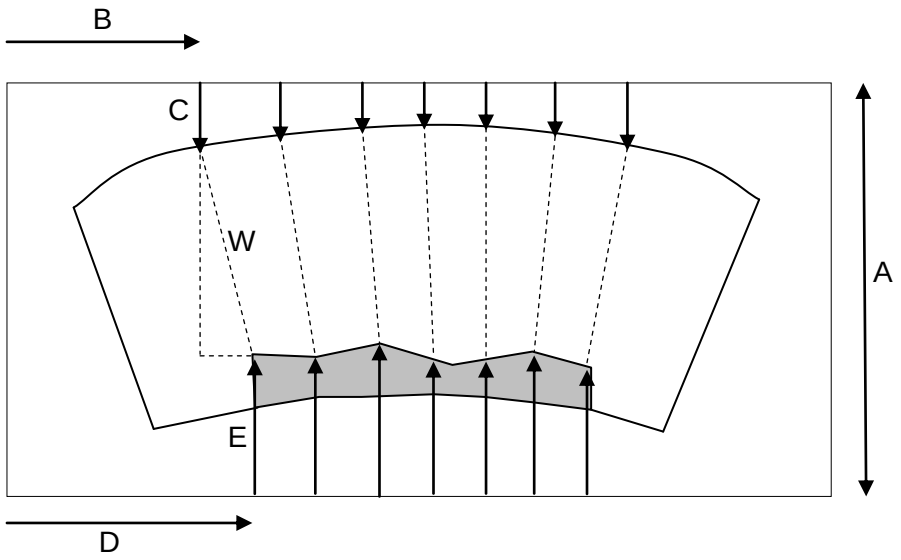

By Pythagoras, the width at each point along the damaged profile (W_i) can then be calculated from the equation,

$$W_i = \sqrt{(B_i - D_i)^2 + (A - C_i - E_i)^2} \tag{3.4}$$

Measurements are also taken at corresponding points on an undamaged vehicle to generate the undamaged width at those points. The difference between the two widths is the crush sustained by the vehicle at that point. From a series of such measurements the damage profile can then be calculated.

3.4.4 Determining the principal direction of force (PDOF)

As shown in Chapter 2, the CRASH algorithm calculates the total change in velocity and it is the direction of the user defined PDOF which determines the orientation of that impulse. The PDOF also affects the magnitude of any energy adjustment factor as discussed in Chapter 4.

In practice the PDOF in generally estimated from a visual inspection of identifiable components on the vehicle. It is rarely possible to estimate the PDOF precisely. An estimate is also made of the likely range of values the PDOF might take for a particular vehicle. By Newton's Third Law the estimates of PDOF for each vehicle then determine the orientation of the vehicles at impact since the impulse acting on one vehicle must be opposite in direction to the impulse acting on the other. It follows that the angle between the two vehicles at impact (Ψ) can be determined from the two PDOF angles (θ) as

$$\Psi = \pi - \theta_1 - \theta_2 \tag{3.5}$$

For some collisions it is possible to align the damage profiles of the two vehicles to assist in determining the angle between the vehicles at impact (Ψ). Where the PDOF on one vehicle can be estimated reasonably well, the orientation of the two vehicles can then be used to estimate the likely value for the PDOF of the other vehicle.

In a substantial number of collisions some indication of the pre-impact behaviour of the vehicles is known, such as the direction of travel. The orientation of the vehicle crush profiles to estimate the attitude of the vehicles at impact can then be used to limit the range of possible values for the PDOF on each vehicle.

In collisions where sufficient data exists to perform calculations using some other model, such as the momentum models described by Brach [**11**] and Ishikawa [**42**] an alternative estimate of the impulse angle becomes available. This can then be used to determine the PDOF values used in the CRASH model.

The requirement to estimate a PDOF in CRASH is a regarded as a major weakness by several commentators (e.g. Brach [**11**], Woolley [**132**]). It is noted however that the models of Brach and Ishikawa also require an estimate to be made to determine the orientation of the impact plane. As explained in Chapter 2, CRASH also defines an impact plane, albeit implicitly. CRASH effectively defines an impact place that is orientated perpendicular to the impulse. It is suggested that the requirement to

determine an impact plane for the models of Brach and Ishikawa inherently suffers therefore from similar problems as those involved in determining the PDOF.

Ishikawa [**42**] suggests that this plane is formed by the common surface forming the damage profile of each vehicle. A similar choice in CRASH would indicate that the impulse and therefore the PDOFs lie perpendicular to the common damage surface. Brach [**13**] also provides guidelines for choosing the orientation of the impact plane. His suggestion is to nominally define the impact plane to the mean angle between the attitude of the vehicles at impact and use a range of values to examine the uncertainty associated with this choice.

The techniques described above do allow a reasonable estimate to be made of this parameter for each vehicle. Any such estimates will inevitably be subject to error. Smith and Noga [**108**] for example suggest that the PDOF for each vehicle may be subject to a range of ±20° for different investigators. Suitable ranges of estimates should be used to determine the sensitivity of the results as discussed in Chapter 5. A method of refining an initial estimate of the PDOF to match scene data is developed in Chapter 7

3.4.5 Determining the point of application

A common factor in all the planar impact models described, is the assumption that the resultant impulse can be modelled as passing through a single point on each vehicle. A variety of techniques have been proposed to establish the location of this point. In reality the impact centre varies during the impact as demonstrated by Ishikawa [**42**]. It is difficult to accurately determine the location of the impact centre at any particular time so any technique which generates a single point can only be an approximation.

CRASH [**65**] defines the point of application as the centroid of the damaged area. Geometric methods can be used to establish the relative position of this point to the centre of mass. Brach [**9**] suggests that this point may be located by using a suitable location on the residual crush surface or along the maximum deformed surface. Ishikawa [**42**] proposes a systematic technique for determining the location of this point. However this technique requires a knowledge of the linear impulse components and angular velocity. Since these values themselves depend on the choice of the point of application, the practical utility of the technique is questionable. An analysis of the

sensitivity of the position of the point of application to the overall result is discussed in Chapter 5.

3.5 Variations in stiffness

In the CRASH algorithm, it is assumed that the face of the vehicle in question is homogeneous. The stiffness coefficients are generally designed to approximate the entire face of the vehicle. Frontal barrier crash tests most closely approximate this behaviour. In reality individual structural components will have different responses to crush forces and can be expected to distort at different rates. Side impact testing is generally performed using a vehicle sized barrier which is impacted into the centre side of the target vehicle. By design this naturally tends to miss the very stiff parts of the side of a vehicle such as the wheels and suspension. Since a considerable proportion of collisions actually do involve an impact over these areas, then it is reasonable to seek to quantify the effect. One way of performing this adjustment would be to vary the stiffness coefficients for those parts of the crush profile which include the wheels. Neptune [**81**] demonstrated a method designed to approximate more accurately the overall crush sustained by the two vehicles involved in a collision. This was achieved by adjusting the stiffness coefficients in each individual crush zone so that the force acting on each zone was matched to the corresponding zone on the other vehicle. Prasad [**91**] used a similar technique to develop a method for estimating the work done in causing crush where one vehicle was not available for measurement.

From Newton's Third Law, the impulse acting on each vehicle should be of approximately the same magnitude. This suggests that the technique proposed by Neptune [**81**] could be extended to refine the stiffness coefficients for either or both vehicles in a collision. This technique was applied by Long [**60**], Grimes *et al.* [**38**] and Chen *et al*. [**19**]. All noted an improvement in the accuracy of calculated results compared with change in velocity data.

Neptune [**82**] recognised that vehicles are not homogeneous structures and investigated the possibility of determining different sets of stiffness coefficients for impacts which did not involve full-overlap collisions. For frontal impacts he concluded that provided damage was contained within the engine compartment, partial overlap stiffness coefficients were the same as full-frontal stiffness coefficients. Where the crush extended into the passenger compartment, the he noted that a bi-linear model

was more appropriate (Neptune [**76**]). This is effectively the same conclusion as reached by Varat *et al.* [**121**].

It is also noted that vehicle design has changed over the years. This has resulted in more modern vehicles being stiffer than their older counterparts. Considerable research has been devoted into determining the most appropriate stiffness coefficients to use for more modern vehicles. Where possible it is suggested that the most appropriate coefficients are used depending on the age of the vehicle. Ideally vehicle specific coefficients should be used and can be calculated from crash tests as described earlier. Alternatively generic coefficients based on the work of Siddal & Day [**98**] or Hague [**39**] can be used. A discussion of the overall accuracy due to the potential accuracy of stiffness coefficients is developed in Chapter 5.

3.6 Summary

This Chapter has summarised the measurement of damage profiles. Measurement protocols developed over the last few decades in the UK but not covered in the original US training manuals provide a realistic and systematic method for recording most types of damage. The essential differences between the measuring protocols applied in the US and UK have been outlined.

In the next Chapter the validity of an energy adjustment factor is discussed. It is shown that the commonly used factor does not provide an adjustment which is supported by the energy loss calculated by either Brach's PIM or Ishikawa's models. An alternative adjustment factor is proposed which does provide equivalence between the various models.

Chapter 4

Calculation of Total Crush Energy

4.1 Objectives

In this Chapter the key features required to determine the total energy absorbed by the crush damage are examined. This can be achieved through the use of energy adjustment factors which transform the crush damage measurements normal to the undamaged surface into data which account for the direction of the PDOF. These data then provide an estimate of the actual energy. Note that the energy adjustment factors described in this thesis are variously known as 'correction factors' or 'magnification factors' in other texts. Existing adjustment factors are discussed and a new factor is derived which incorporates several new key features namely, the directions of the impulse and closing speed together with coefficients of restitution. This new factor has the advantage of matching the calculated factor using either of Brach's or Ishikawa's methods in simple scenarios.

4.2 Introduction

As outlined earlier, stiffness coefficients are generally derived from test collisions. In essence the assumption is made that residual crush increases linearly with increasing speed. Where impacts occur so that the impulse acts perpendicularly to the face of the vehicle, then these coefficients can be utilised directly to determine the crush energy. Measurement techniques as described in the previous Chapter are designed to measure the crush sustained perpendicularly to the face of a vehicle. As a result all

that can be determined directly is therefore the magnitude of the work done in causing crush perpendicularly to the face of the vehicle.

In collisions where the impulse acts at some angle (α) to the vehicle surface an adjustment factor is required to adjust the value for the work done and relate it to the total work done in the collision. The way in which *α* is defined is illustrated below in Figure 4.1 for an impact to the front face of a vehicle. Corresponding definitions for *α* can also be derived for the other faces of a vehicle.

Figure 4.1: Direction of impulse (PDOF) and angle to vehicle face

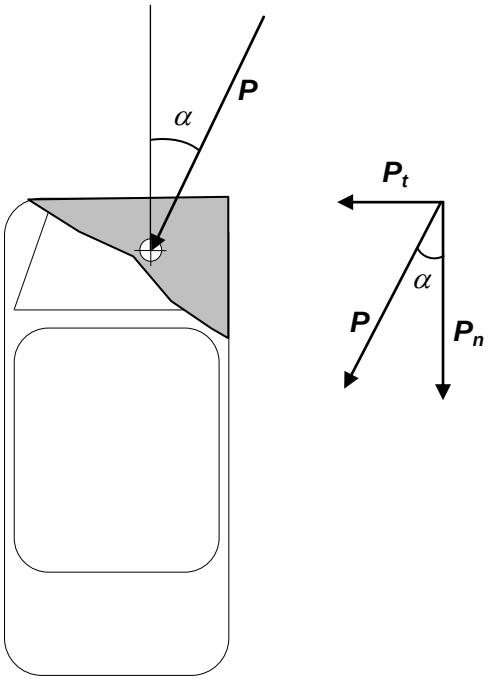

A variety of adjustment factors have been proposed to determine the total crush energy from the normal crush energy. The original adjustment factor was proposed by McHenry [**65**] to be

$$E = E_m(1+\tan^2\alpha) \tag{4.1}$$

where *E* is the actual crush energy and E_m is the crush energy perpendicular to the vehicle face obtained directly from crush measurements and stiffness coefficients. More recently McHenry [**66**] suggested an alternative adjustment factor

$$E = E_m(1+\mu_v\tan\alpha) \tag{4.2}$$

where μ_v is defined as a coefficient of friction at the vehicle to vehicle interface and is constrained so that $0.40 \leq \mu_v \leq 0.55$. Fonda [**31**] explains however that this particular adjustment factor does not follow from physical principles and instead proposes the simple adjustment factor

$$E = E_m(1/\cos\alpha)\,. \tag{4.3}$$

In 2009 Vangi [**119**] proposed another adjustment factor which requires an additional series of measurements to determine an estimate of the principal direction of deformation (PDOD). The PDOD is a measure of the force direction for each crush zone. This is applied to each crush zone to determine an energy adjustment factor

$$E = E_m[1+\tan(\alpha)\tan(PDOD)]\,. \tag{4.4}$$

This method appears to offer a significant improvement in estimating total crush energy. As outlined in a letter to the editor Brach [**5**] suggests that this improvement may simply be as a result of the improved estimation of the PDOF which results from the application of this technique. Equation (4.1) remains the standard adjustment factor used by the majority of CRASH derivative programs and is discussed in more detail in the next section.

4.3 Standard energy adjustment factor

The energy adjustment factor described by McHenry [**65**] and shown in equation (4.1) can be determined from an analysis of the impulse and the direction that impulse makes with the face of the vehicle being measured as shown in Figure 4.1. Crush measurements $\boldsymbol{C_n}$ can be made perpendicular to the vehicle face, i.e. parallel to $\boldsymbol{P_n}$ from which the force $\boldsymbol{F_n}$ can be calculated. McHenry states that the actual force and actual crush can then be given by the expressions

$$\boldsymbol{F} = \frac{\boldsymbol{F}_n}{\cos\alpha}, \qquad \boldsymbol{C} = \frac{\boldsymbol{C}_n}{\cos\alpha}\,. \tag{4.5}$$

Since work done is calculated as the dot product of force and displacement, McHenry suggests that the total energy can be calculated as

$$\begin{aligned} E_n &= \boldsymbol{F}_n \cdot \boldsymbol{C}_n \\ E = \boldsymbol{F}\cdot\boldsymbol{C} &= \frac{\boldsymbol{F}_n}{\cos\alpha}\cdot\frac{\boldsymbol{C}_n}{\cos\alpha} = \frac{E_n}{\cos^2\alpha} = E_n(1+\tan^2\alpha) \end{aligned} \tag{4.6}$$

Brach [**9**], [**11**], [**13**], [**10**], claims that McHenry's approach effectively treats energy as a vector quantity. Force and displacement are vectors which in principle can be transformed in this way for non-normal forces to calculate energy so this model does not appear to treat energy as a vector. However McHenry's approach does make the implicit assumption that vehicle stiffness coefficients are isotropic as identified by Tanny [**116**] and Vangi [**119**]. There does not appear to be any practical reason upon which to base this assumption and vehicles may well exhibit different deformation behaviour when subject to impulses with an additional tangential component to the original vehicle face.

There is also a subsidiary problem as this energy adjustment factor is unbounded in this model. At large angles of incidence the adjustment factor increases substantially. In order to compensate for this, the maximum value that this adjustment factor takes is limited to a value of 2.0 This is achieved at an angle of incidence of 45°. McHenry [**65**] suggests that the reason for this limitation is that '*the tangential frictional force component cannot grow larger than the normal force*.' Whether this claim is justified is not considered but is does provide a useful way of constraining the energy adjustment factor. In the next section an analysis is presented which outlines the principles governing the estimation of energy loss in a collision.

4.4 Energy loss in vehicle collisions

Although energy loss is a not a vector quantity, it is helpful to determine the work done by an impulse in two orthonormal directions. This is the approach adopted by Brach [**9**], [**11**], [**13**], [**10**]. A useful result first noted by Kelvin and Tait [**53**] and expanded by Stronge [**113**] enables the total work in a collision to be partitioned into normal and tangential terms. Using the subscript *i* for each term, their results states that the partial work (W_i) done on colliding bodies by the component of the reaction impulse (P_i) equals the scalar product of this component and half the sum of the initial (U_i) and final (V_i) velocities of the contact point in the direction of this impulse component i.e.

$$W_i = \frac{P_i}{2}(U_i + V_i)\,. \tag{4.7}$$

The total work is equal to the sum of the of the work done by individual terms. In a planar collision therefore the total work done can be expressed as the sum of the normal and tangential contributions so that

$$W = W_n + W_t . \tag{4.8}$$

The impulse is equal in magnitude and opposite in direction for each vehicle giving rise to separate expressions for equation (4.7). As demonstrated by Vangi [**119**], relative velocity components of the contact point can be used in equation (4.7). Equation (4.7) can then be substituted into equation (4.8) to provide the more useful equation

$$W = \frac{P_n}{2}[(U_{2n} - U_{1n}) + (V_{2n} - V_{1n})] + \frac{P_t}{2}[(U_{2t} - U_{1t}) + (V_{2t} - V_{1t})] . \tag{4.9}$$

In the absence of external forces, the work done by the impulse *W* is assumed to be the same as the loss in kinetic energy *E*. Together with the definitions of e_n and e_t as defined earlier in equation (2.14) and U_{Rn}, U_{Rt}, V_{Rn}, and V_{Rt} as defined in equation (2.15) this allows the total work done in a collision to be expressed as

$$E = \frac{P_n U_{Rn}}{2}(1 - e_n) + \frac{P_t U_{Rt}}{2}(1 - e_t) . \tag{4.10}$$

A ratio W_r relating the work performed by the normal and tangential impulse components can also be derived using the earlier definitions of μ, which is the ratio of the tangential and normal components of the impulse [equation (2.7)], and *r*, which is the ratio of the tangential and normal closing velocity components [equation (2.12)] so that

$$W_R = \frac{W_t}{W_n} = \mu r \frac{(1 - e_t)}{(1 - e_n)} . \tag{4.11}$$

It follows from equation (4.11) that the total energy lost as a result of the collision can be found from

$$E = E_n \left[1 + \mu r \frac{(1 - e_t)}{(1 - e_n)} \right] . \tag{4.12}$$

Equation (4.12) is of central importance to this analysis. It shows that the total work done by the impulse is equivalent to the work done by the normal impulse component

multiplied by an adjustment factor. This adjustment factor consists of the product of the tangent of the impulse ratio, the tangent of the ratio of the closing speed and the ratio formed by $(1-e_t)/(1-e_n)$. Note that equation (4.12) remains valid for all orientations of the axis system and the parameters μ and r change depending upon that orientation. In this analysis however the orientation with respect to each of the individual vehicle faces is required to determine the values of the parameters μ and r. For an individual vehicle, the value of μ can be defined as the tangent of the angle that the impulse makes with the face of the vehicle (i.e. angle α as defined earlier). A value for r can be defined similarly as the tangent of the angle (β) that the closing speed vector makes with the face of the vehicle. The parameter r is defined by the impact configuration and can be expressed in terms of the restitution coefficients e_n and e_t together with A, B, C and μ by solving equation (2.45) to give

$$r = \frac{(1+e_{\mathrm{t}})[B-\mu(1+C)]}{(1+e_{\mathrm{n}})(\mu B-A)}. \tag{4.13}$$

The value of the angle β may be difficult to quantify. It is noted however that α and β are angles which will have a fixed orientation for any particular collision. It follows that there will be a difference between them (angle ζ) which will remain constant for any orientation of the impact plane. The value of ζ can therefore be calculated from any arbitrary orientation of the impact plane from the values of μ and r obtained for that particular orientation such that

$$\zeta = \tan^{-1}(\mu) - \tan^{-1}(r). \tag{4.14}$$

With the substitution of $\tan(\alpha)$ for μ and ζ, equation (4.12) can then be expressed as

$$E = E_n\left[1+\tan(\alpha)\tan(\alpha-\zeta)\frac{(1-e_t)}{(1-e_n)}\right]. \tag{4.15}$$

Since equation (4.15) does not explicitly contain r it should be easier to use in practical situations. The manner in which the adjustment factor described in equations (4.12) or (4.15) can be applied to actual vehicle collisions is discussed in subsequent sections.

4.5 Application to actual collisions

4.5.1 Common post-impact velocity scenarios

To determine how equation (4.15) can be used to establish the total energy in practical situations, it is helpful to consider collisions where there is a common post-impact velocity in both the normal and tangential directions before considering more general scenarios. All the existing adjustment factors implicitly make the assumption and do not deal with the more general case. Where there is a common post-impact velocity, $e_n = e_t = 0$ so that equation (4.15) can be simplified to become

$$E = E_n\left[1+\tan(\alpha)\tan(\alpha-\zeta)\right]. \tag{4.16}$$

Note that if ζ is zero then equation (4.16) reduces to equation (4.1). To further simplify this discussion an example collision is chosen such that the measured faces of the vehicles are parallel. A suitable collision for these purposes is RICSAC test 9 as described in Smith and Noga [**109**]. The impact configuration and angles are illustrated in Figure 4.2

Figure 4.2: RICSAC 9 impact configuration

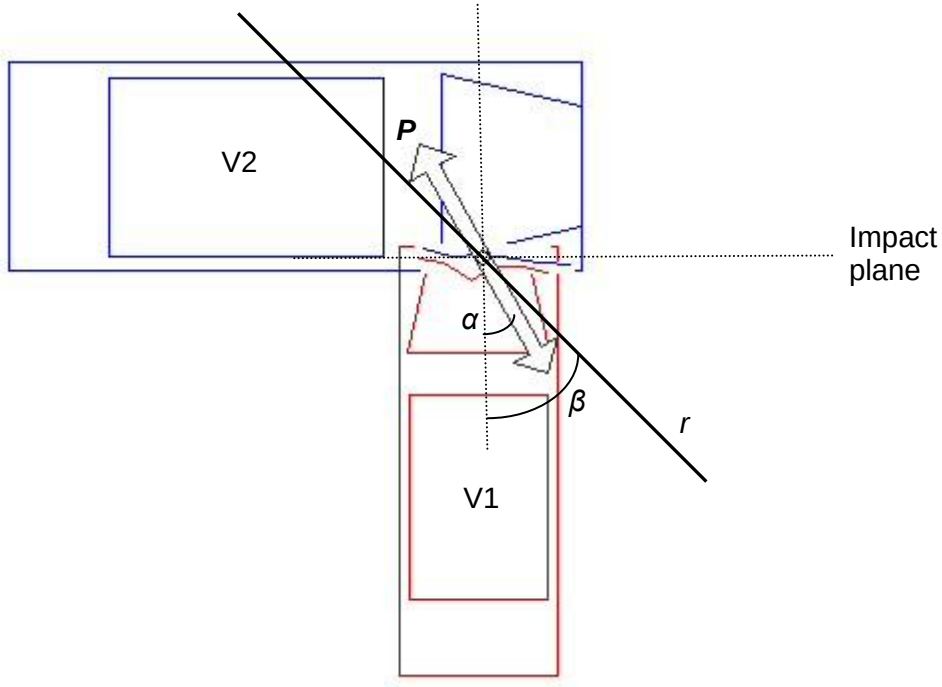

In this collision both vehicles were reported to have been travelling at the same speed at impact and collided at 90°. There was no pre-impact rotation hence the angle that the closing speed vector makes with the vehicle face is 45° for both vehicles. The impact and configuration and vehicle parameters define the values of *A*, *B* and *C* used in each of the models and, assuming a common post-impact velocity, the impulse and therefore the PDOF is found [using equation (2.45) or equation (2.11)] to be at an angle of 31.7° to the front of vehicle 1.

As previously discussed, Brach [**13**] identified that the orientation of the impact plane is immaterial whenever there is a common post-impact velocity. This means that in such collisions the impact plane can in principle be rotated so that it is aligned to either of the measured faces of the vehicle. In this collision the impact plane can be rotated so that it is parallel to the front of V1 and right hand side of V2 as shown in Figure 4.2. Once aligned the normal and tangential energy values can be calculated using either Brach's PIM or Ishikawa's PIM models and compared with the energy values calculated using the method proposed here. This provides a useful check on the correspondence of this method to the results of Brach or Ishikawa's models.

In this collision CRASH measurements and generic stiffness coefficients suggest that the work done in causing crush normal to the respective vehicle faces was 28436 J for vehicle 1 and 7867 J for vehicle 2. With the values for α and β for this impact configuration the adjustment factor is the same for each vehicle i.e. 1.6174 giving a total amount of work done in causing crush of 58716 J. This suggests a pre-impact speed of about 10.68 ms^{-1} for each vehicle. This overestimates the measured pre-impact speed of each vehicle of 9.43 ms^{-1} but matches well with the experimental energy loss of 56066 J reported for this collision by Brach [**6**]. More importantly the normal and tangential crush energies calculated using this adjustment factor are identical to the normal and tangential crush energies calculated by either Brach's or Ishikawa's models.

Also of interest is that with the recorded pre-impact speeds, the momentum only based models of Brach and Ishikawa indicate a total energy loss of 45796 J with a normal component of 28314 J. Since this figure is somewhat less than that calculated previously, this suggests that the normal crush energies calculated by CRASH using the generic stiffness coefficients may be overestimated in this case. Assuming that 28314 J is the correct value for the normal crush energy, a comparison between the various energy adjustment factors for this collision are shown in Table 4.1

Table 4.1: Comparison between various energy adjustment factors

Method	Factor	Tangential (J)	Total (J)
Brach	N/A	17482	45796
1+tan(α)tan(β)	1.6174	17482	45796
$1+\tan^2(\alpha)$	1.3811	10790	39104
$1+\mu_v \tan(\alpha)$ $\mu_v = 0.45$	1.2778	7866	36180
$1+\mu_v \tan(\alpha)$ $\mu_v = 0.55$	1.3396	9615	37929
1/cos(α)	1.1752	4961	33275

This comparison shows that for this particular collision the adjustment factor presented here is larger than the other adjustment factors. (Note: The adjustment factor proposed by Vangi [**119**] has not been considered as insufficient information exists to calculate the values of the principal direction of deformation (PDOD) for each of the crush zones.)

It is helpful to examine the effect of the adjustment factors with differing values of α and β for a collision. For any collision the angle β depends on the relative speeds of the vehicles. In RICSAC 9 both vehicles were moving forwards at impact. The angle β can in theory range between 0° indicating that vehicle 2 was stationary at impact and approach 90° indicating that V1 was almost stationary. Note that V1 cannot actually be stationary at impact otherwise no crush in the normal direction can be sustained. Values outside this range imply a negative velocity for one or other of the vehicles which can be discounted for this collision.

Assuming that the damage sustained and point of application of the impulse remain constant, the direction of the impulse (and therefore α) can be calculated from equation (2.45). Figure 4.3 shows how α varies with different values of β assuming a common post-impact velocity

Figure 4.3: Graph to show variation in *α* with *β*

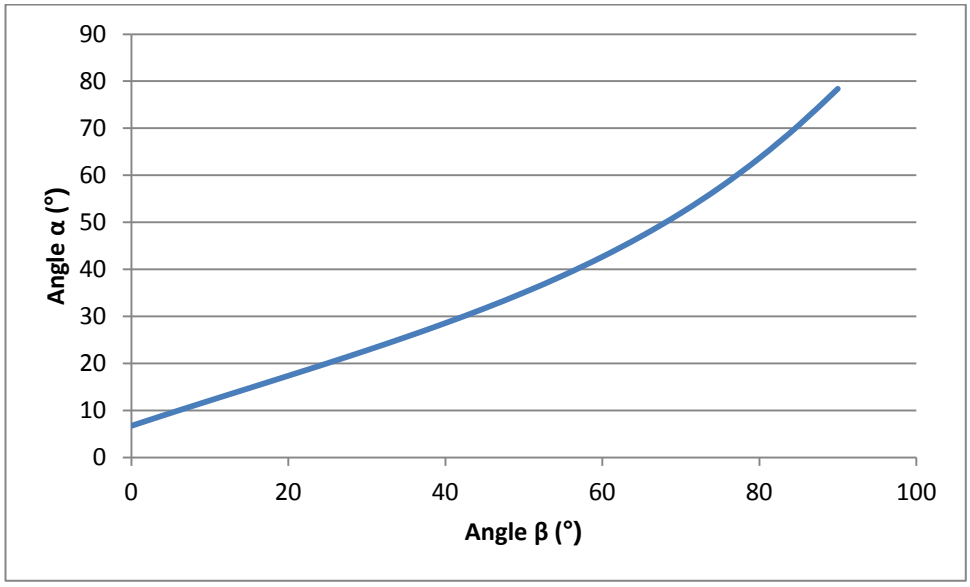

For this collision the difference between the two values is about -6.7° when *β* is zero and increases to about 11.6° when *β* is 90°. Using the values for *α* derived by these calculations a graphical comparison can be made between the various energy adjustment factors as shown in Figure 4.4

Figure 4.4: Comparison of adjustment factors

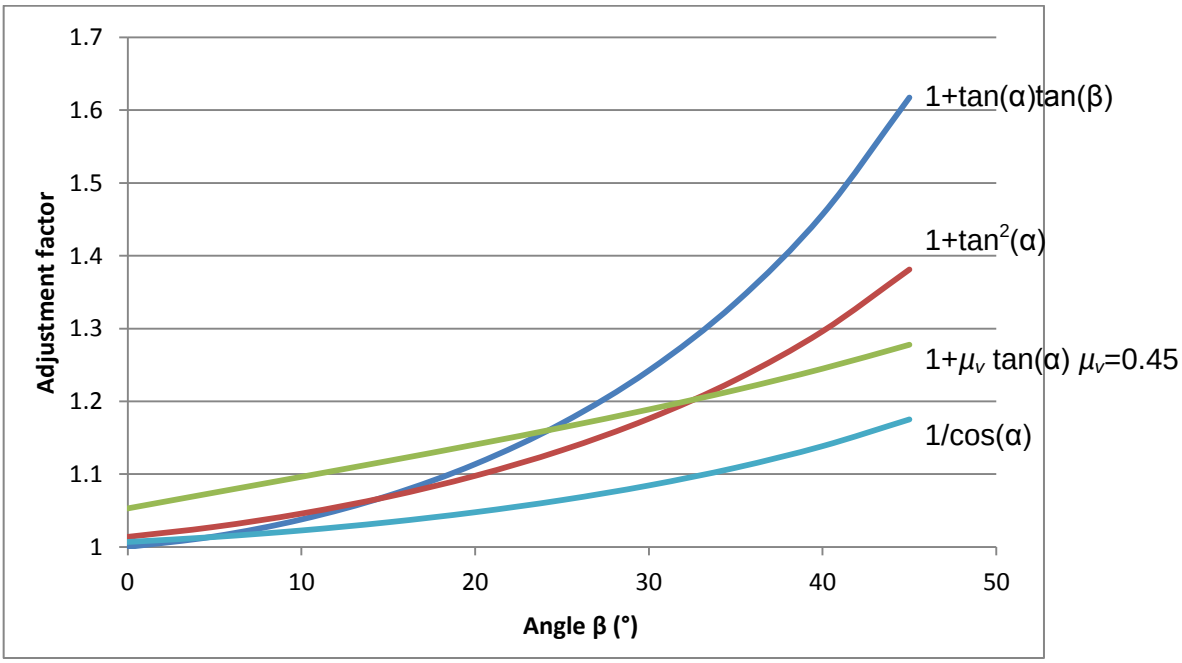

4.5.2 Tangential slip

Although the adjustment factor proposed here is lower than the standard adjustment factor for angles of β up to about 15° in this collision, above this value the adjustment factor increases more rapidly. This will of course be true whenever β is greater than α provided there is a common post-impact velocity. At high angles of incidence however there in an increased likelihood that the relative tangential velocities will not reach a common value along the contact plane resulting in slip. Any such slip will be manifested in a value for e_t such that $-1 \le e_t \le 0$. Tangential slip along the contact plane also affects the value for μ and as a consequence the value of α as shown in equation (2.45) which is reproduced below

$$\mu = \frac{(1+e_t)rA + B(1+e_n)}{(1+e_n)(1+C) + rB(1+e_t)}. \tag{4.17}$$

Since $r = \tan(\beta)$ and $\mu = \tan(\alpha)$ the relationship between e_t and α can be established from this equation for a particular value of β. The graph in Figure 4.5 shows such relationships for the RICSAC 9 collision with various values of β.

Figure 4.5: Graph showing relationship between α and e_t

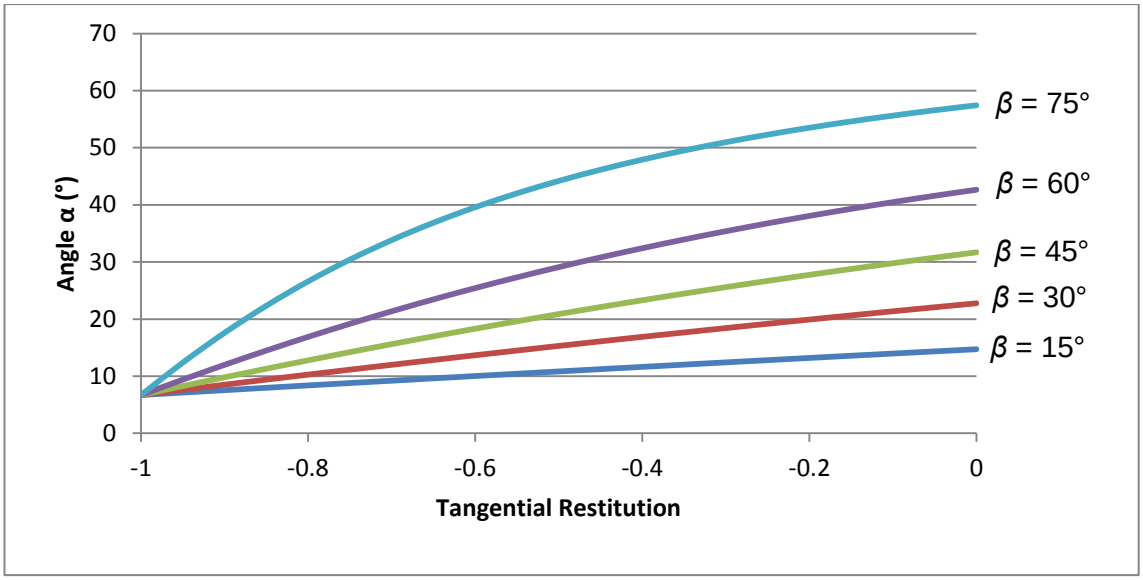

As shown in Figure 4.4 the energy adjustment factor suggested by equation (4.12) appears to be unbounded. This is only true in the theoretical case where a common

post-impact velocity is assumed. In practice the energy adjustment factor is effectively bounded by the onset of tangential slip which reduces the angle α and alters the ratio $(1-e_t)/(1-e_n)$. The overall effect of tangential slip on the adjustment factor is illustrated in Figure 4.6

Figure 4.6: Graph showing overall effect of e_t on the new adjustment factor

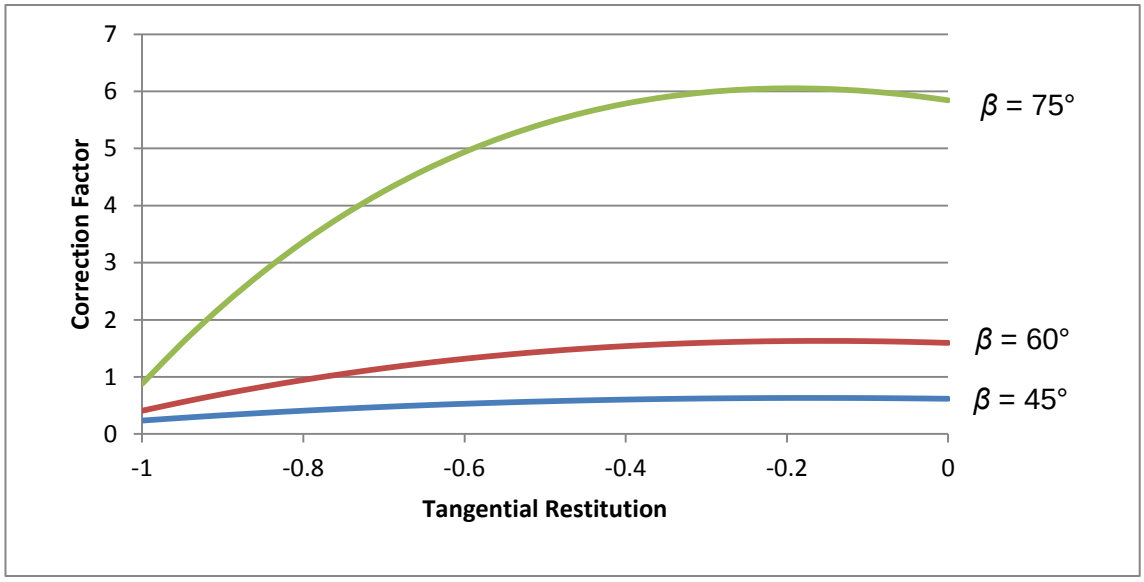

4.5.3 Collisions with stationary vehicles and barriers

It is noted that when one vehicle is stationary and in the absence of sideslip, the closing speed vector β will be zero. (Sideslip in this context is defined as the angle between the direction in which the vehicle is travelling and the direction in which it is heading.) This implies that the energy adjustment factor defined by equation (4.15) will also be zero. Suitable data with which to test this hypothesis for car to barrier collisions does not appear to exist at a sufficiently high level of precision. Since there is generally little difference between α and β any differences between the various energy adjustment factors are also likely to be small. In frontal barrier impacts this is particularly relevant since α is likely to be close to zero for such collisions. However the process for comparing results can be illustrated using the Ford Escort repeated crash tests in the NHTSA database [**83**] and analysed by Kerkhoff *et al*. [**54**]. Using these test collisions it is noted that for the first four tests the speed / crush response is linear as shown in Figure 4.7

Figure 4.7: Speed / Crush graph for US Ford Escorts

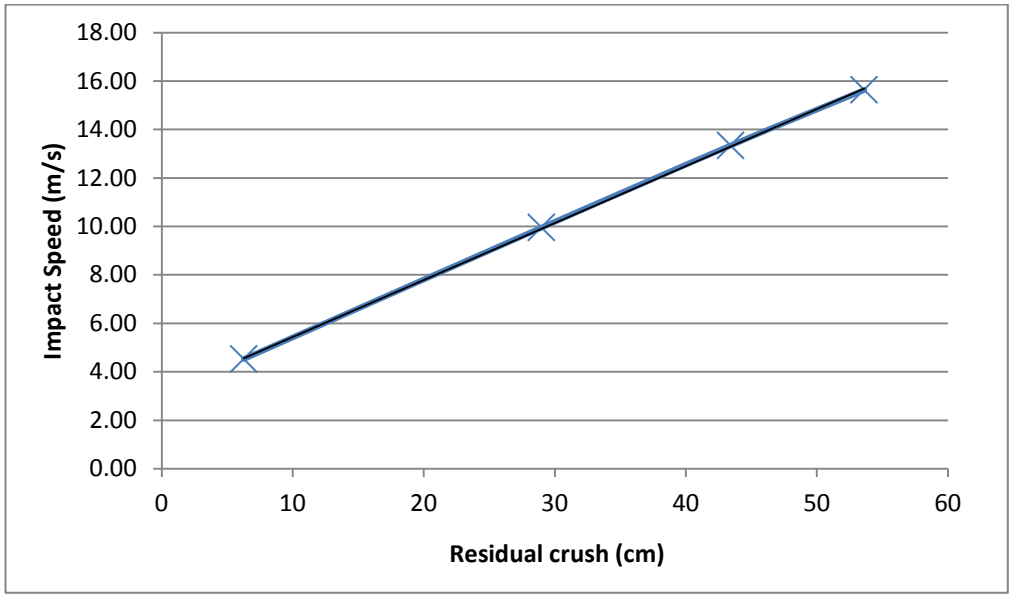

From these tests the intercept with the y-axis is 3.09 ms^{-1}. This data produces the following stiffness coefficients A = 611.3 N/cm and B = 46.2 N/cm^2. A suitable angled barrier test (Test No. 353) was found in the NHTSA database involving a US Ford Escort. In this test, the Ford Escort was guided into impact with a rigid barrier angled at 30° to the direction of travel. Using the stiffness coefficients calculated above the recorded crush measurements indicate a normal crush energy of 110.6 kJ. In this collision a small PDOF can be expected due to the impact configuration. The impact configuration and PDOF are shown in Figure 4.8

Figure 4.8: Impact configuration for NHTSA test 353

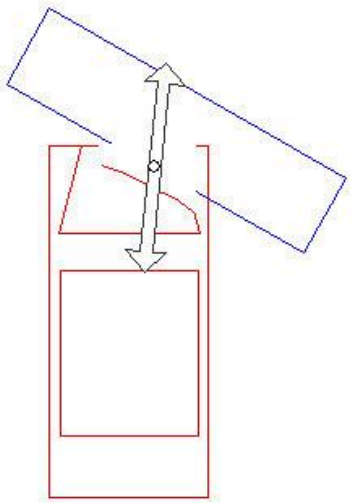

From Brach's PIM model a PDOF value of -6.8° is calculated together with a pre-impact speed for the Escort of 13.86 ms^{-1}. This underestimates the actual pre-impact speed of 15.70 ms^{-1} by 12%. It is apparent however that the recorded damage profile does not match the damage profile as shown in photographs of the vehicle post-impact. The photographs show that damage extends across the entire front of the vehicle. It seems likely that the investigators recording this collision only recorded the direct contact damage and did not record the induced damage. If such information were available it would increase the area of damage thereby increasing the total energy and increasing the calculated impact speed.

A series of angled barrier tests involving the repeated testing of a Ford Escort were also found, tests 1633, 1634 and 1635 refer. These tests comprised of a rigid mobile barrier (mass 1235 kg) colliding with the front left corner of the Escort at an angle of 21°. The results from the first test (No. 1633) show that the work done in causing crush normal to the front of the Escort was 13312 J. This indicates an initial speed for the barrier of about 6.63 ms^{-1} which overestimates the actual impact speed of 6.36 ms^{-1} by 4%. In this collision the relative closing speed lies along an angle of 21° to the front face of the Escort so β is not zero. Applying the energy adjustment factor in equation (4.12) or (4.15) adds an additional 1445 J increasing the calculated pre-impact speed to 6.98 ms^{-1} which represents an overestimate of nearly 10%.

The second test (No. 1634) showed that the work done in causing crush was 46065 J with a calculated initial speed for the barrier of 12.33 ms^{-1} (13.00 ms^{-1} after energy adjustment) The recorded initial speed was 12.57 ms^{-1} suggesting a close match. However these were a series of cumulative crash tests. As shown by Prasad [**90**] the total work done in causing crush using repeated crash tests is

$$\begin{aligned} E_1 &= \tfrac{1}{2} m v_1^2, \\ E_2 &= \tfrac{1}{2} m v_1^2 + \tfrac{1}{2} m v_2^2, \\ E_3 &= \tfrac{1}{2} m v_1^2 + \tfrac{1}{2} m v_2^2 + \tfrac{1}{2} m v_3^2. \end{aligned} \tag{4.18}$$

Equation (4.18) indicates that the equivalent impact speed for test 1634 was 14.08 ms^{-1} thus the calculated value of 13.00 ms^{-1} underestimates the equivalent impact speed by about 7%. Vehicle crush measurements are not recorded for test 1635 so this test is unsuitable for analysis. The spread of these results from this limited series of tests does not indicate whether or not the energy adjustment factor given in equation (4.12) or (4.15) is a suitable adjustment factor for real-world collisions.

Vangi [**119**] also recognised the paucity of suitable data and as an alternative used a finite element model (LS-DYNA) in order to generate validation data. This series of tests involved simulations of crash tests with rigid barriers at a range of values from 10° to 50°. Vangi [**119**] did not report the PDOF or the pre-corrected energy values used. Vangi [**120**] has subsequently provided the pre-corrected energy values he calculated for this series of simulations. These are shown in Figure 4.9 and Figure 4.10

Figure 4.9: 20 km/h simulations (Vangi 2009)

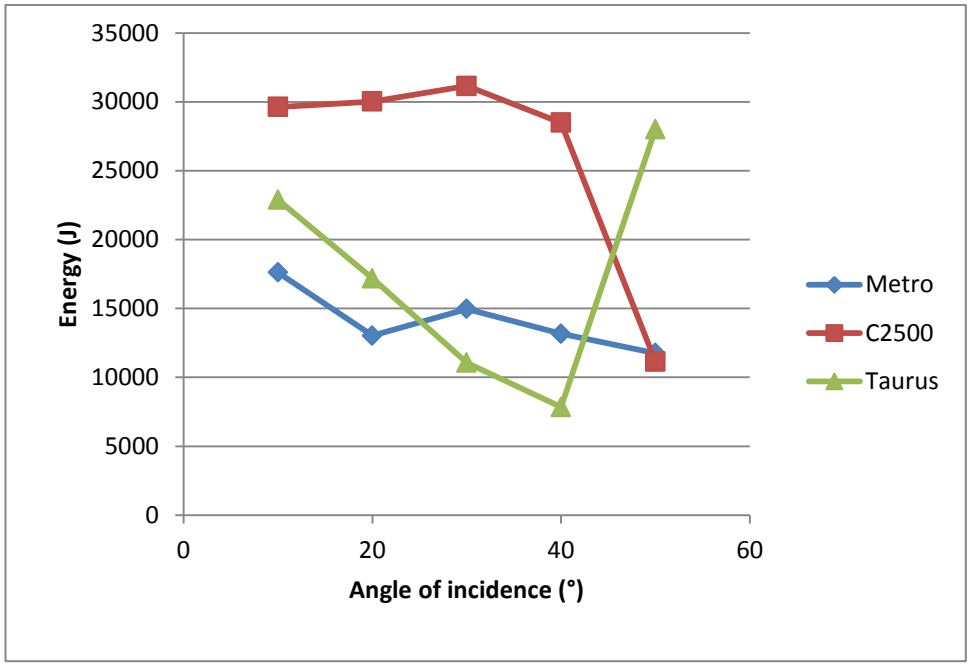

Figure 4.10: 40 km/h simulations (Vangi 2009)

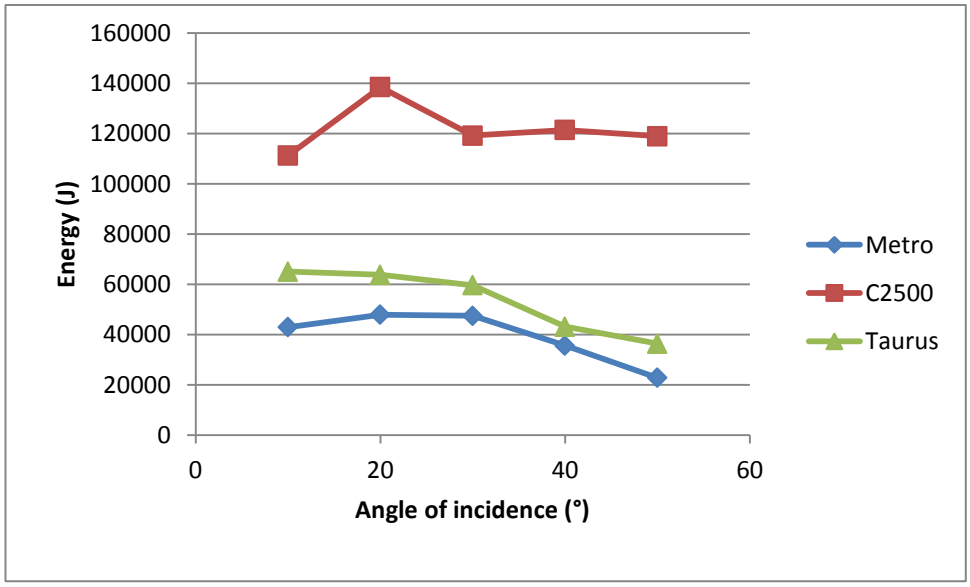

Vangi has not published the damage profiles sustained in his series of simulations. However, in a series of angled barrier tests, increasing the angle of incidence will produce increasing damage to the corner of the vehicle which is struck in the same manner as shown in Figure 4.8. This has the effect of moving the point of application of the impulse towards the struck corner. In turn this increases the total increase in rotation which can be expected as a result of the collision. It follows that although the initial kinetic energy may be the same in each collision, as consequent on using the same vehicle at the same speed, less damage will be sustained with increasing angles of incidence since some of that kinetic energy will be transferred into kinetic energy of rotation.

The results of simulations from Brach's model at 40 km/h with increasing movement of the point of application away from the centre of the vehicle are shown in Figure 4.11

Figure 4.11: 40 km/h simulations using Brach's PIM

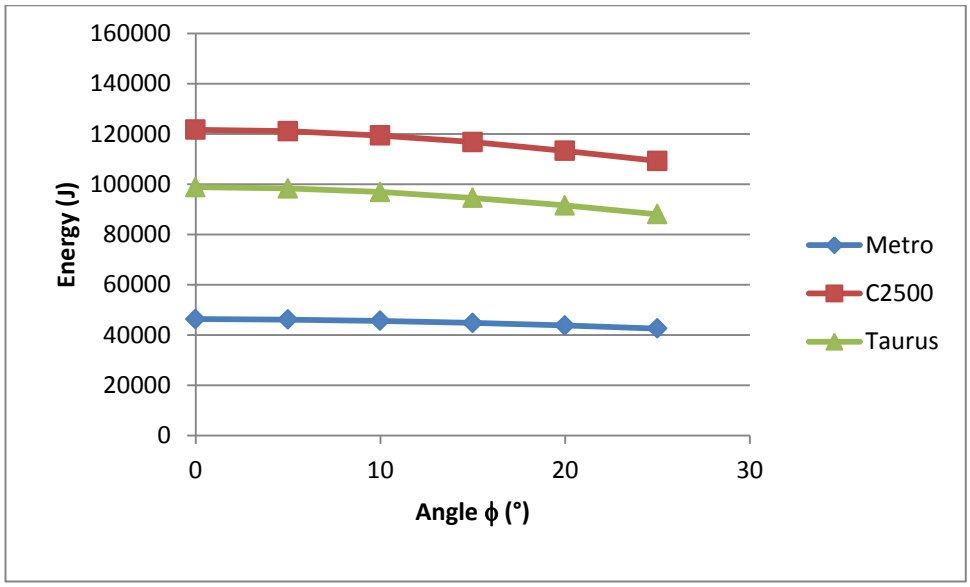

Vangi's results do appear to demonstrate this effect. However the data available is insufficient to determine the point of application of the impulse accurately for each of Vangi's simulated collisions so a direct comparison is not possible. Further work on this aspect will therefore be required in order to establish whether or not the zero adjustment factor indicated by equation (4.12) is valid in collisions with stationary objects. It is suggested that a series of barrier tests at a variety of known slip angles may assist in resolving this issue.

4.5.4 Other impact configurations

The examples used thus far have considered only collisions where an impact plane can be defined such that the values of α and β are common to both vehicles. In such collisions it has been shown that the adjustment factor defined by equation (4.12) provides energy adjustment factors and total energy loss which match those predicted using Brach's and Ishikawa's models. Neither of these models can be used to estimate the energy dissipated by each vehicle due to the component of the impulse in a particular direction; they merely provide the total loss in any particular direction.

In collisions where α and β are different for each vehicle a different adjustment factor will apply to each vehicle and neither of the momentum based models can be utilised to provide comparison data. Figure 4.12 shows a generalised collision where the impact angle (Ψ) is defined as the angle between the vehicles.

Figure 4.12: Generalised impact configuration

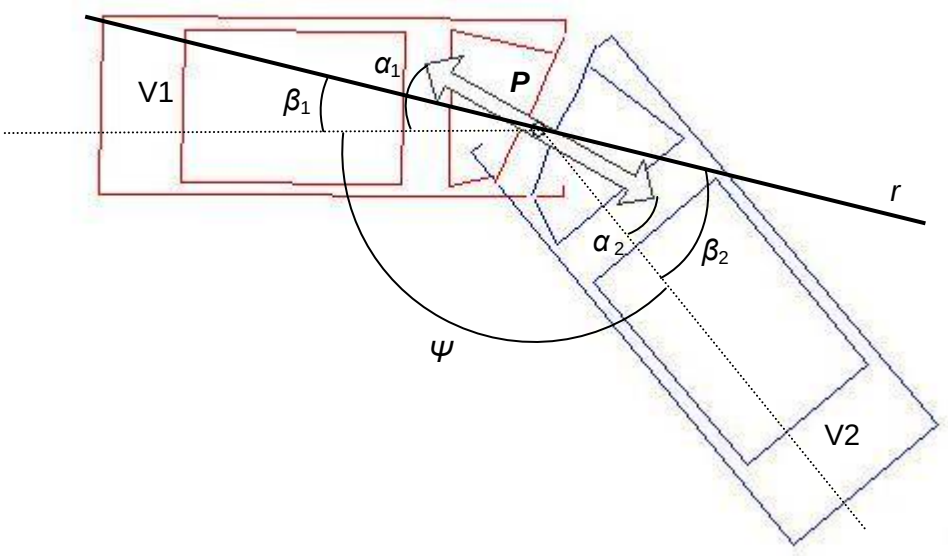

In a similar manner to the way in which the two PDOF values are related by equation (3.5), the values of α and β for each vehicle can be found from

$$\pi = \Psi + \alpha_1 + \alpha_2, \tag{4.19}$$

$$\pi = \Psi + \beta_1 + \beta_2. \tag{4.20}$$

One the corrected energy value is computed it can be entered into the CRASH equation to determine the total change in speed for each vehicle. This equation, described in Chapter 2 is repeated below

$$\Delta v_1 = \sqrt{\frac{2m_2(E_1 + E_2)(1+e_p)}{m_1(m_1\delta_2 + m_2\delta_1)(1-e_p)}}. \tag{4.21}$$

As explained in Chapter 2, the Δv obtained from equation (4.21) is the total change in velocity along the line of application of the impulse $\boldsymbol{P}$. It is apparent from equation (4.21) that although changing the values of E_1 and E_2 in this equation will affect the magnitude of Δv, altering these values has no effect on the values of δ_1 or δ_2. These are defined solely by the yaw moments of inertia and the lengths of the moment arms.

Changing the values of the work done in causing crush to each vehicle makes no difference therefore to the relative magnitudes of their closing or separation velocities. Although their absolute magnitudes will change, the directions of the velocity vectors do not. It follows that once the pre and post-impact velocity directions are defined, it is only their magnitudes which will be determined by altering the total energy work done by using any adjustment factor. What does have an effect however is restitution. In the next section the effects of restitution coefficients and how they can be related to collisions are discussed in more detail.

4.6 Restitution effects

The energy adjustment factor given in equations (4.12) and (4.15) is the product of three factors. The closing speed and impulse angles (α and β respectively) are multiplied by the third factor, consisting of the ratio $(1-e_t)/(1-e_n)$. The discussion so far has only considered collisions where a common post-impact velocity could be assumed so that this ratio could be ignored. The effect of a non-zero tangential coefficient of restitution e_t was also mentioned to show that it provides a constraint on the otherwise unbounded behaviour of the overall factor. In this section the nature of restitution coefficients are discussed along with their effect on the adjustment factor as a whole.

As shown previously, the calculation of work done in causing crush damage is related to both the impulse and the closing speed. It is helpful first to determine how these parameters can be related to each other. In Brach's PIM model [**11**] the impulse

components normal and tangential to an impact plane can be calculated from the equations

$$P_n = \frac{\bar{m}(1+e_n)U_{Rn}}{A-\mu B}, \tag{4.22}$$

$$P_t = \mu P_n = \frac{\mu\bar{m}(1+e_n)U_{Rn}}{A-\mu B}. \tag{4.23}$$

Substitution of equations (4.22) and (4.23) into equation (4.10) produces

$$E = \frac{\bar{m}(1-e_n^2)U_{Rn}^2}{2(A-\mu B)} + \frac{\mu\bar{m}(1+e_n)(1-e_t)U_{Rn}U_{Rt}}{2(A-\mu B)} \tag{4.24}$$

or alternatively

$$E = \frac{\bar{m}(1-e_n^2)U_{Rn}^2}{2(A-\mu B)} + \frac{\mu\bar{m}(1-e_t^2)U_{Rt}^2}{2[\mu(1+C)-B]}. \tag{4.25}$$

Note that in both equations (4.24) and (4.25) the first term corresponds to the energy loss from the component of the impulse normal to the impact plane and the second term to the loss of energy from the component of the impulse tangential to the impact plane.

The magnitude of the total impulse *P* can be derived from equations (4.22) and (4.23). Substitution of equation (4.10) and the definition of *r* as defined in equation (2.12) leads to an expression relating the total energy loss to the impulse

$$P = \sqrt{\frac{2E\bar{m}(1+e_n)(1+\mu^2)}{(A-\mu B)[1-e_n+\mu r(1-e_t)]}}. \tag{4.26}$$

Equation (4.26) is effectively the same as equation (2.46) derived by Brach [**9**]. However in equation (2.46) Brach uses an additional term μ_c which he defines so that μ_c is just sufficient to halt relative tangential motion during the impact. Brach defines the term μ_c in terms of the relative closing speed *r* and e_t as

$$\mu_c = r/(1+e_t). \tag{4.27}$$

Equation (4.26) provides a description of the magnitude of the total impulse in terms of the energy lost through causing crush damage. A similar expression can also be

derived using Ishikawa's impulse components. As shown in Chapter 2, equation (4.26) is equivalent to the CRASH equation [equation (2.51)] whenever μ is zero. A zero value for μ occurs when the impact plane required in Brach and Ishikawa's models is rotated so that the plane is perpendicular to the impulse thereby eliminating any tangential impulse component.

A potential problem in determining coefficients of restitution is that they are effectively defined in Brach's and Ishikawa's models relative to an impact plane. In Ishikawa's model a separate tangential coefficient of restitution is explicitly defined, whereas in Brach's model the tangential coefficient is implicitly defined through the coefficient μ_0. As already discussed, these models are generally utilised by defining a suitable impact plane and adjusting the pre-impact velocities and coefficients with that impact plane to produce some desired output scenario. Once the coefficients and pre-impact velocities are set, any rotation of the impact plane necessarily requires different values for the coefficients to maintain the same output scenario.

The energy adjustment factor defined by equation (4.12) or (4.15) requires however the effective coefficients of restitution normal and tangential to the face of the vehicle under investigation. The problem is that in order to determine these coefficients relative to the face of each vehicle, the impact plane must be rotated for each vehicle so that it is perpendicular to the original face of the vehicle. This is illustrated in Figure 4.13 where a collision is depicted together with the arrows showing the desired paths of the centres of mass.

Figure 4.13: Impact configuration and desired output

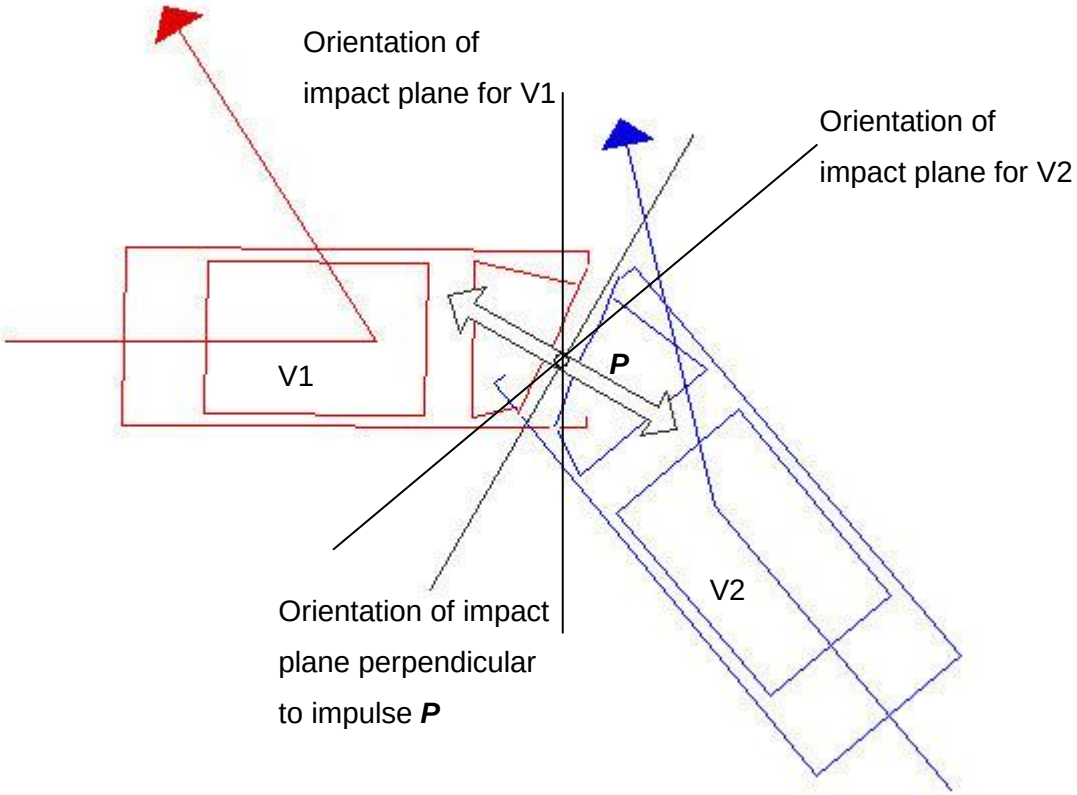

The solution to this problem requires that some method of transforming the coefficients from one orientation of the impact plane to another must be derived. As discussed in Chapter 3, Brach [**11**], [**13**] suggests that a nominal impact plane for a collision is one that is orientated so that it bisects the angle between the two vehicles at impact. Ishikawa [**42**] suggests that the impact plane should be parallel to the common damaged surface between the two vehicles. It is contended however that orientating the impact plane perpendicular to the impulse approximately satisfies both Brach's and Ishikawa's suggestions as is shown in Figure 4.13. Orientating the impact plane so that it is perpendicular to the impulse also eliminates the tangential impulse component. As a secondary benefit, this orientation ensures that any coefficient of restitution normal to the impulse is common to not only the momentum models of Brach and Ishikawa but also to CRASH. This facilitates direct comparison between the various models since with this particular orientation $e_n = e_p$.

To simplify this discussion, it is assumed further that relative motion tangential to the impulse ceases at some stage during the collision so that $e_t = 0$. In reality, this additional assumption is also likely to be true in practice, unless the collision is a

sideswipe. Brach [**10**] notes for example that in all the RICSAC series of tests relative tangential motion did cease during impact. Furthermore, Brach [**11**], [**13**] recommends that a common tangential post-impact velocity should be assumed '*unless the physical evidence strongly indicates otherwise'*. In Brach's model a common tangential velocity is assured when $\mu = \mu_0$ With the impact plane orientated so that it is perpendicular to the impulse $\mu = \mu_0 = 0$.

Some work has been done to determine ranges for [normal] coefficients of restitution likely in vehicle to vehicle collisions and a comprehensive analysis using the NHTSA crash tests [**83**] is provided by Monson and Germane [**71**]. They conclude that the closing speed is highly influential in determining the magnitude of restitution. Their results show a spread of coefficients from 0 to about 0.3 which generally decrease with increasing closing speed. They note however that sufficient data to establish firm results only exists for full frontal vehicle to barrier collisions. Their results for vehicle to vehicle impacts, angled impacts, side impacts and rear impacts are less conclusive. These results broadly mirror earlier studies by Prasad [**87**], Ishikawa [**43**], [**42**] and Kerkhoff *et al.* [**54**].

It is arguable whether the normal coefficient of restitution e_n determined from empirical data should be applicable in a direction normal to the original face of a vehicle or along the line of action of the impulse. The method developed here however allows conversion of coefficients to and from any orientation of the impact plane. Equation (4.17) can be written

$$(1+e_t) = \frac{(1+e_n)[\mu(1+C)-B]}{r(A-\mu B)}, \tag{4.28}$$

so that

$$(1-e_t) = 2 - \frac{(1+e_n)[\mu(1+C)-B]}{r(A-\mu B)}. \tag{4.29}$$

Equation (4.29) can then be substituted into equation (4.26) to eliminate e_t and then solved for e_n to yield

$$e_n = \frac{[R(1+2\mu r)-S-T]}{R+S+T}, \tag{4.30}$$

where

$$R = A - \mu B,$$
$$S = \mu^2(1+C) - \mu B, \qquad (4.31)$$
$$T = \frac{2E\bar{m}}{P^2}(1+\mu^2).$$

For any collision once *E*, the total values for the work done in causing crush and *P,* the total impulse, are established for one particular orientation of the impact plane, then these totals must apply to every orientation of the impact plane. As the impact plane is rotated about the impulse, the value of μ also changes as the proportion of normal and tangential components varies. Equation (4.30) can then be utilised to find the value of e_n for any other orientation. Once e_n has been found, the tangential coefficient of restitution e_t can be found with either of equations (4.28) or (4.26).

To demonstrate the effects of this technique, the source data from RICSAC 9 is used. In this test collision two vehicles collided at 90° as shown in Figure 4.2 For this illustration, when the impact plane is orientated perpendicular to the impulse a nominal value e_n = 0.3 is assumed. In this orientation a tangential coefficient of restitution e_t = 0 is also assumed. Figure 4.14 shows the variation of μ with different orientations of the impact plane about the impulse.

Figure 4.14: Variation in μ compared with angle of Γ from impulse

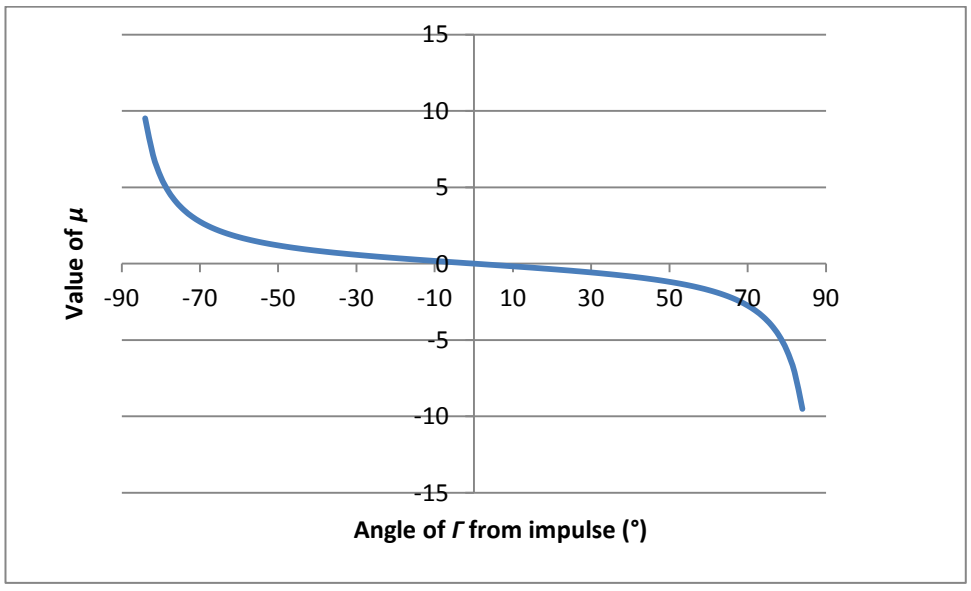

Note: Although it may be expected that the value of μ should lie between -1 and +1, it can be seen from Figure 4.14 that once the impact plane lies outside the range -45° to 45° from the direction of the impulse then the value of μ is not so bounded. Outside this range the magnitude of the tangential impulse component is greater than the magnitude of the normal impulse component which produces a value for μ greater than unity.

A zero value for μ is obtained when Γ is orientated perpendicular to the impulse. In this example this occurs at an angle of about 29.5° from the face of the vehicles. With the further assumption that the vehicles were travelling at their measured speed of 9.43 ms^{-1} the total work done in causing crush is calculated to be 41573 J and the total impulse was about 9243 kg ms^{-1}. From equations (4.30) and (4.28) the relationship between the two coefficients of restitution and the angle of Γ from the impulse is as shown in Figure 4.15

Figure 4.15: Graph to show e_n and e_t compared with angle of Γ from impulse

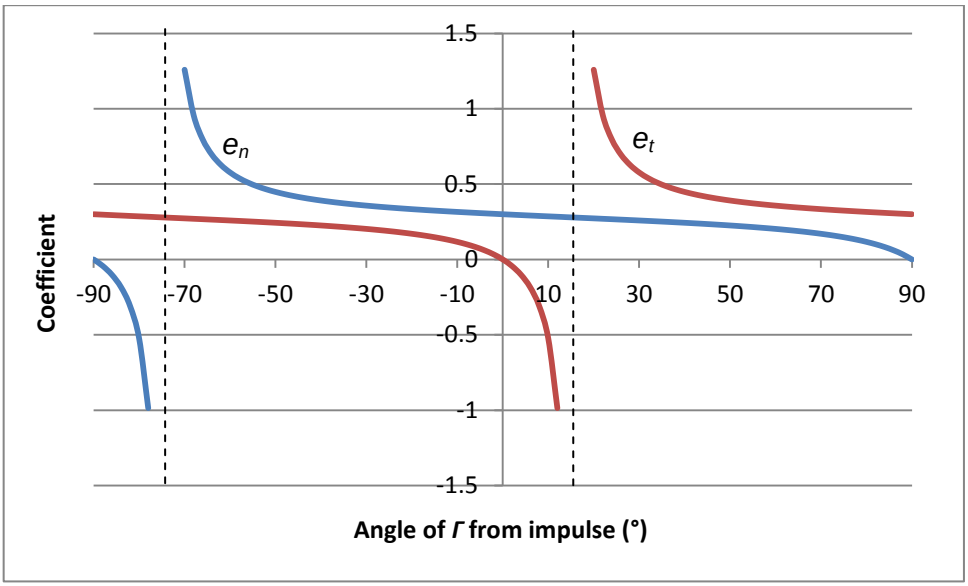

For any particular orientation of the impact plane, Figure 4.15 shows the corresponding values for the coefficients of restitution required to maintain the same total work done (E) and total impulse (P). In order to maintain the same total work done and total impulse, it can be seen that the coefficients tend towards asymptotes corresponding to orientations of the impact plane normal and parallel to closing speed vector r.

In this example nominal values of e_n = 0.3 and e_t = 0 were assumed with the impact plane orientated perpendicular to the impulse. The same technique [using equations (4.30) and (4.28)] can also be used if the values for e_n and e_t are known at some other orientation of the impact plane. For example, Brach [**6**] reports that for RICSAC test 9 he determined a normal coefficient of restitution e_n = 0.4 with an impulse ratio μ of 0.486 and that there was a common post-impact velocity tangential to the impact plane, i.e. e_t = 0. This impulse ratio corresponds to an impact plane aligned with the faces of the vehicles as shown in Figure 4.2 From this data the impulse is about 25.9° from the faces of the vehicles. Calculation shows that the effective coefficients when the impact plane is orientated to the impulse are e_n = 0.27 and e_t = -0.38 A graph to show the values of coefficients at other orientations of the impact plane is shown in Figure 4.16

Figure 4.16: Graph to show e_n and e_t with e_n = 0.4 when Γ = -25.9

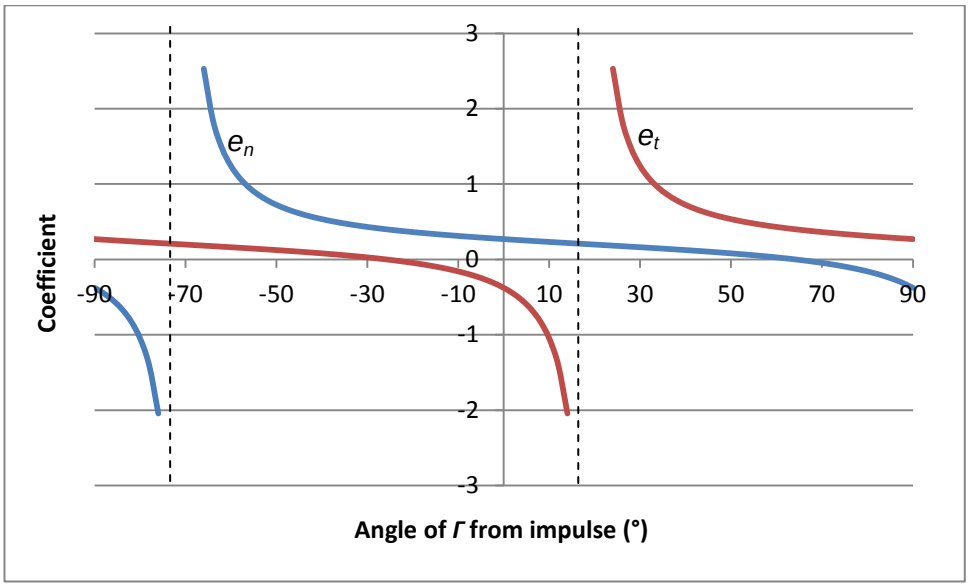

Note that since a common pre-impact speed is assumed as before together with no change to the other data, the graph in Figure 4.16 shows asymptotes in the same location as in Figure 4.15. The points where the coefficients intersect the x-axis however are displaced to the left by 25.9°. Again this shows that with arbitrary orientation of the impact plane, equations (4.30) and (4.28) can be used to determine the exact coefficients of restitution required.

4.7 Summary

In this Chapter a new method was derived to determine the energy adjustment factor applicable to each vehicle in a particular collision. It incorporates the key features which can affect adjustment factors, the direction of the impulse, the direction of the closing speed and restitution in both the normal and tangential directions. This method also has the advantage of matching the calculated factor using either of Brach's or Ishikawa's methods. In some scenarios this method provided results which correspond to practical solutions. However further work is required to determine whether this new method can be used to model all real life collisions.

The new energy adjustment factor described in this Chapter has the disadvantage of requiring knowledge about the direction of the closing velocity of the two vehicles. This appears to preclude its utility in scenarios where there is no scene data from which to determine the angle between the vehicles' closing speeds. However a technique is developed in Chapter 7 which addresses this shortcoming. In that Chapter it is shown how the pre- and post-impact velocities may be determined for the majority of vehicle to vehicle collisions from an analysis of their changes in velocity. As outlined above, once the direction of the closing velocity vector is established, the adjustment factor only affects the magnitude of the two values for crush energy. This suggests a two stage process, the first stage using arbitrary values for E_1 and E_2 simply to establish the angle of the closing velocity vector and a second stage where the adjusted values for E_1 and E_2 are used to determine the magnitude of the respective vehicles' velocities.

An analysis of the potential accuracy of this new energy adjustment factor is described in Chapter 7 once a technique is available from which to determine the closing speed angle. Before describing the development of that new technique however, the next Chapters examine and discuss the potential accuracy of the CRASH model.

Chapter 5

Accuracy of the CRASH Model

5.1 Objectives

In this Chapter the potential accuracy of the various impact models is examined and compared with previously published work. Major sources of error are identified and their likely magnitudes are estimated to provide an estimate of the overall accuracy which can be expected from the impact models.

5.2 Introduction

Three impact models are considered in detail by this thesis, the planar impact mechanics model by Brach [**11**], a similar model by Ishikawa [**43**] and the CRASH model described by McHenry [**65**]. As shown previously Brach's and Ishikawa's models are equivalent and produce identical results with identical input data. The CRASH model can also produce identical results provided the impact plane required in the Brach and Ishikawa models is orientated so that it is perpendicular to the impulse as demonstrated in Chapter 2.

The models by Brach and Ishikawa are essentially forward iteration models and require an estimate of the initial velocities in order to determine the post impact velocities and Δv as the output. CRASH provides Δv directly as an output from an estimate of the work done in causing crush to each vehicle. Provided that a realistic estimate of the work done in causing crush (crush energy) is available, then a reasonable estimate of Δv can be obtained. The estimate of work done in causing crush can be obtained after

the event using techniques developed in Chapter 3 and Chapter 4. CRASH therefore has a potential advantage over the other models in that it does not require any knowledge of the post-impact conditions upon which to base initial estimates of the impact speed. However, estimates of crush energy are not precise and are subject to error.

An obvious way of calibrating all the models is to compare the output of the models with known data. Both Brach [**11**], [**7**], [**9**], [**10**], [**12**], [**13**] and Ishikawa [**43**], [**42**], [**41**] provide comparisons in their works to full scale crash tests. Brach has also performed several comparison tests between his model and CRASH. These comparisons have however tended mainly to highlight differences between Brach's model and CRASH. As shown in Chapter 4, Brach's comparisons do not necessarily match the orientations of the impact plane required to directly compare the results using his model with those generated by CRASH. In particular Brach does not allow CRASH to utilise coefficients of restitution. Without restitution a direct comparison between these models cannot be entirely valid. Although the original formulation of CRASH does not incorporate such coefficients, Smith [**105**] shows that it is possible to incorporate restitution into the CRASH model. In this Chapter Brach's results are re-analysed to provide a more realistic comparison between the models.

Several others have also provided comparisons between real-world collisions and the CRASH model in an effort to demonstrate the overall accuracy. One notable paper concerning the accuracy of CRASH was provided in 1982 by Smith and Noga [**108**]. Lenard *et al*. [**56**], [**57**] discuss the potential accuracy of CRASH in vehicle collisions. A similar earlier study by Jennings and Jones [**48**] investigated whether CRASH was suitable for use with European vehicles. Little work has been performed however into determining the theoretical accuracy of CRASH compared with other models. This Chapter also provides an analysis to determine the theoretical accuracy which can be expected from CRASH. Before describing the theoretical accuracy however, the next section examines the results of empirical studies.

5.3 Empirical Studies

The majority of existing studies investigate the accuracy of CRASH when compared to actual vehicle to vehicle (VTV) or vehicle to barrier (VTB) collisions. Due to the inherent problems in determining actual Δv values for real-world collisions these

studies are all based on the results of instrumented test collisions. For convenience these comparisons are separated into two groups. UK based studies by Jennings and Jones [**48**] and Lenard *et al*. [**56**], [**57**] and US based studies by Smith and Noga [**107**] Brach [**6**], Ishikawa [**42**] and Day and Hargens [**25**]. Particular attention is paid to the well known RICSAC series of crash tests summarised by Jones and Baum [**51**].

5.3.1 UK Based studies

The study by Jennings and Jones [**48**] was designed primarily to determine whether or not the version of CRASH in use at that time (CRASH2) was suitable for use with European vehicles. CRASH was developed originally in the USA as an algorithm to determine Δ*v* and the stiffness coefficients were determined solely using American vehicles which potentially could be significantly different to European vehicles. The accident environment was also considered to be significantly different to that in the USA and the majority of the paper is devoted to analysing differences between the two environments. A total of 200 cases were considered of which 100 were considered suitable for analysis using CRASH. The remainder were mainly rejected for analysis as they were thought to violate one or more of the CRASH assumptions listed by McHenry [**65**] and described in Chapter 2.

As part of the study Jennings and Jones updated the stiffness coefficients to match more accurately the threshold damage level for European vehicles developed from a series of crash tests. They noted that in all but five collisions the estimated Δ*v* was within ±10 mph of the actual Δ*v* compared with 13 collisions falling outside this range using the CRASH2 default stiffness coefficients.

The study by Lenard *et al*. [**56**] analysed 26 front and 26 side barrier tests performed under EuroNCAP between 1996 and 1998. The Δ*v* values were determined using CRASH3 and default stiffness coefficients. They determined that without using custom vehicle stiffness coefficients in frontal VTB collisions the Δ*v* was systematically underestimated by about 7 kmh^{-1} with a range of about ±10 kmh^{-1} for CRASH results. For side impacts they concluded that CRASH underestimated by 1 kmh^{-1} with a range of about ±5 kmh^{-1}. Of note is that in this study the energy absorbed by deformable barriers was also analysed and incorporated into the calculations. Comparative tests excluding the work done in causing crush to the barriers was not provided. However the mean value for work done in causing crush to the barriers was estimated to be about 30% in the EuroNCAP tests which were considered.

Lenard *et al*. [**57**] update their earlier work to provide a comparison with a total of 137 test collisions involving VTV and VTB (rigid and deformable) crash tests. The results from these test collisions are summarised in Table 5.1

Table 5.1: Statistical properties of CRASH3 results (Lenard *et al.* 2000)

		Absolute Error (km/h) $\Delta V_{crash} - \Delta V_{test}$		**Relative Error (%)** $(\Delta V_{crash} - \Delta v_{test}) / \Delta V_{test}$	
Impact Type	**No. of vehicles**	**Mean**	**Standard deviation**	**Mean**	**Standard deviation**
Front	91	-5	9	-9	17
Car to car	22	+2	7	+5	13
Rigid barrier	25	-10	11	-21	19
Deformable barrier	44	-5	7	-8	12
Side	44	-2	3	-9	12
Rigid barrier	5	-6	N/A	-27	N/A
Deformable barrier	39	-1	2	-6	9
Rear					
Rigid barrier	2	-4	N/A	-19	N/A
TOTAL	137	-4	8	-19	15

Lenard *et al*. concluded that the default stiffness coefficients in CRASH3 are sufficiently well suited for modern European cars for statistical studies but make the point that for individual collisions custom stiffness coefficients may be desirable. These results show that for frontal impacts CRASH appears to underestimate Δ*v* for rigid and deformable barrier impacts but overestimate Δ*v* in car to car impacts. In side and rear impacts CRASH can underestimate Δ*v* significantly. They call for further research to collate vehicle crush data from crash tests. Insufficient detail is provided to further analyse their results.

5.3.2 US based studies

The first comprehensive study into the accuracy of CRASH appears to be that performed by Smith and Noga [**107**] in 1982 This was later summarised the same year as an SAE paper by the same authors [**108**]. Staged collisions using 53 American vehicles and 29 using European vehicles were examined using the default coefficients in CRASH3. They determined that for low changes in velocity in the range 10 – 15 mph (16 – 24 kmh^{-1}) the mean calculated value of Δv was accurate to ±17.8%. For higher changes in velocity in the range 25 – 30 mph (40 – 48 kmh^{-1}) the mean calculated value of Δv was accurate to ±14%. Both these figures are for a 95% level of confidence and weighted according to their assumed frequency of occurrence based on the US towaway accident population.

The version of CRASH used by Smith and Noga did not have the facility to incorporate restitution effects and in [**107**] they note that this may have had an adverse effect on the results, particularly at lower speeds. Smith and Noga also utilised the standard energy adjustment factor as described in Chapter 4. They observed that although CRASH generally tended to underestimate the total Δv, for oblique side impacts CRASH overestimated Δv. Smith and Noga attribute this to the adjustment factor. They found that in each of these cases the angle of incidence of the impulse to the original face of the vehicle was 45° or greater resulting in a large adjustment factor greater or equal to 2. They suggest that the simple model describing the standard adjustment factor may not be appropriate to higher angles of incidence.

Smith and Noga also investigated the probable limits on ranges for input (measurement) data. The ranges on the input data were estimated by comparing the results obtained from 34 pairs of measurements. One set of measurements were obtained by skilled team of investigators who attended the scene and the other set were obtained by a single person with limited training who measured the vehicles after they had been removed from the scene. For this comparison the skilled 2-person team measurements were taken to be the ‘true’ values and the lesser skilled single person’s results were taken to be the ‘field’ measurements.

It should be noted that although this study appears somewhat crude, it is the only such study that appears to have been recorded. On the basis of this investigation, Smith and Noga determined the confidence levels on individual measurements that could be expected. Their results are shown in Table 5.2

Table 5.2: 95% confidence levels for measurements (Smith & Noga 1982)

Measurement	Mean error	Standard deviation	95% confidence limits
Weight (lbs)	24	65	±130
$C_1 - C_6$ (inches)	0.3	1.5	±3.0
Offset D (inches)	-0.1	1.8	±3.6
Damage length L (inches)	-0.5	3.0	±6.0
PDOF (degrees)	N/A	N/A	±20[1]

[1]The PDOF measurements are based on 10° increments

Smith and Noga's study also examined to some extent the theoretical accuracy of the CRASH model. For this part they used a simplified version of the CRASH equation described in equation (2.24). Excluding restitution, equation (2.24) can be written as

$$\Delta v_1 = \sqrt{\frac{2\gamma_1(E_1 + E_2)}{m_1\left(1 + \frac{\gamma_1 m_1}{\gamma_2 m_2}\right)}}\,. \tag{5.1}$$

Assuming that the parameters in this equation are independent of each other it is possible to use standard error propagation theory to determine an approximation to likely error in the result. A similar technique is utilised in the next section where it is discussed in more detail. Smith and Noga made the further assumptions that six crush measurements were obtained in each case and that the standard energy adjustment factor was used. With these assumptions they determined that with the 95% confidence limits shown in Table 5.2, the overall uncertainty in Δv for individual collisions resulting from measurement error was between 9 and 25%. The greatest source of error was found to be in the estimation of the PDOF. Uncertainty in this variable alone accounted for about 4 times as much error in the final result as the other factors. They further calculated that a 10% uncertainty in the *A* and *B* stiffness coefficients produced errors of approximately 2 to 5% in Δv.

Woolley *et al*. [**132**] also analysed data presented by Smith and Noga using the CRASH3 coefficients. They point out that individual Δv values could be in error by as much as ±40%. As a result of this and an incorrect analysis of the theory underpinning CRASH they concluded that CRASH does not produce accurate results and instead proposed the IMPAC model [**130**]. (Note: The IMPAC model is essentially a

conservation of momentum model, similar to those described herein but with the assumption of a common post-impact velocity i.e. $e_n = e_t = 0$)

5.3.3 RICSAC tests

In this section the data from the well known RICSAC (Research Input for Computer Simulation of Automobile Collisions) tests series is discussed. The data has been used for several comparative studies. More pertinently for this research the RICSAC tests include crush measurement data for each vehicle. The RICSAC series comprises twelve tests, each involving a collision between full size US vehicles travelling at known speeds. The data is summarised by Jones and Baum [**51**] from several volumes of a US DOT report by Shoemaker [**96**], [**97**] and Jones and Baum [**52**].

Data from the tests is spread over a number of publications and there are discrepancies between the data reported in different sources, e.g. Smith and Noga [**109**] and Brach [**6**]. In addition, the actual changes in velocity (Δv) as initially reported were found to be incorrect due to a failure to adjust the velocities to account for accelerometer positions located remotely to the centre of mass. This has provoked considerable discussion in the literature. These errors have since been corrected independently by Brach and Smith [**12**] and McHenry and McHenry [**69**] with slightly different results as shown in Table 5.3.

Table 5.3: Comparison between uncorrected and corrected Δv (speeds in ms^{-1})

RICSAC test No.	Untransformed [51]		Brach & Smith [12]		McHenry & McHenry [69]	
	V1	V2	V1	V2	V1	V2
1	5.45	6.93	5.27	6.62	5.50	7.55
3	4.25	7.06	4.20	6.88	4.25	7.06
4	8.36	10.01	8.31	9.66	8.36	9.92
5	7.29	11.22	7.06	11.13	7.24	11.40
6	4.02	5.36	4.11	6.53	4.07	6.39
7	5.36	7.38	5.36	8.81	5.36	8.85
8	6.84	4.83	6.97	4.78	6.66	4.92
9	9.57	3.98	8.72	3.84	8.90	3.67
10	15.69	6.30	12.83	5.86	15.20	5.59
11	10.73	7.02	11.18	7.20	10.95	7.02
12	17.92	11.80	18.77	11.26	18.24	11.93

Data from test 2 is omitted as there was a failure of the accelerometers during this test and no data was recorded. The majority of the transformed changes in velocity are within 5% of the untransformed values, although there are some exceptions, such as in tests 6, 9 and 10. The differences between the two sets of corrections indicates that the RICSAC data requires some interpretation to obtain usable results.

The Δ*v* values for a damage-only analysis of the RICSAC series of tests have been recalculated for this research using the RICSAC sample data provided with the EDCRASH [**26**] implementation of the CRASH algorithm. This is the same data set as used by Day and Hargens [**22**] and [**25**] in their validation of the EDCRASH computer program. The measurements used and other source data corresponds well with the original measurements recorded by Jones and Baum [**51**]. The crush analysis results obtained for the damage-only analyses are shown in Appendix E with the source data shown in Appendix D. The results in Appendix E were generated using AiDamage [**74**]. These results have been compared with results from Brach's model as shown in Table 5.4 and are summarised graphically in Figure 5.1 below. In this comparison the measured Δ*v* and Brach Δ*v* PIM results are both taken from Brach and Smith [**12**] using corrected accelerometer data.

Table 5.4: Comparative Δ*v* results PIM and raw CRASH (Speeds in ms^{-1})

RICSAC test No.	Corrected Speeds Brach & Smith [12]		PIM Results [12]		Raw CRASH	
	V1	V2	V1	V2	V1	V2
1	5.27	6.62	4.61	6.90	6.20	9.30
3	4.20	6.88	3.50	5.54	2.79	4.43
4	8.31	9.66	6.45	10.06	7.05	11.00
5	7.06	11.13	6.00	10.90	6.89	12.54
6	4.11	6.53	4.62	7.57	6.97	11.44
7	5.36	8.81	6.76	9.58	8.84	19.25
8	6.97	4.78	5.23	4.97	4.84	4.60
9	8.72	3.84	6.85	3.15	6.32	2.91
10	12.83	5.86	11.02	5.39	7.08	3.46
11	11.18	7.20	10.91	6.84	9.33	5.85
12	18.77	11.26	16.17	11.21	11.74	8.15

Figure 5.1: Graph to show comparative Δ*v* results (Speeds in ms^{-1})

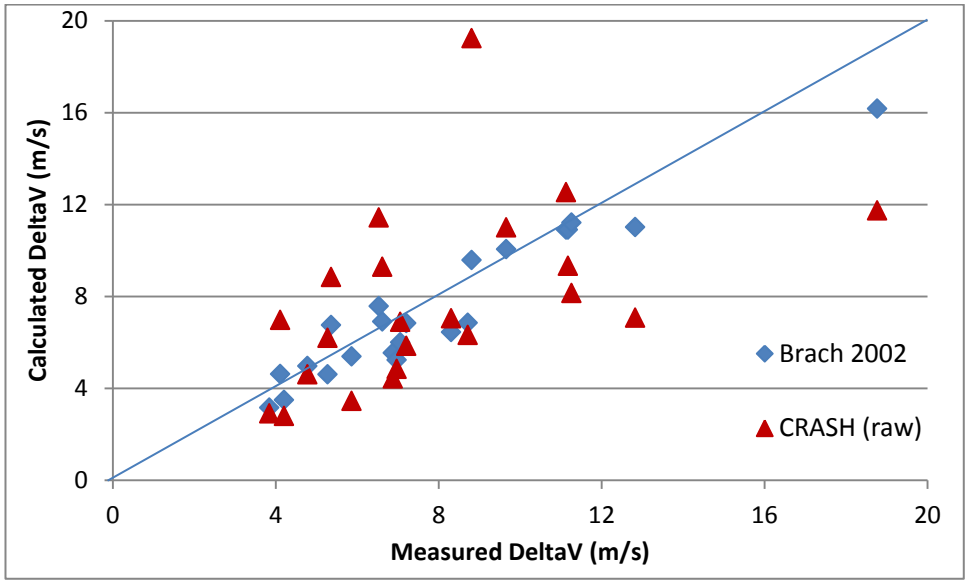

The results from this comparison show a much wider spread of results for the CRASH algorithm than for Brach's model. Brach's model shows a mean underestimate from the actual change in velocity of 5% with a standard deviation of 14% whereas CRASH overestimates with a mean error of 2% with a large standard deviation of 45%.

It is helpful at this stage to discuss some of the other comparisons which have been made with CRASH. Day and Hargens [**25**] also produced a table of results for their validation of their EDCRASH program. Their results show some variation in the calculated values of Δ*v* to those calculated here and shown in Figure 5.1, particularly in tests 6, 9, 10 and 12 where differences of over 2 ms^{-1} are apparent. Since the vehicle data, crush data and stiffness coefficients used by Day and Hargens are identical to those used in this analysis, this is somewhat surprising. Day and Hargens perform two series of analyses, one without trajectory simulations and the other with such simulations. (Note: The trajectory simulation model used by some implementations of CRASH is an analysis of the post-impact motion of the vehicle to derive the post-impact velocities of each vehicle.)

Although it is unclear from their text, it appears that their quoted results are not based on the calculation of Δ*v* from crush damage analyses, but instead are based upon the determination of pre-impact velocity and Δ*v* using the conservation of linear momentum as outlined by equations (2.1) and (2.2). Day and Hargens do not appear to record the 'Damage Only' Δ*v* results of their EDCRASH program runs. As such, the EDCRASH

validation performed by Day and Hargens can only be considered as a validation of the momentum only and trajectory simulation models contained within EDCRASH. The EDCRASH study does not validate the damage part of the CRASH algorithm.

Brach also performed earlier analyses of the RICSAC tests in 1991 [**8**] and 1998 [**10**] which show different results for his planar impact mechanics model. The reasons for the differences between each of Brach's results appear to be due the optimisation process used on each occasion and that early versions of the PIM model used a slightly different formulation. In each it appears that the same initial velocities were used and the e and μ parameters adjusted to obtain a close match to some desired output. For example in the 1991 series, Brach optimised the tests to minimise the differences from the calculations to the post-impact velocities. In the 1998 series, the optimisation process used (if any) is not specified. In the 2002 series, Brach and Smith state that the results were optimised to match a "*weighted combination of DeltaV and energy loss"*. They further state that that the best fit with this optimisation in all cases was for the common velocity conditions i.e. $e = 0$ and $\mu = \mu_0$ A comparison between the three analyses of the RICSAC data performed by Brach is shown in Table 5.5 and summarised graphically in Figure 5.2

Table 5.5: Comparison between Brach's RICSAC results (Speeds in ms^{-1})

RICSAC test No.	**1991 Results** [**8**]		**1998 Results** [**10**]		**2002 Results** [**12**]	
	V1	**V2**	**V1**	**V2**	**V1**	**V2**
1	4.91	7.38	4.60	6.92	4.61	6.90
3	4.30	6.83	4.27	6.77	3.50	5.54
4	6.83	10.64	6.74	10.52	6.45	10.06
5	6.25	11.37	6.22	11.49	6.00	10.90
6	4.48	7.35	4.63	7.56	4.62	7.57
7	6.22	8.81	6.77	9.57	6.76	9.58
8	5.88	5.61	5.58	5.30	5.23	4.97
9	9.75	4.48	8.78	4.05	6.85	3.15
10	15.73	7.68	13.96	6.83	11.02	5.39
11	11.16	6.98	10.88	6.83	10.91	6.84
12	18.07	12.62	17.77	12.31	16.17	11.21

Figure 5.2: Graphical comparison of Brach's RICSAC results (Speeds in ms^{-1})

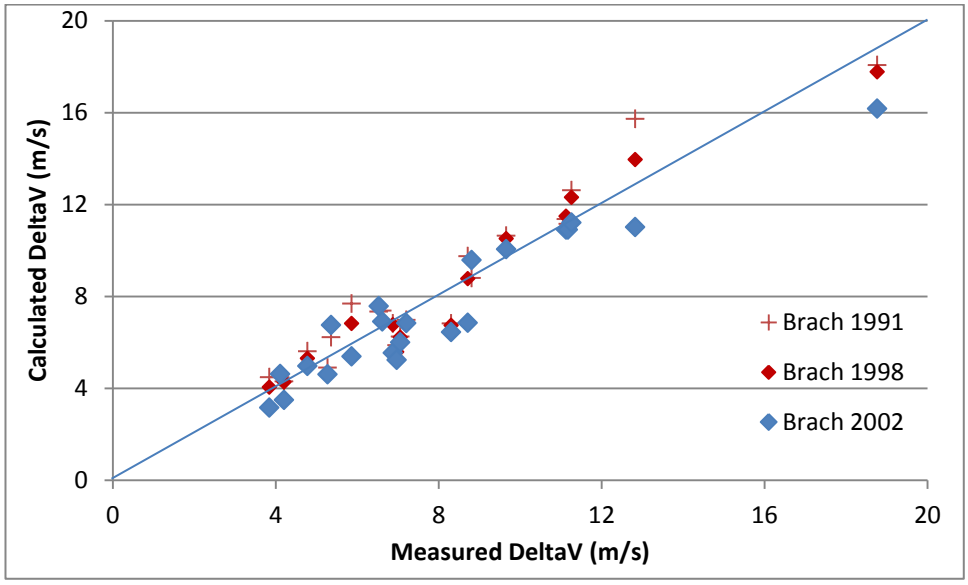

Although differences exist between Brach's three analyses, the difference between his calculated results and those measured from for the accelerometers are similar. There remain discrepancies with the CRASH results which further explanation and this forms the basis of the next section.

5.3.4 Errors in crush data measurements

Potential problems with the crush measurements in the RICSAC data are discussed in this section together with methods which can be used to compensate for such errors. A study of the photographs of the damaged vehicles in the RICSAC tests indicates that vehicle crush measurements were not necessarily obtained at the correct height. For example, side impacts crush measurements appear in some instances to have been taken at the height of maximum intrusion rather than along sill level as described in Chapter 3. This is confirmed by Smith and Noga [**109**] who state that damage profiles were measured at the level of maximum intrusion. This has resulted in a significant overestimate to the damage sustained by some vehicles and a consequent increase in the calculated crush energy absorbed by those vehicles. In other collisions the reported damage length *L* or offset *D* are clearly incorrect when compared with photographs.

Also, and as identified by Smith and Noga [**108**], the estimation of the PDOF values applicable to each vehicle are somewhat subjective and prone to error. The CRASH results shown in Figure 5.1 and Appendix D are based on the original PDOF estimates. In general, by Newton's Third Law, the force acting on one vehicle should be equal in magnitude to the force acting on the other vehicle. The force required to cause damage to each vehicle can be calculated and a comparison between those forces used to estimate the validity of the analysis. Any errors in the measurements to one or other vehicle tend to be manifested in an obvious difference between the forces calculated as causing the damage to each vehicle. Table 5.6 shows a summary of the force differences determined for each of the RICSAC test collisions and the impact type.

Table 5.6: RICSAC tests comparison of force difference and impact type

Test	Force Difference (%)	Impact Type
1	363	60° front to side
2	469	60° front to side
3	47	10° front to rear
4	99	10° front to rear
5	385	10° front to rear
6	577	60° front to side
7	608	60° front to side
8	14	90° front to side
9	80	90° front to side
10	66	90° front to side
11	4	10° front to front
12	29	10° front to front

Tests 1, 5, 6, and 7 reveal force differences well in excess of 100% and no systematic relationship is apparent between the scale of error and type of collision. Comparison with the photographs indicates that some adjustment to the crush measurements is desirable. The author has examined and measured scores of damaged vehicles. Based on this experience, photographs and the measurements an estimate of the likely crush at the load bearing level have been made for each vehicle. The adjustments made vary dependent on the particular damage to each vehicle. Although such a process is somewhat rough and ready the resulting measurements provide a better

approximation of the damage profiles to the stiff parts of the vehicles. Suitable adjustments are detailed in Table 5.7

Table 5.7: RICSAC tests measurement adjustments

Test	Damage Adjustments
1	v2 subtract 10 cm from each C_1 to C_6
2	v2 subtract 15 cm from each C_1 to C_6
3	v1 add 5 cm to each C_1 to C_6. Set v2 offset to -50 cm
4	v2 subtract 15 cm from each C_1 to C_6
5	v2 subtract 20 cm from each C_1 to C_6
6	v2 subtract 15 cm from each C_1 to C_6
7	v2 subtract 20 cm from each C_1 to C_6
8	No adjustment
9	v2 subtract 10 cm from each C_1 to C_6
10	v2 add 10 cm to each C_1 to C_6
11	No adjustment
12	Expand damage length *L* for both vehicles to 140 cm

It is possible to refine the PDOF values used by replacing the estimated values with values calculated using Brach's or Ishikawa's models and the actual speeds of the vehicles at impact. Adjusting the crush measurement profiles as indicated in Table 5.7 also has a secondary effect. As discussed in Chapter 3, McHenry [65] indicates that the position of the point of application of the impulse can be assumed to be the centre of mass of the damaged area, the damage centroid. Adjusting the damage profile alters the calculated position of the damage centroid. Assuming that the calculated damage centroid is the point of application of the impulse, and further assuming a common post-impact velocity at the damage centroids, the refined PDOF values obtained from the momentum only models are as shown in Table 5.8

Table 5.8: Adjusted PDOF values (degrees)

RICSAC test No.	Original values		Adjusted values		Difference	
	V1	V2	V1	V2	V1	V2
1	-30	30	-11.3	48.7	-18.7	-18.7
2	-30	30	-11.7	48.3	-18.3	-18.3
3	0	170	14.1	-175.9	-14.1	-14.1
4	-0.5	170.5	11.1	-178.9	-11.6	-10.6
5	0	170	11.6	-178.4	-11.6	-11.6
6	-30	30	-11	49	-19	-19
7	-30	30	-12.7	47.3	-17.3	-17.3
8	-30	60	-20.5	69.5	-9.5	-9.5
9	-30	60	-21.8	68.2	-8.2	-8.2
10	-65	25	-25.3	64.7	-39.7	-39.7
11	4.5	-4.5	-2.9	-11.9	7.4	7.4
12	4.5	-4.5	1	-8	3.5	3.5

Table 5.8 shows that the visual estimates of the PDOF are considerably different from the PDOF values required to cause the desired change in velocity. Such a difference has been noted previously by many commentators, e.g. Smith and Noga [**108**] and Brach [**12**]. (Note: In test 10 it appears that the initial estimates of -65 and 25° may have been transposed. However for consistency the data is retained as recorded.)
The amended data is used in subsequent sections.

5.3.5 Post-impact directions of travel

Interestingly, using the actual pre-impact speeds, the momentum only models of Brach and Ishikawa predict post-impact directions of travel which are close to the actual post-impact directions of travel recorded by Jones and Baum [**51**] The values and differences between the post-impact directions of travel measured from Jones and Baum and those calculated using Brach's PIM are shown in Table 5.9

Table 5.9: Post-impact directions of travel (degrees)

RICSAC test No.	Actual Values		PIM Values		Difference	
	V1	V2	V1	V2	V1	V2
1	17	67	14	65	3	2
2	19	64	14	64	5	0
3	2	10	8	14	-6	-4
4	4	9	6	11	-2	-2
5	0	4	5	12	-5	-8
6	8	61	11	64	-3	-3
7	11	54	10	57	1	-3
8	50	56	25	58	25	-2
9	59	65	29	76	30	-11
10	65	66	33	72	32	-6
11	6	26	18	39	-12	-13
12	7	32	7	39	0	-7

The results for collision 11 appear to be anomalous, the reasons for which have not been ascertained. However the results in Table 5.9 for the three 90° collisions (numbers 8, 9 and 10) do not match the post-impact trajectories as precisely as the other collisions. This is particularly pronounced as far as the less massive vehicle (vehicle 1) is concerned in each collision.

In these particular collisions the recorded post impact directions of travel show that the centres of mass of each vehicle moved approximately parallel to each other post-impact. In these calculated scenarios, assuming a common post-impact velocity at the damage centroids predicts that the vehicles ‘pass through’ each other. This is a physically impossible result. Allowing restitution along the line of action of the impulse, but maintaining a common tangential velocity produces calculated results which match the recorded output scenarios.

This is illustrated in Figure 5.3 where the predicted motion of the vehicles in RICSAC 9 is shown with $e_p = 0$ and $e_p = 0.3$

Figure 5.3: Motion of Centres of Mass with varying coefficients (RICSAC 9)

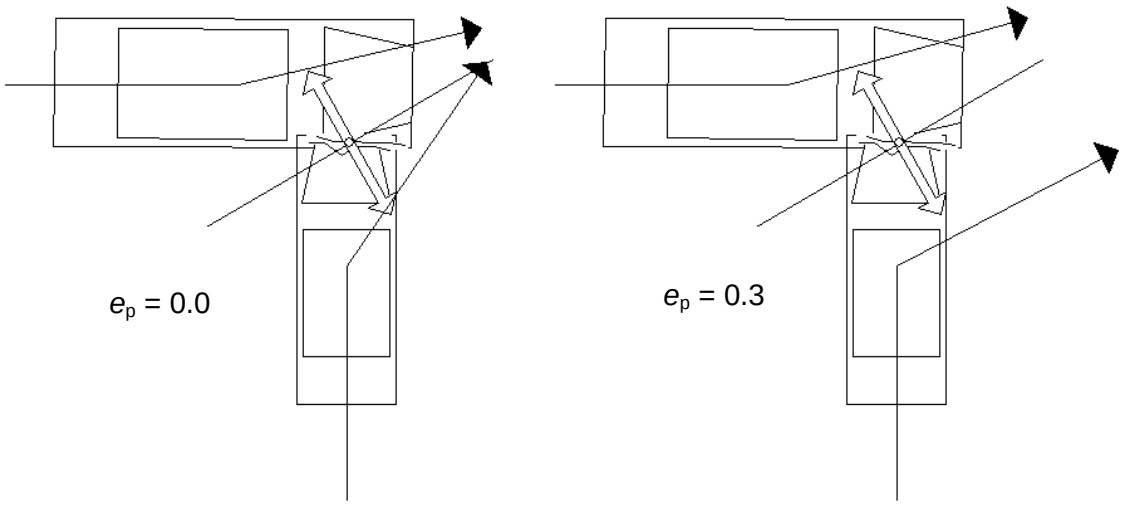

With the adjustments to the coefficient of restitution for collisions 8, 9 and 10, the post-impact directions of travel calculated using PIM are shown in Table 5.10

Table 5.10: Post impact directions of travel with e=0.3 (degrees)

RICSAC test No.	Actual Values		PIM Values		Difference	
	V1	V2	V1	V2	V1	V2
8	50	56	41	49	9	7
9	59	65	45	69	14	-4
10	65	66	54	66	2	0

The correspondence between the calculated post-impact directions of travel using Brach's PIM and the actual directions suggests that the momentum based models of Brach and Ishikawa do predict accurately the post-impact directions of travel provided suitable estimates can be made for the pre-impact speeds. This important finding that the predicted post-impact directions of travel match very well with the actual post-impact directions of travel is utilised in Chapter 7 to provide a way of refining initial estimates of the PDOF to generate more accurate and reliable results.

5.3.6 RICSAC analysis using adjusted data

The adjustments suggested in Table 5.7 and Table 5.8 have been included in a second set of AiDamage analyses. These results are shown in Appendix F and summarised in Figure 5.4 below

Figure 5.4: Comparison of original (raw) and adjusted CRASH results

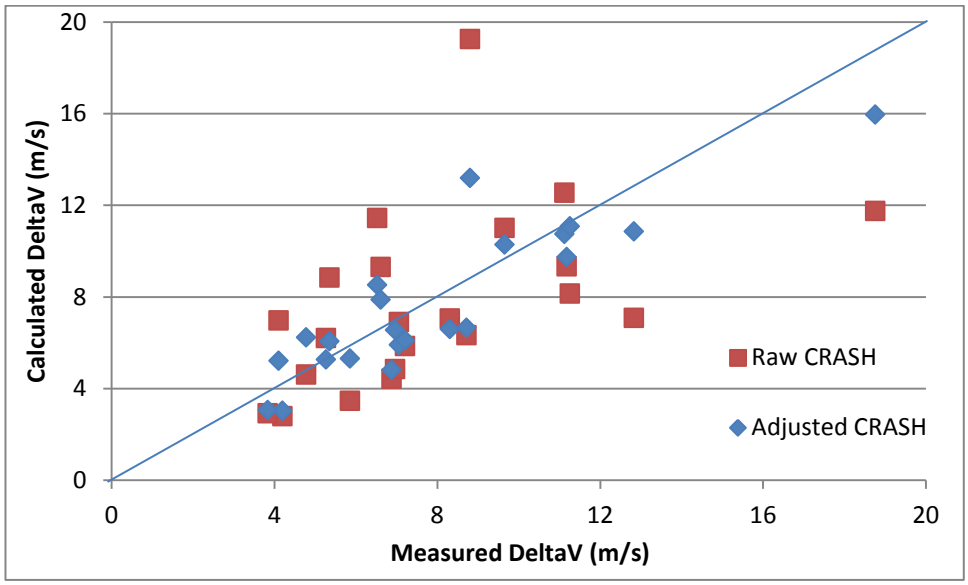

Using the adjusted measurements and PDOF values these tests now show that CRASH underestimates Δ*v* by a mean of 2% with a standard deviation of about 22%. An analysis of the error associated with each test is shown in Figure 5.5

Figure 5.5: Errors per individual test

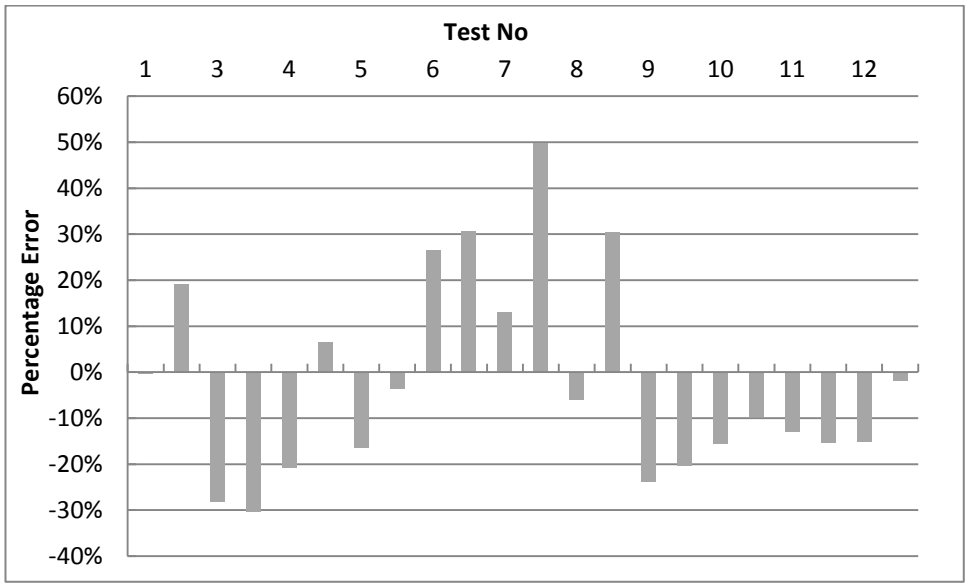

Although the majority of results show a range of differences less than about ±30%, test 7 produces an anomalous result. In this calculation the change in velocity for vehicle 2 is calculated to be nearly 50% greater than the change in velocity determined from the accelerometers. A similar overestimate is also noted using the momentum based models of Brach and Ishikawa. This suggests that some other factor is responsible. It has not been possible to definitively identify this factor. However in their DOT report Jones and Baum [**52**] also report an overestimated Δv for vehicle 2 in test 7 (35.5 mph). They suggest that this may be due to the fact that in this collision there was significant rotation of vehicle 2 during the impact itself of approximately 22° and that this is not modelled by CRASH. Excluding test 7 from the analysis suggests that damage only algorithm of CRASH underestimates the true Δv by 4% with a standard deviation of 18%. Although the variation in the results remains relatively large, comparing these adjusted results with the original raw data results tends to indicate that improvements to the measuring process and in particular adjusting the PDOF to match reality do produce more accurate results.

5.4 Theoretical Accuracy of CRASH

With the exception of the work performed by Smith and Noga [**107**] little work has been performed to determine the theoretical accuracy of CRASH. As discussed previously Smith and Noga utilised a simplified version of the CRASH equation, assumed a fixed number of crush measurements and adopted the standard energy adjustment factor proposed by McHenry [**65**]. There does not appear to be however a rigorous study to quantify how potential error in any one of the input parameters to the CRASH equation is likely to affect the overall result. Singh [**100**] determined the theoretical accuracy of CRASH stiffness coefficients assuming normally distributed input parameters. This approach of assuming normally distributed input parameters is also adopted here to quantify how the errors in the input data affect the overall result. This approach was adopted so that a confidence interval for the final result could be computed and compared with Monte Carlo simulations which form the subject of the next Chapter.

Repeated measurements of a variable generally produce a result which has a normal (Gaussian) distribution and can be written as $x = N(\mu, \sigma^2)$ where μ is the mean and σ is the standard deviation so that σ^2 represents the variance. A function f comprising a number of such variables, $x_1 \ldots x_n$ can be written

$$y = \mathrm{f}(x_1, x_2, \ldots, x_n)\,. \tag{5.2}$$

Error propagation theory shows that the variance in the result σ_y^2 can then be approximated by

$$\sigma_y^2 = \sum_{i=1}^{n}\left(\frac{\partial f}{\partial x_i}\right)^2 \sigma_i^2 + \sum_{i=1}^{n}\sum_{j=1(j\neq i)}^{n}\left(\frac{\partial f}{\partial x_i}\right)\left(\frac{\partial f}{\partial x_j}\right)\sigma_{ij} \tag{5.3}$$

The second term in equation (5.3) represents the covariance between the variables x_i and x_j. If the variables are independent and therefore uncorrelated, then σ_{ij} is zero so that the second term in equation (5.3) vanishes. As a result the variance in a function f for a number of independent variables is approximately given by

$$\sigma_y^2 = \sum_{i=1}^{n}\left(\frac{\partial f}{\partial x_i}\cdot\sigma_x\right)^2\,. \tag{5.4}$$

Similarly the absolute uncertainty Δy can be expressed as

$$\Delta y^2 = \sum_{i=1}^{n}\left(\frac{\partial f}{\partial x_i}.\Delta x_i\right)^2\,. \tag{5.5}$$

As demonstrated earlier the CRASH algorithm can be considered as two separate parts, one to determine the crush energy values and the second to determine the change in velocity. As such the variance may be determined for each calculation to determine the crush energy which may then be used in the second part to determine the overall variance in Δv. Singh [**99**] shows that the work done in causing crush for an arbitrary number of crush zones n can be determined from equation

$$E = \frac{L}{(n-1)}\left(\frac{A\eta}{2} + \frac{B\kappa}{6} + \frac{(n-1)A^2}{2B}\right) \tag{5.6}$$

where

$$\begin{aligned}\eta &= \sum_{i=1}^{n-1}[C_i + C_{i+1}]\\ \kappa &= \sum_{i=1}^{n-1}\left[C_i^2 + C_iC_{i+1} + C_{i+1}^2\right].\end{aligned} \tag{5.7}$$

By applying equation (5.4) the variance in equation (5.6) can then be written as

$$\sigma_E^2 = \left(\frac{\partial E}{\partial A}\right)^2 \sigma_A^2 + \left(\frac{\partial E}{\partial B}\right)^2 \sigma_B^2 + \left(\frac{\partial E}{\partial L}\right)^2 \sigma_L^2 + \left(\frac{\partial E}{\partial \eta}\right)^2 \sigma_\eta^2 + \left(\frac{\partial E}{\partial \kappa}\right)^2 \sigma_\kappa^2 \tag{5.8}$$

where the partial derivatives are defined in Appendix G and the variance in η and κ are defined as

$$\begin{aligned} \sigma_\eta^2 &= \sum_{i=1}^{n-1}\left[\left(\frac{\partial \eta}{\partial C_i}\right)^2 \sigma_{c_i}^2 + \left(\frac{\partial \eta}{\partial C_{i+1}}\right)^2 \sigma_{c_{i+1}}^2\right], \\ \sigma_\kappa^2 &= \sum_{i=1}^{n-1}\left[\left(\frac{\partial \kappa}{\partial C_i}\right)^2 \sigma_{c_i}^2 + \left(\frac{\partial \kappa}{\partial C_{i+1}}\right)^2 \sigma_{c_{i+1}}^2\right]. \end{aligned} \tag{5.9}$$

Note that the partial derivatives were evaluated symbolically using Mathcad Version 13. The input data to these and other equations is frequently quoted in the form $x \pm \delta x$ where the δx term represents the confidence limit applicable to that parameter (usually 95%). Assuming a normal distribution for the data and using a two-tailed hypothesis test corresponding to 95% (i.e. $\alpha = 0.025$) the standard deviation σ can be expressed as

$$\sigma = \frac{\delta x}{1.96}. \tag{5.10}$$

5.4.1 Example: RICSAC 8

Applying equation (5.10) to the data allows the variance to be determined for each parameter and thereby permits the calculation of the total variance or standard deviation. This process is illustrated using the data from RICSAC tests [**51**] as shown in Appendix D together with the 95% measurement confidence limits suggested by Smith and Noga [**108**] in Table 5.2 Confidence limits are not available for the default CRASH3 stiffness coefficients so a nominal value of ±10% was used which matches the confidence interval used by Smith and Noga. This may well underestimate the true confidence interval however as suggested by the work of Siddall and Day [**98**] where their confidence limits on updated stiffness coefficients are generally higher. The effect of using alternative confidence limits is discussed in later sections. RICSAC test 8 is used for this example as it was one of the few tests where the measurements did not

require adjustment. From this data the crush energy and confidence limits for each vehicle were calculated using Mathcad. The model and results are shown in Appendix H (Part I) and show that the 95% confidence limits applicable to this calculation is about ±23%. The contribution to the confidence limits by each of the parameters in equation (5.6) is shown in Table 5.11

Table 5.11: Contribution of individual energy parameters to overall confidence limit

Variable	Standard Deviation		Fraction of overall result (%)		Fraction of total error (%)	
	V1	V2	V1	V2	V1	V2
A (N/cm)	31.8	12.8	15.4	5.86	42.91	6.58
B (N/cm^2)	1.19	1.78	5.4	4.14	5.27	3.29
L (cm)	7.78	7.78	8.22	7.10	12.24	9.67
η (cm)	16.5	16.5	14.3	8.2	37.12	12.89
κ (cm^2)	342	816	3.69	18.8	2.47	67.57
Total (J)	3130	2470	23.5	22.8	100	100

These results demonstrate that the overall uncertainty in the determination of the crush energy cannot be ascribed to one particular input parameter. For vehicle one, the value of *A* and *η* are dominant but for vehicle 2, the dominant factor is the uncertainty in the factor *κ*. This suggests that an alternative approach is required to determine what factors are dominant in calculating crush energy. This is discussed in more detail below.

Once the variance in crush energy has been determined however, this can be multiplied by the energy adjustment factor to calculate the corrected crush energy. As explained in Chapter 4 a number of energy adjustment factors have been proposed so each will have a different error term. For consistency with existing work the standard energy adjustment factor is used here

$$E = E_m(1+\tan^2\alpha) \tag{5.11}$$

where E is the corrected energy, E_m is the energy calculated from the measured data and α is the angle of impulse with the original face of the vehicle. The result of

equation (5.11) can then be used in equation (2.24) to calculate Δ*v*. Equation (2.24) is repeated here for convenience

$$\Delta v_1 = \sqrt{\frac{2m_2(E_1+E_2)(1+e_p)}{m_1(m_1\delta_2+m_2\delta_1)(1-e_p)}}\,. \tag{5.12}$$

where m_1 and m_2 are the masses for each vehicle, E_1 and E_2 are the corrected crush energy values and δ_1 and δ_2 are defined as

$$\delta_1 = 1+\frac{h_1^2}{k_1^2}, \qquad \delta_2 = 1+\frac{h_2^2}{k_2^2} \tag{5.13}$$

where k_1 and k_2 are the radii of gyration and h_1 and h_2 are the lengths of the moment arms about the centres of mass. The lengths of the moment arms can be found from the expression

$$h = (x-\bar{x})\sin\theta - \bar{y}\cos\theta \tag{5.14}$$

where θ is the PDOF, x is the displacement of the centre of mass of the vehicle to the original surface and $\bar{x}$ and $\bar{y}$ are the displacements of the point of application of the impulse perpendicular and parallel to the original surface. McHenry's method [**65**] for determining the location of the point of application of the impulse, by assuming this point is the damage centroid, depends on the crush measurements and offset. It follows therefore that h will be affected by any error in these measurements as well as any error in the PDOF. As an alternative to equation (5.14) the position of the point of application of the impulse can be defined using polar coordinates, d and ϕ about the centre of mass in a manner similar to that described by Brach [**11**] so that

$$h = d\sin(\theta+\phi) \tag{5.15}$$

Using polar coordinates is an effective way defining the position of the point of application and is used here in preference to Cartesian coordinates to allow for greater consistency and avoid potential problems when different surfaces of the vehicle are considered. In any event the fact that any error in the PDOF affects h and E means that the δ and E parameters in equation (5.12) are likely to be correlated to some extent. Since this cannot easily be determined analytically, a detailed discussion on this aspect is deferred until the next Chapter. Assuming however that this correlation

can be considered to be negligible, the variance of equation (5.11) can be calculated in a similar manner as previously. The partial derivatives required for this series of calculations are defined in Appendix G.

No data appears to be available on which to base suitable error bounds for the parameters *k*, *d* or ϕ. The 95% confidence limits for the radius of gyration is assumed here therefore to be 0.1 m. The length of the moment arm (*h*) is determined by the PDOF (θ) and the position of the point of application of the impulse which is itself defined through the parameters *d* and ϕ. It is supposed here that the error in *h* is constrained to lie within the same bounds as crush measurements, i.e. ± 3" (7.62 cm). Permitting a simple bound on the angular value of ϕ has the undesirable effect that the lateral error in *h* is then also dependent upon the length of *d*. To negate this effect, the model here constrains variation in the angle ϕ so that the lateral variation is the same as the variation in *d*.

The model and results for RICSAC test 8 are shown in the Mathcad implementation of the model. The full listing is in Appendix H (Part II). The results show that the 95% confidence limits applicable to the calculation of Δv when using the raw data reported by Jones and Baum [**51**] is about ±18%. The contribution to the confidence limits by each of the parameters in equation (5.12) is shown in Table 5.12

Table 5.12: Contribution of individual Δv parameters to overall confidence limit

Variable	Standard Deviation		Fraction of result (%)		Fraction of total error (%)	
	V1	V2	V1	V2	V1	V2
m_1	25.5	25.5	1.69	2.46	0.90	1.86
m_2	25.5	25.5	0.43	2.31	0.06	1.68
E_1	4665	-	7.25	-	16.68	-
E_2	3898	-	6.06	-	11.65	-
δ_1	0.402	-	14.9	-	70.20	-
δ_2	0.036	-	1.28	-	0.52	-
e_p	0.00	-	0.00	-	0.00	-
Δv_1	-	0.438	-	17.5	-	96.46
Total	0.438	0.424	17.7	18.1	100	100

The results for this one test shows that the largest contributor to the overall error by far is the error in δ_1. For this collision δ_1 is 1.67 with a 95% confidence limit of ±47% which is due almost entirely to a large uncertainty in h_1. In turn the uncertainty in h_1 can be tracked back to the uncertainty in $PDOF_1$. Reducing the uncertainty in the PDOF parameters by setting the confidence limit to ±10° reduces the overall uncertainty in Δv to around ±12% and eliminating it entirely reduces the overall uncertainty to around ±9%. It appears therefore that an accurate estimate of PDOF is essential if a realistic result is to be obtained.

5.4.2 Application to RICSAC tests

As discussed earlier, a more accurate estimate of the PDOF has been determined for the RICSAC collisions along with more realistic measurements. The analytical model developed here for RICSAC 8 and shown in Appendix H has been applied to each of the collisions and including restitution where necessary, an estimate of the theoretical accuracy has been be obtained. A comparison showing the calculated difference in change in velocity (from Brach [**12**]) and theoretical limits of accuracy for the RICSAC test series are shown in Figure 5.6

Figure 5.6: RICSAC - Comparison between calculated and theoretical accuracy

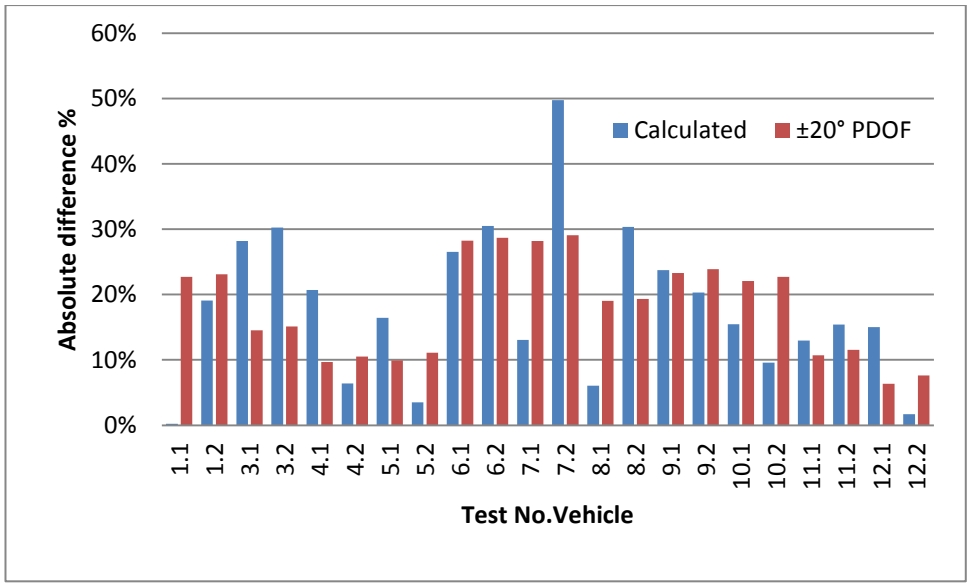

The mean 95% confidence limit using ±20° in the PDOF for each vehicle was found to be ±18%. Reducing the variability in the PDOF to ±10° reduced the mean confidence limit to ±12.3% suggesting that if achievable, increased accuracy in estimating the PDOF should produce significantly more accurate results. In several of the tests

however it is noted that the calculated error is somewhat greater than the theoretical error. This indicates that either the theoretical error is not taking some major factor into account, the model itself is flawed, or that the source data itself contains one or more errors. As previously indicated the measurement data is not ideal and examination of the recorded changes in velocity indicate that these were themselves calculated from potentially flawed sources. Although a record of the accelerometer data is present in the RICSAC source data compiled by Shoemaker [**96**] and [**97**] no obvious reference to actual post-impact speeds appears to have been recorded from which a change in velocity could be calculated.

5.4.3 Application to Lotus test series

Alternative series of tests do exist from which additional comparisons can be made. For example the Lotus series of tests performed by ITAI [**45**] were designed so that post-impact data was available from which post-impact speeds could be determined. A similar comparison as above using uncorrected data from the Lotus tests and changes in velocity calculated using post-impact data has also been performed. These results are shown in Figure 5.7

Figure 5.7: Lotus - Comparison between calculated and theoretical accuracy

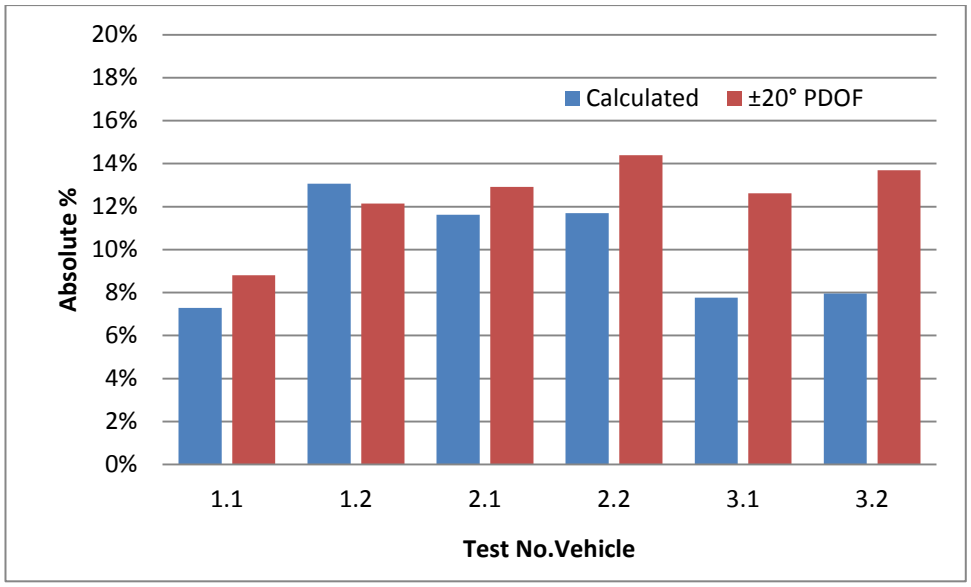

The results show that for all but one vehicle the error in the calculated change in velocity was smaller than the theoretical error. Although these vehicles appear to have been measured more consistently and accurately than in the RICSAC series of tests, flaws in the data have been noted e.g. Smith [**103**]. This is reflected in the results. The

mean calculated error compared with the actual changes in speed was +10% with a standard deviation of 3%. The mean 95% confidence limit using ±20° in the PDOF for each vehicle was found to be ±12.4%.

5.5 Contribution to uncertainty by individual input parameters

A more useful comparison of the effect of uncertainty in individual input parameters can be obtained by considering the overall confidence limits to Δv achieved using a range of uncertainty in individual input parameters. This allows a direct comparison to be made with Smith and Noga's [**108**] results. The CRASH algorithm as a whole can be considered to be a sequence of individual components each taking various input parameters as shown in Figure 5.8

Figure 5.8: Relationship between input parameters

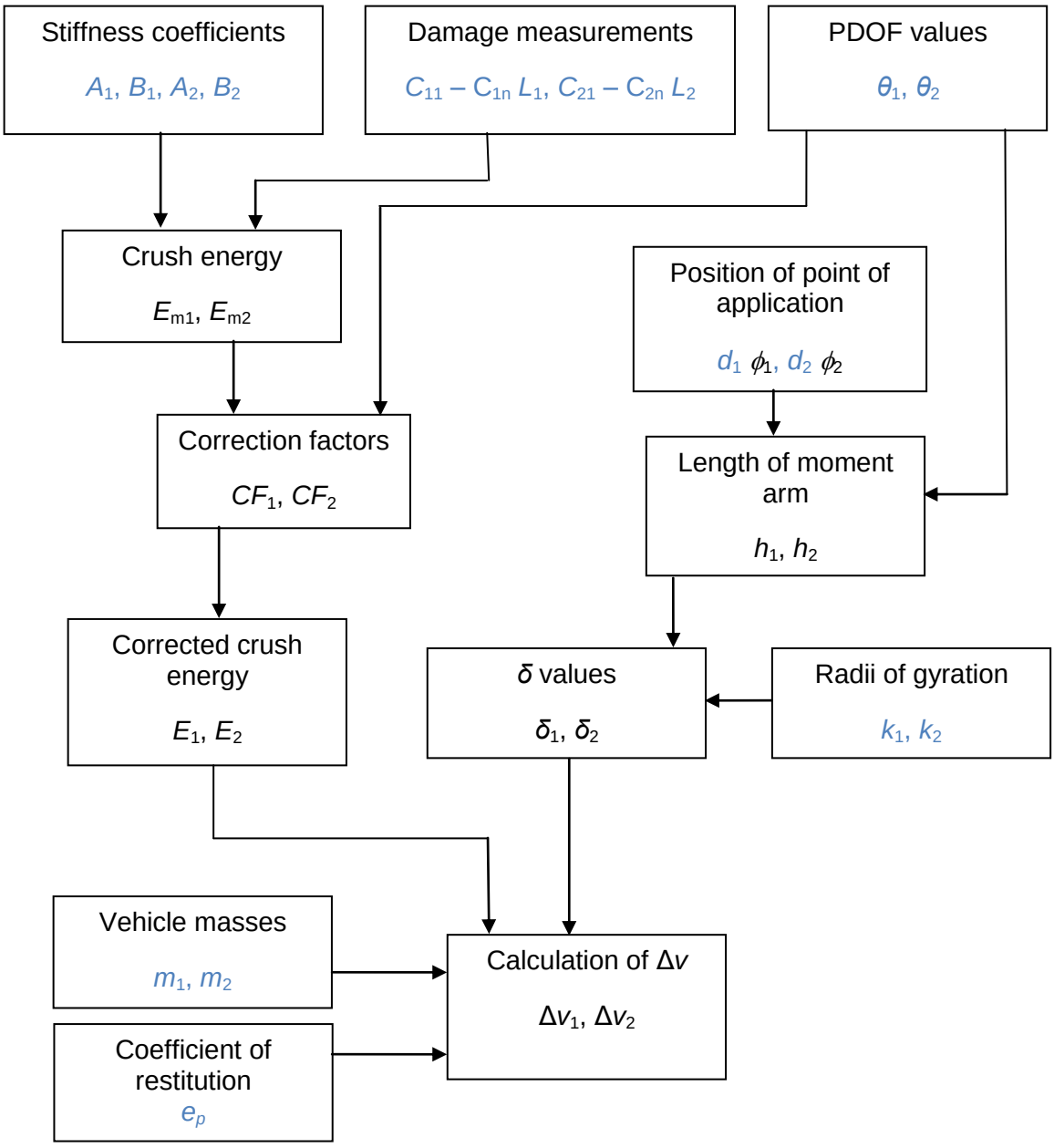

The parameters shown in blue in Figure 5.8 are measured or otherwise determined by the user. Other parameters are interim values dependent upon those inputs. Each of the input parameters will have an uncertainty associated with it. By eliminating the uncertainty in all inputs except for the parameter under investigation the effect of uncertainty in each input parameter can be investigated. Suitable ranges for each of the parameters have been designed as shown in Table 5.13. These are designed to encompass the uncertainties suggested by Smith and Noga [**108**] as shown in Table 5.2 and also to examine the relationship between uncertainty in each parameter and the overall uncertainty in the result.

Table 5.13: Uncertainty in individual parameters

Parameter	Description	Uncertainty used
δC	Uncertainty in crush measurements	0.01, 0.05, 0.1 m
δL	Uncertainty in damage length	0.01, 0.05, 0.1, 0.15, 0.2 m
δm	Uncertainty in mass	10, 25, 50 100 kg
$\delta PDOF$	Uncertainty in PDOF	1, 5, 10, 15, 20, 25°
δd	Uncertainty in position of point of application	0.01, 0.05, 0.1, 0.2 m
δk	Uncertainty in radius of gyration	0.01, 0.05, 0.1, 0.2 m
δA	Uncertainty in A stiffness coefficient	5, 10, 15, 20%
δB	Uncertainty in B stiffness coefficient	5, 10, 15, 20%

5.5.1 Application to RICSAC tests

The results from this analysis as applied to the RICSAC series of crash tests are shown in Appendix I. The overall uncertainty shown in Table I.1 is calculated using the 95% confidence levels suggested by Smith and Noga which allows a direct comparison to be made with their work. Since no uncertainty was ascribed by Smith and Noga to the position of the point of application (d), a 95% confidence level identical to the crush measurement uncertainty was used, i.e. ±3” (0.0762 m). Siddall and Day [**98**] as part of their update to the vehicle stiffness coefficients shows that the radius of gyration (k) varies from about 1.25 m for small cars up to about 1.55 m for large cars. The range of probable values for k is therefore likely to be relatively small. Thus a 95% confidence

level of 0.1 m was assigned to the uncertainty in the radii of gyration (*k*) measurements.

The tables in Appendix I show results show a linear response with respect to each of the parameters under investigation. For example multiplying the uncertainty in any one parameter by a factor of two, doubles the resultant contribution to uncertainty by that parameter. Since the uncertainty in each factor is determined from the product of the appropriate partial derivative and associated uncertainty, such a linear response may be expected for all collisions. The total uncertainty can then be found from application of equation (5.5) as the sum of the squares of the individual uncertainties. It is important to note however that in any particular collision the uncertainty in a parameter may be identical to the uncertainty in another collision, but the numerical result of the associated partial derivative is unlikely to be the same. This leads to different results for different collision scenarios.

The results have been grouped by impact configuration which highlights some obvious trends. Figure 5.9 shows the overall uncertainty grouped by impact configuration. It is clear from Figure 5.9 that the front to front and front to rear impact configurations appear to be inherently more accurate than the front to side impact configurations with the 60° front to side impacts predicting overall uncertainty of around 27%

Figure 5.9: Overall uncertainty grouped by impact type

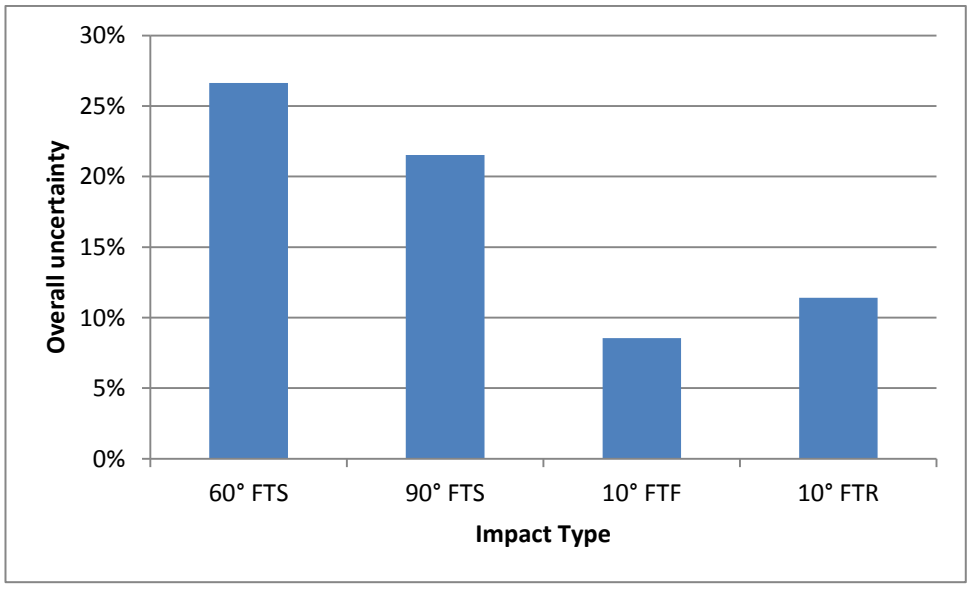

An analysis of the individual contributions made by each of the input parameters shows the main sources of uncertainty in the overall result. An analysis of the relative contribution made by each of the input parameters grouped by impact type reveals the results shown in Figure 5.10

Figure 5.10: Percentage contribution to uncertainty grouped by impact type

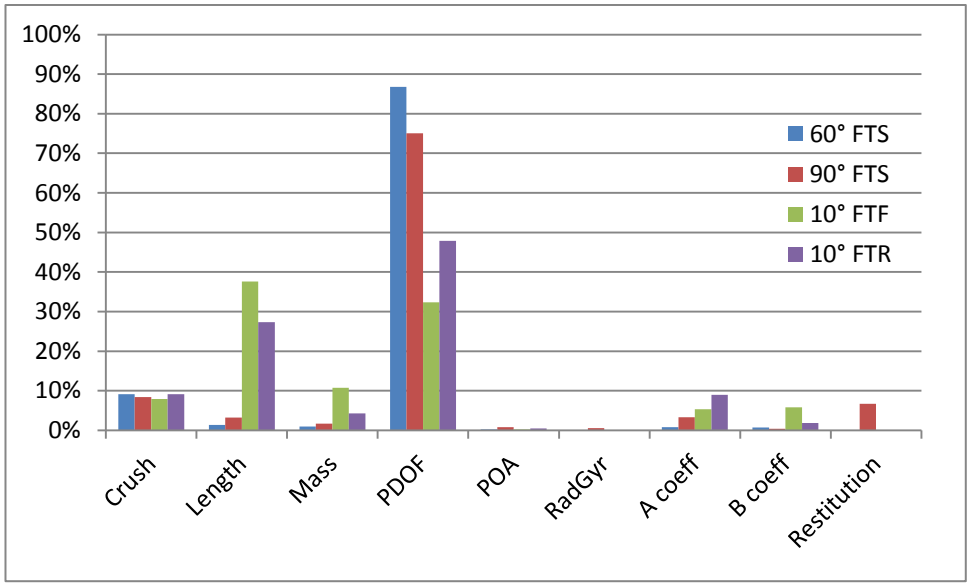

The major contributor to overall uncertainty in Δv is clearly the uncertainty in the PDOF which confirms the findings of Smith and Noga [**108**]. Although the overall contribution of uncertainty in the PDOF at 61% is lower than that found by Smith and Noga, these new results provide significant insight into the overall uncertainty. The results here show the effect of a larger range of input parameters rather than simply the three parameters of PDOF, crush and mass considered by Smith and Noga.

It is clear from these results that the uncertainty associated with some parameters are unlikely to have any significant effect on the overall uncertainty. For example uncertainty in the position of the point of application of the impulse to each vehicle and radii of gyration has a negligible effect. A 0.0762 m (3") uncertainty in the crush measurements generates a contribution of 4% to 10%. As may be expected, a larger contribution to the overall error is noted for those tests where the crush measurements

were relatively small. Similarly a fixed uncertainty of 0.1524 m (6”) in damage length becomes more significant for shorter damage lengths.

5.5.2 Analysis of effect of uncertainty in estimate of PDOF

When grouped by impact configuration, it can be seen that the uncertainty in the PDOF mirrors the overall uncertainty for that configuration which is itself indicative of the dominant role played by the uncertainty in the PDOF. Figure 5.11 shows the percentage contribution to uncertainty of the PDOF measurement compared with the overall uncertainty for each of the RICSAC tests. As can be seen, in the three 60° front to side impacts (tests 1, 6 and 7) the percentage contribution of the uncertainty in the PDOF measurement approaches 90%. For the front to front (tests 11 and 12) and front to rear (tests 2, 3 and 5) collisions the contribution of the PDOF uncertainty is significantly lower.

Figure 5.11: Relative contribution of uncertainty in PDOF to overall uncertainty

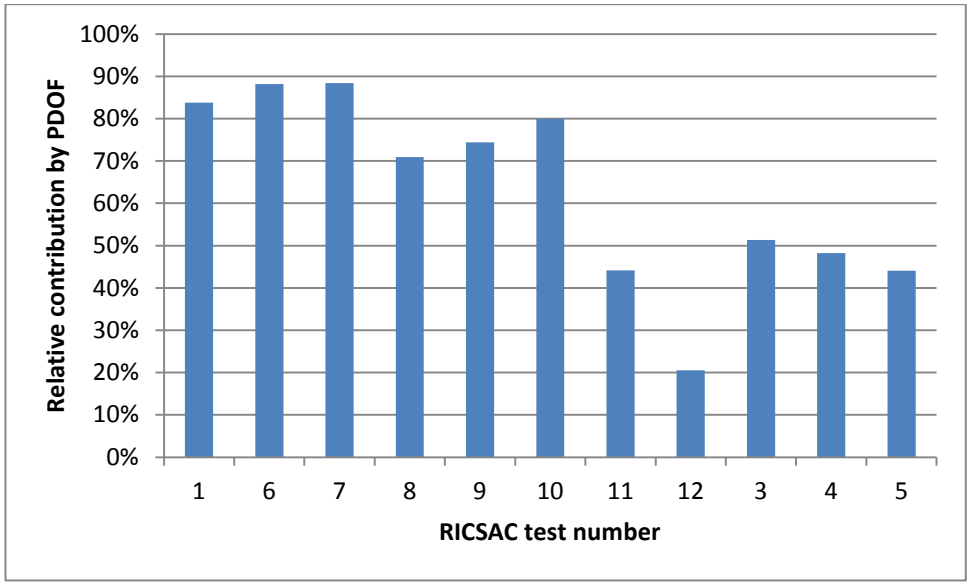

This pattern is due in part to the behaviour of the standard energy adjustment factor. In these tests the energy adjustment factor shown in equation (5.11) is unbounded and increases with more oblique angles of incidence as described in Chapter 4. In the front to front and front to rear impacts the nominal angle of incidence is close to

perpendicular to the vehicle surface. Thus any variation in the angle of incidence α will produce relatively small changes to the adjustment factor. In the 60° front to side impacts the nominal angle of incidence is around 40° to 50° for one of the vehicles in each of these collisions. In such cases a variation in PDOF of ±20° therefore produces a possible range of adjustment factors from around 1.1 to 8.5. Applying an upper bound on this factor of 2 was suggested by McHenry [**65**] to eliminate excessive adjustment factors. Such a modification is generally utilised in practical applications of the CRASH algorithm and thereby reduces the overall uncertainty.

In the analysis presented in this Chapter the error term associated with the adjustment factor is determined from the partial differentiation of the adjustment factor with respect to α as shown in Appendix G and reproduced below

$$\frac{\partial E}{\partial \alpha} = 2\sec^2 \alpha \tan \alpha = 2\tan \alpha (1 + \tan^2 \alpha). \tag{5.16}$$

Equation (5.4) can be applied to the result of equation (5.16) to determine the variance and standard deviation in the adjustment factor. It is noted that the result of equation (5.16) will be zero for a nominal angle of incidence of zero indicating that at such angles the standard deviation in the adjustment factor is also zero. However at larger angles of incidence the standard deviation will become progressively larger as it depends in part on the term tan(α) which increases with increasing angle. At larger nominal angles the result of equation (5.16) is therefore larger producing a larger variance in the overall result. It is possible to mitigate this effect somewhat by constraining the adjustment factor to a maximum value of 2. This requires some modification to the Mathcad implementation of the model shown in Appendix H. This can be achieved by conditionally replacing the standard deviation determined from equation (5.16) and (5.4) with a value determined from

$$\sigma_{CF} = \frac{2 - (1 + \tan^2 \alpha)}{1.96} = \frac{1 - \tan^2 \alpha}{1.96}. \tag{5.17}$$

This modification is necessary only where the standard deviation is such that the 95% confidence limits applied to the nominal value exceed 2 as is the case in the 60° front to side impacts. Applying this modification produces results shown in tables I.11 and I.12 in Appendix I and reduces the overall uncertainty in the 60° front to side impacts to around 15%. The remaining RICSAC tests are unaffected by this modification. A

comparison between the original contribution to uncertainty by variation in the PDOF and the effect of reducing the variability in the adjustment factor to zero is shown in Figure 5.12

Figure 5.12: Effect of eliminating energy adjustment

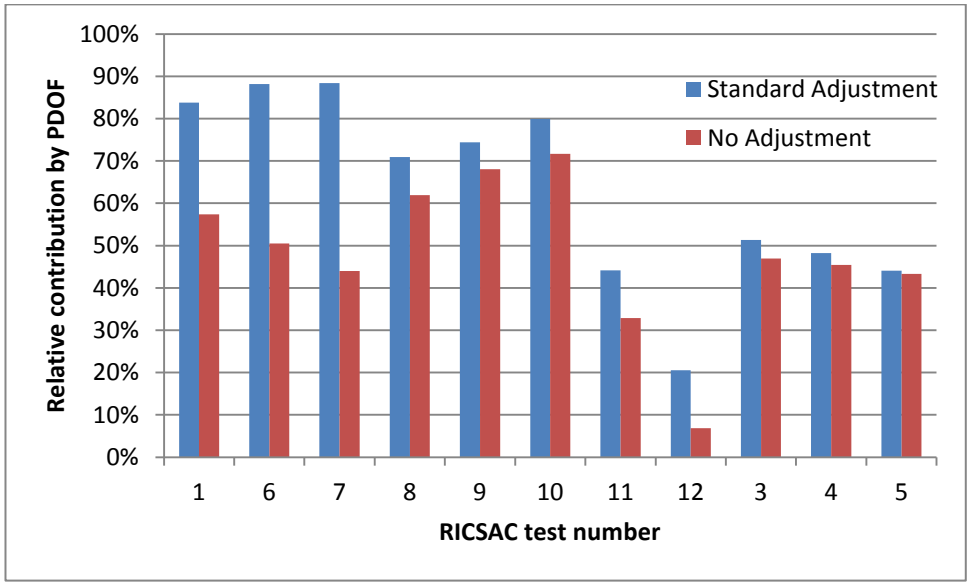

The remaining contribution of variation in the PDOF to uncertainty in the overall result is due to the variation in the length of the moment arm (h). Some correlation is apparent between the sum of the lengths of the two moment arms ($h_1 + h_2$) and the contribution to overall uncertainty in the PDOF. This correlation is explored in more detail in the next Chapter. The 90° front to side impacts in the RICSAC test series generate moment arm sums which are considerable longer than the moment arm sums found for the front to front or front to side impacts. Some impact configurations appear therefore be inherently more sensitive in this respect.

As a result of this analysis it appears that an uncertainty in the PDOF of ±20° can produce results which have a relatively high level of overall uncertainty of over 25% for some impact configurations. It appears that the only method available to reduce this uncertainty to more acceptable limits is to reduce the uncertainty in the estimate of the PDOF. For real-world collisions this may of course be impractical. As outlined earlier, using the actual pre-impact speeds for the RICSAC tests in the momentum only

models generated post-impact directions of travel which matched the empirical results. As a consequence the derived PDOF values were considerably more accurate than initial visual estimates. This suggests that the reverse situation is also likely to be valid; if the post-impact directions of travel can be ascertained, then it should be possible to generate more realistic estimates for the PDOF. Such an approach is developed in Chapter 7.

5.6 Summary

In this Chapter several empirical studies were examined and these appear to show that CRASH has the potential at least to produce changes in velocity results to within about 15% of the true change in velocity. The well known RICSAC tests were examined in detail to determine whether the claimed accuracy could be replicated using a known data set. Several problems with the RICSAC data were encountered and only partially resolved. Although the mean results did show an acceptable level of accuracy individual test collisions produced results which were not as accurate. Raw data from another series of tests was also examined which appear to show a greater level of accuracy.

The theoretical accuracy expected from variation in the empirical measurements was derived and examined. As found by Smith and Noga [**107**] the largest individual contribution to the overall uncertainty was the estimation of the PDOF parameter for each vehicle.

In the next Chapter, the issue of overall accuracy in the CRASH model is examined in more detail. A Monte Carlo simulation model is developed both to compare the results with the analytical process adopted in this Chapter and with real-world collisions.

Chapter 6

Monte Carlo Simulation to Determine Probable Limits of Accuracy

6.1 Objectives

In this Chapter the work of the previous Chapter is extended and a simulation model is developed to analyse the probable limits on accuracy of the CRASH model in more detail. The input parameters are chosen randomly from a known distribution and the Monte Carlo method used to determine the results.

6.2 Description and development of model used

6.2.1 Introduction

In the previous Chapter an analytical approach was adopted to determine the likely accuracy that can be expected from use of the CRASH model. Useful results were obtained. However a number of potential problems were identified such as possible correlation between some of the input parameters. In order to remove these potential problems another method to determine the likely accuracy is desirable. The approach adopted is to develop a model using the Monte Carlo method on a range of values for the input parameters.

In essence the Monte Carlo method relies on a large number of individual calculations of the result using randomly assigned input parameters. A statistical analysis can then

be performed on the results to determine the probable outcome. Monte Carlo methods can only yield probabilistic and not true results, i.e. it is only possible to give a probability that the Monte Carlo estimate lies within a certain range of the true value. The error term associated with any such estimate is also probabilistic and has a mean value of σ^2/N where σ^2 is the variance in the estimate and N is the number of iterations performed in the simulation. It follows therefore that the standard deviation of a Monte Carlo simulation scales as $1/\sqrt{N}$. To obtain a likely precision in the standard deviation of a result to ±0.01 therefore at least 10^4 iterations are required.

Monte Carlo methods rely on a large number of calculations to determine a mean value and probable range of uncertainty. The analytical approach is computationally simpler and easier to implement in practical scenarios than an equivalent Monte Carlo simulation. It is also desirable therefore to determine whether the analytical results obtained previously can be confirmed using a Monte Carlo simulation. Such a result would enable the calculation of error bounds on the overall results.

6.2.2 Input parameters

The input parameters to the Monte Carlo method are required to be randomly distributed about the desired mean value according to some probability distribution. Some method for determining the assignment of values is therefore required. Computers are essentially deterministic machines and as such any computer based random number generator will be at best a pseudo-random number generator. As indicated by Weinzierl [**122**] the true randomness of the generated numbers is not particularly relevant to Monte Carlo methods. It is more important that the sampling of the distribution is as uniform as possible. The requirement for a uniform distribution is also highlighted by Robert and Casella [**92**]. A potential problem with random numbers is that the numbers need not be distributed evenly over a finite sample. Levy [**58**] illustrates the clustering and gaps that may occur in pseudo-random sequences. For Monte Carlo simulations Levy shows that it is preferable to use quasi-random sequences where the numbers are distributed uniformly.

The Mathcad documentation [**64**] indicates that the random number generator used by Mathcad generates quasi-random numbers distributed according to the required probability density function. As mentioned in the previous Chapter, repeated measurements of a variable generally produce a result which has a normal or

Gaussian distribution. For this reason it is assumed initially that the input parameters to the CRASH equation will also be normally distributed about a nominal mean value. The assumption of a normal distribution may not be valid for all parameters so the effect of different distributions is also investigated.

6.3 Testing methodology

To determine the effect of uncertainty in each input parameter a series of collisions are simulated. A simple vehicle colliding head-on into a barrier is modelled initially with more complex scenarios developed where necessary. Each of the input parameters are varied systematically to determine the overall confidence limits on the results. The simulation is also applied to the RICSAC [**51**] series of crash tests to provide a comparison with the analytical method described in the previous Chapter. The same input parameters and confidence limits are used as described in Table 5.13. This allows a direct comparison to be made with the analytical model for the RICSAC tests.

The Mathcad implementation of the model developed for this analysis is shown in Appendix J. For comparison with Appendix H and Chapter 5 the data from RICSAC 8 is displayed.

One adverse effect of using a random normal distribution about a nominal mean value is that certain values may be generated which are physically impossible. For example crush measurements should to be constrained so that they do not become negative. Similarly A and B stiffness coefficients cannot be less than zero. The basic model has therefore been modified so that physically impossible values are not utilised but are replaced with realistic values. The method developed here to constrain the generation of values is to truncate the lower end of the data to zero. Where individual values are negative the random number generator is utilised to generate a replacement value which is positive. To avoid unnecessary bias, the upper end of the data is similarly constrained. The combined effect maintains the nominal mean value v but reduces the range so that the parameter falls within the range $0 \le v \le 2v$ and as such will reduce the variance.

An illustration of the effect of these constraints is shown in Figure 6.1. In this example a nominal mean value of 20 was used with a 95% confidence limit of ±15. The histogram on the left shows the raw distribution obtained from 10^4 samples. The

second histogram to the right shows the same distribution after adjustment to remove the lower and upper tails of data.

Figure 6.1: Effect of constraints (Sample of 10^4 normally distributed values)

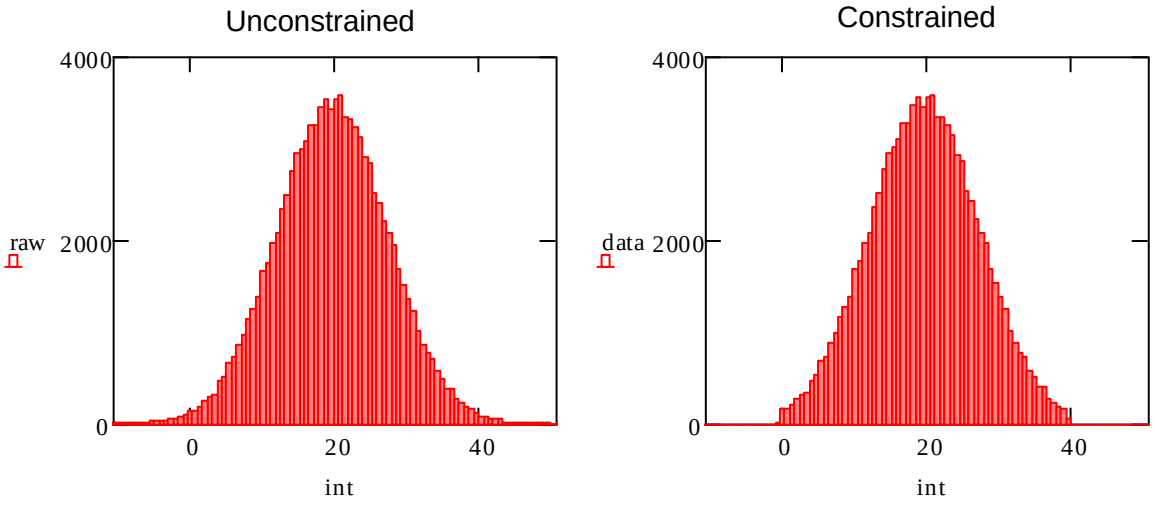

In general, unless the uncertainty in a particular parameter is more than approximately 75% of the value of the parameter (as in this example) the effect of this modification is likely to be negligible. In any case the only effect should be simply to reduce the standard deviation in the parameter under investigation. In this example the unconstrained standard deviation was found to be 7.63 and the constrained standard deviation was 7.42. The only parameters that are likely to be significantly affected therefore are the crush measurements which may be close to or equal to zero.

6.4 Results for a rigid barrier

The analysis of a series of simulations of a vehicle colliding head-on into a rigid barrier reveals much about the way in which uncertainty in the input parameters affect the overall accuracy. Three collisions were simulated assuming uniform crush of 0.1, 0.2 and 0.4 metres respectively. The input data and results obtained from the Mathcad implementation of the model in Appendix J are shown in Appendix K. Assuming 95% confidence limits on the input parameters suggested by Smith and Noga [**108**] and discussed in Chapter 5, the overall uncertainty in the final result is around 19% for the 0.1 m crush reducing to 10% for the 0.4 m crush. As in the previous Chapter, the contribution to overall uncertainty by each of the input parameters is analysed. Again

as noted in the previous Chapter, the overall uncertainty can be found as the square root of the sum of the individual squared uncertainties. The results however can only be an approximation to the overall confidence limits since the exact values found differ on each program run due to the random assignment of input values.

6.4.1 Effect of uncertainty in crush measurements

As suggested by the overall results and confirmed by a detailed analysis, the major contribution to uncertainty in head-on barrier collisions is the uncertainty in the crush measurements. Assuming 95% confidence levels suggested by Smith and Noga [**108**] uncertainty in the crush measurements contributes about 84% of the total uncertainty for the 0.1 m crush and about 45% for the 0.4 m crush. The individual contribution of uncertainty in the crush measurements to the overall result is approximately linear up to the ±0.1 m level. However, extending the uncertainty well beyond this range reveals a non-linear response as shown in Figure 6.2

Figure 6.2: Contribution to uncertainty by variation in crush measurements

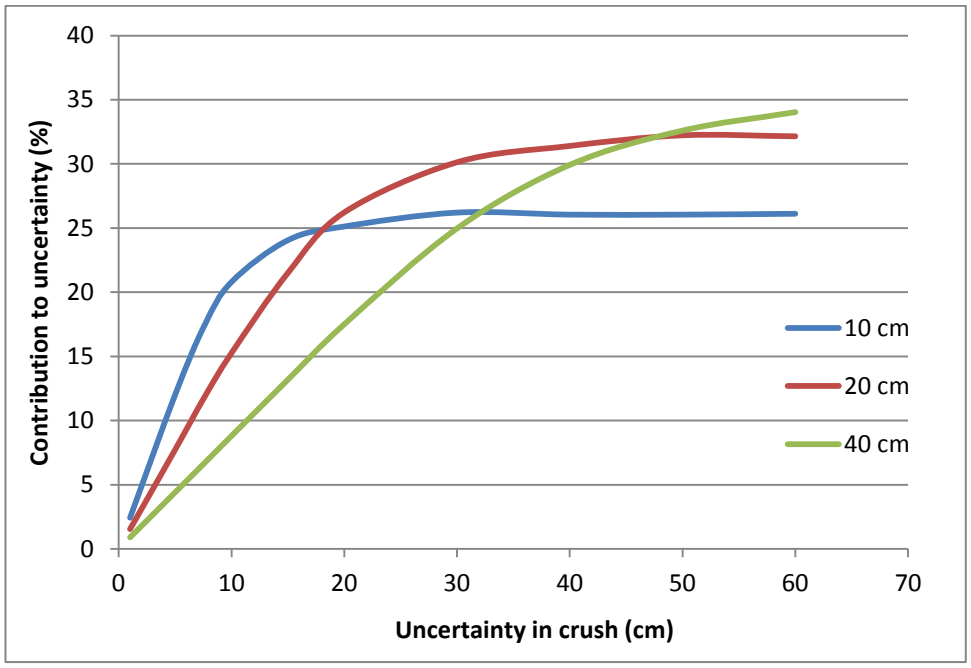

This response at increasing levels of uncertainty is due to the constraint limiting the variability in crush measurements C to the range $0 \leq C \leq 2C$ as programmed into the model and described above. Importantly these results confirm the earlier suggestion that provided the uncertainty in the crush measurement is not greater than about 75% of the nominal crush value, the effect of the constraint is not significant. As might be expected these results show too that at low levels of overall crush, uncertainty in the crush measurements can contribute a significant uncertainty to the overall result. At low levels of overall crush therefore, measurements need to be taken with as much precision as possible.

Although the result can be sensitive to uncertainty in the depth of crush, the Monte Carlo simulations suggest that Δv is not as sensitive to uncertainty in the length of the damaged area. In these simulations the damage length was assigned a nominal value of 1.3 m which is typical of the width of the front of a small car. Assuming an uncertainty of 0.1524 m (6”) in the damage length as suggested by Smith and Noga [**108**] the contribution to uncertainty is approximately 5.6 % and is identical for each of the simulations. The results show a linear response to increasing uncertainty and are illustrated in Figure 6.3

Figure 6.3: Contribution to uncertainty by variation in damage length

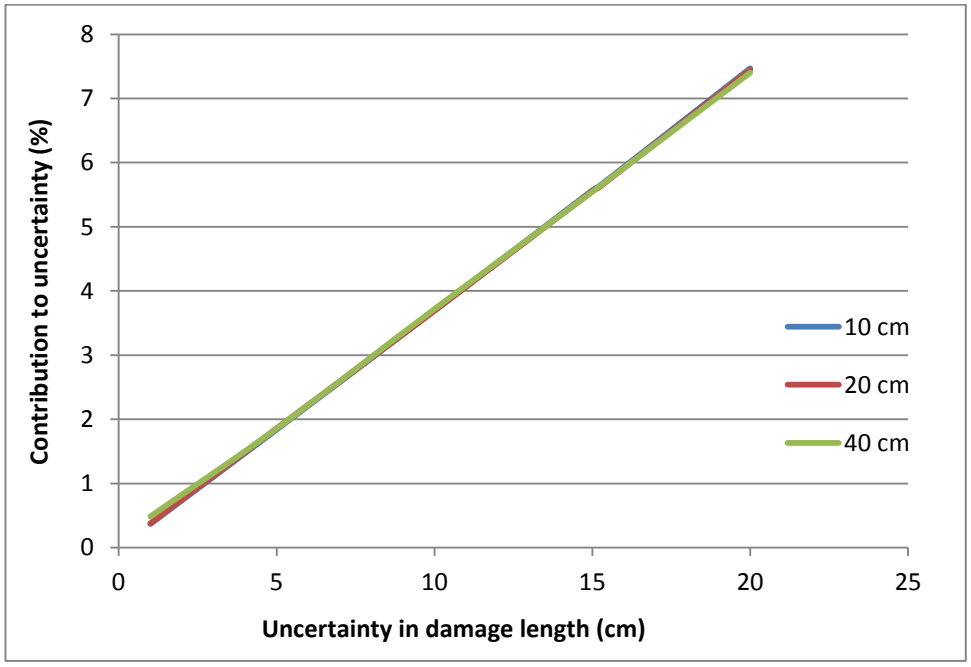

6.4.2 Effect of uncertainty in PDOF

The high contribution to overall uncertainty by crush found in these results conflicts with the findings of the previous Chapter where the major contributor was found to be the uncertainty in the PDOF. In these simulations the contribution by the PDOF is relatively small and represents less than 1% of the total uncertainty in the 0.1 m crush simulation up to about 3% in the 0.4 m crush simulation. Although the proportion of the total uncertainty varies, the numerical value for the contribution to uncertainty for each of the simulations is identical. (A slight variation is expected due to the random nature of the inputs.) The response of uncertainty in the result to increasing uncertainty in the PDOF is shown in Figure 6.4

Figure 6.4: Contribution to uncertainty by variation in PDOF

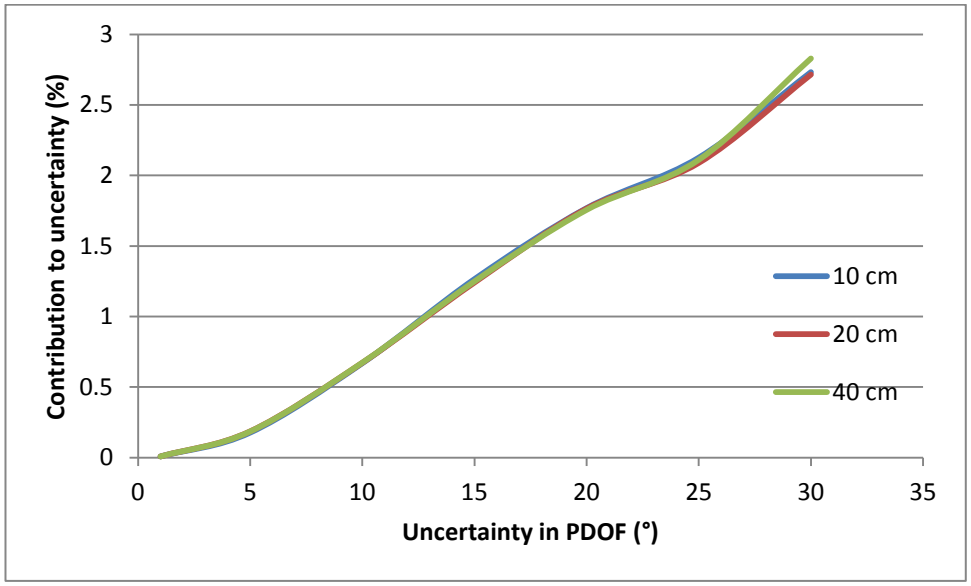

The response to increasing uncertainty in PDOF obtained by these results is clearly non-linear. Further analysis reveals the reasons for this non-linearity and also the reasons for the relatively small contribution to overall uncertainty in these simulations. Variation in the PDOF has two effects. One is the effect on the length of the moment arm, h which in turn affects the numerical value for δ used in the denominator of the CRASH equation as shown by equations (5.13) and (5.15). The second effect is that variation in the PDOF affects the energy adjustment factor. In these analyses the standard energy adjustment factor proposed by McHenry [**65**] is utilised as shown in

equation (5.11). Variation in this factor affects the overall value of E used in the numerator of the CRASH equation. The relative values of each of these terms therefore contributes in a non-linear way to the overall result. In these simulations the nominal PDOF value is zero and variations either side of the nominal value can be used to show the relationship between the changes in the values of δ_1 and E_1. Ignoring restitution, the CRASH equation [equation (2.24)] can be written as

$$\Delta v_1 = \sqrt{\frac{2(E_1 + E_2)}{m_1\delta_1 + \dfrac{m_1^2\delta_2}{m_2}}}\,. \tag{6.1}$$

In collisions such as these where the barrier is assumed to have an effectively infinite mass, the second term in the denominator of equation (6.1) vanishes. In addition the term E_2 is zero since the barrier does not deform to absorb energy. This produces the simplified expression

$$\Delta v_1 = \sqrt{\frac{2E_1}{m_1\delta_1}}\,. \tag{6.2}$$

The change in E_1 as a result of the change in PDOF ($\Delta\theta$) can be found from equation (5.11) as

$$\Delta E_1 = \tan^2(\Delta\theta)\,. \tag{6.3}$$

Substituting equation (5.15) into (5.13) produces an expression for δ_1 so that the change in δ_1 as a result of uncertainty in the PDOF ($\Delta\theta$) can be expressed as

$$\Delta\delta_1 = \frac{d_1^2\sin^2(\Delta\theta + \phi)}{k_1^2}\,. \tag{6.4}$$

Thus the overall change in Δv_1 as a result in the change in PDOF is given by the square root of the ratio ΔE_1 / $\Delta\delta_1$ i.e.

$$\Delta(\Delta v_1) = \sqrt{\frac{k_1^2\tan^2(\Delta\theta)}{d_1^2\sin^2(\Delta\theta + \phi)}} = \frac{k_1\tan(\Delta\theta)}{d_1\sin(\Delta\theta + \phi)}\,. \tag{6.5}$$

In the car to barrier simulations described here the point of application of the impulse lies on the centre line of the vehicle so that ϕ is zero. This leads to a simplification of equation (6.5) giving

$$\Delta(\Delta v_1) = \sqrt{\frac{k_1^2 \tan^2(\Delta\theta)}{d_1^2 \sin^2(\Delta\theta)}} = \frac{k_1}{d_1 \cos(\Delta\theta)}. \tag{6.6}$$

Equation (6.6) shows that error in the estimate of PDOF produces an overall effect which is inversely proportional to the cosine of the error in angle, with a magnitude dependent on the ratio of k_1 / d_1. This is illustrated in Figure 6.5 where a range of ratios for k_1 / d_1 are shown

Figure 6.5: Effect of ratio *k*/*d* with uncertainty in estimate of PDOF (ϕ = 0)

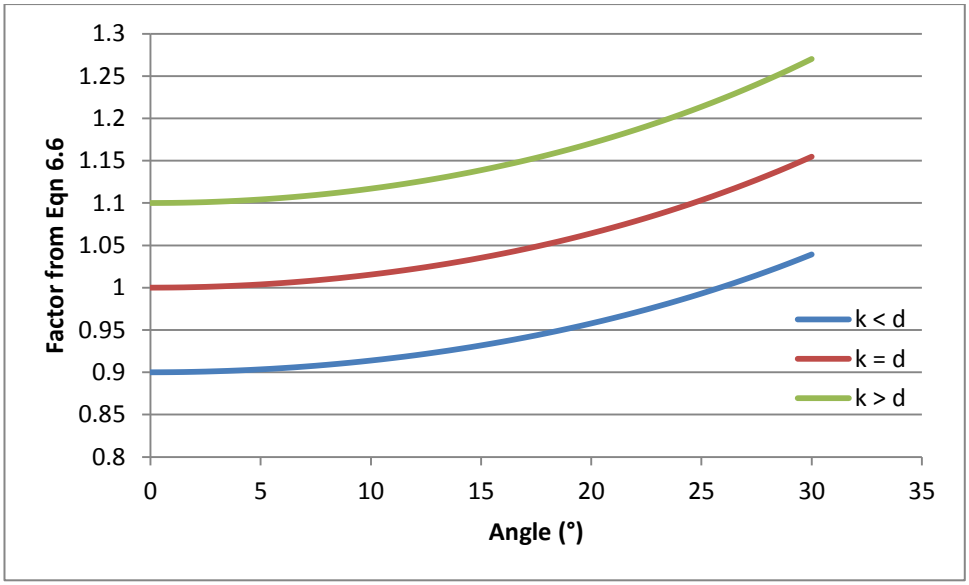

If $k_1 < d_1$ therefore variations in the estimate of PDOF close to the nominal estimate for the PDOF produce a result smaller than the nominal value for Δv_1. The actual angle where the overall response again produces a result equal to the nominal value for Δv_1 can be found from equation (6.6). In Figure 6.5 for example the 90% ratio between k_1 and d_1 indicates that the nominal result for Δv_1 is not reached until the PDOF angle is greater than 25.8° from head-on. In turn this has a significant effect on the shape of the distribution of results from the Monte Carlo simulation. Results from two Monte Carlo simulations showing the distributions obtained from a simulation where k_1 is 120% of d_1 and where k_1 has a value of 80% of d_1 are shown in Figure 6.6

Figure 6.6: Shape of distribution showing dependence on ratio *k*/*d* ($\phi = 0$)

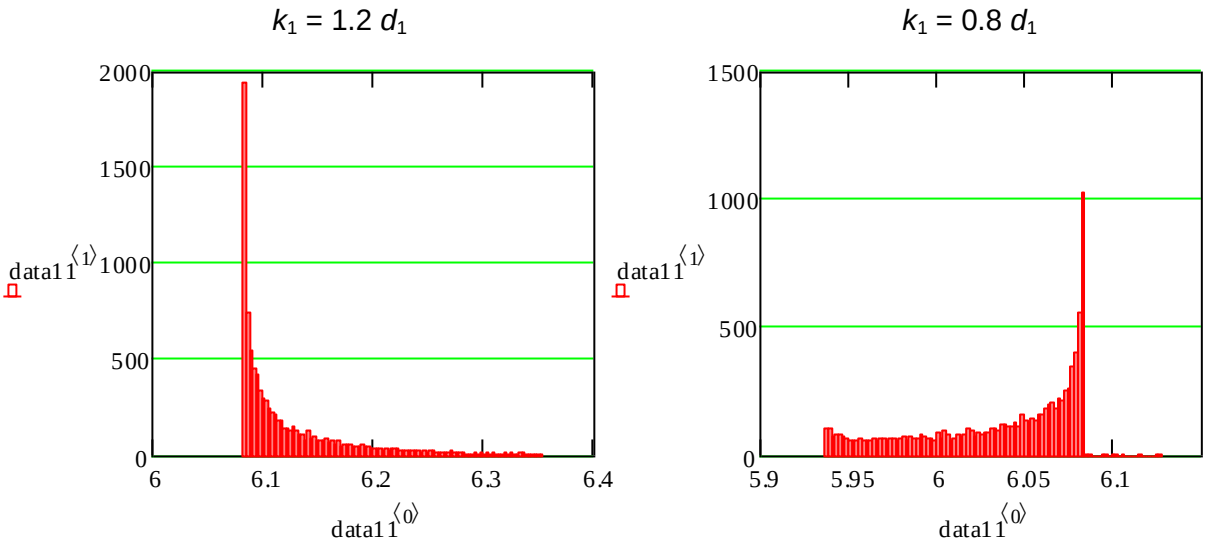

These results can be expressed in a more general way. Where the $k \geq d$ the distribution has a lower bound at the nominal value of Δv and tails off towards an upper bound determined by the uncertainty in the estimation of PDOF. If $k < d$ however there is a small peak below the nominal value with few or no values above the nominal value peak. In both scenarios the mode corresponds to the nominal mean value. The magnitude of uncertainty in the final result due to the uncertainty in PDOF is also found to be dependent on the ratio *k*/*d* as shown in Figure 6.7

Figure 6.7: Dependence of overall uncertainty in PDOF on ratio *k*/*d* ($\phi = 0$)

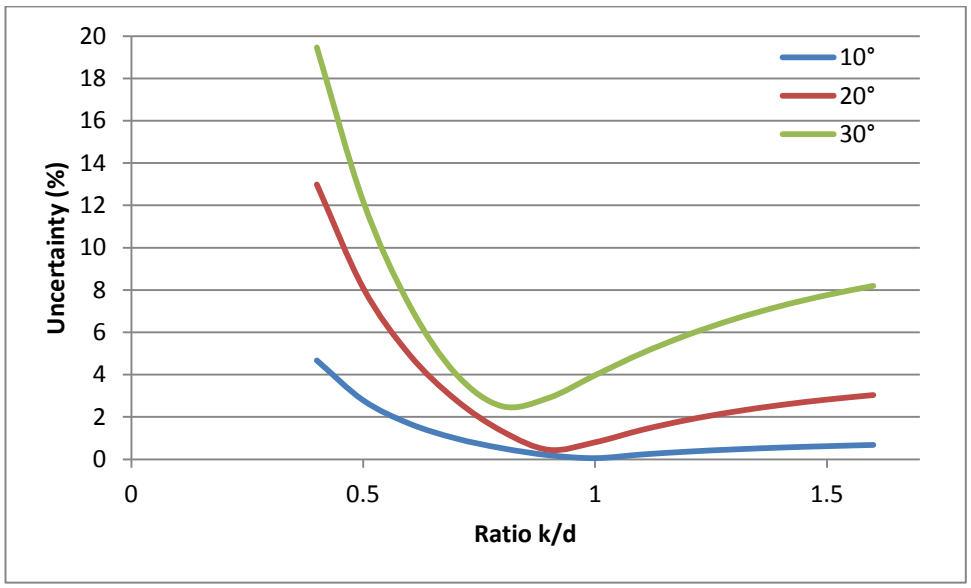

Figure 6.7 shows that if *k* is much larger or smaller than *d* then the overall uncertainty in Δv increases significantly from a minimum value. (The minimum value itself is dependent on the uncertainty in the estimation of PDOF.) The overall uncertainty appears to be more sensitive where *k* is smaller than *d*. In the frontal barrier simulations used in this section, the ratio *k*/*d* is about 0.77. The dependence on sensitivity in PDOF to the ratio *k*/*d* is independent of the actual values for *k* or *d*. This means that the same overall uncertainty introduced by uncertainty in PDOF will apply to all vehicle to barrier collisions with a similar *k*/*d* ratio.

Figure 6.5 and equation (6.6) utilise the simplifying assumption that the angle ϕ was zero as is the case for the frontal barrier impacts considered here. In real-world collisions ϕ is unlikely to be zero as the point of application of the impulse is unlikely to lie of the centre line of a vehicle. The inclusion of a non-zero value for ϕ as shown in equation (6.5) alters the dependence of overall uncertainty on the ratio *k*/*d*. For example utilising a 10° value for ϕ produces the graph shown in Figure 6.8

Figure 6.8: Effect of ratio *k*/*d* with uncertainty in estimate of PDOF (ϕ = 10°)

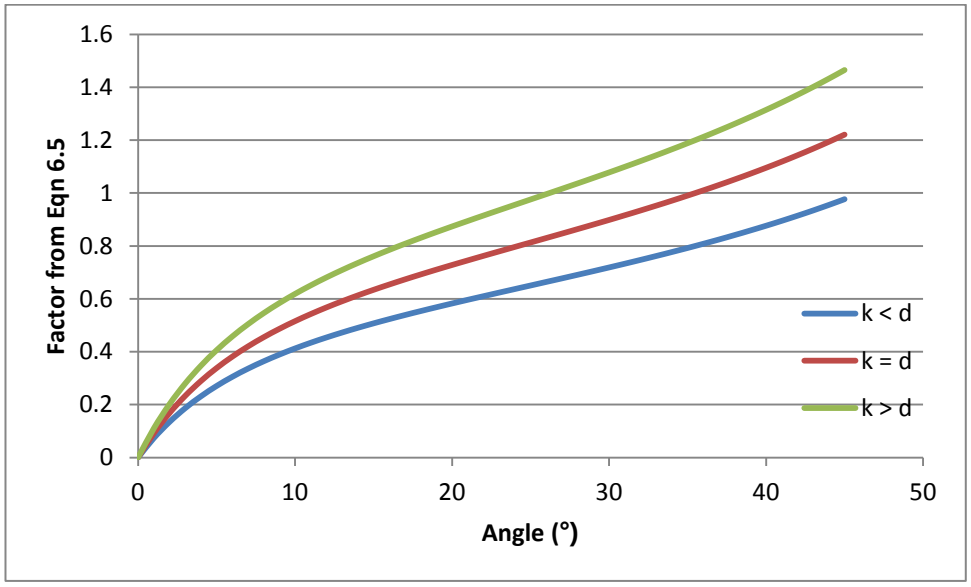

It can be seen from Figure 6.8 that where ϕ is non-zero variations in the estimate of PDOF close to the nominal estimate for the PDOF produce a result lower than the nominal value for Δv regardless of the ratio *k*/*d*. Larger values for ϕ produce a more

linear series of curves. As a consequence the shape of the distribution of results from the Monte Carlo simulations alters so that the mode no longer corresponds to the nominal mean value. The modes tend to be somewhat lower and the data more dispersed than when ϕ is zero. Figure 6.9 shows the results from two Monte Carlo simulations showing the distributions obtained where k is 120% and 80% of d respectively

Figure 6.9: Shape of distribution showing dependence on ratio k/d (ϕ = 10°)

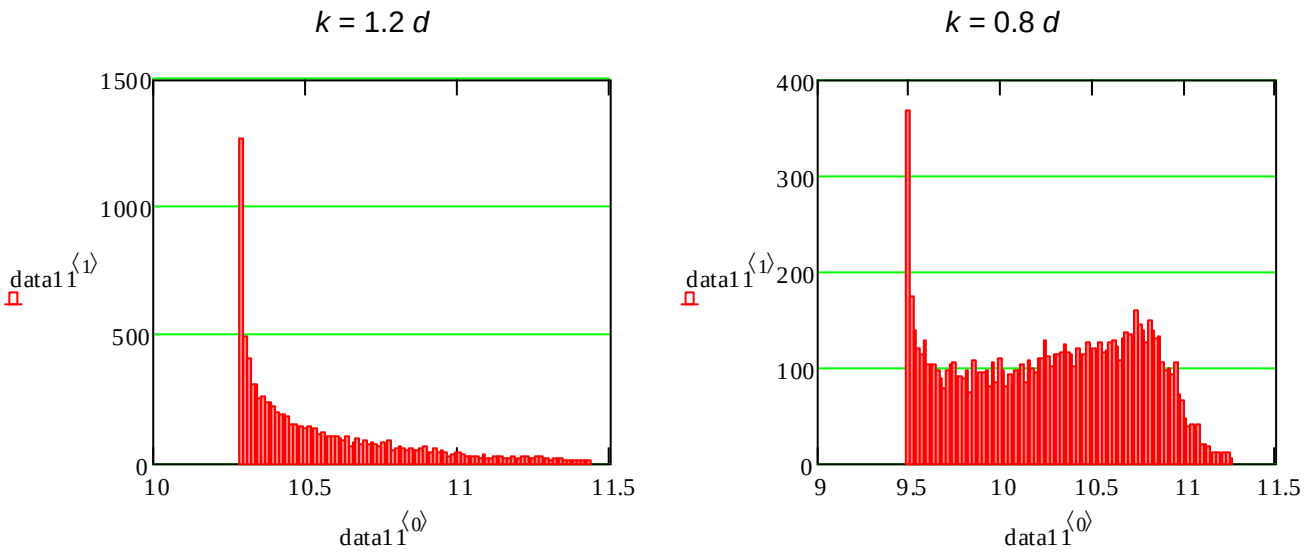

In these particular simulations, when k = 1.2 d the nominal mean value for Δv is 10.4 ms^{-1} and when k = 0.8 d Δv is 10.3 ms^{-1}. It can be seen therefore that the mode in each of the histograms shown in Figure 6.9 underestimate the nominal mean values. It can also be seen that when $k < d$ the discrepancy between the nominal mean value and the mode value tends to be greater than when $k > d$. The mean Δv value from Monte Carlo simulation also underestimates the nominal Δv when $k < d$ but overestimates when $k > d$.

The overall sensitivity of Δv to changes in PDOF where ϕ is non-zero follow similar curves to those shown in Figure 6.7. However the overall uncertainty is greater and the lower bound less pronounced. In addition the lower bound is displaced towards the right towards higher values for the ratio k/d. The dependence of overall uncertainty where ϕ is non-zero is illustrated in Figure 6.10

Figure 6.10: Dependence of overall uncertainty in PDOF on ratio *k*/*d* (ϕ = 10°)

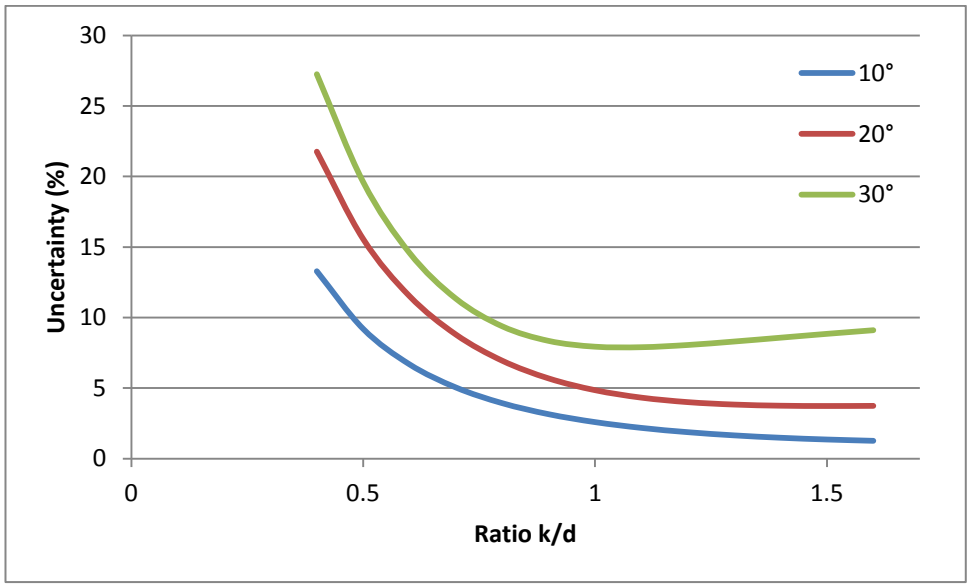

Although the discussion above is directly applicable to frontal collisions only, a similar argument can be applied to the rear and sides of a vehicle and a similar distribution can be expected. In two vehicle collisions, the overall uncertainty will be partially dependent on both of the *k*/*d* ratios and to a lesser extent the values for ϕ. It follows therefore that if the two *k*/*d* ratios are both close to unity then Δv is not particularly sensitive to uncertainty in the PDOF. If one or both of the *k*/*d* ratios are significantly greater or less than unity however, then the same uncertainty in PDOF will produce a greater uncertainty in the overall result.

An analysis of the generic vehicle data provided by Siddall and Day [**98**] as part of their update to the vehicle stiffness coefficients shows that the radius of gyration (*k*) varies from about 1.25 m for small cars up to about 1.55 m for large cars. The range of probable values for *k* is therefore relatively small. The range of distances of the point of application to the centre of mass (*d*) is dependent to a large extent on the part of vehicle which has been struck and the size of the vehicle. The front and rear of a vehicle are somewhat further away from the centre of mass than either side of the vehicle. A collision which strikes a vehicle on the side close to the centre of the vehicle is likely to produce a small value for *d* and consequently a relatively large *k*/*d* ratio. It can be expected from this analysis therefore that some impacts are likely to be more sensitive to uncertainty in the PDOF.

6.4.3 Effect of uncertainty in position of point of application

The simulations performed here suggest that the overall uncertainty in Δv is not particularly sensitive to changes in the position of the point of application. The overall contribution to uncertainty is less than 1% for a 0.2 m potential error in estimating the point of application. The results obtained by these simulations are identical for all three crush depths and are shown in Figure 6.11

Figure 6.11: Contribution to uncertainty by variation in point of application

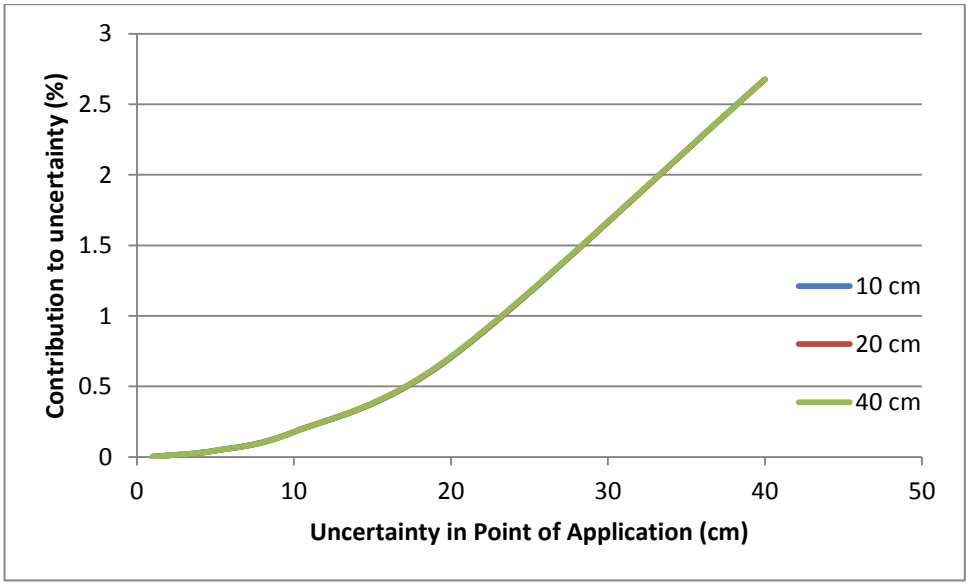

Uncertainty in the point of application affects the length of the moment arm (h) as shown by equation (5.15) and reproduced below

$$h = d\sin(\theta + \phi)\,. \tag{6.7}$$

As the nominal values for θ and ϕ are both zero in these simulations, the length h may be expected to be zero regardless of the actual value for d. As explained in the previous Chapter however, permitting a simple bound on the angular value of ϕ has the effect that the lateral error in h is then also dependent upon the length of d. The model here constrains variation in the angle ϕ so that the lateral variation is the same as the variation in d. It follows that in this model the value of the angle ϕ is also dependent on the uncertainty in d which produces a non-zero value for h. The consequent

uncertainty in h affects the magnitude of δ which appears in the denominator of equation (6.2).

6.4.4 Effect of uncertainty in mass

The results of the simulations performed here confirm the earlier findings of Smith and Noga [**108**] to the extent that the result does not appear to be particularly sensitive to uncertainty in the measurement of mass. Assuming the same confidence limit of 50kg as suggested by Smith and Noga, the contribution to the overall uncertainty is less than 2% and is identical for all three simulations. The results show a linear response to increasing uncertainty and are illustrated in Figure 6.12

Figure 6.12: Contribution to uncertainty by variation in mass

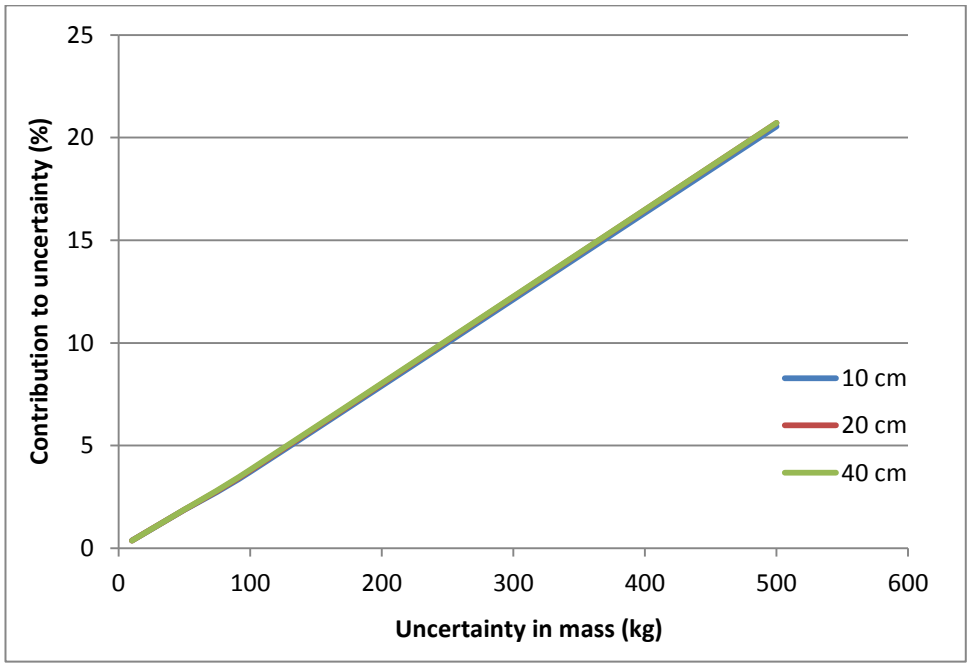

6.4.5 Effect of uncertainty in stiffness coefficients

Smith and Noga [**108**] determined that an uncertainty of 10% in the stiffness coefficients produced errors of between 2 to 6% in the calculation of Δv. The simulations performed here confirm these results and yield significant new ones. As may be expected the response to uncertainty is dependent on the crush

measurements. The results obtained by varying the individual stiffness coefficients are shown below in Figure 6.13 and Figure 6.14

Figure 6.13: Contribution to uncertainty by variation in *A* stiffness coefficient

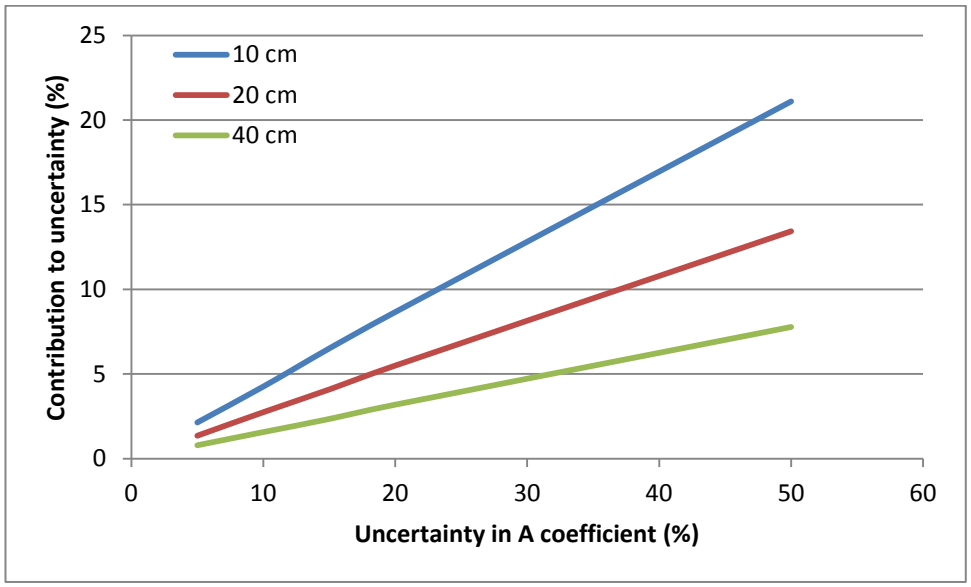

Figure 6.14: Contribution to uncertainty by variation in *B* stiffness coefficient

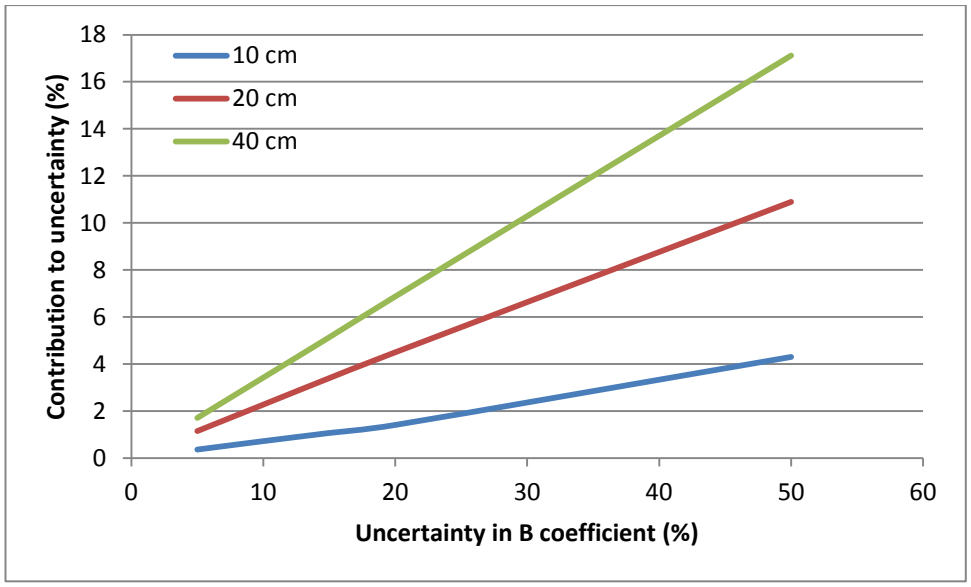

As can be seen the overall uncertainty responds approximately linearly to increasing uncertainty in each of the stiffness coefficients. At low levels of crush the overall uncertainty is dominated by the potential error in the *A* stiffness coefficient. With higher levels of uncertainty the *B* stiffness coefficient becomes dominant. This is due to the behaviour of the equation to determine the work done in causing crush. As outlined earlier, Singh [**99**] shows that the work done in causing crush can be determined from equation (2.35). This may be rewritten as the sum of three terms, i.e.

$$E = \frac{LA\eta}{(n-1)2} + \frac{LB\kappa}{(n-1)6} + \frac{LA^2}{2B} \tag{6.8}$$

where

$$\eta = \sum_{i=1}^{n-1}[C_i + C_{i+1}], \qquad \kappa = \sum_{i=1}^{n-1}\left[C_i^2 + C_iC_{i+1} + C_{i+1}^2\right]. \tag{6.9}$$

The first and second terms in equation (6.8) determine the contributions made by the *A* and *B* coefficients respectively with variable crush measurements and the third term is a constant which is not dependent on crush. The contribution by each of the terms can be plotted against increasing crush to determine the relative contribution made by each term as a function of crush depth. This is illustrated in Figure 6.15

Figure 6.15: Contribution by each term to total energy

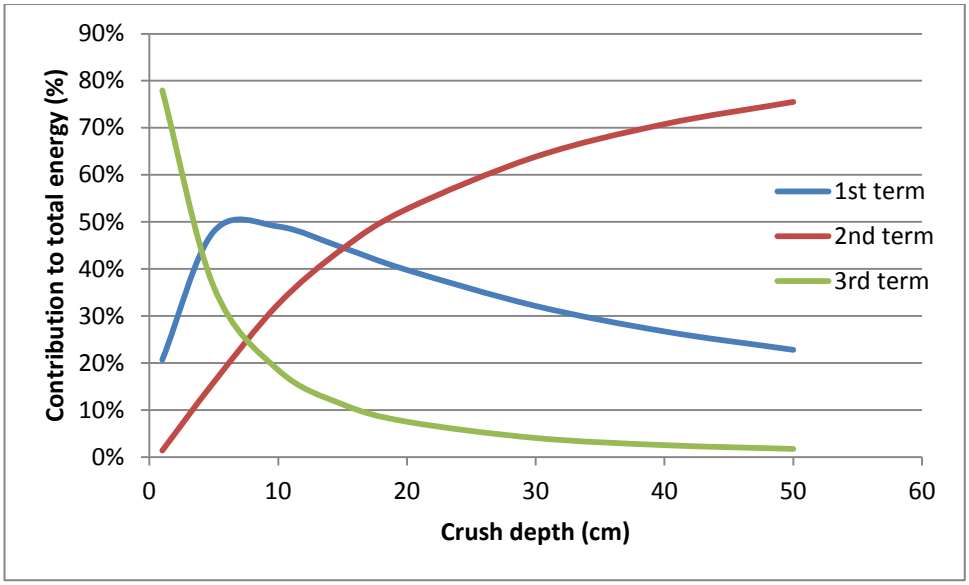

Figure 6.15 shows that that the relative contribution by the constant third term rapidly falls with increasing crush. The 1st term peaks where the point where the contribution by the 2nd and 3rd terms are equal and then falls away leaving the 2nd term as the dominant contributor above a certain critical value. Of minor interest is that assuming a uniform crush depth, this critical value is reached when the crush depth reaches 2*A*/*B* and the 1st term peaks where crush depth is equal to *A*/*B*. This indicates that there is a certain level of crush below which uncertainty in the A coefficient will be dominant and above which uncertainty in the B coefficient will be dominant. Again assuming uniform crush, this level is at 3*A*/*B*.

6.5 Monte Carlo simulation of RICSAC tests

The Monte Carlo simulation shown in Appendix J was applied to the RICSAC series of crash tests. A similar approach is adopted as outlined in the previous chapter. Figure 5.8 shows in blue the input parameters which are measured or otherwise determined by the user. Each of the input parameters has an uncertainty associated with it. By eliminating the uncertainty in all inputs except for the parameter under investigation the effect of uncertainty in each input parameter can be investigated. Suitable ranges for each of the input parameters are shown in Table 5.13 and are chosen to match those used for the analysis in the previous Chapter.

The results from these simulations are shown in Appendix L. The overall uncertainty in DeltaV as shown in Table L.1 is calculated using the 95% confidence levels suggested by Smith and Noga [**108**] As in the previous Chapter, since no uncertainty was ascribed by Smith and Noga to the position of the point of application (*d*), a 95% confidence level identical to the crush measurement uncertainty was used, i.e. ±3" (0.0762 m). A 95% confidence level of 0.1 m was assigned to the uncertainty in the radii of gyration (*k*) measurements. As noted earlier, the overall uncertainty can be found as the square root of the sum of the individual squared uncertainties. The results however can only be an approximation to the overall confidence limits since the exact values found differ on each run of the simulation due to the random assignment of input values.

In general the results from this analysis match closely those obtained from the analysis in the previous Chapter. The same pattern is evident showing that some impact configurations appear to be inherently more sensitive to uncertainty in the input

parameters than others. In addition it can be seen that the major contributor is the uncertainty remains the uncertainty in PDOF. However the mean contribution to overall uncertainty in this parameter is reduced from the 61% found using the analytical model to 52%. The mean contribution made by uncertainty in the crush measurements is increased from 9% using the analytical model to 15% using the Monte Carlo model. These differences are discussed in more detail below. Since uncertainty due to the remaining parameters is virtually the same, these other parameters are not considered in detail. A comparison between the two sets of results is shown in Figure 6.16

Figure 6.16: Comparison of percentage contributions to uncertainty

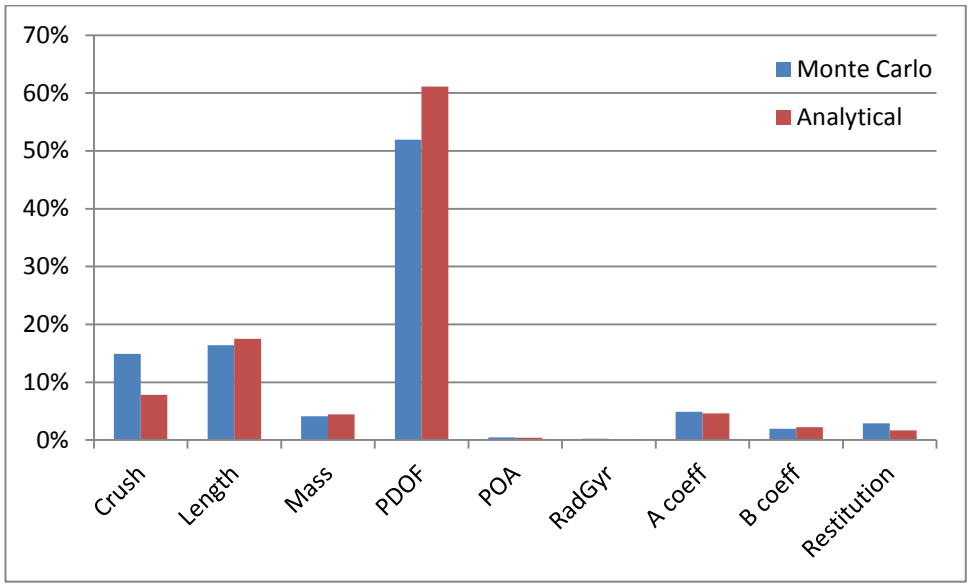

The results shown in Figure 6.16 show that even if there are differences between the models it is clear that both models rank the effect of uncertainty in the same order. So in both models uncertainty in PDOF is by far the most important parameter, followed by length and the crush measurements.

6.5.1 Contribution by uncertainty in crush measurements

The contribution by uncertainty in the crush measurements is somewhat higher in the Monte Carlo simulation than in the analytical model. In all cases and for all levels of uncertainty in crush, the Monte Carlo simulations predict a higher contribution to overall uncertainty. Uncertainty in the crush measurements directly affects the values for η

and κ determined by equation (6.9) and these parameters are subsequently used to determine the crush energy in equation (6.8). Analysis of the results derived from equation (6.9) show that the Monte Carlo model generates mean values for κ which are higher than the nominal mean value and that there is a small positive skew. This appears to be due to the fact that the κ term is the sum of squared and therefore positive values.

Figure 6.17 shows the difference between Monte Carlo model and analytical model for each of the RICSAC tests at three levels of crush uncertainty, 0.01, 0.05 and 0.10 metres.

Figure 6.17: Difference in contribution by crush uncertainty between models

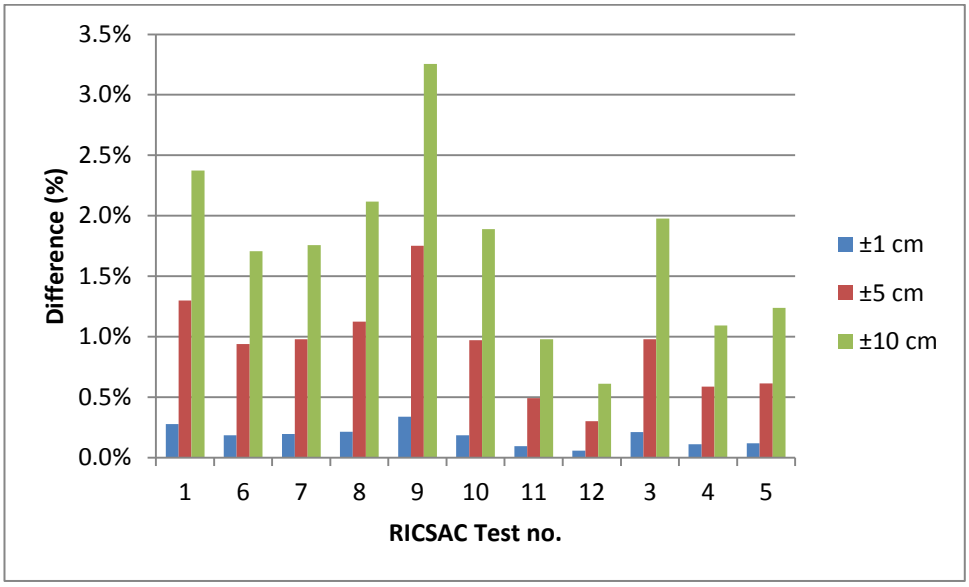

The difference between the actual contributions to overall uncertainty range from less than 1% to just over 3.2% even for uncertainty in crush of 0.1 m. The worst case from this analysis was RICSAC test 9 where the overall contribution to uncertainty was 12.7% in the Monte Carlo simulation and 9.5% in the analytical model. For this particular collision this represents a difference of less than 0.2 ms^{-1} in the uncertainty in Δv_1. Lower levels of uncertainty in crush produce a much smaller overall contribution. It is considered therefore that although there is clearly a difference between the analytical and Monte Carlo models, for practical purposes that difference can be considered to be negligible.

6.5.2 Contribution by uncertainty in PDOF

The effect of uncertainty in the PDOF averaged over all the collisions is 52% in the Monte Carlo simulations compared with 61% in the analytical model considered in the previous Chapter. The results shown in Appendix L show a much greater variation between individual collisions as shown in Figure 6.18

Figure 6.18: Difference in contribution by uncertainty in PDOF between models

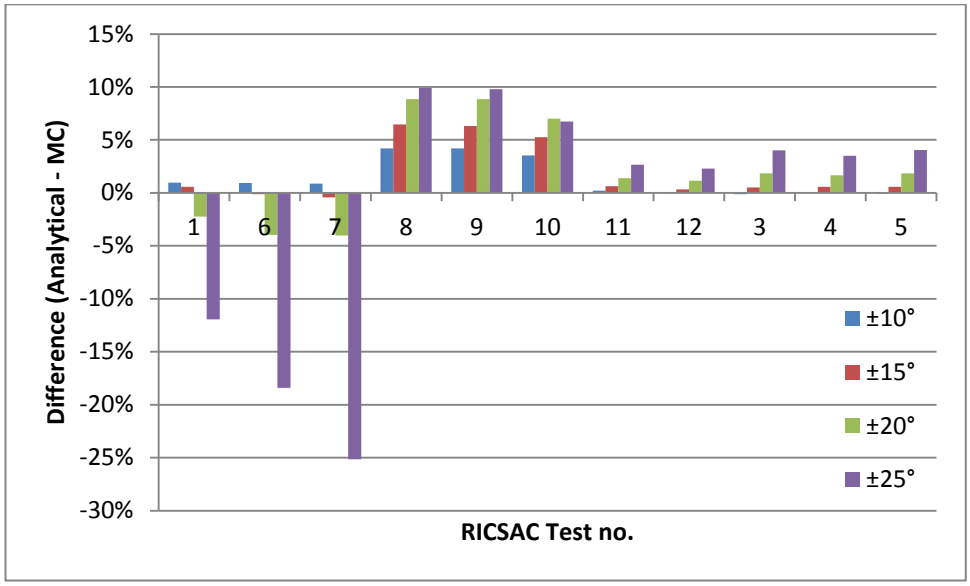

The difference between the effect of uncertainty in the PDOF is clearly dependent on impact configuration. The green bars in Figure 6.18 show the overall uncertainty at the Smith and Noga level of ±20° At this level of uncertainty the Monte Carlo simulations overestimate the uncertainty calculated by the analytical model 60° front to side impacts by 2 – 4%. However in the 90° front to side impacts the Monte Carlo simulation underestimates the analytical model by 7 – 9%.

As outlined previously uncertainty in the PDOF affects the equation used to calculate Δv in two ways. One effect is that variation in PDOF alters the value of h which in turn affects δ. The second effect is that variation in the PDOF alters E through the energy adjustment factor. The overall effect on the crash equation [equation (2.24)] is that changes in δ and E can add constructively or partially cancel each other as was shown previously when considering car to barrier collisions. This correlation between the E and δ is not included in the analytical model and can therefore can be expected to affect those results. Eliminating the effect of δ and E separately in both the analytical

and Monte Carlo models allows the effect of variation in PDOF on each parameter to be examined. A comparison between the contribution to uncertainty predicted by both models for the parameters δ and E separately are shown in Figure 6.19 and Figure 6.20.

Figure 6.19: Comparison of PDOF contribution to uncertainty (δ only)

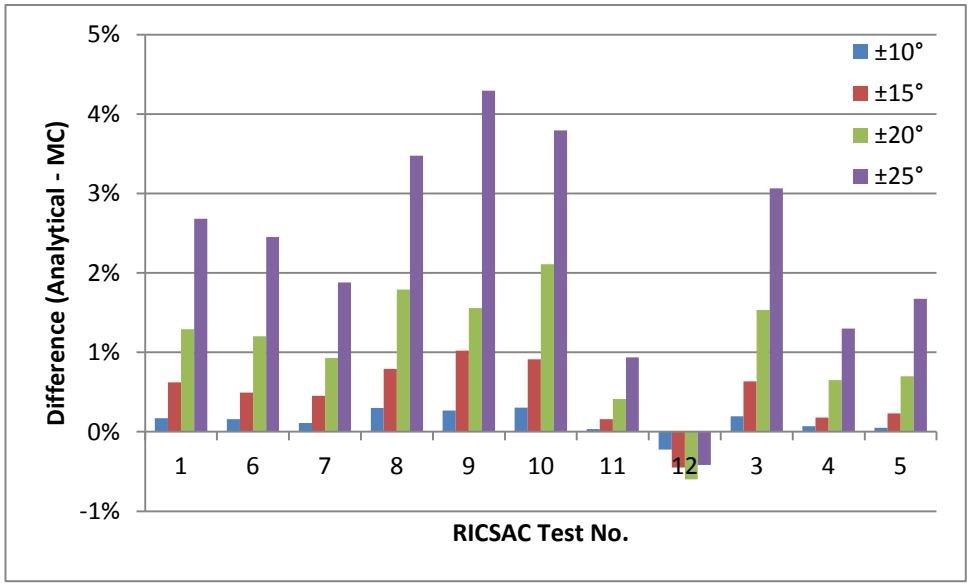

Figure 6.20: Comparison of PDOF contribution to uncertainty (E only)

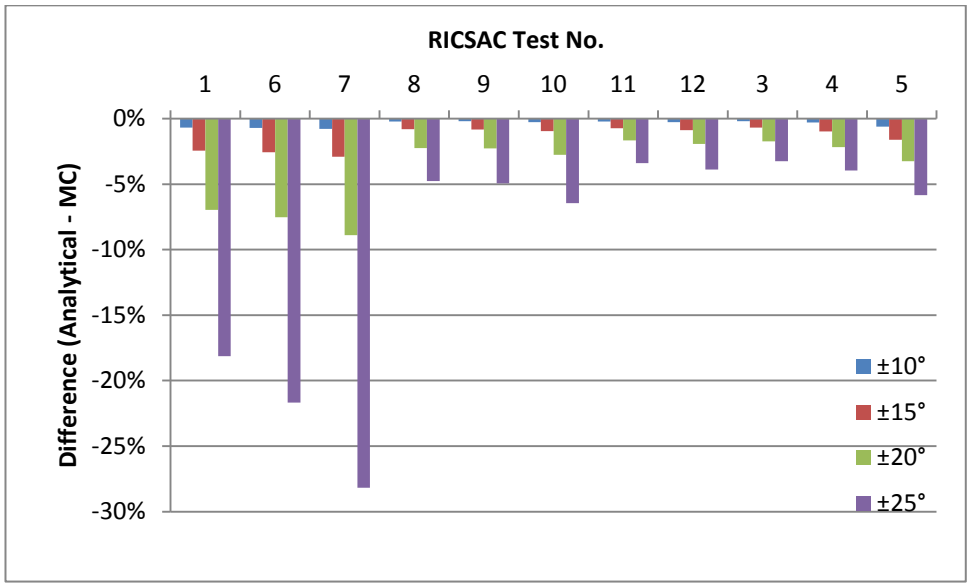

If the parameters δ and E were completely independent the combined response would be the sum of the effects shown in Figure 6.19 and Figure 6.20. The fact that the actual response is as shown in Figure 6.18 indicates the correlation between the two parameters. It is clear too that the major contributor to overall uncertainty is due to the energy adjustment factor as shown in Figure 6.20. For direct comparison with the analytical model and existing studies in this area, the energy adjustment factor used here is the commonly used factor proposed by McHenry [**65**] and shown in equation (5.11). In the results presented in Appendix L the effect of equation (5.11) is unconstrained. As discussed in Chapter 4, the energy adjustment proposed by McHenry is normally constrained so that it does not exceed 2.0 Constraining the Monte Carlo simulation in a similar manner reduces uncertainty in the 60° front to side impacts substantially, as it did with the analytical method described in the previous Chapter. As with the analytical model, such a constraint has little effect on the other impact configurations. This result is shown in Figure 6.21

Figure 6.21: Overall uncertainty grouped by impact type

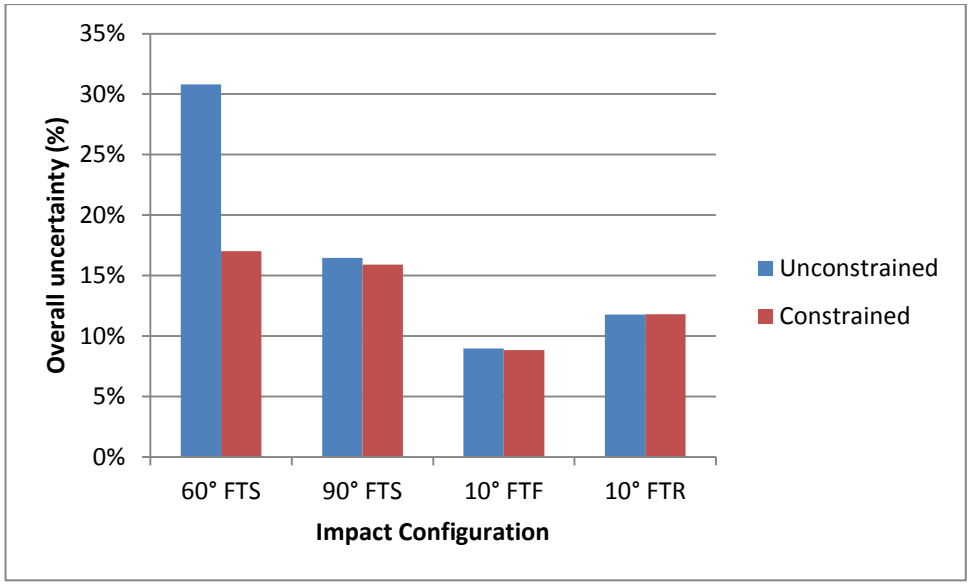

As shown in Figure 6.21 the contribution to uncertainty by PDOF using a constrained energy adjustment factor shows some dependence on impact configuration as previously noted. Figure 6.22 shows a more detailed analysis of this effect with varying levels of uncertainty in the PDOF. Thus a ±20° uncertainty in the PDOF suggests a contribution of between 5 to 8% to overall uncertainty and a contribution of between 10

to 13% for front to side (FTS) impacts. The contribution made by uncertainty in the PDOF is smaller for front to front (FTF) and front to rear (FTR) impact configurations.

Figure 6.22: Contribution by PDOF to total uncertainty grouped by impact type

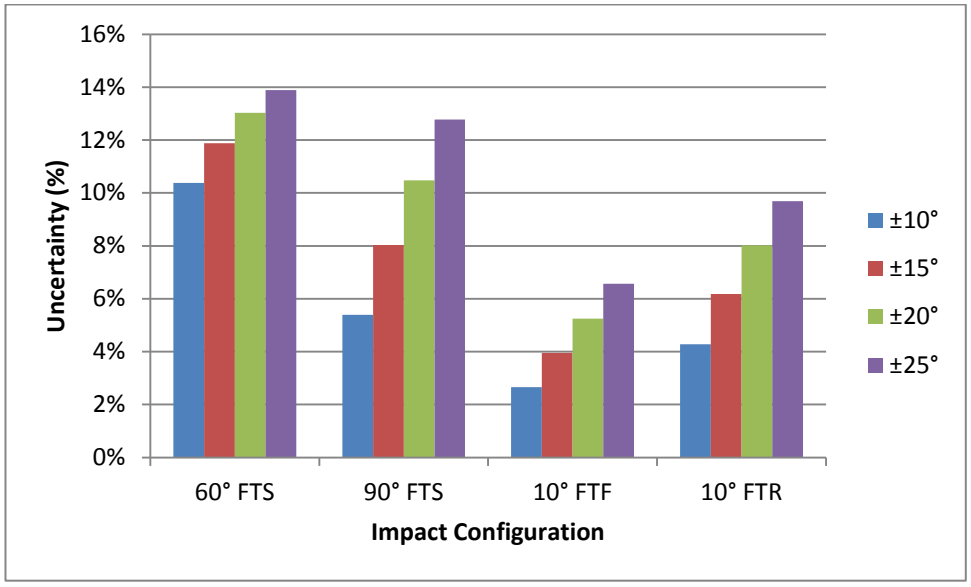

The contribution made by uncertainty in the PDOF tends to dominate overall uncertainty. It is instructive therefore to consider the contribution to uncertainty made by all the parameters excluding uncertainty in the PDOF. Figure 6.23 shows a comparison of the overall (constrained) uncertainty including and excluding the effects of uncertainty in the PDOF.

Figure 6.23: Overall uncertainty including and excluding PDOF by impact type

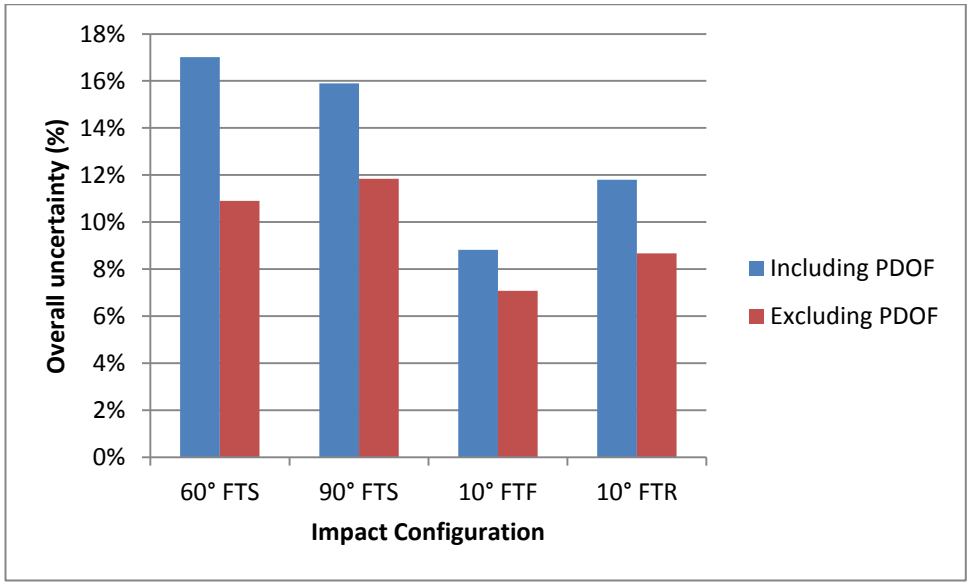

In this analysis front to side (FTS) impacts remain significantly more sensitive than front to front (FTF) or front to rear (FTR) impacts whether or not the PDOF is included in the analysis. The contribution made by variance in the other parameters accounts suggests that even if uncertainty in the PDOF were to be eliminated completely, FTS impacts appear to have an overall uncertainty of around 11 – 12% whereas FTR and FTF impacts have an uncertainty of around 7 – 9%. It is also noted that the slight ~1% difference between the FTS 60° and 90° impacts appears to be due to the inclusion of uncertainty in the coefficient of restitution (e_p) for the three FTS 90° impacts.

6.6 Determining overall uncertainty per-collision

The ultimate aim in forensic collision investigation is the determination of the vehicle speeds in a particular collision. For other purposes it may be sufficient to determine a probable range of results for a statistically large data set. For forensic work however, the actual speeds and associated uncertainty is required. This theme is developed in the next Chapter, where actual vehicle speeds are determined. In this Chapter however the uncertainty associated with the change in velocity is under investigation.

Figure 6.24: Comparison of overall uncertainty (constrained PDOF)

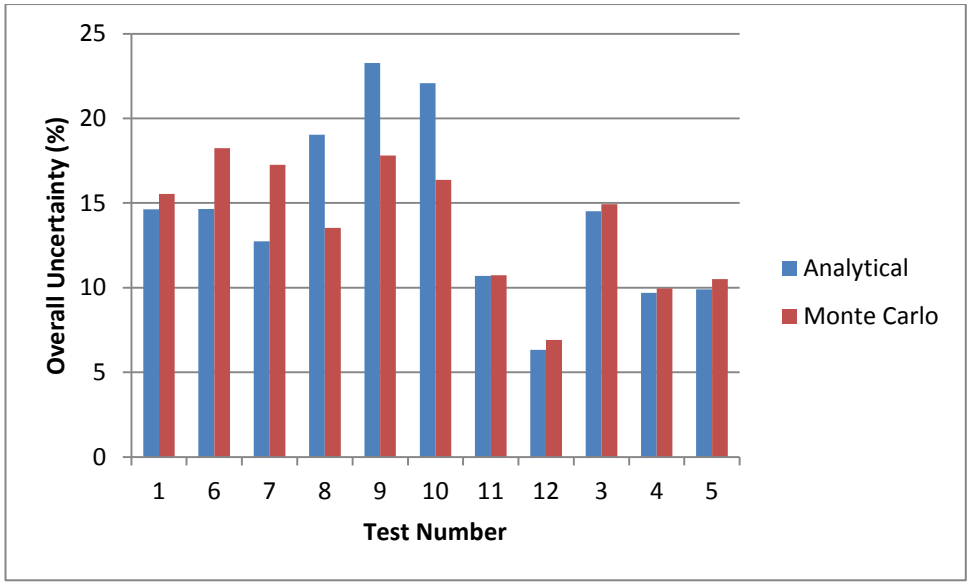

Figure 6.24 shows a direct comparison between the overall uncertainty using the analytical approach in the previous Chapter and the Monte Carlo method for each of

the RICSAC test collisions. When grouped by impact type the differences become more apparent as shown in Figure 6.25

Figure 6.25: Comparison between models by impact type (±20° PDOF)

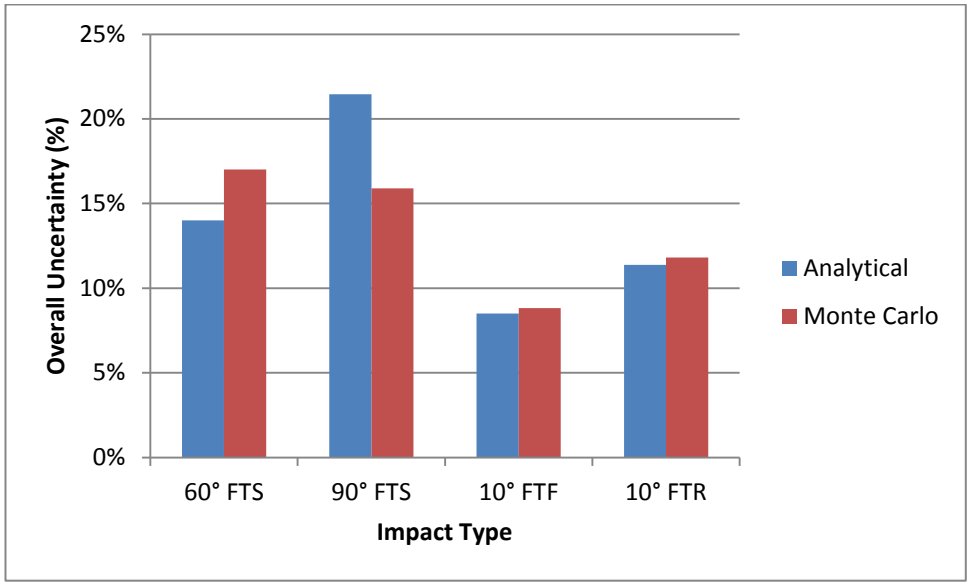

Although the FTF and FTR impacts produce very similar results (about 0.4%), there remains a difference between the results obtained from each of the models in the front to side impacts (3 – 6%). This difference can be alleviated by reducing the uncertainty in the PDOF to ±10° as shown in Figure 6.26

Figure 6.26: Comparison between models by impact type (±10° PDOF)

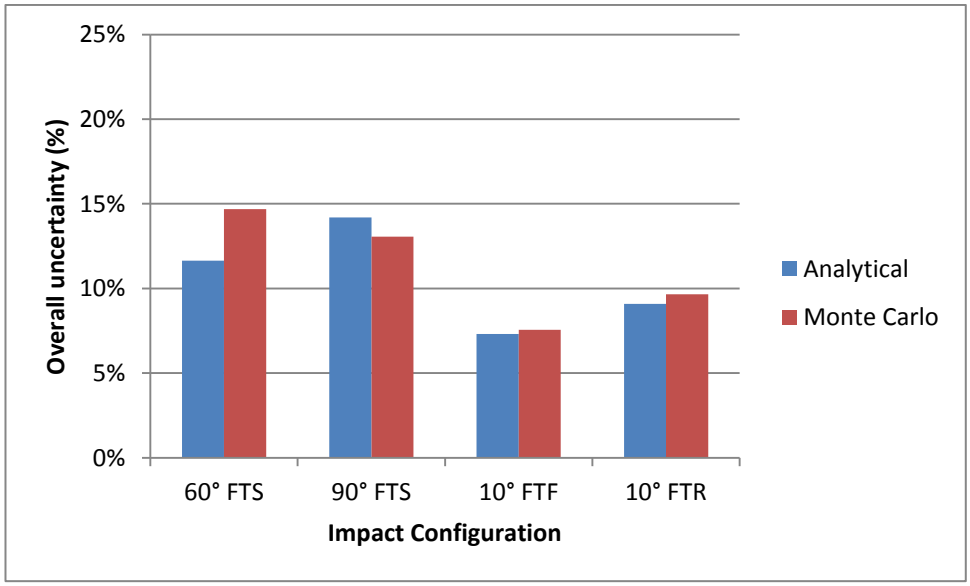

Reducing uncertainty in the PDOF to ±10° reduces the difference between the analytical and Monte Carlo models. It is noted that the remaining differences in the 60° FTS impacts (about 3%) appear to be due to the use of the constrained energy adjustment factor described previously in section 5.5.2. It is apparent that the constraint applied in this section reduces the variability in the adjustment factor significantly more than the corresponding constraint applied in the Monte Carlo model. It appears that this is due to the way in which the constraint described in equation (5.17) applies equally to truncate both the upper and lower extents of variability in the adjustment factor. For example, in RICSAC 7 the nominal adjustment factor for vehicle 2 is found to be 1.85 The non-constrained approach produces a standard deviation for the adjustment factor of 0.3. However the constrained approach reduces the standard deviation in the adjustment factor to around 0.08. This subsequently limits the uncertainty in the crush energy for vehicle 2 to ±8% as compared with ±32% in the unconstrained version. The corresponding constrained uncertainty in crush energy from the Monte Carlo method is approximately ±28% Where this constraint is not applicable, such as for vehicle 1 in the same collision, the analytical model provides a limit on uncertainty in crush energy to ±7.9% whereas the Monte Carlo model suggests ±8.6%; a much closer correspondence. It may be prudent therefore to consider further work on the analytical constraint in an effort to resolve these differences.

6.7 Summary

These results here suggest that front to side (FTS) impacts are inherently less accurate and therefore produce a greater range of overall uncertainty than front to front (FTF) or front to rear (FTR) impacts when using the same variance in input parameters. The reasons for this are complex and are dependent on a combination of the effects explored in section 6.4. The main effects include the uncertainty in crush, the contribution to uncertainty by the *A* and *B* coefficients each of the terms in the crush damage equation and the effect of variability in the PDOF. All of these parameters respond in a non-linear manner and it has not been possible to determine a suitable correlation between any one factor and overall uncertainty.

Assuming Smith and Noga's [**108**] input uncertainties, overall uncertainty in DeltaV is about 15 – 17% for front to side impacts reducing to 9 – 12% for front to front or front to rear impacts. The largest individual contribution is that due to uncertainty in PDOF.

This is consistent with Smith and Noga's earlier conclusion and this new analysis generates significant new results. A reduction in this one parameter therefore is likely to have the greatest overall effect. Reducing uncertainty in the PDOF to ±10° reduces overall uncertainty to 13 – 15% for front to side impacts and 8 – 10% for end to end impacts.

It should be appreciated however that this analysis is based on a relatively small data set with only two or three test collisions in each category. Larger data sets may produce different results. Additional work may be considered in this area to validate the conclusions reached.

The analytical model produces results comparable to the Monte Carlo method. It is clear too that the two methods produce closer results if the uncertainty in PDOF is minimised. In the next Chapter a method is presented which allows the actual velocities of vehicles to be determined. A useful side effect to this method is that it enables better estimates to be made of the PDOF values applicable in a particular collision. The PDOF values used in this and the previous Chapter were determined using this technique. The technique essentially involves adjusting the PDOF values so that predicted post-impact trajectories match those determined from field data. It is found that even small variations in PDOF (around 0.1°) can produce significant changes in the post-impact trajectories so that estimates of PDOF to within ±1° are possible.

Chapter 7

Determination of actual vehicle speeds from change in velocity data

7.1 Objectives

In this Chapter the work of the previous Chapters is extended and a method is developed whereby the actual speeds of the vehicles in a collision may be determined from change in velocity data. For practical collision investigation purposes it is anticipated that change in velocity data will generally be derived from the CRASH equation as described earlier. However change in velocity data from any other suitable source can be used. The method relies solely on conservation laws and is also applicable to situations where the coefficient of restitution is non-zero. An extension to the method is also developed which allows a better estimate to be made of the principal directions of force applicable to each vehicle.

The material presented in this Chapter forms the basis of a paper published in the Journal of Automobile Engineering Proc IMechE Part D 225 (1) (2011).

7.2 Introduction

As outlined in Chapter 2 the scientific reconstruction of road traffic collisions often requires the calculation of the speeds of vehicles involved. An estimate of the actual vehicle speeds is of prime importance to forensic practitioners as for the courts the

speed of the vehicles is usually a key factor in the allocation of liability or in the decision about criminal offences. The determination of actual speeds have traditionally centred on the analysis of tyre and other marks on the road surface to model the behaviour of the vehicles involved and their speeds. With the increased use of anti-lock braking systems (ABS), tyre marks are becoming less common. The presence of water on a road surface also decreases the chance of suitable tyre marks being found on the road surface. In situations where there are no tyre marks, any model based on the analysis of those marks cannot succeed and the determination of pre-impact speeds in particular becomes more problematic. There are a variety of methods that provide information on vehicle speeds in the absence of tyre marks, such as the determination of vehicle speed from pedestrian throw distance as discussed by Evans and Smith [**106**].

In the context of this work, a determination of the change in velocity of vehicles can be made using the CRASH algorithm described in Chapter 2. As shown earlier the CRASH algorithm can be considered as two distinct algorithms, one to determine the energy absorbed in causing deformation and the second to determine the change in velocity of each vehicle. The CRASH algorithm has the advantage that it does not rely on the presence of residual marks on the road surface, but requires only that there is crush damage suitable for measuring. The main disadvantage however is that the CRASH method only provides the change in velocity of each vehicle and not the actual velocities.

Normally the pre-impact direction of travel of each vehicle are also known or can be estimated for a particular collision. The method developed in this Chapter shows how this information together with knowledge of the change in velocity of each vehicle can be used to derive the actual pre and post impact velocities of both vehicles. This method is derived from an analysis of the collision based on the conservation laws of linear and angular momentum and includes restitution. It has the advantage of not being limited to any particular method by which the changes in velocity are generated. So it can be used as well with in-car accident data recorders that provide data on change in velocity as impact phase models such as CRASH.

Models for the impact phase of collisions commonly make a number of assumptions and these are described in Chapter 2. The same assumptions are also adopted here and are summarised below. First tyre and other external forces are assumed to be negligible during the impact, so that momentum is conserved. Second, the vehicle

masses and moments of inertia are maintained throughout the collision. That is the deformations caused by the collision do not significantly change the moments of inertia and the masses of the vehicles are not significantly changed, for example, by parts of a vehicle becoming detached as a result of the collision. Third, the time-dependent force can be modelled by one resultant impulse which acts at some point on or in the vehicles. Similarly as with CRASH and the other impact models described in this work, the discussion here is restricted to two vehicle planar collisions. For collisions involving significant vertical motion, this analysis will need modification. In the next section planar collisions are analysed to develop a new model to calculate the change in velocity of vehicles and also to derive expressions for the closing speed.

7.3 Planar Collisions

In this section the conservation laws of momentum are used to derive expressions for the change in velocity ($\Delta\boldsymbol{v}$). Smith [**105**] shows how the equations for $\Delta\boldsymbol{v}$ can be derived from the conservation of momentum and conservation of energy without recourse to a specific model for how the energy absorbed by the vehicles is related to damage. In this section an alternative derivation of the equations for $\Delta\boldsymbol{v}$ is also presented. Rose *et al.* [**95**] use a heuristic method based on McHenry's spring model [**65**] to obtain some interesting and helpful results for collisions. Also in this section, new equations are developed which provide expressions for the closing speeds which includes the energy absorbed by the vehicles. Such an analysis provides a rigorous and general basis for the results. However more importantly the analysis yields a yields new results. Equations (2.1) - (2.4) described in Chapter 2 form a system of four equations describing the conservation of momentum. These equations lead to an expression relating the two changes in velocity, i.e.

$$\Delta\boldsymbol{v}_1 = -\Delta\boldsymbol{v}_2 \frac{m_2}{m_1}. \tag{7.1}$$

In addition, the change in rotation of the two vehicles can be expressed as

$$\Delta\omega_1 = \frac{h_1}{k_1^2}\Delta v_1, \qquad \Delta\omega_2 = \frac{h_2}{k_2^2}\Delta v_2. \tag{7.2}$$

Lower case symbols are used for motion at the centre of mass. Upper case symbols are used to distinguish motion at the point of application of the impulse so that U_p is

denotes the component of the vehicle's velocity before impact in the direction of ***p*** at the point where the impulse ***P*** acts then

$$U_{1\mathrm{p}} = \boldsymbol{u}_1 \cdot \boldsymbol{p} + h_1\omega_1, \qquad U_{2\mathrm{p}} = \boldsymbol{u}_2 \cdot \boldsymbol{p} + h_2\omega_2 \tag{7.3}$$

where ***p*** is a unit vector in the direction of ***P***. Similarly V_p may be used to describe the component of vehicle's velocity after impact in the direction of ***p***

$$V_{1\mathrm{p}} = \boldsymbol{v}_1 \cdot \boldsymbol{p} + h_1\Omega_1, \qquad V_{2\mathrm{p}} = \boldsymbol{v}_2 \cdot \boldsymbol{p} + h_2\Omega_2 . \tag{7.4}$$

The coefficient of restitution (e_p) for the vehicles in the direction of ***P*** at the point where the impulse acts may be defined so that

$$V_{2\mathrm{p}} - V_{1\mathrm{p}} = -e_\mathrm{p}(U_{2\mathrm{p}} - U_{1\mathrm{p}}) . \tag{7.5}$$

The substitution of equations (7.2) to (7.5) into equation (7.1) produces

$$m_2(1+e_\mathrm{p})(U_{2\mathrm{p}} - U_{1\mathrm{p}}) = (m_1 + m_2)\Delta v_1 + m_2h_1\Delta\omega_1 - m_2h_2\Delta\omega_2 . \tag{7.6}$$

Further substitution of equations (7.1) and (7.2) into equation (7.6) then produces

$$\Delta v_1 = \frac{m_2(1+e_\mathrm{p})(U_{2\mathrm{p}} - U_{1\mathrm{p}})}{(m_1\delta_2 + m_2\delta_1)} \tag{7.7}$$

where

$$\delta_1 = 1 + \frac{h_1^2}{k_1^2}, \qquad \delta_2 = 1 + \frac{h_2^2}{k_2^2} . \tag{7.8}$$

Using a similar notation to that used by Brach [**11**] it is noted that result (7.7) can also be written as

$$\Delta v_1 = \frac{\bar{m}(1+e_\mathrm{p})(U_{2\mathrm{p}} - U_{1\mathrm{p}})}{Am_1} \tag{7.9}$$

where

$$A = 1 + \frac{\bar{m}h_1^2}{m_1k_1^2} + \frac{\bar{m}h_2^2}{m_2k_2^2} , \tag{7.10}$$

$$\bar{m} = \frac{m_1 m_2}{m_1 + m_2}. \tag{7.11}$$

Results (7.7) and (7.9) describe the changes in velocity at the centre of mass of the vehicle in terms of the closing speed of the points of contact between the vehicles. Since the closing speed of the vehicles is unknown for the majority of collisions, such a result is of limited use. However following a method similar to that of Smith [**105**] it is possible to determine the closing speed in terms of the total work done in causing crush to the vehicles as a result of the collision. This allows the unknown closing speed parameter in equation (7.7) to be replaced by a value which can be calculated from post-impact data. The work done in causing crush can be estimated using the methods described by McHenry [**65**], as described earlier, or any other suitable method. The total work done in causing crush (crush energy) to the vehicles as a result of the collision can be expressed as

$$E = E_T + E_R \tag{7.12}$$

where

$$E_T = m_1 \Delta v_1 (\boldsymbol{u}_2 \cdot \boldsymbol{p} - \boldsymbol{u}_1 \cdot \boldsymbol{p}) - \tfrac{1}{2} m_1 (\Delta v_1)^2 \left(1 + \frac{m_1}{m_2}\right), \tag{7.13}$$

$$E_R = m_1 \Delta v_1 (h_2 \omega_2 - h_1 \omega_1) - \tfrac{1}{2} m_1 (\Delta v_1)^2 \left(\frac{h_1^2}{k_1^2} + \frac{m_1 h_2^2}{m_2 k_2^2}\right). \tag{7.14}$$

Equation (7.12) can be solved for the closing speed $U_{2\mathrm{p}} - U_{1\mathrm{p}}$ to yield result (7.15)

$$U_{2\mathrm{p}} - U_{1\mathrm{p}} = \frac{E}{m_1 \Delta v_1} + \frac{\Delta v_1 (m_1 \delta_2 + m_2 \delta_1)}{2 m_2}. \tag{7.15}$$

As described by Smith [**105**], the substitution of $U_{2\mathrm{p}} - U_{1\mathrm{p}}$ from result (7.15) into equation (7.7) leads to the commonly used formula to calculate velocity change

$$\Delta v_1 = \sqrt{\frac{2 E m_2 (1 + e_{\mathrm{p}})}{m_1 (m_1 \delta_2 + m_2 \delta_1)(1 - e_{\mathrm{p}})}}. \tag{7.16}$$

Equations (7.7) and (7.16) both describe the change in velocity at the centre of mass ($\Delta \boldsymbol{v}$) along the line of action of the impulse. From equations (7.3) and (7.4) the change

in velocity at the point of application of the impulse in the direction of $\boldsymbol{p}$ (ΔV_{p}) may be described by the expression

$$\Delta V_{\mathrm{p}} = \Delta \boldsymbol{v} \cdot \boldsymbol{p} + h\Delta\omega\,. \tag{7.17}$$

The substitution of equations (7.2) and (7.8) into equation (7.17) produces the result

$$\Delta V_{\mathrm{p}} = \delta\,(\Delta \boldsymbol{v} \cdot \boldsymbol{p})\,. \tag{7.18}$$

Equation (7.18) shows that along the line of action of the impulse $\boldsymbol{P}$, the change in velocity of the point of application is equal to the product of the change in velocity at the centre of mass and the scalar value DeltaV. It should be noted that in addition to the change in velocity along the line of action of the impulse there is also a tangential change in velocity at the points of action (ΔV_{t}) due to the consequent change in rotation as defined by equation (7.2). If U_{t} and V_{t} are used to denote the component of the vehicle's velocity before impact in a direction perpendicular to $\boldsymbol{p}$ at the point where the impulse $\boldsymbol{P}$ acts then

$$U_{\mathrm{t}} = \left|\boldsymbol{u} \times \boldsymbol{p}\right| + h_{\mathrm{t}}\omega, \qquad V_{\mathrm{t}} = \left|\boldsymbol{v} \times \boldsymbol{p}\right| + h_{\mathrm{t}}\Omega \tag{7.19}$$

where h_{t} is related by Pythagoras to h as shown by equation (7.20) where d is the distance from the point of application of the impulse to the centre of mass

$$d^2 = h^2 + h_{\mathrm{t}}^2\,. \tag{7.20}$$

From Newton's laws of motion there can be no change in velocity at the centre of mass perpendicular to the impulse $\boldsymbol{P}$**.** Thus any change in velocity of the points of action tangential to the impulse can only be due to a change in the angular velocity of the vehicle. The change in velocity tangential to the direction of the impulse for each vehicle can now be obtained by equation (7.21)

$$\Delta V_{1\mathrm{t}} = h_{1\mathrm{t}}\ \Delta\omega_1, \qquad \Delta V_{2\mathrm{t}} = h_{2\mathrm{t}}\ \Delta\omega_2. \tag{7.21}$$

7.4 Closing Speeds

The changes in velocity of each vehicle at the centres of mass and at the point of application of the impulse are described in the previous section. In this section the total closing speed of the vehicles is derived as the vector sum of the closing speed in the

direction of the impulse and the closing speed perpendicular to the impulse. A method is then described which uses the total closing speed to determine the actual speeds of the vehicles at impact. From result (7.7) an expression for the closing speed along the line of action of the impulse at the point of action of the impulse can readily be obtained

$$U_{2\mathrm{p}} - U_{1\mathrm{p}} = \frac{\Delta v_1 (m_1 \delta_2 + m_2 \delta_1)}{m_2 (1 + e_{\mathrm{p}})} . \tag{7.22}$$

Alternatively, as Smith [**105**] demonstrates, the total energy absorbed in the collision may be expressed as

$$E = E_{\Delta} + E_e \tag{7.23}$$

where

$$E_{\Delta} = \left(\frac{m_1}{2m_2} \right) (\Delta v_1)^2 (m_1 \delta_2 + m_2 \delta_1) , \tag{7.24}$$

$$E_e = m_1 \Delta v_1 (\mathbf{v}_2 \cdot \boldsymbol{p} + h_2 \Omega_2 - \mathbf{v}_1 \cdot \boldsymbol{p} + h_1 \Omega_1) . \tag{7.25}$$

The closing speed in the direction of ***P*** can now be found by substituting equations (7.4) and (7.5) into equation (7.25) to yield

$$E_e = -e_{\mathrm{p}} m_1 \Delta v_1 (U_{2\mathrm{p}} - U_{1\mathrm{p}}) . \tag{7.26}$$

Equations (7.18), (7.24), and (7.26) can then be used in equation (7.23) to produce

$$U_{2\mathrm{p}} - U_{1\mathrm{p}} = \sqrt{\frac{2E(m_1 \delta_2 + m_2 \delta_1)}{m_1 m_2 (1 - e_{\mathrm{p}}^2)}} . \tag{7.27}$$

Equation (7.27) is similar to that derived by Rose *et al* [**95**] but is more general as it includes the effect of restitution. Rose *et al* restrict their subsequent analysis to one dimension along the line of the impulse. As highlighted previously, it must be noted that there is also a tangential change in velocity at the point of application of the impulse due to the change in rotation. The component change in velocity for each vehicle tangential to the impulse where the impulse acts is given by equation (7.21). The tangential change in velocity for vehicle 1 can be subtracted from that for vehicle 2 to yield

$$\Delta V_{2t} - \Delta V_{1t} = h_{2t}\ \Delta\omega_2 - h_{1t}\ \Delta\omega_1 . \tag{7.28}$$

Substitution of equations (7.1), (7.2) and (7.19), into equation (7.28) produces

$$\Delta V_{2t} - \Delta V_{1t} = -m_1 \Delta v_1 \left[\frac{h_{1t} h_1}{m_1 k_1^2} + \frac{h_{2t} h_2}{m_2 k_2^2} \right]. \tag{7.29}$$

Equation (7.7) can be substituted into (7.29) to produce

$$\frac{\Delta V_{2t} - \Delta V_{1t}}{(U_{2p} - U_{1p})} = \frac{-m_1 m_2 (1 + e_p)}{(m_1 \delta_2 + m_2 \delta_1)} \left[\frac{h_{1t} h_1}{m_1 k_1^2} + \frac{h_{2t} h_2}{m_2 k_2^2} \right]. \tag{7.30}$$

This may be written in a format similar to that of equation (7.9) to yield

$$\frac{(V_{2t} - V_{1t})}{(U_{2t} - U_{1t})} = 1 - \frac{B}{rA}(1 + e_p). \tag{7.31}$$

where A and $\bar{m}$ are given by equations (7.10) and (7.11) respectively and

$$B = \left[\frac{\bar{m} h_{1t} h_1}{m_1 k_1^2} + \frac{\bar{m} h_{2t} h_2}{m_2 k_2^2} \right], \tag{7.32}$$

$$r = \frac{(U_{2t} - U_{1t})}{(U_{2p} - U_{1p})}. \tag{7.33}$$

Analogously to equation (7.5), and in a similar manner to that used by Ishikawa [**43**] a tangential coefficient of restitution (e_t) can be defined such that

$$V_{2t} - V_{1t} = -e_t (U_{2t} - U_{1t}). \tag{7.34}$$

Substitution of equation (7.34) into equation (7.31) produces a result showing the relationship between the tangential closing speed and the closing speed along the line of action of the impulse

$$(U_{2t} - U_{1t})(1 + e_t) = \frac{B}{A}(U_{2p} - U_{1p})(1 + e_p). \tag{7.35}$$

The coefficient e_t will be zero when relative tangential motion between the two points of application ceases at or before separation of the vehicles. It is suggested that this situation will occur in the majority of vehicle to vehicle collisions so that it may be

assumed that e_t is zero leading to a simplification of the following equations. Where e_t is zero (i.e. $V_{1t} = V_{2t}$), equation (7.29) becomes

$$U_{2t} - U_{1t} = m_1 \Delta v_1 \left[\frac{h_{1t} h_1}{m_1 k_1^2} + \frac{h_{2t} h_2}{m_2 k_2^2} \right]. \tag{7.36}$$

This formula gives the component of the closing speed perpendicular to the direction of the PDOF. This formula gives the tangential closing speed component in terms of Δv and includes the effects of restitution along the line of action of the impulse (e_p) via equation (7.16). This is a key equation in the calculation of the closing speeds and so of the vehicles speed.

In addition, where e_t is zero equation (7.35) can be written

$$rA + B(1 + e_p) = 0. \tag{7.37}$$

As explained in Chapter 2, Brach [**11**] develops his Planar Impact Mechanics model (PIM) to demonstrate how using the conservation of momentum, a model can be derived which models the behaviour of vehicles during the impact phase. His model partitions the impulse into normal and tangential components which are related to each other by an impulse ratio μ and also includes a normal coefficient of restitution. Although the choice of impact plane is not critical in his model, the choice of impact plane effectively determines the impulse ratio μ and the coefficients of restitution. A critical impulse ratio μ_0 is also defined by Brach as the impulse ratio at which a common tangential post-impact velocity may be determined. With an orientation of the impact plane perpendicular to the impulse as defined in Chapter 2, then there can be no tangential impulse component so that Brach's critical impulse ratio μ_0 will also be zero.

It is noted that the left hand side of result (7.37) is identical to the numerator in Brach's equation to determine the critical impulse ratio μ_0. This indicates that Brach's model and the model presented here both predict a common tangential post-impact speed with the same initial conditions and orientation of the impact plane. Collisions where relative tangential motion continues beyond separation implies a non-zero tangential coefficient e_t Such a non-zero tangential coefficient will occur for example in sideswipe type collisions. Without loss of generality, the substitution of equation (7.34)

into equation (7.21) yields an expression for the closing speed perpendicular to the impulse

$$U_{2t} - U_{1t} = (h_{1t}\ \Delta\omega_1 - h_{2t}\ \Delta\omega_2)/(1+e_t) \tag{7.38}$$

The total closing speed (U_R) can now be expressed as the vector sum of the component results from equations (7.22) [or (7.27)] and (7.38)

$$U_R = \sqrt{(U_{2p} - U_{1p})^2 + (U_{2t} - U_{1t})^2} \tag{7.39}$$

Of note is that an alternative to result (7.39) can be determined by using result (7.35). Using this result the total closing speed can be expressed without explicit reference to the tangential closing speed to give

$$U_R = \sqrt{(U_{2p} - U_{1p})^2 \left(1 + \frac{B^2(1+e_p)^2}{A^2(1+e_t)^2}\right)} \tag{7.40}$$

The angle of the closing speed vector to the impulse ***P*** (β) can be found from equation (7.33)

$$\tan\beta = r = (U_{2t} - U_{1t})/(U_{2p} - U_{1p}) \tag{7.41}$$

Using result (7.35), angle β can also be defined solely in terms of *A* and *B* and the two coefficients of restitution e_p and e_t

$$\tan\beta = \frac{B(1+e_p)}{A(1+e_t)} \tag{7.42}$$

In CRASH analyses it is usual to define a principal direction of force (PDOF) for each vehicle as the direction in which the impulse acts so as to cause the observed damage. Brach [**11**] suggests that the requirement to estimate the PDOF is a major weakness in CRASH and the work of the previous Chapters shows that an accurate estimate of the PDOF is important in reducing uncertainty. A new method is presented later in this Chapter which permits a more realistic estimate to be made of the actual impulse and therefore the PDOF values applicable to each vehicle.

The impact geometry of a typical collision is illustrated in Figure 7.1 where two vehicles V1 and V2 collide obliquely as shown in the insert.

Figure 7.1: Impact Configuration

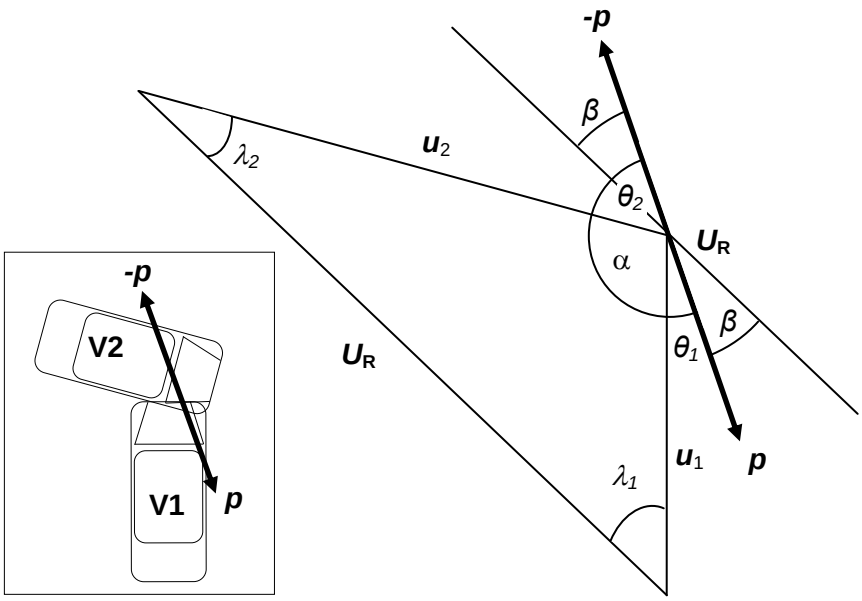

Defining the PDOF values for each vehicle uniquely determines the angle between the two vehicles at impact by Newton's Third Law. This value (α) can be determined from the PDOF values (θ) as

$$\alpha = \pi - \theta_1 - \theta_2 \tag{7.43}$$

It follows that the angle (λ) between the initial heading of vehicles and the closing speed can then be described by the expressions

$$\lambda_1 = \beta + \theta_1, \qquad \lambda_2 = \pi - \alpha - \lambda_1 = \theta_2 - \beta. \tag{7.44}$$

When there is no pre-impact rotation by either vehicle, the closing velocity of the points of action for each vehicle must also be the closing velocity of their centres of mass. The absence of significant pre-impact rotation is a common feature in many collisions and the simplifying assumption that pre-impact rotation is zero, or at least negligible, does not severely limit the number of collisions amenable to this technique. If there is significant pre-impact rotation, then this method cannot distinguish between the closing velocity due to the translational motion of the vehicles or that due to rotational motion.

If there is pre-impact rotation therefore, additional information will be required to resolve this difference.

Consideration of the triangle of vectors formed by the closing speed vector and the initial velocity vectors, indicates that the Sine Rule can be used to determine the actual speed of the vehicles. Where there is no pre-impact rotation as described earlier, result (7.45) determines the initial vehicle speeds where α is the angle between the two vehicles at impact

$$U_2 = u_2 = \frac{U_R \sin(\lambda_1)}{\sin\alpha}, \qquad U_1 = u_1 = \frac{U_R \sin(\lambda_2)}{\sin\alpha}. \tag{7.45}$$

Once the pre-impact velocities have been found it is straightforward to determine the post-impact velocities using the change in velocity ($\Delta\boldsymbol{v}$) for each vehicle.

This method has been used with the RICSAC tests to compute the initial speeds. These calculations are discussed in more detail in following sections. It should be emphasised that no knowledge of how the values for Δv are obtained is assumed in this derivation. As a result equation (7.45) is equally applicable to any model yielding the changes in velocity of each vehicle.

7.5 Discussion

7.5.1 Practical Considerations

Using this technique requires that some way is available to determine the changes in velocity sustained by each vehicle. These values may be calculated using any suitable force-crush model, or generated by some other method, such as from in-car accident data recorders. In the situation where a data recorder was fitted to only one vehicle, equation (7.1) may allow the Δv of the other vehicle to be estimated from the relative masses of each vehicle.

A commonly used model used to generate values for Δv is that provided by CRASH. As demonstrated previously the CRASH model uses a linear force-crush model to determine the work done in causing crush to each vehicle in a collision (E_1 and E_2) (See *e.g.* Day and Hargens [**22**] or McHenry [**65**]) Practical considerations for measuring vehicles are described more fully by Neades and Shephard [**75**] and are

outlined in Chapter 3. CRASH based programs calculate the positions of the damage centroids using the geometry of the deformed areas and these are frequently used to define the points of application of the impulse ***P***. The shape of the damaged area is also used to assist in estimating the PDOF. Ishikawa [**42**] provides an alternative method to estimate the PDOF for the vehicles from the damage profiles which may be helpful in determining these values. He proposes a method whereby the impact centre is assumed to be the mid-point of the contacting surfaces at the point of maximum deformation. The PDOF is then assumed to lie along a line perpendicular to the line of the contacting surfaces through the impact centre. The difference between these two methods is usually small and the choice of PDOF is discussed further in section 7.7.

Essentially the CRASH algorithm consists of two distinct processes. One to determine the crush energy and a second process where those energy values are utilised to determine the changes in velocity. The derivation here does not rely on any particular deformation law and describes the second process.

7.5.2 The effect of restitution

In the majority of substantial vehicle to vehicle collisions, the points of application of the impulse reach a common velocity tangential to the impulse so that $V_{2t} = V_{1t}$. If the coefficient of restitution in the direction of the impulse (e_p) is also zero this implies that the points of action reach a common velocity during the collision phase. This is the common velocity assumption present in many of the CRASH derivations. As described previously, Smith [**105**] shows that the common velocity assumption may be relaxed somewhat by the inclusion of a non-zero coefficient of restitution along the line of action of the impulse. This leads to equation (7.16) which can be viewed as an extension to the standard or zero restitution CRASH model. If the coefficient of restitution in the direction of the impulse is greater than zero, then the points of application of the impulse reach a common velocity along the line of action of the impulse at the moment of maximum engagement. At the moment of maximum engagement the maximum amount of energy has been absorbed by the vehicle structures. If energy is then returned to the vehicles due to restoration of the vehicle structure, the velocities of the vehicles continue to change beyond that required simply to reach a common velocity at the point of application of the impulse as outlined by Brach [**11**].

In situations where the points of action do not reach a common velocity, such as in a sideswipe type of collision, the common velocity assumption becomes invalid. In such situations it is likely too that the impulse no longer dominates the tyre forces so that there is also unlikely to be any major engagement between the vehicles and a corresponding lack of residual crush to the structural members of vehicles. In such collisions any assumption that there is a common tangential post-impact velocity (i.e. $V_{2t} = V_{1t}$) is no longer valid.

Smith and Tsongas [**110**] report a series of staged collisions where they found that the coefficient of restitution was between 0 and 0.26. In general, they report that lower values of restitution tend to be found as the closing speed increases. Little information is available to indicate their methodology but it seems likely that these collisions were central and that restitution was calculated along the line of action of the impulse. Wood [**125**] also suggests a similar relationship based on a series of full scale crash tests with a maximum restitution of about 0.3 More recently Rose, Fenton and Beauchamp [**94**] investigated the effects of restitution for a single type of vehicle (a Chevrolet Astro van) in head-on collisions with a barrier. Here they found that the coefficient of restitution varied from 0.11 to 0.19 for impact speeds around 47 – 57 kmh^{-1}. Cipriani *et al* [**21**] studied a series of vehicle to vehicle collinear impacts with low speeds up to 7 ms^{-1} and discovered that restitution varied from about 0.2 to 0.6 with the lower values found for higher impact speeds. At lower closing speeds it is apparent that restitution effects can be significant.

The use of a positive coefficient of restitution e_p increases the calculated closing speed and as a result tends to increase the pre-impact speeds determined for each vehicle. Minimum pre-impact speeds are therefore calculated when e_p is zero, which as previously noted is likely to be close to the actual value for higher speed collisions. Determining the minimum impact speed for each vehicle is often of prime importance particularly in criminal forensic collision investigation.

7.6 Example Collisions

7.6.1 Standard Energy Adjustment Factor

This model has been applied to the data from the Research Input for the Computer Simulation of Automobile Collisions full scale tests (RICSAC) [**51**] using the standard

energy adjustment factor defined by McHenry [**65**] and examined in Chapter 4. An analysis using the new energy adjustment factor also defined in Chapter 4 is presented in the next section. This is the same data set as used in earlier Chapters investigating the overall accuracy of the CRASH algorithm. As highlighted earlier it is apparent that in several of the tests there are significant discrepancies between the recorded damage profiles and the photographs of the damage. These discrepancies result in very large force differences in the calculations. This is particularly evident in tests 2, 6 and 7 where force differences of 469%, 577% and 608% respectively were obtained. As detailed earlier, the data from these tests has been adjusted in an attempt to rectify some of the more obvious discrepancies. The changes in velocity for each of the collisions is show in Appendix F.

As an illustration of the entire process, Test 8 of the RICSAC series is analysed in detail. Test 8 of the series was a set up to be representative of a 90° intersection collision with both vehicles travelling at 9.2 ms^{-1} at impact. A CRASH damage analysis shows that with the PDOF values as recorded, the work done in causing deformation to the vehicles was 63 kJ. Using the recorded PDOF values and a zero coefficient of restitution ($e_p = 0$), the method described here uses equation (7.16) to determine the speed change in the direction of the PDOF. Equation (7.27) gives the closing speed in the direction of the impulse as 12.83 ms^{-1}. Equation (7.38) gives the closing speed perpendicular to the impulse as 5.86 ms^{-1}. These component results can be used in equation (7.39) to determine the total closing speed as 14.1 ms^{-1}. With this configuration the angle λ_1 is 24.5° and angle α is 90°. Using equation (7.45) the pre-impact speeds are found to be 8.18 ms^{-1} for vehicle 1 and 11.49 ms^{-1} for vehicle 2. From these values and the calculated changes in velocity from equation 16 the post-impact motion can be determined from the definition of $\Delta\boldsymbol{v}$.

Diagrams in Jones and Baum [**51**] show that for Test 8 the centres of mass of each vehicle moved off along a common post-impact direction of approximately 40° - 50° to the original direction of travel of vehicle 1. The calculated post-impact motion of the vehicles for Test 8 with a zero coefficient of restitution shows that the centres of mass of the vehicles do not follow the recorded post-impact direction of travel. Indeed when the coefficient of restitution is close to zero the vehicles appear to pass through each other as shown in the first part of Figure 7.2. This cannot be a realistic scenario for this type of impact configuration. A more realistic model can be achieved however by using a non-zero coefficient of restitution e_p. The post-impact motion predicted for

RICSAC Test 8 using coefficients of restitution of 0.0 and 0.3 are shown in Figure 7.2 to illustrate this effect. The PDOF for each vehicle and the coefficient of restitution are difficult to determine accurately. Various reasonable values were tried and the best ones selected on the basis of the force balance and post-impact direction of travel. The optimum values gave pre-impact speeds of 8.9 ms^{-1} for vehicle 1 and 9.0 ms^{-1} for vehicle 2 which underestimate the measured speeds by 0.3 and 0.2 ms^{-1} respectively.

Figure 7.2: RICSAC Test 8: Motion of centres of mass with varying restitution

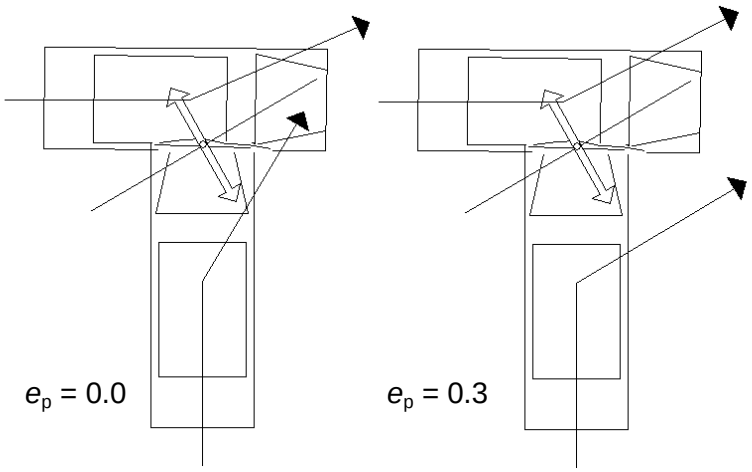

The remainder of the RICSAC tests can be treated in a similar way to calculate pre-impact speeds for these tests. Early versions of the CRASH measuring protocols indicated that crush damage should be measured at the level of maximum intrusion. Later versions of CRASH suggest that crush damage should be measured at the main load bearing level, i.e. at bumper and sill level as described in Chapter 3 and in Neades and Shephard [75].

Comparison between the photographs and the recorded measurements suggest that the early measurement version was used to determine the damage profiles. For example the photographs of vehicle 2 in both tests 1 and 2 show considerable intrusion at about mid-door level but much less intrusion at sill level. The author has examined and measured scores of damaged vehicles. Based on this experience, photographs and the measurements an estimate of the likely crush at the load bearing level have been made for each vehicle. The adjustments made vary dependent on the particular damage to each vehicle. Although such a process is somewhat rough and ready the

resulting measurements provide a better approximation of the damage profiles to the stiff parts of the vehicles.

In addition the PDOF values for each vehicle were adjusted so that although the configuration of the vehicles at impact remained constant, the post-impact directions of travel for the centres of mass matched those recorded for each of the tests as shown in the diagrams presented by Jones and Baum [51]. Three 90° impact tests were conducted (Tests, 8, 9 and 10). As outlined previously in each of these collisions a coefficient of restitution of 0.3 has been applied so that a reasonable match was achievable with the recorded post-impact motion. Note that using a coefficient of 0.3 produces a reasonable match for each of these three tests. Further adjustment around 0.3 can produce a marginally closer fit but with little change in the calculated closing speed. The actual adjustments made are detailed in Table 5.7 and

Table 5.8. The results from this analysis are shown in Table 7.1.

Table 7.1: RICSAC Closing speed results – Standard energy adjustment (ms^{-1})

Test	Calculated Δ*v*		Total Closing Speed	Measured Pre-impact Speed		Calculated Pre-impact Speed	
	V1	V2		V1	V2	V1	V2
1	5.3	7.9	16.0	8.8	8.8	9.2	9.3
2	8.4	12.6	25.6	14.0	14.0	14.8	14.8
3	3.0	4.8	8.5	9.4	0.0	8.5	0.1
4	6.6	10.3	17.6	17.2	0.0	17.6	0.2
5	5.9	10.7	17.3	17.7	0.0	17.3	-0.4
6	5.2	8.5	17.3	9.6	9.6	10.0	10.0
7	6.1	13.2	24.0	13.0	13.0	13.9	13.9
8*	6.6	6.2	12.6	9.2	9.2	8.9	9.0
9*	6.7	3.1	12.2	9.4	9.4	8.6	8.6
10*	10.9	5.3	18.6	14.8	14.8	13.1	13.2
11	9.7	6.1	16.3	9.1	9.1	8.0	8.4
12	16.0	11.1	27.1	13.6	14.0	13.6	13.7
*Coefficient of restitution e_p = 0.3							

A graph summarising these results comparing the measured pre-impact speed of each vehicle with the pre-impact speed calculated by this method is shown in Figure 7.3. (Note that the stationary target vehicles used in tests 3, 4 and 5 have been omitted from the results.)

Figure 7.3: Percentage error of calculated and actual pre-impact speed

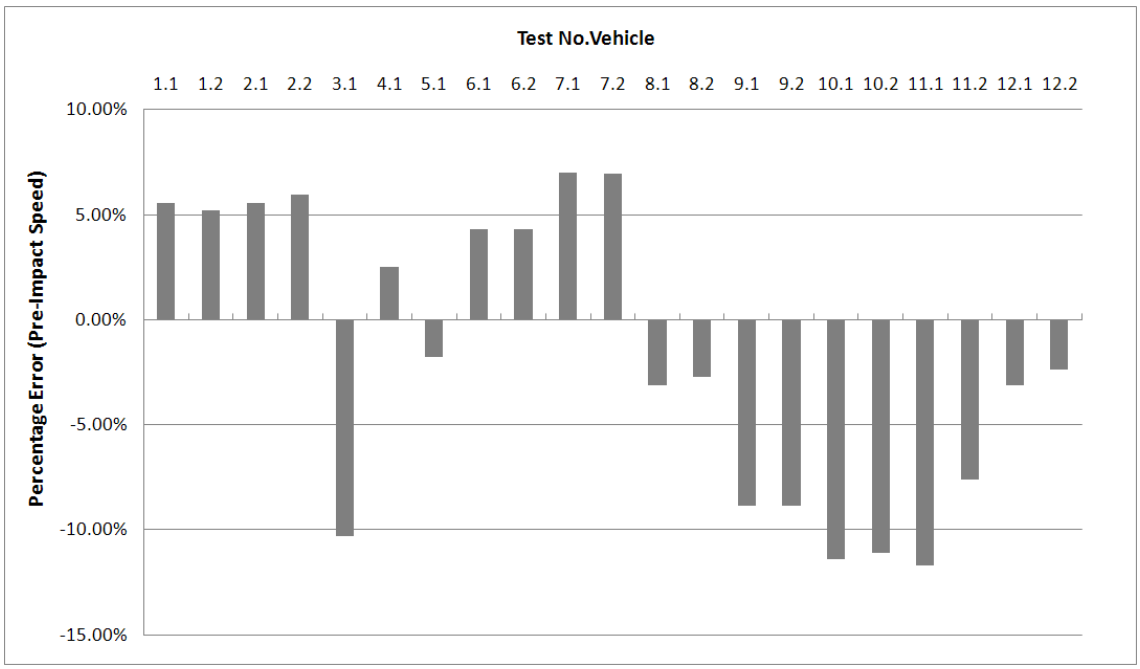

These results indicate that the pre-impact speeds calculated using this technique for the RICSAC tests range from -12% to +8% with a mean underestimate of 2%. Smith and Noga [**107**] note that in the collisions they considered, CRASH tended to underestimate Δv with a mean error of ±13.8% for higher speed collisions (40 – 48 kmh^{-1}) and ±17.8% for lower speed collisions (16 – 24 kmh^{-1}). The results here seem also to indicate that the work done in causing crush has been underestimated. One source of error may be that in several of the RICSAC collisions the crush damage profile recorded does not seem to replicate the crush profile as shown in photographs. Although the damage profiles were adjusted in this analysis to better replicate the damage profiles, with more representative measurements a better correspondence to the actual speeds is to be expected.

In the Lotus crash tests [**45**] vehicles were crashed into stationary target vehicles. A similar analysis of the crash data as performed for the RICSAC tests reveals a correspondence of calculated impact speeds to actual speeds of between -9.6% to +3.7% A detailed analysis of the likely sources and magnitude of error is presented in Chapters 5 and 6.

7.6.2 New Energy Adjustment Factor

The data from the RICSAC tests has also been applied using the new energy adjustment factor defined in Chapter 4. The development of this factor in Chapter 4 also resulted in the development of a method to transform coefficients of restitution to alternative orientation of the impact plane. This permits the analysis of those collisions where a non-zero coefficient of restitution parallel to the impulse was required. The tests affected by this adjustment are tests 8, 9 and 10. The results using the new adjustment factor for all the RICSAC tests are shown in Table 7.2. Further details of this analysis are provided in Appendix M

Table 7.2: RICSAC Closing speed results – New energy adjustment (ms^{-1})

Test	Calculated Δ*v*		Total Closing Speed	Measured Pre-impact Speed		Calculated Pre-impact Speed	
	V1	V2		V1	V2	V1	V2
1	5.3	7.9	15.6	8.8	8.8	8.97	9.00
2	8.4	12.6	24.2	14.0	14.0	13.97	14.02
3	3.0	4.8	8.4	9.4	0.0	8.37	0.00
4	6.6	10.3	17.6	17.2	0.0	17.56	0.01
5	5.9	10.7	17.3	17.7	0.0	17.35	0.00
6	5.2	8.5	16.3	9.6	9.6	9.44	9.44
7	6.1	13.2	22.5	13.0	13.0	13.02	13.00
8*	6.6	6.2	14.5	9.2	9.2	10.23	10.28
9*	6.7	3.1	14.0	9.4	9.4	9.89	9.89
10*	10.9	5.3	21.3	14.8	14.8	15.07	15.11
11	9.7	6.1	16.2	9.1	9.1	7.95	8.31
12	16.0	11.1	27.1	13.6	14.0	13.53	13.63
*Coefficient of restitution e_p = 0.3							

The results using the new energy adjustment factor produce a slightly closer set of values to those calculated using the standard energy adjustment factor. Overall the accuracy is just under 0.2% with a standard deviation of 5.5%. A direct comparison between the sets of results with the recorded pre-impact speeds are shown in Figure 7.4 and Figure 7.5. For clarity the comparison between vehicle 1 and vehicle 2 are shown separately

Figure 7.4: Comparison between energy adjustment models Vehicle 1

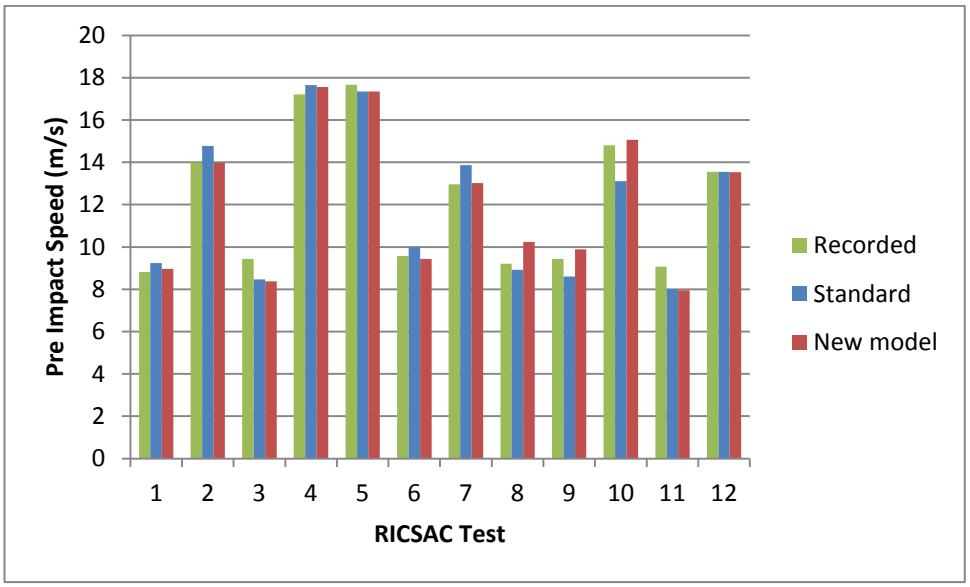

Figure 7.5: Comparison between energy adjustment models Vehicle 2

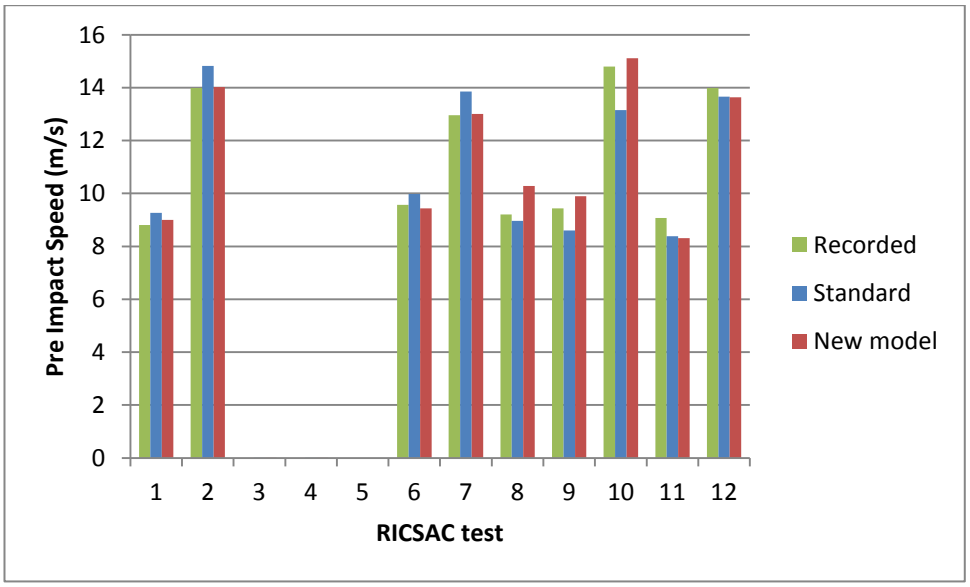

As can be seen, the overall correlation between the recorded pre-impact speed and the calculated speed is remarkably close with both models. Although in percentage terms the accuracy ranges up to about ±12% this corresponds to inaccuracy in the actual speeds of no more than ±1.1 ms^{-1} using the new model and one example (test 10) at

+1.6 and 1.7 ms^{-1} for vehicles 1 and 2 respectively using the standard energy adjustment model.

7.7 Accuracy

In this section the accuracy of this method is discussed. Three parameters are identified as key values affecting the overall accuracy and each is considered in turn. These are the impact angle alpha, the method used to determine Δv in the first place and the choice of the point through which the impulse acts.

The techniques developed in this Chapter cannot be applied to all collisions. As α tends towards 0 or 180°, sin α will tend towards zero leading to a singularity in result (47). With α at 0 or 180° therefore all that can be calculated is the closing speed of the vehicles and not the actual speeds of either vehicle. Without additional information concerning the pre-impact speed of one of the vehicles, it is not possible to determine the individual speeds of either vehicle. At angles close to these extremes, any results from result (7.45) will become sensitive to the exact angle and should therefore be treated with caution. This is very similar to the way in which conservation of momentum calculations become sensitive to changes in angles at near-collinear calculations.

The most important factor which affects the accuracy of the calculations are the inaccuracies in the method used to determine the change in velocity itself. Thus if using CRASH to generate Δv values the overall accuracy will be broadly similar to those inherent when using CRASH. However techniques to improve the accuracy of those calculations have been developed and outlined in this Chapter. Implicit in the overall accuracy is the estimation of the direction of the impulse (PDOF) and also the angle α. In CRASH this choice will also affect directly the calculation of energy absorbed by each vehicle as explained in Chapter 6. The estimation of the direction of the impulse determines the proportion of the closing speed allocated to each vehicle. Thus an accurate choice is important. Figure 7.6 shows how the initial speeds of the vehicles are affected by varying the PDOF. Data from RICSAC Test 9 is used together with a zero coefficient of restitution. It is also assumed that the attitude of the vehicles remains constant throughout the impact.

Figure 7.6: RICSAC Test 9. Variation of initial vehicle speeds with PDOF

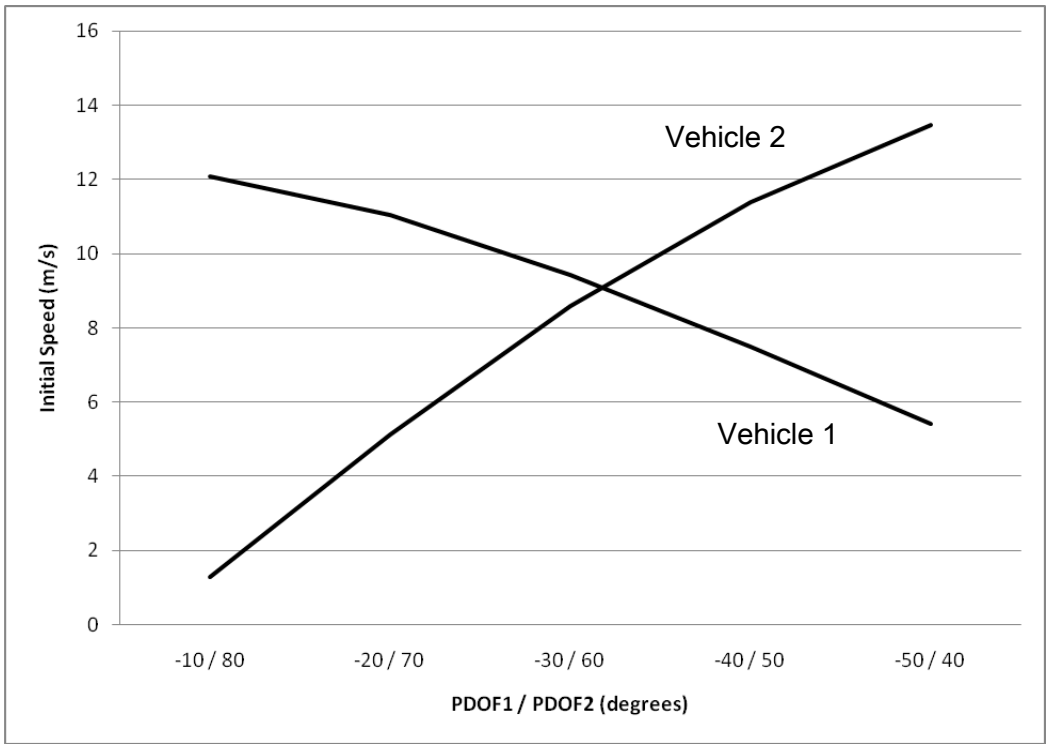

The sensitivity of the results to the actual direction of the impulse as indicated by Figure 7.6 suggests that a visual estimation of the direction of the PDOF may not be sufficiently precise. This is the normal method of operation for investigators using CRASH which requires an estimate of the PDOF for each vehicle. Investigators commonly estimate the direction of the impulse from the pattern of damage sustained by each vehicle. As described earlier, in real-world collisions the immediate post-impact directions of motion of each vehicle can often be deduced from an analysis of tyre and other marks on the roads surface. With the techniques described here, the post-impact velocity is straightforward to obtain. Using this information it is then possible to refine the initial estimate of the PDOF and restitution values so that the calculated post-impact directions of travel match those recorded for actual collisions.

The value of Δv is dependent on the value h for each vehicle since this factor not only determines the change in velocity of the centre of mass, but also determines the change in rotation $\Delta\omega$. This value is itself dependent upon the point chosen as the point through which the impulse acts. Thus the choice of this point on each vehicle will

have an effect on the calculated speeds. In CRASH calculations the point through which the impulse acts is normally assumed to be the centroid of the damaged area. Ishikawa [**42**] proposes a method whereby the impact centre is assumed to be the mid-point of the contacting surfaces at the point of maximum deformation. He provides a method whereby that point can be calculated. Unfortunately this calculation requires knowledge of the impulse and post-impact rotation which are themselves affected by the location of this point. It is apparent however that the position of this point could vary by as much as half the crush depth. An analysis of the RICSAC tests produce differences of less than 1 ms^{-1} for each vehicle. As confirmed by the analyses in Chapters 5 and 6 this suggests that the calculation of the initial speeds is not particularly sensitive to variations in this parameter.

7.8 Summary

The method presented in this Chapter demonstrates that the pre-impact speed of a vehicle can be determined from an analysis of the changes in velocity sustained by each vehicle. This data can be from any suitable algorithm that provides such changes in velocity. The technique has been applied to a series of crash tests where changes in velocity were determined using the commonly used CRASH algorithm. Results are presented using the standard energy adjustment factor and a new adjustment factor both of which are described in Chapter 4. It is shown that the new adjustment factor produces results which are slightly closer to the actual vehicle speeds than the standard adjustment factor. However it is recognised that this is a limited data set and a more comprehensive series of tests is desirable.

A technique has also been suggested to improve the accuracy of the estimation of the PDOF which is required as an input parameter to CRASH. Application of these techniques should provide more reliable results for crash investigators involved in analysing collisions.

Chapter 8

Conclusions

8.1 Overview

This Chapter provides a summary of the thesis and an evaluation based on the criteria specified in Chapter 1. Suggestions are also made for future work in this area. As outlined in Chapter 1 this thesis considers the impact phase of road vehicle collisions and has three main aims

- To quantify factors affecting accuracy of DeltaV and predicted speeds
- To determine the relevance and accuracy of energy adjustment factors in CRASH calculations
- To develop a method to determine actual vehicle velocities from DeltaV values

These aims have been discussed in depth throughout the body of the thesis. The main finding of this work are summarised in the next sections. Of note throughout this work is that CRASH can be viewed as two separate algorithms. The first is an algorithm to estimate the amount of work done in causing crush damage (crush energy). The second part of the algorithm uses the crush energy estimates to determine DeltaV. The two algorithms are described in detail in Chapter 2.

Since the estimation of crush energy and the overall accuracy of the CRASH algorithm depends crucially on crush damage measurements, Chapter 3 contains details of measuring protocols which can be used to consistently measure that damage.

8.2 Equivalence of impact phase models

It has been shown that the momentum models of Brach [**11**] and Ishikawa [**43**] which do not utilise the conservation of energy are equivalent and differ mainly in the way in which tangential sliding is treated. Both models make use of an impact plane in their specification to partition the impulse into normal and tangential components. Chapter 2 explains how Brach uses an effective tangential sliding coefficient of friction μ whereas Ishikawa utilises a second coefficient of restitution e_t. Ishikawa identified that there was an explicit conversion between μ and e_t. The two momentum models also use somewhat different coefficients. Conversion between μ and e_t and between the various coefficients can be achieved using the equations listed in Appendix C.

If the impact plane is orientated so that it is perpendicular to the impulse then the tangential impulse component vanishes. With this orientation Chapter 2 shows that second part of the CRASH algorithm is also equivalent to the momentum only models. It is shown that the second part of the CRASH algorithm uses only conservation laws as described by Smith [**105**] and provides a new model to allow for tangential restitution. This is an important result since it shows that any perceived differences and inaccuracies of the CRASH model as compared to the momentum models do not lie in the second part of the CRASH algorithm. Any differences and inaccuracies can only be due to the first part of the algorithm where the crush damage is estimated. The consequent dependence on accuracy to the first part of the CRASH algorithm motivates the discussion on measuring protocols detailed in Chapter 3.

8.3 Energy adjustment factors

As shown in Chapter 3 the measuring process requires that the crush measurements are made perpendicular to the damaged face of the vehicle. The raw crush energy values obtained from these measurements are then transformed into values suitable as input to the second part of the algorithm. This is achieved through the use of energy adjustment factors which effectively scale the raw crush energy into suitable estimates. The nature and effect of the energy adjustment factors are described in Chapter 4. It should be noted that the energy adjustment factors only affect the first part of CRASH algorithm where the estimates of crush damage are made.

Methods are detailed which allow the crush energy to be estimated using the momentum models. This permits a comparison to be made between the estimates of

crush energy obtained by measurement and theoretical values obtained from the momentum models. It is shown that the standard energy adjustment factor as described by McHenry [**65**] does not produce results consistent with the momentum models. Similarly other adjustment factors proposed by Fonda [**31**] or a later revision by McHenry [**66**] also do not provide results consistent with the momentum models. An alternative adjustment factor is derived in Chapter 4 which does provide a scale factor which matches energy values obtained from the momentum models. In essence this new method partitions the crush energy into two terms, one produced by the component of the impulse perpendicular to the damaged surface and the other by the component of the impulse which is tangential to the surface.

The new adjustment factor requires an estimate to be made of the angle between the pre-impact velocity vectors of the two vehicles (closing velocity angle). It also takes into account restitution both parallel and perpendicular to the damaged surface. It is recognised that this information may not be readily available which may reduce the utility of the new adjustment factor. This shortcoming is addressed in Chapter 7 where a method to determine the pre-impact velocities of the vehicles is developed. This information does then allow for the closing velocity angle to be determined.

Chapter 4 also details a new method whereby the two coefficients of restitution e_n and e_t used by the impact phase models can be transformed to different orientations of the impact plane. The new energy adjustment factor requires such a conversion to transform coefficients of restitution parallel and perpendicular to the impulse to their equivalent values perpendicular and parallel to the impact surface. In addition this transformation may prove useful more generally whenever converting between different orientations of the impact plane.

8.4 Theoretical accuracy of CRASH

Chapters 5 and 6 describe a detailed discussion concerning the overall accuracy of the CRASH algorithm. Chapter 5 discusses accuracy from a theoretical viewpoint whereas Chapter 6 contains details of a Monte Carlo simulation designed to explore overall accuracy and the effect of uncertainty in the CRASH input parameters

These analyses show that front to side (FTS) impacts are inherently less accurate and therefore produce a greater range of overall uncertainty than front to front (FTF) or front

to rear (FTR) impacts. Some of the input parameters respond in a non-linear manner such as uncertainty in crush depth or PDOF. As a result it has not been possible to determine a simple guide to indicate overall uncertainty from any one parameter.

Utilising typical uncertainties matching those of Smith and Noga [**108**] as listed in Table 5.2, overall uncertainty in DeltaV is found to be about 15 – 17% for front to side impacts. This reduces to around 9 – 12% for front to front or front to rear impacts. The largest individual contribution is that due to uncertainty in PDOF. A reduction in this one parameter therefore is likely to have the greatest overall effect. Reducing uncertainty in the PDOF to ±10° reduces overall uncertainty to 13 – 15% for front to side impacts and 8 – 10% for end to end impacts.

A careful analysis of one of the standard data sets has shown that this behaviour is due to the significantly larger length of the side of a vehicle when compared with its width. However this analysis is based on a relatively small data set with only two or three test collisions in each category. Nevertheless larger data sets are not expected to produce significantly different results.

The analytical model produces results which are comparable to the Monte Carlo method. It is clear too that the two methods produce closer results if uncertainty in PDOF is minimised. A method for reducing the uncertainty in PDOF is discussed in Chapter 7.

8.5 Determining actual vehicle speeds

A new technique is developed in Chapter 7 which permits the actual speeds of vehicles involved in a collision to be determined from the changes in velocity which each vehicle sustains as a result of that collision. This is a significant new result based on the assumptions of the CRASH algorithm. However it should be noted that this method is equally applicable to any technique which provides change in velocity data. The new method takes into account the effects of restitution both parallel and tangentially to the impulse and as such should be applicable to the majority of vehicle to vehicle collisions.

This new method cannot be used however where the angle between the closing velocities is either zero or 180° as the solution relies upon the sine of this angle in the denominator leading to a singularity in the solution equations. At angles close to zero

or 180° the results become very sensitive to the exact angle and any results should be treated with caution.

The determination of vehicle pre-impact velocities with knowledge of the changes in velocity means that the post impact velocities can also be determined. Using an iterative process the PDOF values for each vehicle can be refined so that the desired post impact trajectories are achieved. This too is a significant development in forensic collision investigation as it enables a better estimate to be made of the PDOFs which traditionally have been difficult to estimate. It is found that even small variations in PDOF (around 0.1°) can produce significant changes in the post-impact trajectories so that estimates of PDOF to within ±1° are possible.

The new technique to estimate pre-impact speeds was applied to the RICSAC series of test collisions. Using the standard energy adjustment factor discussed in Chapter 4 it was found that the new method produced results which underestimated DeltaV by about 2% with a standard deviation of 6.4%

The new energy adjustment factor was also applied to the RICSAC collisions and compared with the standard adjustment factor. Using the new factor produced a slightly better correspondence with actual pre-impact speeds with an average error of less than 0.2% with a standard deviation of 5.5%. This shows that a combination of the new techniques to estimate pre-impact speeds, coupled with the new adjustment factor may yield an estimate of pre-impact speeds with a 95% confidence interval of about ±11%.

8.6 Evaluation

In Chapter 1 a series of specific objectives were formulated by which this research could be evaluated. For convenience these are addressed in turn

Determine how the various impact phase models are interrelated

> Chapter 2 shows how the impact phase models considered by this research are related. The two momentum models of Brach [**11**] and Ishikawa [**43**] are shown to be equivalent. The relationship of the momentum models to the CRASH model developed by McHenry [**65**] is also established. That is, if the impact

plane required by the models of Brach and Ishikawa is orientated so that it is perpendicular to the impulse, then all three models produce identical results.

So that consistency can be achieved, describe a systematic method to determine crush damage profiles

Chapter 3 provides a consolidated set of measuring protocols. Although many of the techniques are addressed elsewhere, there is not a single document summarising them or their application. In particular a new technique for measuring severely bowed vehicles is presented.

Determine whether the energy adjustment factor commonly used by CRASH accurately models reality. If not, determine whether there an alternative adjustment factor which can be utilised or developed

These objectives are considered in Chapter 4. A number of energy adjustment factors have been proposed in addition to the standard factor proposed by McHenry [**65**]. None of these factors produce total crush energy values which correspond to the loss of energy predicted by the momentum only models of Brach [**11**] and Ishikawa [**43**]. An alternative energy adjustment factor is developed and evaluated which does produce crush energy results which match those predicted by the momentum models.

Determine the overall accuracy that can be expected from CRASH analyses

This aspect is considered in Chapters 5 and 6. Overall accuracy is found to be dependent on the impact type. For example, front to side impacts are inherently less accurate than front to front or front to end impacts.

Determine the most significant factors affecting the accuracy of CRASH

The most significant factor affecting the accuracy of CRASH is the requirement for user estimated values for the principal direction of force (PDOF). Uncertainty in the PDOF is typically in the order of ±20°. Such a level of uncertainty in the PDOF accounts for some 52% of the total uncertainty in the overall result.

Ascertain whether it is possible to determine the actual velocities of vehicles from DeltaV values

Chapter 7 describes the development of a new technique which allows the determination of actual pre- and post-impact velocities from an analysis of the changes in velocity sustained by each of the vehicles in a collision. This technique is applicable to the majority of vehicle to vehicle collisions. When compared to the results of a series of test collisions the new technique is able to predict the actual pre-impact speeds with a 95% confidence interval of ±11%. This is comparable to the accuracy obtained with many of the other techniques used in forensic collision investigation.

Describe techniques which can be used or developed to reduce uncertainty in the most significant factors affecting accuracy

Chapter 7 presents a new technique which can be used to refine an initial estimate of the PDOFs. Matching the post-impact trajectories predicted by the determination of actual speeds algorithm, enables the initial estimate of the PDOF to be adjusted thereby significantly reducing the uncertainty in the estimate of PDOF. Small changes in the PDOF estimates can have a large effect on the post impact trajectories which means that potential uncertainty in the PDOF can be reduced to less than ±1°.

8.7 Limitations of findings

The investigation has demonstrated the accuracy of CRASH from a theoretical and experimental viewpoint. However, the study was restricted by a relatively small sample of collisions (mainly the RICSAC series of tests), covering a limited range of collision typologies. The CRASH algorithm can be viewed as two separate techniques; the first to establish an estimate of the work done in causing deformation and the second to calculate the change in velocity. The study has clearly evaluated the relative importance of the factors applied to the second part of the model. For the first part, the work done is significantly affected by the accuracy of the residual crush measurements and the stiffness coefficient values (*A* and *B*). These were considered for the test data available. However, it is possible that the *A* and *B* values used over-simplify the force-crush relationship for a modern vehicle, where a non-linear response may be observed

for some cars. The assessment of this was beyond the practicable scope of this study, largely because of the data restrictions.

8.8 Recommendations for future work

The validation of the theoretical models developed as part of this thesis is based on a relatively small sample of test collisions, mainly those from the RICSAC series of tests. A study using a more extensive series of tests would yield more detail of the likely accuracy of the CRASH algorithm. It would also provide additional information which may help to refine the details of the analytical and Monte Carlo models presented here.

The new energy adjustment factor described in Chapter 4 has been validated for a range of scenarios Further work would assist in determining the validity of its use in a wider range of collisions. Chapter 4 considered some collisions where the new adjustment factor generated results which matched those from the momentum models of Brach [**11**] and Ishikawa [**43**]. The technique was applied to the RICSAC tests, a standard data set, with considerable success. There are few if any other data set available. The production and publication of other data sets would enable a wider investigation of all the models discussed here. Additional work in this area is desirable.

Bibliography

1 Anon. *Collision Deformation Classification.* Vol J224MAR80. (1980) SAE.

2 Anon. *Road Vehicle Collisions British Standard Automobile Series.* BS AU 191: 1983 ISO 6813-1981; 1983.

3 Bartlett W. *Evaluating the Uncertainty in Various Measurement Tasks Common to Accident Reconstruction.* (2002) SAE. 2002-01-0546.

4 Brach R. *An impact moment coefficient for vehicle collision analysis.* (1977) 770014.

5 Brach RM. *Comments on Energy loss in vehicle to vehicle impact by Dario Vangi.* (2009) International Journal of Impact Engineering. May 2009.

6 Brach RM. *Energy Loss in Vehicle Collisions.* (1987) SAE. 871993.

7 Brach RM. *Impact analysis of two-vehicle collisions.* (1983) SAE. 830468.

8 Brach RM. *Mechanical Impact Dynamics.* (1990) John Wiley & Sons.

9 Brach RM, Brach RM. *A Review of Impact Models for Vehicle Collision.* (1987) SAE. 870048.

10 Brach RM, Brach RM. *Crush Energy and Planar Impact Mechanics for Accident Reconstruction.* (1998) SAE. 980025.

11 Brach RM, Brach RM. *Vehicle Accident Analysis and Reconstruction Methods.* (2005) SAE International.

12 Brach RM, Smith RA. *Re-Analysis of the RICSAC Car Crash Accelerometer Data.* (2002) SAE. 2002-01-1305.

13 Brach RM, Welsh KJ, Brach RM. *Residual Crush Energy Partitioning, Normal and Tangential Energy Losses.* (2007) SAE. 2007-01-0737.

14 Burkhard PM. *DeltaV, BEV and Coefficient of Restitution Relationships as Applied to the Interpretation of Vehicle Crash Test Data.* (2001) SAE. 2001-01-0499.

15 Burkhard PM. *Determination of b1 coefficients from lower and higher speed impacts using peak force.* (2001) SAE. 2001-01-0501.

16 Campbell KL. *Energy Basis for Collision Severity.* (1974) SAE. 740565.

17 Cannon JW. *Dependence of a Coefficient of Restitution on Geometry for High Speed Vehicle Collisions.* (2001) SAE. 2001-01-0892.

18 Carpenter NJ, Welcher JB. *Stiffness and Crush Energy Analysis for Vehicle.* (2001) SAE. 2001-01-0500.

19 Chen HF, Tanner CB, Cheng PH, Guenther DA. *Application of Force Balance Method in Accident Reconstruction.* (2005) SAE. 2005-01-1188.

20 Cipriani AL. *Low Speed Collinear Impact Severity: A comparison Between Full Scale Testing and Analytical Prediction Tools with Restitution Analysis.* (2002) SAE. 2002-01-0540.

21 Cipriani AL, Bayan FP, Woodhouse ML, Cornetto AD, Dalton AP, Tanner CB, Timbario TA, Dererl ES. *Low Speed Collinear Impact Severity: A Comparison Between Full Scale Testing and Analytical Prediction Tools with Restitution Analysis.* (2002) SAE. 2002-01-0540.

22 Day TD, Hargens RL. *An Overview of the Way EDCRASH Computes Delta-V.* (1987) SAE. 870041.

23 Day TD, Hargens RL. *An Overview of the Way EDSMAC Computes Delta-V.* (1988) SAE. 880069.

24 Day TD, Hargens RL. *Differences Between EDCRASH and CRASH3.* (1985) SAE. 850253.

25 Day TD, Hargens RL. *Further Validation of EDCRASH Using the RICSAC Staged Collisions.* (1989) SAE. 890740.

26 *EDCRASH.* Beaverton, USA: Engineering Dynamics Corporation.

27 Emori RI. *Analytical approach to automobile collisions.* (1968) SAE. 680016.

28 Engineering Dynamics Corporation. *EDCRASH Training Manual.* (1986) Engineering Dynamics Corporation.

29 Fell M, Hughes M. *Summary of data for the ITAI field day at Leyland.* (1993) Impact. Impact Special.

30 Fonda AG. *Nonconservation of Momentum During Impact.* (1995) SAE. 950355.

31 Fonda AG. *Principles of Crush Energy Determination.* (1999) SAE. 1999-01-0106.

32 Fonda AG. *The Effects of Measurement Uncertainty on the Reconstruction of Various Vehicular Collisions.* (2004) SAE. 2004-01-1220.

33 Fonda AG, Metz LD. *Post-Impact Spin.* (1993) SAE. 930653.

34 Funk JR, Cornier JM, Bain CE. *Analytical Model for Investigating Low-Speed Sideswipe Collisions.* (2004) SAE. 2004-01-1185.

35 Gabler HC, Hampton CE, Hinch J. *Crash Severity: A Comparison of Event Data Recorder Measurements with Accident Reconstruction Estimates.* (2004) SAE. 2004-01-1194.

36 Garrott WR. *Measured Vehicle Inertial Parameters - NHTSA's Data Through September 1992.* (1993) SAE. 930897.

37 Garrott WR, Christos J, Monk M. *Vehicle Inertial Parameters.* (?) Accident Reconstruction Journal.

38 Grimes WD, Hesser R, Hunter J, Neptune JA. *Developing a crush profile estimate by balancing impact forces.* (1997) SAE. 970942.

39 Hague D. *Frontal Generic Stiffness Coefficients and CRASH3 Analysis.* In: ITAI Conference Proceedings; 2005.

40 Huang M. *Vehicle Crash Mechanics.* (2002) CRC Press.

41 Ishikawa H. *Computer simulation of automobile collision – reconstruction of accidents.* (1985) SAE. 851729.

42 Ishikawa H. *Impact Center and Restitution Coefficients for Accident Reconstruction.* (1994) SAE. 940564.

43 Ishikawa H. *Impact model for accident reconstruction~Normal and tangential restitution coefficients.* (1993) SAE. 930654.

44 ISO. Uncertainty of measurement -- Part 3: Guide to the expression of uncertainty in measurement. [Internet]. 1998 [cited 2010 March]. Available from: http://www.iso.org/sites/JCGM/GUM/JCGM100/C045315e-html/C045315e.html?csnumber=50461.

45 ITAI. *Field Day – Lotus 16th October 1994, Results Issue.* (1995) Impact.;4(3):67-98.

46 Jean B. *Calculating Stiffness Coefficients from Barrier Test Data. Accident.* (1992) Accident Reconstruction Journal. 4(5).

47 Jennings PW. *Methods For Assessing Vehicle Speed From Impact Damage.* (1999) Accident Reconstruction Seminar.

48 Jennings PW, Jones IS. *Development and Evaluation of the CRASH2 Program for Use under European Conditions.* (1981) SAE. 810473.

49 Jewkes DB. *Reconstruction of Accident Severity in a Multiple Vehicle Collision.* (2001) SAE. 2001-01-1283.

50 Jones IS. *The Effect of Impact Type and Vehicle Velocity on Vehicle Crush.* (1983) American Association for Automotive Medicine. 27th Annual Proceedings.

51 Jones IS, Baum AS. *Research Input for Computer Simulation of Automobile Collisions.* Vol DOT HS-805 040. (1978) Calspan Corporation.

52 Jones IS, Baum AS. *Research Input for Computer Simulation of Automobile Collisions, Vol IV.* Department of Transportation; 1978. DOT HS 805 040.

53 Kelvin WT, Tait PG. *Treatise on Natural Philosophy.* (1912) Cambridge University Press.

54 Kerkhoff JF, Husher SE, Varat MS, Busenga AM, Hamilton K. *An investigation into vehicle frontal impact stiffness, BEV and repeated testing for reconstruction.* (1993)

SAE. 930899.

55 Kimborough S. *Determining the Relative Likelihoods of Competing Scenarios of Events Leading to an Accident.* (2004) SAE. 2004-01-1222.

56 Lenard J, Hurley B, Thomas P. *The Accuracy of Crash3 for Calculating Collision Severity in Modern European Cars.* (1998) 98-S6-O-08.

57 Lenard J, Hurley B, Thomas P. The Statistical Accuracy Of Delta-V In Systematic Field Accident Studies. [Internet]. 2000 [cited 2010 February 24]. Available from: http://www.ukccis.org/downloads/download_publication.asp?file=publications/Statistical accuracy of delta v.pdf.

58 Levy G. An introduction to quasi-random numbers. [Internet]. [cited 2010 March]. Available from: http://www.nag.co.uk/IndustryArticles/introduction_to_quasi_random_numbers.pdf.

59 Levy RA. *Speed Determination in Car-Truck Sideswipe Collisions.* (2000) SAE. 2000-01-0463.

60 Long TJ. *A validation study for the force balance method in determination of stiffness coefficients.* (1999) SAE. 1999-01-0079.

61 Marine MC, Wirth JL, Thomas TM. *Crush Energy Considerations in Override/Underride Impacts.* (2002) SAE. 2002-01-0556.

62 Marquard JF. *Collision Severity - Measurement by Delta-V.* (1974) SAE. 740303.

63 Mason R, Whitcomb D. *The Estimation of Accident Impact Speed.* (1972) YB-3109-v-1.

64 Mathsoft Engineering & Education, Inc. *Mathcad Help* [Internet]. 2005.

65 McHenry R. *CRASH3 Users Guide and Technical Manual.* Vol HS-805-732. (1981) DOT.

66 McHenry BG. *The Algorithms of CRASH.* In: Southeast Coast Collision Conference; 2001; Cocoa Beach, Florida.

67 McHenry RR, McHenry BG. *A Revised Analysis Procedure for the CRASH Computer Program.* (1986) SAE. 861894.

68 McHenry RR, McHenry BG. *Effect of Restitution in the Application of Crush Coefficients.* (1997) SAE. 970960.

69 McHenry BG, McHenry RR. *RICSAC-97 A Re-evaluation of the Reference Set of Full Scale Crash Tests.* (1997) SAE. 970961.

70 Moffat. *Highway Collision Reconstruction.* In: Winter Annual Meeting; 1980; Chicago.

71 Monson KL, Germane GJ. *Determination and Mechanisms of Motor vehicle Structural Restitution from Crash Test Data.* (1999) SAE. 1999-01-0097.

72 Navin F, MacNabb M, Miyasaki GW. *Elastic Properties of Selected Vehicles.* (1988) SAE. 880223.

73 Navin F, Navin N, MacNabb M. *CRASH III and Canadian test data.* (1987) SAE. 870499.

74 Neades J. *AiDamage.* Ai Training Services Ltd; 1996 - 2010.

75 Neades J, Shephard R. *Review of Measurement Protocols Applicable to Speed from Damage Programs.* (2009) Impact.;17(1):4-12.

76 Neptune JA. *A Comparison of Crush Stiffness Characteristics from Partial-Overlap and Full-Overlap Frontal Crash Tests.* (1999) SAE. 1999-01-0105.

77 Neptune JA. *Crush Stiffness Coefficients, Restitution Constants, And a Revision of CRASH3 and SMAC.* (1998) SAE. 980029.

78 Neptune JA. *Impact Analysis Based Upon the CRASH3 Damage Algorithm.* (1995) SAE. 950358.

79 Neptune JA. *Speed from Skids: A Modern Approach.* (1995) SAE. 950354.

80 Neptune JA, Blair GY, Flynn JE. *A Method for Quantifying Vehicle Crush Stiffness Coefficients.* (1992) SAE. 920607.

81 Neptune JA, Flynn JE. *A Method for Determining Accident Specific Crush Stiffness Coefficients.* (1994) SAE. 940913.

82 Neptune JA, Flynn JE. *A Method for Determining Crush Stiffness Coefficients from Offset Frontal and Side Crash Tests.* (1998) SAE. 980024.

83 NHTSA. Vehicle Crash test Database. [Internet]. 2010 [cited 2010 January 14]. Available from: http://www-nrd.nhtsa.dot.gov/database/veh/veh.htm.

84 Otubushin A, Galer M. *Crashed Vehicle Examination Techniques.* (1986) SAE. 860372.

85 Otubushin A, Galer M. *Crashed vehicle examination techniques.* (1986) SAE. 860372.

86 Pepper JV. *Harriot's Manuscript on the Theory of Impacts.* (1976);33(2):131-151.

87 Prasad AK. *Coefficient of Restitution of Vehicle Structures and its Use in Estimating the Total DeltaV in Automobile Collisions.* (1991) AMD Vol. 126/BED-Vol. 19.

88 Prasad AK. *CRASH3 Damage Algorithm Reformulation for Front and Rear Collisions.* (1990) SAE. 900098.

89 Prasad AK. *Energy absorbed by vehicle structures in side-impacts.* (1991) SAE. 910599.

90 Prasad AK. *Energy Dissipated in Vehicle Crush - A Study Using the Repeated Test Technique.* (1990) SAE. 900412.

91 Prasad AK. *Missing Vehicle Algorithm (OLDMISS) Reformulation.* (1991) SAE. 910121.

92 Robert C, Casella G. *Monte Carlo Statistical Methods.* (2004) Springer.

93 Robinette RD, Fay RJ, Paulsen RE. *Delta-V: basic concepts, computational methods, and misunderstandings.* (1994) SAE. 940915.

94 Rose NA, Fenton SJ, Beauchamp G. *Restitution Modeling for Crush Analysis: Theory and Validation.* (2006) 2006-01-0908.

95 Rose NA, Fenton SJ, Ziernicki RM. *An Examination of the CRASH3 Effective Mass Concept.* (2004) SAE. 2004-01-1181.

96 Shoemaker NE. *Reseach Input for Computer Simulation of Automobile Collisions Vol II.* US Department of Transportation; 1978. DOT HS 805 038.

97 Shoemaker NE. *Reseach Input for Computer Simulation of Automobile Collisions Vol III.* US Department of Transportation; 1978. DOT HS 805 039.

98 Siddall DE, Day TD. *Updating the Vehicle Class Categories.* (1996) SAE. 960897.

99 Singh J. *Estimating Constant Stiffness Model Parameters from Collisions Tests.* (2006) Impact. Spring.

100 Singh J. *Uncertainty Relationships for Derived Stiffness Coefficients from Full Width to Rigid Barrier Collision Tests using Normally Distributed Input Parameters.* (2004) Impact.

101 Smith GC. *Conservation of Momentum Analysis of Two-Dimensional Colliding Bodies, With or Without Trailers.* (1994) SAE. 940566.

102 Smith R. *Critical Speed Motion.* (1991) Impact.;2:12-14.

103 Smith R. *Reconstructions of the Collisions Staged at the Field Day at Norwich.* In: ITAI 2nd International Conference; 1995; Plymouth.

104 Smith R. *Skidding to a Stop.* (1990) Impact.;1(1):11-12.

105 Smith R. *The formula commonly used to calculate velocity change in vehicle collisions.* (1998) IMechE. 212(Part D): p. 73-78.

106 Smith R, Evans AK. *Vehicle Speed calculation from pedestrian throw distance.* (1999) IMechE. 213 PartD.

107 Smith RR, Noga JT. *Accuracy and Sensitivity of Crash.* US Dept of Transportation; 1982. DOT HS 906 152.

108 Smith RA, Noga JT. *Accuracy and Sensitivity of CRASH.* (1982) SAE. 821169.

109 Smith RA, Noga JT. *Examples of Staged Collisions in Accident Reconstruction. Highway Collision Reconstruction.* (1980).

110 Smith RA, Tsongas NG. *Crash Phase Accident Reconstruction.* (1986) SAE. 860209.

111 Steffan H, Moser A. *The Collision and Trajectory Models of PC-CRASH.* (1996) SAE. 960666.

112 Stonex K, Nelson W, Garrett J. *Collision Damage Severity Scale.* (1970) SAE. 700136.

113 Stronge WJ. *Impact Mechanics.* (2000) Cambridge University Press.

114 Strother CE, Woolley RL, James MB. *A Comparison Between NHTSA Crash test Data and CRASH3 Frontal Stiffness Coefficients.* (1990) SAE. 900101.

115 Struble DE. *Generalizing CRASH3 for Reconstructing Specific Accidents.* (1987) SAE. 870041.

116 Tanny S. *The Linear Elastic-Plastic Vehicle Collision.* (1992) SAE. 921073.

117 Tsongas NG. *CRASH3 User's Guide and Technical Manual.* US Department of Transportation; 1986.

118 Tumbas NS, Smith RA. *Measuring Protocol for Quantifying Vehicle Damage from an Energy Basis Point of View.* (1988) SAE. 880072.

119 Vangi D. *Energy loss in vehicle to vehicle oblique impact.* (2009) International Journal of Impact Engineering.;36:512-521.

120 Vangi D. *Personal correspondence.* 2010.

121 Varat MS, Husher SE, Kerkhoff JF. *An analysis of trends of vehicle frontal impact stiffness.* (1994) SAE. 940914.

122 Weinzierl S. Introduction to Monte Carlo methods. [Internet]. 2000 [cited 2010 March]. Available from: http://arxiv.org/abs/hep-ph/0006269v1.

123 Welsh KJ. *Crush energy and structural characterization.* (1999) SAE. 1999-01-0099.

124 *WinCrash.* Tucson, USA: ARSoftware.

125 Wood D. *Structural Rebound Characteristics of the Car Population in Frontal Impacts.* (2000) SAE. 2000-01-0461.

126 Wood D, Adamson D, Ydenius A. *Car frontal collisions: occupant compartment forces, interface forces and stiffnesses.* (2004) IJCrash. 9(3): p. 311-325.

127 Wood DP, Doody M, Mooney S. *Application of a Generalised Frontal Crush Model of the Car Population to Pole and Narrow Object Impacts.* (1993) SAE.;930894.

128 Wood D, Walsh D. *Car to Car Interaction in Frontal Collisions: A Model for the Behaviour of the Car Population and Options for Improved Crashworthiness.* (2000) International Journal of Crashworthiness.;7(1):79 - 96.

129 Woolley RL. *Non-Linear Damage Analysis in Accident Reconstruction.* (2001) SAE. 2001-01-0504.

130 Woolley RL. *The IMPAC Computer Program for Accident Reconstruction.* (1985) SAE. 850254.

131 Woolley RL, Kinney JR. *Reference Cases for Comparison of Collision Algorithms Used in Accident Reconstruction.* (1994) SAE. 940567.

132 Woolley RL, Warner CY, Tagg MD. *Inaccuracies in the CRASH3 Program.* (1985) SAE. 850255.

Appendices

Appendix A: Solution Equations of Planar Impact Mechanics (PIM)

The planar impact mechanics model is discussed in section 2.3. Brach [**11**] shows that the solution to this model can be expressed as

$$
\begin{aligned}
v_{1n} &= u_{1n} + \bar{m}(1+e_n)U_{Rn}q/m_1,\\
v_{1t} &= u_{1t} + \mu\bar{m}(1+e_n)U_{Rn}q/m_1,\\
v_{2n} &= u_{2n} - \bar{m}(1+e_n)U_{Rn}q/m_2,\\
v_{2t} &= u_{2t} - \mu\bar{m}(1+e_n)U_{Rn}q/m_2,\\
\Omega_1 &= \omega_1 + \bar{m}(1+e_n)U_{Rn}(h_1-\mu h_{1t})q/(m_1k_1^2),\\
\Omega_2 &= \omega_2 + \bar{m}(1+e_n)U_{Rn}(h_2-\mu h_{2t})q/(m_2k_2^2)
\end{aligned}
$$

where

$$
\begin{aligned}
&\bar{m} = m_1m_2/(m_1+m_2),\\
&e_n = -(V_{Rn}/U_{Rn}),\\
&\mu = P_t/P_n,\\
&U_{Rn} = u_{2n} - h_2\omega_2 - u_{1n} + h_1\omega_1, \qquad V_{Rn} = v_{2n} - h_2\Omega_2 - v_{1n} + h_1\Omega_1,\\
&U_{Rt} = u_{2t} - h_{2t}\omega_2 - u_{1t} + h_{1t}\omega_2, \qquad V_{Rt} = v_{2t} + h_{2t}\Omega_2 - v_{1t} + h_{1t}\Omega_1,\\
&\frac{1}{q} = 1 + \frac{\bar{m}h_1^2}{m_1k_1^2} + \frac{\bar{m}h_2^2}{m_2k_2^2} - \mu\left(\frac{\bar{m}h_1h_{1t}}{m_1k_1^2} + \frac{\bar{m}h_2h_{2t}}{m_2k_2^2}\right) = A + \mu B,\\
&h_2 = d_2\sin(\theta_2+\phi_2-\Gamma) \qquad h_{2t} = d_2\cos(\theta_2+\phi_2-\Gamma),\\
&h_1 = d_1\sin(\theta_1+\phi_1-\Gamma) \qquad h_{1t} = d_1\cos(\theta_1+\phi_1-\Gamma).
\end{aligned}
$$

The critical impulse ratio μ_0 is defined as

$$
\mu_0 = \frac{rA + B(1+e)}{(1+e)(1+C) + rB}
$$

where

$$
\begin{aligned}
r &= U_{Rt}/U_{Rn},\\
A &= 1 + \frac{\bar{m}h_1^2}{m_1k_1^2} + \frac{\bar{m}h_2^2}{m_2k_2^2},\\
B &= \frac{\bar{m}h_1h_{1t}}{m_1k_1^2} + \frac{\bar{m}h_2h_{2t}}{m_2k_2^2},\\
C &= \frac{\bar{m}h_{1t}^2}{m_1k_1^2} + \frac{\bar{m}h_{2t}^2}{m_2k_2^2}.
\end{aligned}
$$

Appendix B: Solution Equations For Ishikawa's Model

Ishikawa's impact model is discussed in section 2.4. Ishikawa [**43**] and [**42**] shows that the solution to this model can be expressed as

$$P_n = \frac{1}{(1-m_n m_t m_0^2)}\left[m_n U_{Rn}(1+e_n) + m_n m_t m_0 U_{Rt}(1+e_t)\right],$$
$$P_t = \frac{1}{(1-m_n m_t m_0^2)}\left[m_t U_{Rt}(1+e_t) + m_n m_t m_0 U_{Rn}(1+e_n)\right]$$

where e_n and e_t can be found from

$$V_{Rn} = -e_n U_{Rn}, \qquad V_{Rt} = -e_t U_{Rt}$$

The relative speeds of the point of application of the impulse are defined as

$$U_{Rn} = u_{2n} - h_2\omega_2 - u_{1n} + h_1\omega_1$$
$$V_{Rn} = v_{2n} - h_2\Omega_2 - v_{1n} + h_1\Omega_1$$
$$U_{Rt} = u_{2t} + h_{2t}\omega_2 - u_{1t} - h_{1t}\omega_1$$
$$V_{Rt} = v_{2t} + h_{2t}\Omega_2 - v_{1t} - h_{1t}\Omega_1$$

The mass ratios used extensively by Ishikawa are defined as

$$m_n = \frac{\gamma_{1n} m_1 \gamma_{2n} m_2}{\gamma_{1n} m_1 + \gamma_{2n} m_2}$$
$$m_t = \frac{\gamma_{1t} m_1 \gamma_{2t} m_2}{\gamma_{1t} m_1 + \gamma_{2t} m_2}$$
$$m_0 = \frac{h_1 h_{1t}}{m_1 k_1^2} + \frac{h_2 h_{2t}}{m_2 k_2^2}$$

where

$$\gamma_{1n} = \frac{k_1^2}{k_1^2 + h_1^2} \qquad \gamma_{2n} = \frac{k_2^2}{k_2^2 + h_2^2}$$
$$\gamma_{1t} = \frac{k_1^2}{k_1^2 + h_{1t}^2} \qquad \gamma_{2t} = \frac{k_2^2}{k_2^2 + h_{2t}^2}$$

,

$$e_t = \frac{m_n U_{Rn}(1+e_n)(\mu - m_t m_0)}{m_t U_{Rt}(1-\mu m_n m_0)} - 1$$

$$\mu = \frac{P_t}{P_n}$$

Appendix C: Conversion between PIM and Ishikawa's Models

PIM by Brach [**11**] and the impact model by Ishikawa [**43**] are shown to be equivalent in Chapter 2. The equivalence between the various coefficients used by each of these model is summarised below

$$m_n = \frac{\bar{m}}{A}, \qquad m_t = \frac{\bar{m}}{(1+C)}, \qquad m_0 = \frac{B}{\bar{m}}.$$

From these equivalences the following products can be derived

$$m_n m_0 = \frac{B}{A},$$
$$m_t m_0 = \frac{B}{(1+C)},$$
$$\frac{m_n}{m_t} = \frac{1+C}{A},$$
$$m_n m_t m_0^2 = \frac{B^2}{A(1+C)},$$
$$m_n m_t m_0 = \frac{\bar{m}B}{A(1+C)}.$$

Using Ishikawa's notation μ can be expressed as

$$\mu = \frac{P_t}{P_n} = \frac{m_n m_t m_0 U_{Rn}(1+e_n) + m_t U_{Rt}(1+e_t)}{m_n m_t m_0 U_{Rt}(1+e_t) + m_n U_{Rn}(1+e_n)}$$

Using the conversion factors specified above, μ can be expressed using Brach's notation and e_t as

$$\mu = \frac{(1+e_t)rA + B(1+e_n)}{(1+e_n)(1+C) + rB(1+e_t)}$$

Appendix D: Raw RICSAC Test Data (From Jones & Baum [51])

This data forms the raw source data used by several analyses in this thesis and is introduced in Chapter 5.

Test.Veh	L	D	c1	c2	c3	c4	c5	c6	A	B	Cg to F	Cg to R	Length	Width	Mass	Inertia
	(cm)	(cm)	(cm)	(cm)	(cm)	(cm)	(cm)	(cm)	(N/cm)	(N/cm^2)	(cm)	(cm)	(cm)	(cm)	(kg)	(kgm^2)
1.1	117	36	10	14	18	26	31	38	624	23	251	290	541	196	2096	5054
1.2	288	55	1	30	27	30	23	10	246	46	212	233	444	171	1398	2659
2.1	192	0	1	6	9	18	30	42	624	23	251	290	541	196	2096	5054
2.2	301	35	17	58	60	54	25	0	246	46	212	233	444	171	1397	2658
3.1	76	56	5	5	4	4	5	6	624	23	251	290	541	196	2244	5413
3.2	76	13	17	17	15	13	10	8	684	28	212	233	444	171	1415	2692
4.1	105	41	16	20	25	32	38	46	624	23	251	290	541	196	2259	5447
4.2	106	-23	91	81	74	61	50	38	684	28	212	233	444	171	1447	2752
5.1	85	52	4	4	5	5	6	7	624	23	251	290	541	196	2086	5031
5.2	135	-4	91	93	80	58	34	15	641	26	193	213	406	154	1147	1484
6.1	138	25	1	1	3	4	4	6	624	23	251	290	541	196	1950	4703
6.2	196	-8	10	30	45	49	43	21	246	46	212	233	444	171	1190	2263
7.1	168	10	0	3	5	10	13	16	624	23	251	290	541	196	1678	4047
7.2	276	-22	0	28	45	53	54	20	246	46	212	233	444	171	771	1467
8.1	185	0	7	9	0	0	0	0	624	23	251	290	541	196	2031	4899
8.2	215	38	16	21	23	15	11	2	251	35	251	290	541	196	2136	5152
9.1	126	4	13	15	32	19	19	24	528	32	193	213	406	154	1023	1323
9.2	138	173	20	12	12	8	7	4	251	35	251	290	541	196	2222	5359
10.1	121	-7	18	26	36	23	23	23	528	32	193	213	406	154	1046	1352
10.2	135	169	23	17	15	13	11	1	251	35	251	290	541	196	2141	5162
11.1	83	-32	56	51	47	43	38	32	454	30	212	233	444	171	1379	2624
11.2	82	-33	75	67	58	47	36	28	624	23	251	290	541	196	2200	5305
12.1	81	7	98	88	75	66	50	36	454	30	212	233	444	171	1420	2700
12.2	72	-27	100	84	73	60	49	38	624	23	251	290	541	196	2046	4935

Appendix E: RICSAC Results from raw Jones & Baum [51] data using AiDamage [74]

This appendix shows the impact configurations, PDOF and DeltaV results from the raw (unadjusted) RICSAC test data as described in Chapter 5 and listed in Appendix D. Note that the zero entries for pre-impact motion in the AiDamage results merely indicate that this calculation was not performed.

RICSAC 1 Base
(Damage based)

	Veh 1	Veh 2	
Total Delta-V:	6.20	9.29	m/s
Longitudinal Delta-V:	-5.37	-8.05	m/s
Lateral Delta-V:	3.10	-4.65	m/s
Angular velocity change:	237.41	99.48	deg/s
Energy dissapated:	45.17	102.89	kJ
Magnitude of force	154.67	716.43	kN
Force direction:	-30.00	30.00	deg
Pre-impact motion			
Total speed:	0.00	0.00	m/s
Longitudinal component:	0.00	0.00	m/s
Lateral component:	0.00	0.00	m/s
Sideslip:	0.00	0.00	deg

RICSAC 1 Base
(Impact attitude)

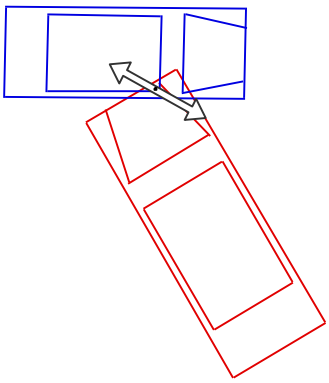

RICSAC 2 Base
(Damage based)

	Veh 1	Veh 2	
Total Delta-V:	10.34	15.51	m/s
Longitudinal Delta-V:	-8.96	-13.43	m/s
Lateral Delta-V:	5.17	-7.75	m/s
Angular velocity change:	373.92	211.12	deg/s
Energy dissapated:	61.43	344.43	kJ
Magnitude of force	225.92	1286.51	kN
Force direction:	-30.00	30.00	deg
Pre-impact motion			
Total speed:	0.00	0.00	m/s
Longitudinal component:	0.00	0.00	m/s
Lateral component:	0.00	0.00	m/s
Sideslip:	0.00	0.00	deg

RICSAC 2 Base
(Impact attitude)

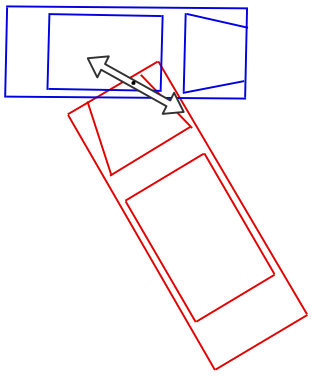

RICSAC 3 Base
(Damage based)

	Veh 1	Veh 2	
Total Delta-V:	2.79	4.43	m/s
Longitudinal Delta-V:	-2.79	4.36	m/s
Lateral Delta-V:	0.00	-0.77	m/s
Angular velocity change:	37.47	42.05	deg/s
Energy dissapated:	8.82	15.67	kJ
Magnitude of force	55.96	81.65	kN
Force direction:	0.00	170.00	deg
Pre-impact motion			
Total speed:	0.00	0.00	m/s
Longitudinal component:	0.00	0.00	m/s
Lateral component:	0.00	0.00	m/s
Sideslip:	0.00	0.00	deg

RICSAC 3 Base
(Impact attitude)

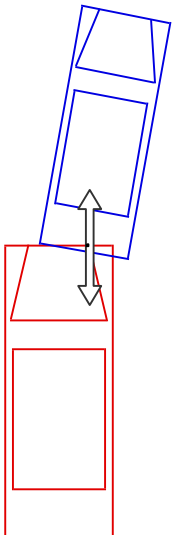

RICSAC 4 Base
(Damage based)

	Veh 1	Veh 2	
Total Delta-V:	7.05	11.00	m/s
Longitudinal Delta-V:	-7.05	10.85	m/s
Lateral Delta-V:	0.06	-1.82	m/s
Angular velocity change:	87.25	206.84	deg/s
Energy dissapated:	39.23	128.61	kJ
Magnitude of force	137.11	273.06	kN
Force direction:	-0.50	170.50	deg
Pre-impact motion			
Total speed:	0.00	0.00	m/s
Longitudinal component:	0.00	0.00	m/s
Lateral component:	0.00	0.00	m/s
Sideslip:	0.00	0.00	deg

RICSAC 4 Base
(Impact attitude)

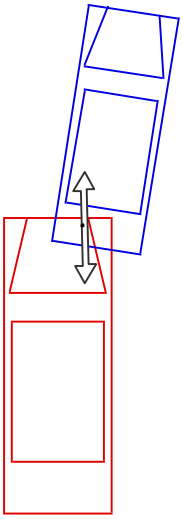

RICSAC 5 Base
(Damage based)

	Veh 1	Veh 2	
Total Delta-V:	6.89	12.54	m/s
Longitudinal Delta-V:	-6.89	12.35	m/s
Lateral Delta-V:	0.00	-2.18	m/s
Angular velocity change:	92.78	276.12	deg/s
Energy dissapated:	10.05	153.47	kJ
Magnitude of force	63.09	316.33	kN
Force direction:	0.00	170.00	deg
Pre-impact motion			
Total speed:	0.00	0.00	m/s
Longitudinal component:	0.00	0.00	m/s
Lateral component:	0.00	0.00	m/s
Sideslip:	0.00	0.00	deg

RICSAC 5 Base
(Impact attitude)

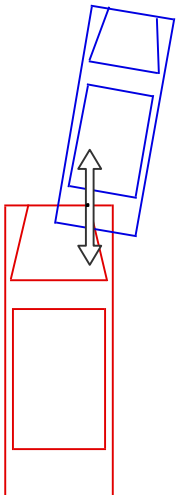

RICSAC 6 Base
(Damage based)

	Veh 1	Veh 2	
Total Delta-V:	6.97	11.43	m/s
Longitudinal Delta-V:	-6.04	-9.90	m/s
Lateral Delta-V:	3.49	-5.72	m/s
Angular velocity change:	265.68	196.25	deg/s
Energy dissapated:	19.39	169.58	kJ
Magnitude of force	111.71	756.66	kN
Force direction:	-30.00	30.00	deg
Pre-impact motion			
Total speed:	0.00	0.00	m/s
Longitudinal component:	0.00	0.00	m/s
Lateral component:	0.00	0.00	m/s
Sideslip:	0.00	0.00	deg

RICSAC 6 Base
(Impact attitude)

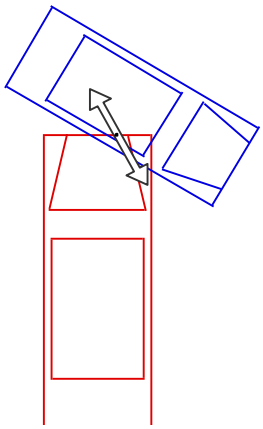

RICSAC 7
(Damage based)

	Veh 1	Veh 2	
Total Delta-V:	8.84	19.25	m/s
Longitudinal Delta-V:	-7.66	-16.67	m/s
Lateral Delta-V:	4.42	-9.62	m/s
Angular velocity change:	330.08	324.45	deg/s
Energy dissapated:	31.47	267.59	kJ
Magnitude of force	155.34	1099.85	kN
Force direction:	-30.00	30.00	deg
Pre-impact motion			
Total speed:	0.00	0.00	m/s
Longitudinal component:	0.00	0.00	m/s
Lateral component:	0.00	0.00	m/s
Sideslip:	0.00	0.00	deg

RICSAC 7
(Impact attitude)

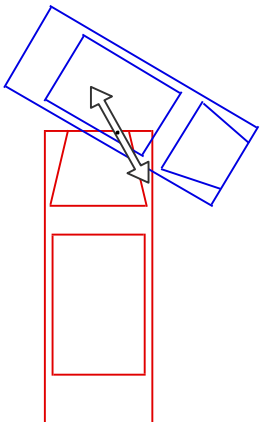

RICSAC 8
(Damage based)

	Veh 1	Veh 2	
Total Delta-V:	4.84	4.60	m/s
Longitudinal Delta-V:	-4.19	-2.30	m/s
Lateral Delta-V:	2.42	-3.99	m/s
Angular velocity change:	146.22	29.89	deg/s
Energy dissapated:	34.81	28.27	kJ
Magnitude of force	173.38	199.27	kN
Force direction:	-30.00	60.00	deg
Pre-impact motion			
Total speed:	0.00	0.00	m/s
Longitudinal component:	0.00	0.00	m/s
Lateral component:	0.00	0.00	m/s
Sideslip:	0.00	0.00	deg

RICSAC 8
(Impact attitude)

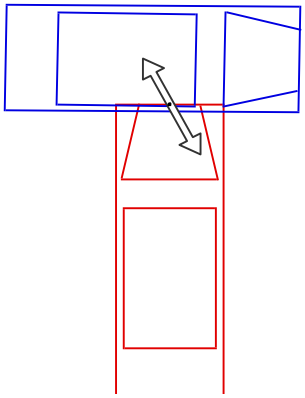

RICSAC 9
(Damage based)

	Veh 1	Veh 2	
Total Delta-V:	6.32	2.91	m/s
Longitudinal Delta-V:	-5.47	-1.45	m/s
Lateral Delta-V:	3.16	-2.52	m/s
Angular velocity change:	272.37	-62.99	deg/s
Energy dissapated:	37.85	10.16	kJ
Magnitude of force	174.51	96.70	kN
Force direction:	-30.00	60.00	deg
Pre-impact motion			
Total speed:	0.00	0.00	m/s
Longitudinal component:	0.00	0.00	m/s
Lateral component:	0.00	0.00	m/s
Sideslip:	0.00	0.00	deg

RICSAC 9
(Impact attitude)

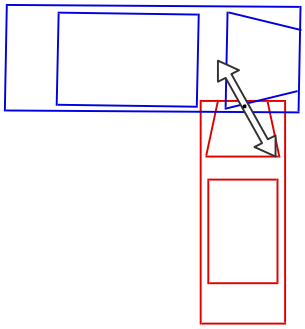

RICSAC 10
(Damage based)

	Veh 1	Veh 2	
Total Delta-V:	7.08	3.46	m/s
Longitudinal Delta-V:	-2.99	-3.13	m/s
Lateral Delta-V:	6.42	-1.46	m/s
Angular velocity change:	500.78	12.96	deg/s
Energy dissapated:	68.99	21.82	kJ
Magnitude of force	386.54	233.29	kN
Force direction:	-65.00	25.00	deg
Pre-impact motion			
Total speed:	0.00	0.00	m/s
Longitudinal component:	0.00	0.00	m/s
Lateral component:	0.00	0.00	m/s
Sideslip:	0.00	0.00	deg

RICSAC 10
(Impact attitude)

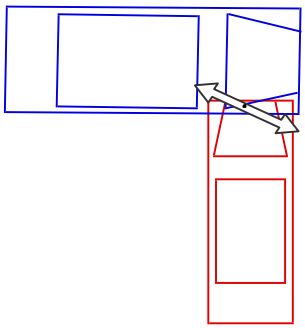

RICSAC 11
(Damage based)

	Veh 1	Veh 2	
Total Delta-V:	9.33	5.85	m/s
Longitudinal Delta-V:	-9.30	-5.83	m/s
Lateral Delta-V:	-0.73	0.46	m/s
Angular velocity change:	-142.41	-30.01	deg/s
Energy dissapated:	44.89	61.60	kJ
Magnitude of force	147.75	150.95	kN
Force direction:	4.50	-4.50	deg
Pre-impact motion			
Total speed:	0.00	0.00	m/s
Longitudinal component:	0.00	0.00	m/s
Lateral component:	0.00	0.00	m/s
Sideslip:	0.00	0.00	deg

RICSAC 11
(Impact attitude)

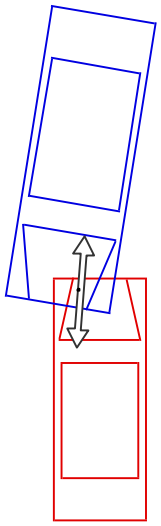

RICSAC 12
(Damage based)

	Veh 1	Veh 2	
Total Delta-V:	11.74	8.15	m/s
Longitudinal Delta-V:	-11.70	-8.12	m/s
Lateral Delta-V:	-0.92	0.64	m/s
Angular velocity change:	-45.24	-29.66	deg/s
Energy dissapated:	90.69	76.60	kJ
Magnitude of force	205.08	157.37	kN
Force direction:	4.50	-4.50	deg
Pre-impact motion			
Total speed:	0.00	0.00	m/s
Longitudinal component:	0.00	0.00	m/s
Lateral component:	0.00	0.00	m/s
Sideslip:	0.00	0.00	deg

RICSAC 12
(Impact attitude)

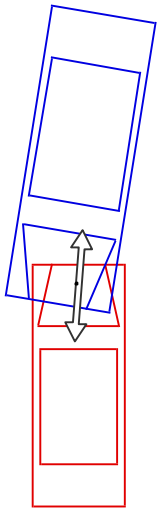

Appendix F: RICSAC Results from adjusted data using AiDamage [74]

This appendix shows the impact configurations, PDOF and DeltaV results from the adjusted RICSAC test data as described in Chapter 5. The pre and post-impact vectors showing motion of the vehicles' centres of mass are also shown, superimposed on the impact configuration diagrams. Note that as in Appendix F, the zero entries for pre-impact motion in the AiDamage results merely indicate that this calculation was not performed.

RICSAC 1 v2 -10cm
(Damage based)

	Veh 1	Veh 2	
Total Delta-V:	5.26	7.88	m/s
Longitudinal Delta-V:	-5.16	-5.20	m/s
Lateral Delta-V:	1.03	-5.92	m/s
Angular velocity change:	117.77	35.16	deg/s
Energy dissapated:	35.23	48.35	kJ
Magnitude of force	136.60	342.71	kN
Force direction:	-11.30	48.70	deg
Pre-impact motion			
Total speed:	0.00	0.00	m/s
Longitudinal component:	0.00	0.00	m/s
Lateral component:	0.00	0.00	m/s
Sideslip:	0.00	0.00	deg

RICSAC 1 v2 -10cm
(Impact attitude)

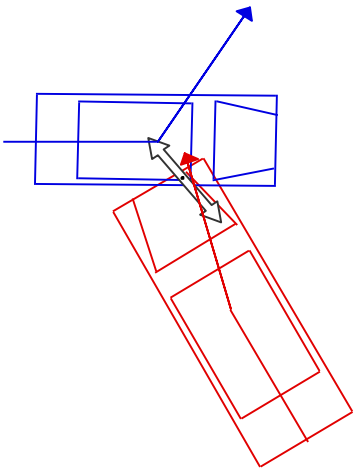

RICSAC 2 v2 -15cm
(Damage based)

	Veh 1	Veh 2	
Total Delta-V:	8.37	12.55	m/s
Longitudinal Delta-V:	-8.19	-8.35	m/s
Lateral Delta-V:	1.70	-9.37	m/s
Angular velocity change:	170.35	135.79	deg/s
Energy dissapated:	48.05	165.20	kJ
Magnitude of force	199.80	611.18	kN
Force direction:	-11.70	48.30	deg
Pre-impact motion			
Total speed:	0.00	0.00	m/s
Longitudinal component:	0.00	0.00	m/s
Lateral component:	0.00	0.00	m/s
Sideslip:	0.00	0.00	deg

RICSAC 2 v2 -15cm
(Impact attitude)

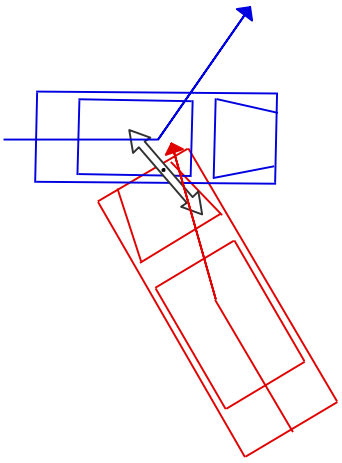

RICSAC 3 V1 +5 cm V2 offset -50
(Damage based)

	Veh 1	Veh 2	
Total Delta-V:	3.03	4.80	m/s
Longitudinal Delta-V:	-2.93	4.79	m/s
Lateral Delta-V:	-0.74	0.34	m/s
Angular velocity change:	-3.92	56.09	deg/s
Energy dissapated:	12.59	15.28	kJ
Magnitude of force	66.85	80.62	kN
Force direction:	14.10	-175.90	deg
Pre-impact motion			
Total speed:	0.00	0.00	m/s
Longitudinal component:	0.00	0.00	m/s
Lateral component:	0.00	0.00	m/s
Sideslip:	0.00	0.00	deg

RICSAC 3 V1 +5 cm V2 offset -50
(Impact attitude)

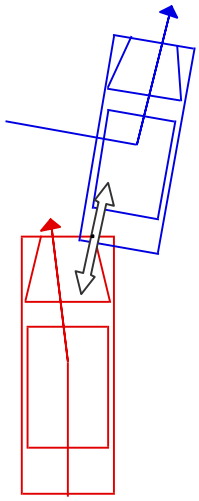

RICSAC 4 v2 -15cm
(Damage based)

	Veh 1	Veh 2	
Total Delta-V:	6.59	10.28	m/s
Longitudinal Delta-V:	-6.46	10.28	m/s
Lateral Delta-V:	-1.27	0.20	m/s
Angular velocity change:	6.04	88.25	deg/s
Energy dissapated:	40.73	88.10	kJ
Magnitude of force	139.72	224.59	kN
Force direction:	11.10	-178.90	deg
Pre-impact motion			
Total speed:	0.00	0.00	m/s
Longitudinal component:	0.00	0.00	m/s
Lateral component:	0.00	0.00	m/s
Sideslip:	0.00	0.00	deg

RICSAC 4 v2 -15cm
(Impact attitude)

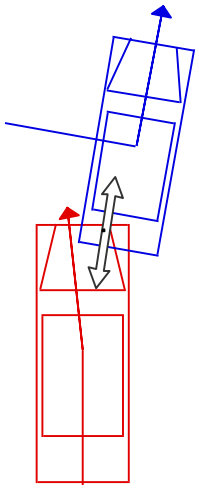

RICSAC 5 -20cm
(Damage based)

	Veh 1	Veh 2	
Total Delta-V:	5.90	10.74	m/s
Longitudinal Delta-V:	-5.78	10.73	m/s
Lateral Delta-V:	-1.19	0.30	m/s
Angular velocity change:	7.80	97.45	deg/s
Energy dissapated:	10.47	94.16	kJ
Magnitude of force	64.41	242.52	kN
Force direction:	11.60	-178.40	deg
Pre-impact motion			
Total speed:	0.00	0.00	m/s
Longitudinal component:	0.00	0.00	m/s
Lateral component:	0.00	0.00	m/s
Sideslip:	0.00	0.00	deg

RICSAC 5 -20cm
(Impact attitude)

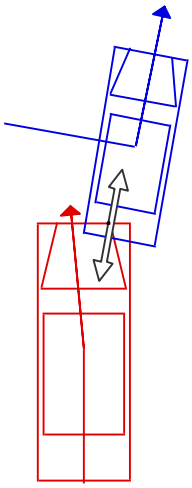

RICSAC 6 -15cm
(Damage based)

	Veh 1	Veh 2	
Total Delta-V:	5.20	8.52	m/s
Longitudinal Delta-V:	-5.10	-5.59	m/s
Lateral Delta-V:	0.99	-6.43	m/s
Angular velocity change:	108.83	117.95	deg/s
Energy dissapated:	15.09	67.68	kJ
Magnitude of force	98.55	328.19	kN
Force direction:	-11.00	49.00	deg
Pre-impact motion			
Total speed:	0.00	0.00	m/s
Longitudinal component:	0.00	0.00	m/s
Lateral component:	0.00	0.00	m/s
Sideslip:	0.00	0.00	deg

RICSAC 6 -15cm
(Impact attitude)

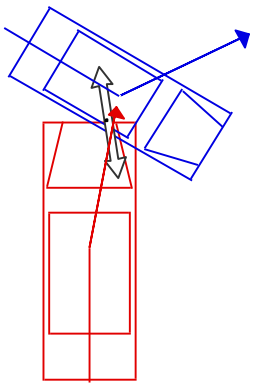

RICSAC 7 -20cm
(Damage based)

	Veh 1	Veh 2	
Total Delta-V:	6.06	13.19	m/s
Longitudinal Delta-V:	-5.91	-8.94	m/s
Lateral Delta-V:	1.33	-9.69	m/s
Angular velocity change:	133.32	186.45	deg/s
Energy dissapated:	24.80	91.76	kJ
Magnitude of force	137.90	438.30	kN
Force direction:	-12.70	47.30	deg
Pre-impact motion			
Total speed:	0.00	0.00	m/s
Longitudinal component:	0.00	0.00	m/s
Lateral component:	0.00	0.00	m/s
Sideslip:	0.00	0.00	deg

RICSAC 7 -20cm
(Impact attitude)

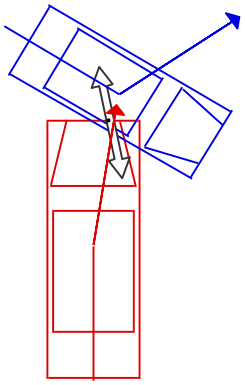

RICSAC 8 e=0.3
(Damage based)

	Veh 1	Veh 2	
Total Delta-V:	6.55	6.23	m/s
Longitudinal Delta-V:	-6.14	-2.18	m/s
Lateral Delta-V:	2.29	-5.84	m/s
Angular velocity change:	140.82	18.66	deg/s
Energy dissapated:	29.75	24.16	kJ
Magnitude of force	160.31	184.24	kN
Force direction:	-20.50	69.50	deg
Pre-impact motion			
Total speed:	0.00	0.00	m/s
Longitudinal component:	0.00	0.00	m/s
Lateral component:	0.00	0.00	m/s
Sideslip:	0.00	0.00	deg

RICSAC 8 e=0.3
(Impact attitude)

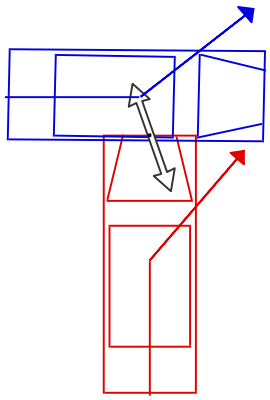

RICSAC 9 v2 -10cm e=0.3
(Damage based)

	Veh 1	Veh 2	
Total Delta-V:	6.65	3.06	m/s
Longitudinal Delta-V:	-6.18	-1.14	m/s
Lateral Delta-V:	2.47	-2.84	m/s
Angular velocity change:	232.02	-82.16	deg/s
Energy dissapated:	17.77	8.84	kJ
Magnitude of force	118.66	90.20	kN
Force direction:	-21.80	68.20	deg
Pre-impact motion			
Total speed:	0.00	0.00	m/s
Longitudinal component:	0.00	0.00	m/s
Lateral component:	0.00	0.00	m/s
Sideslip:	0.00	0.00	deg

RICSAC 9 v2 -10cm e=0.3
(Impact attitude)

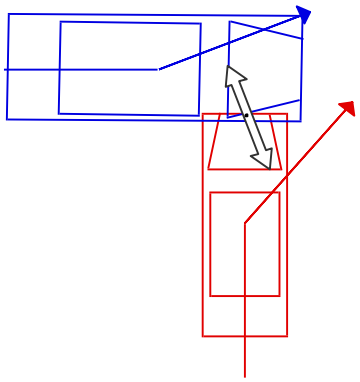

RICSAC 10 v2 +10cm e=0.3
(Damage based)

	Veh 1	Veh 2	
Total Delta-V:	10.85	5.30	m/s
Longitudinal Delta-V:	-9.81	-2.26	m/s
Lateral Delta-V:	4.64	-4.79	m/s
Angular velocity change:	334.60	-134.60	deg/s
Energy dissapated:	42.20	27.21	kJ
Magnitude of force	180.69	155.68	kN
Force direction:	-25.30	64.70	deg
Pre-impact motion			
Total speed:	0.00	0.00	m/s
Longitudinal component:	0.00	0.00	m/s
Lateral component:	0.00	0.00	m/s
Sideslip:	0.00	0.00	deg

RICSAC 10 v2 +10cm e=0.3
(Impact attitude)

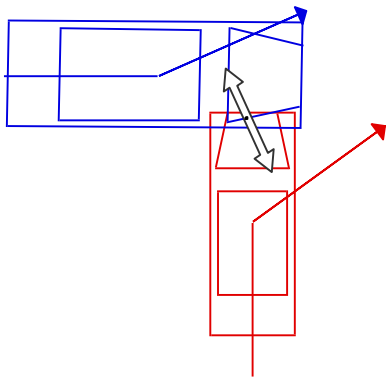

RICSAC 11
(Damage based)

	Veh 1	Veh 2	
Total Delta-V:	9.73	6.10	m/s
Longitudinal Delta-V:	-9.72	-5.97	m/s
Lateral Delta-V:	0.49	1.26	m/s
Angular velocity change:	-77.15	11.04	deg/s
Energy dissapated:	44.73	63.94	kJ
Magnitude of force	147.48	153.79	kN
Force direction:	-2.90	-11.90	deg
Pre-impact motion			
Total speed:	0.00	0.00	m/s
Longitudinal component:	0.00	0.00	m/s
Lateral component:	0.00	0.00	m/s
Sideslip:	0.00	0.00	deg

RICSAC 11
(Impact attitude)

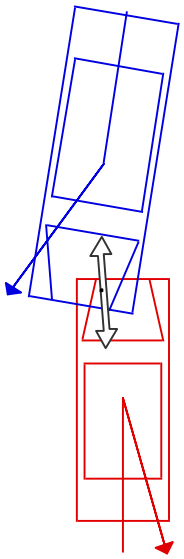

RICSAC 12
(Damage based)

	Veh 1	Veh 2	
Total Delta-V:	15.95	11.07	m/s
Longitudinal Delta-V:	-15.95	-10.96	m/s
Lateral Delta-V:	-0.28	1.54	m/s
Angular velocity change:	-31.08	-18.76	deg/s
Energy dissapated:	155.25	151.37	kJ
Magnitude of force	352.12	308.92	kN
Force direction:	1.00	-8.00	deg
Pre-impact motion			
Total speed:	0.00	0.00	m/s
Longitudinal component:	0.00	0.00	m/s
Lateral component:	0.00	0.00	m/s
Sideslip:	0.00	0.00	deg

RICSAC 12
(Impact attitude)

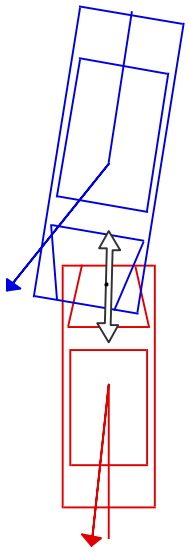

Appendix G: Partial Derivatives. Evaluated symbolically using Mathcad V.13

The potential accuracy of CRASH is discussed in Chapter 5. As part of the analysis to determine the accuracy, the partial derivatives of the equations used to determine crush energy and CRASH are required. These are detailed in this Appendix.

Partial derivatives for the crush energy equation (from Singh [**99**])

$$E = \frac{L}{n-1}\left[\frac{A\eta}{2} + \frac{B\kappa}{6} + \frac{(n-1)A^2}{2B}\right]$$

where

$$\eta = \sum_{i=1}^{n-1}[C_i + C_{i+1}],$$
$$\kappa = \sum_{i=1}^{n-1}\left[C_i^2 + C_i C_{i+1} + C_{i+1}^2\right].$$

The partial derivatives of each parameter are then given by

$$\frac{\partial \eta}{\partial C_j} = \frac{\partial\left[\sum_{i=1}^{n-1}\left[C_i + C_{i+1}\right]\right]}{\partial C_j} = \begin{cases} 1 & \text{for } j = 1, n \\ 2 & \text{for } j \neq 1, n \end{cases}$$

$$\frac{\partial \kappa}{\partial C_j} = \frac{\partial\left[\sum_{i=1}^{n-1}\left[C_i^2 + C_i C_{i+1} + C_{i+1}^2\right]\right]}{\partial C_j} = \begin{cases} 2C_j + C_{j+1} & \text{for } j = 1 \\ C_{j-1} + 4C_j + C_{j+1} & \text{for } j \neq 1, n \\ 2C_j + C_{j-1} & \text{for } j = n \end{cases}$$

$$\frac{\partial E}{\partial A} = \frac{L}{n-1}\left[\frac{\eta}{2} + \frac{(n-1)A}{B}\right]$$

$$\frac{\partial E}{\partial B} = \frac{L}{n-1}\left[\frac{\kappa}{6} - \frac{(n-1)A^2}{2B^2}\right]$$

$$\frac{\partial E}{\partial L} = \frac{1}{n-1}\left[\frac{A\eta}{2} + \frac{B\kappa}{6} + \frac{(n-1)A^2}{2B}\right]$$

$$\frac{\partial E}{\partial \eta} = \frac{AL}{2(n-1)}$$

$$\frac{\partial E}{\partial \kappa} = \frac{BL}{6(n-1)}$$

Partial derivatives of standard energy adjustment factor (from McHenry [**65**])

$$E = E_n(1+\tan^2\alpha)\,.$$

This produces the two partial derivatives

$$\frac{\partial E}{\partial E_n} = 1+\tan^2\alpha,$$
$$\frac{\partial E}{\partial \alpha} = 2\sec^2\alpha\tan\alpha = 2\tan\alpha(1+\tan^2\alpha).$$

Partial derivatives of CRASH equation (from McHenry [**65**] and amended by Smith [**105**])

$$\Delta v_1 = \sqrt{\frac{2m_2(E_1+E_2)(1+e_p)}{m_1(m_1\delta_2+m_2\delta_1)(1-e_p)}},$$
$$\Delta v_2 = \frac{m_1\Delta v_1}{m_2}$$

where

$$\delta = 1+\frac{h^2}{k^2},$$
$$h = d\sin(\theta+\phi).$$

This produces the series of partial derivatives for each parameter as follows

$$\frac{\partial\delta}{\partial h} = 2\frac{h}{k^2}$$
$$\frac{\partial\delta}{\partial k} = -2\frac{h^2}{k^3}$$
$$\frac{\partial h}{\partial d} = \sin(\theta+\phi)$$
$$\frac{\partial h}{\partial \theta} = d\cos(\theta+\phi)$$
$$\frac{\partial h}{\partial \phi} = d\cos(\theta+\phi)$$

$$\frac{\partial\Delta v_1}{\partial m_1} = \frac{-\dfrac{m_2(E_1+E_2)(1+e_p)}{m_1^2(m_1\delta_2+m_2\delta_1)(1-e_p)} - \dfrac{m_2\delta_2(E_1+E_2)(1+e_p)}{m_1(m_1\delta_2+m_2\delta_1)^2(1-e_p)}}{\sqrt{\dfrac{2m_2(E_1+E_2)(1+e_p)}{m_1(m_1\delta_2+m_2\delta_1)(1-e_p)}}}$$

$$\frac{\partial \Delta v_1}{\partial m_2} = \frac{\dfrac{(E_1+E_2)(1+e_p)}{m_1(m_1\delta_2+m_2\delta_1)(1-e_p)} - \dfrac{m_2\delta_1(E_1+E_2)(1+e_p)}{m_1(m_1\delta_2+m_2\delta_1)^2(1-e_p)}}{\sqrt{\dfrac{2m_2(E_1+E_2)(1+e_p)}{m_1(m_1\delta_2+m_2\delta_1)(1-e_p)}}}$$

$$\frac{\partial \Delta v_1}{\partial E_1} = \frac{\partial \Delta v_1}{\partial E_2} = \frac{m_2(1+e_p)}{m_1(m_1\delta_2+m_2\delta_1)(1-e_p)\sqrt{\dfrac{2m_2(E_1+E_2)(1+e_p)}{m_1(m_1\delta_2+m_2\delta_1)(1-e_p)}}}$$

$$\frac{\partial \Delta v_1}{\partial \delta_1} = -\frac{m_2^2(E_1+E_2)(1+e_p)}{m_1(m_1\delta_2+m_2\delta_1)^2(1-e_p)\sqrt{\dfrac{2m_2(E_1+E_2)(1+e_p)}{m_1(m_1\delta_2+m_2\delta_1)(1-e_p)}}}$$

$$\frac{\partial \Delta v_1}{\partial \delta_2} = -\frac{m_2(E_1+E_2)(1+e_p)}{(m_1\delta_2+m_2\delta_1)^2(1-e_p)\sqrt{\dfrac{2m_2(E_1+E_2)(1+e_p)}{m_1(m_1\delta_2+m_2\delta_1)(1-e_p)}}}$$

$$\frac{\partial \Delta v_1}{\partial e_p} = \frac{\dfrac{m_2(E_1+E_2)}{m_1(m_1\delta_2+m_2\delta_1)(1-e_p)} + \dfrac{m_2(E_1+E_2)(1+e_p)}{m_1(m_1\delta_2+m_2\delta_1)(1-e_p)^2}}{\sqrt{\dfrac{2m_2(E_1+E_2)(1+e_p)}{m_1(m_1\delta_2+m_2\delta_1)(1-e_p)}}}$$

$$\frac{\partial \Delta v_2}{\partial m_1} = \frac{\Delta v_1}{m_2},$$

$$\frac{\partial \Delta v_2}{\partial m_2} = \frac{-\Delta v_1 m_1}{m_2^2}$$

$$\frac{\partial \Delta v_2}{\partial \Delta v_1} = \frac{m_1}{m_2}$$

Appendix H: Analytical Mathcad Model to Determine Uncertainty in Δ*v* (RICSAC 8)

An analytical model to determine the uncertainty in DeltaV is developed in Chapter 5. The listing below is the Mathcad implementation of that model. Note that the green highlighting indicates user input sections, blue highlighting indicates where uncertainty can be adjusted and yellow indicates key output sections.

CRASH Analytical Error Analysis for RICSAC8

Standard error factor to convert 95% confidence limits to standard deviation:

StdErr := 1.9(

Part I: Calculation of Crush Energy

Measurement Data

Vehicle 1

$$C1 := \begin{pmatrix} 6.9 \\ 7.34 \\ 7.78 \\ 8.22 \\ 8.66 \\ 9.1 \end{pmatrix}$$

Vehicle 2

$$C2 := \begin{pmatrix} 15.7 \\ 21.1 \\ 23.4 \\ 15 \\ 11.2 \\ 2 \end{pmatrix}$$

δC := 7.6 (7.62cm is equivalent to 3 inches)

$\sigma_C := \frac{\delta C}{StdErr}$ $\sigma_C = 3.888$

L1 := 185.

L2 := 214.

δL := 15.2 (15.24cm is equivalent to 6 inches)

$\sigma_L := \frac{\delta L}{StdErr}$ $\sigma_L = 7.776$

Stiffness Coefficients

δCoeff := 10% (Permits simple adjustment of all coefficients)

A1 := 623.

A2 := 250.

δA1 := δCoeff · A1

δA2 := δCoeff · A2

$\sigma_{A1} := \frac{\delta A1}{StdErr}$ $\sigma_{A1} = 31.811$

$\sigma_{A2} := \frac{\delta A2}{StdErr}$ $\sigma_{A2} = 12.781$

B1 := 23.

B2 := 34.

δB1 := δCoeff · B1

δB2 := δCoeff · B2

$\sigma_{B1} := \frac{\delta B1}{StdErr}$ $\sigma_{B1} = 1.189$

$\sigma_{B2} := \frac{\delta B2}{StdErr}$ $\sigma_{B2} = 1.776$

Derived values

$i := 0..4$

$\alpha_1 := \sum_i \left(C1_i + C1_{i+1}\right)$ $\alpha_1 = 80$

$\alpha_2 := \sum_i \left(C2_i + C2_{i+1}\right)$ $\alpha_2 = 159.1$

$\beta_1 := \sum_i \left[\left(C1_i\right)^2 + C1_i \cdot C1_{i+1} + \left(C1_{i+1}\right)^2\right]$ $\beta_1 = 966.05$

$\beta_2 := \sum_i \left[\left(C2_i\right)^2 + C2_i \cdot C2_{i+1} + \left(C2_{i+1}\right)^2\right]$ $\beta_2 = 4.303 \times 10^3$

$\sigma_\alpha := \sqrt{18 \cdot \sigma_c^{\,2}}$ $\sigma_\alpha = 16.494$ (Common value for both vehicles)

$$\sigma_{\beta 1} := \sqrt{\sigma_c^{\,2} \cdot \left[\begin{array}{l}\left(2 \cdot C1_0 + C1_1\right)^2 + \left(C1_0 + 4 \cdot C1_1 + C1_2\right)^2 + \left(C1_1 + 4 \cdot C1_2 + C1_3\right)^2 \ldots \\ + \left(C1_2 + 4 \cdot C1_3 + C1_4\right)^2 + \left(C1_3 + 4 \cdot C1_4 + C1_5\right)^2 + \left(2 \cdot C1_5 + C1_4\right)^2\end{array}\right]} \qquad \sigma_{\beta 1} = 396.841$$

$$\sigma_{\beta 2} := \sqrt{\sigma_c^{\,2} \cdot \left[\begin{array}{l}\left(2 \cdot C2_0 + C2_1\right)^2 + \left(C2_0 + 4 \cdot C2_1 + C2_2\right)^2 + \left(C2_1 + 4 \cdot C2_2 + C2_3\right)^2 \ldots \\ + \left(C2_2 + 4 \cdot C2_3 + C2_4\right)^2 + \left(C2_3 + 4 \cdot C2_4 + C2_5\right)^2 + \left(2 \cdot C2_5 + C2_4\right)^2\end{array}\right]} \qquad \sigma_{\beta 2} = 850.255$$

Note multiplier of 1/100 to convert to joules

$n := 6$

$$E1 := 0.01\left[\left[\frac{(n-1) \cdot A1^2}{2 \cdot B1} + \frac{B1 \cdot \beta_1}{6} + \frac{A1 \cdot \alpha_1}{2}\right] \cdot \frac{L1}{n-1}\right]$$

$E1 = 2.611 \times 10^4$

$$E2 := 0.01\left[\left[\frac{(n-1) \cdot A2^2}{2 \cdot B2} + \frac{B2 \cdot \beta_2}{6} + \frac{A2 \cdot \alpha_2}{2}\right] \cdot \frac{L2}{n-1}\right]$$

$E2 = 2.12 \times 10^4$

$dA1 := \frac{1}{5} \cdot \left(5 \cdot \frac{A1}{B1} + \frac{1}{2} \cdot \alpha_1\right) \cdot L1$

$dB1 := \frac{1}{5} \cdot \left(\frac{-5}{2} \cdot \frac{A1^2}{B1^2} + \frac{1}{6} \cdot \beta_1\right) \cdot L1$

$dL1 := \frac{1}{2} \cdot \frac{A1^2}{B1} + \frac{1}{30} \cdot B1 \cdot \beta_1 + \frac{1}{10} \cdot A1 \cdot \alpha_1$

$d\alpha 1 := \frac{1}{10} \cdot A1 \cdot L1$

$d\beta 1 := \frac{1}{30} \cdot B1 \cdot L1$

$dA2 := \frac{1}{5} \cdot \left(5 \cdot \frac{A2}{B2} + \frac{1}{2} \cdot \alpha_2\right) \cdot L2$

$dB2 := \frac{1}{5} \cdot \left(\frac{-5}{2} \cdot \frac{A2^2}{B2^2} + \frac{1}{6} \cdot \beta_2\right) \cdot L2$

$dL2 := \frac{1}{2} \cdot \frac{A2^2}{B2} + \frac{1}{30} \cdot B2 \cdot \beta_2 + \frac{1}{10} \cdot A2 \cdot \alpha_2$

$d\alpha 2 := \frac{1}{10} \cdot A2 \cdot L2$

$d\beta 2 := \frac{1}{30} \cdot B2 \cdot L2$

Potential Error Calculations

$$\sigma_{E1} := 0.01\sqrt{dA1^2\cdot\sigma_{A1}{}^2 + dB1^2\cdot\sigma_{B1}{}^2 + dL1^2\cdot\sigma_L{}^2 + d\alpha1^2\cdot\sigma_\alpha{}^2 + d\beta1^2\cdot\sigma_{\beta1}{}^2} \qquad \delta E1 := \sigma_{E1}\cdot StdEn$$

$$\sigma_{E1} = 3.13\times 10^3$$

$$\delta E1 = 6.134\times 10^3$$

$$\sigma_{E2} := 0.01\sqrt{dA2^2\cdot\sigma_{A2}{}^2 + dB2^2\cdot\sigma_{B2}{}^2 + dL2^2\cdot\sigma_L{}^2 + d\alpha2^2\cdot\sigma_\alpha{}^2 + d\beta2^2\cdot\sigma_{\beta2}{}^2} \qquad \delta E2 := \sigma_{E2}\cdot StdEn$$

$$\sigma_{E2} = 2.47\times 10^3$$

$$\delta E2 = 4.841\times 10^3$$

$$Ratio1 := \frac{\delta E1}{E1} \qquad Ratio1 = 23.497\% \qquad Ratio2 := \frac{\delta E2}{E2} \qquad Ratio2 = 22.835\%$$

Analysis of Energy Calculations

$$errA1 := 1.960.01\cdot\sqrt{dA1^2\cdot\sigma_{A1}{}^2} \qquad errA2 := 1.960.01\cdot\sqrt{dA2^2\cdot\sigma_{A2}{}^2}$$

$$RerrA1 := \frac{errA1}{E1} \qquad RerrA1 = 15.392\% \qquad RerrA2 := \frac{errA2}{E2} \qquad RerrA2 = 5.86\%$$

$$errB1 := 1.960.01\cdot\sqrt{dB1^2\cdot\sigma_{B1}{}^2} \qquad errB2 := 1.960.01\cdot\sqrt{dB2^2\cdot\sigma_{B2}{}^2}$$

$$RerrB1 := \frac{errB1}{E1} \qquad RerrB1 = \blacksquare\% \qquad RerrB2 := \frac{errB2}{E2} \qquad RerrB2 = 4.14\%$$

$$errL1 := 1.960.01\cdot\sqrt{dL1^2\cdot\sigma_L{}^2} \qquad errL2 := 1.960.01\cdot\sqrt{dL2^2\cdot\sigma_L{}^2}$$

$$RerrL1 := \frac{errL1}{E1} \qquad RerrL1 = 8.22\% \qquad RerrL2 := \frac{errL2}{E2} \qquad RerrL2 = 7.102\%$$

$$err\alpha1 := 1.960.01\cdot\sqrt{d\alpha1^2\cdot\sigma_\alpha{}^2} \qquad err\alpha2 := 1.960.01\cdot\sqrt{d\alpha2^2\cdot\sigma_\alpha{}^2}$$

$$Rerr\alpha1 := \frac{err\alpha1}{E1} \qquad Rerr\alpha1 = 14.315\% \qquad Rerr\alpha2 := \frac{err\alpha2}{E2} \qquad Rerr\alpha2 = 8.198\%$$

$$err\beta1 := 1.960.01\cdot\sqrt{d\beta1^2\cdot\sigma_{\beta1}{}^2} \qquad err\beta2 := 1.960.01\cdot\sqrt{d\beta2^2\cdot\sigma_{\beta2}{}^2}$$

$$Rerr\beta1 := \frac{err\beta1}{E1} \qquad Rerr\beta1 = 3.693\% \qquad Rerr\beta2 := \frac{err\beta2}{E2} \qquad Rerr\beta2 = 18.771\%$$

$$t1 := \sqrt{RerrA1^2 + RerrB1^2 + RerrL1^2 + Rerr\alpha1^2 + Rerr\beta1^2} \qquad t2 := \sqrt{RerrA2^2 + RerrB2^2 + RerrL2^2 + Rerr\alpha2^2 + Rerr\beta2^2}$$

$$t1 = 23.497\% \qquad t2 = 22.835\%$$

Energy Adjustment

Principal Directions of Force (PDOF)
(Base Side: 0=Front, 90=right, 180=rear, 270=left)

$BaseSide1 := 0$

$PDOF1 := -30$

$BaseSide2 := 90$

$PDOF2 := 60$

$\delta PDOF := 20$

$\sigma_{PDOF} := \frac{\delta PDOF}{StdErr}$ $\sigma_{PDOF} = 10.204$

$\theta 1 := PDOF1 - BaseSide1$

$\theta 1 = -30$

$\theta 2 := PDOF2 - BaseSide2$

$\theta 2 = -30$

$CF1 := 1 + \tan\left(\theta 1 \cdot \frac{\pi}{180}\right)^2$

$CF1 = 1.333$

$CF2 := 1 + \tan\left(\theta 2 \cdot \frac{\pi}{180}\right)^2$

$CF2 = 1.333$

$d\theta 1 := 2 \cdot \tan\left(\theta 1 \cdot \frac{\pi}{180\pi}\right) \cdot \left(1 + \tan\left(\theta 1 \cdot \frac{\pi}{180}\right)^2\right)$

$d\theta 1 = -0.449$

$d\theta 2 := 2 \cdot \tan\left(\theta 2 \cdot \frac{\pi}{180\pi}\right) \cdot \left(1 + \tan\left(\theta 2 \cdot \frac{\pi}{180}\right)^2\right)$

$d\theta 2 = -0.449$

$\sigma_{CF1} := \sqrt{d\theta 1^2 \cdot \left(\sigma_{PDOF} \frac{\pi}{180}\right)^2}$

$\sigma_{CF1} = 0.08$

$\sigma_{CF2} := \sqrt{d\theta 2^2 \cdot \left(\sigma_{PDOF} \frac{\pi}{180}\right)^2}$

$\sigma_{CF2} = 0.08$

$EC1 := E1 \cdot CF1$

$EC1 = 3.481 \times 10^4$

$EC2 := E2 \cdot CF2$

$EC2 = 2.827 \times 10^4$

$dE1 := CF1$

$dCF1 := E1$

$dE2 := CF2$

$dCF2 := E1$

$\sigma_{EC1} := \sqrt{dE1^2 \cdot \sigma_{E1}{}^2 + dCF1^2 \cdot \sigma_{CF1}{}^2}$

$\sigma_{EC1} = 4.665 \times 10^3$

$\sigma_{EC2} := \sqrt{dE2^2 \cdot \sigma_{E2}{}^2 + dCF2^2 \cdot \sigma_{CF2}{}^2}$

$\sigma_{EC2} = 3.898 \times 10^3$

Part II: Calculation of DeltaV

δ1 and δ2

$\phi 1 := -0.98557$ $\phi 2 := -77.446$

$d1 := 2.4701$ $d2 := 0.91163$

$\delta d := \frac{7.62}{100}$

$\sigma_d := \frac{\delta d}{StdErr}$ $\sigma_d = 0.039$

Angle defined so that lateral variation is equal to δd

$\delta\phi 1 := \frac{180}{\pi} \cdot \operatorname{asin}\left(\frac{\delta d}{d1}\right)$ $\delta\phi 1 = 1.768$ $\delta\phi 2 := \frac{180}{\pi} \cdot \operatorname{asin}\left(\frac{\delta d}{d2}\right)$ $\delta\phi 2 = 4.795$

$\sigma_{\phi 1} := \frac{\delta\phi 1}{StdErr}$ $\sigma_{\phi 1} = 0.902$ $\sigma_{\phi 2} := \frac{\delta\phi 2}{StdErr}$ $\sigma_{\phi 2} = 2.446$

$h1 := d1 \cdot \sin\left[(PDOF1 + \phi 1) \cdot \frac{\pi}{180}\right]$ $h1 = -1.272$

$h2 := d2 \cdot \sin\left[(PDOF2 + \phi 2) \cdot \frac{\pi}{180}\right]$ $h2 = -0.273$

$dd1 := \sin\left[(PDOF1 + \phi 1) \cdot \frac{\pi}{180}\right]$ $dd1 = -0.515$

$dd2 := \sin\left[(PDOF2 + \phi 2) \cdot \frac{\pi}{180}\right]$ $dd2 = -0.3$

$d\phi 1 := d1 \cdot \cos\left[(PDOF1 + \phi 1) \cdot \frac{\pi}{180}\right]$ $d\phi 1 = 2.118$

$d\phi 2 := d2 \cdot \cos\left[(PDOF2 + \phi 2) \cdot \frac{\pi}{180}\right]$ $d\phi 2 = 0.87$

$dPDOF1 := d\phi 1$ $dPDOF2 := d\phi 2$

$\sigma_{h1} := \sqrt{(dd1 \cdot \sigma_d)^2 + \left(dPDOF1 \cdot \sigma_{PDOF} \cdot \frac{\pi}{180}\right)^2 + \left(d\phi 1 \cdot \sigma_{\phi 1} \cdot \frac{\pi}{180}\right)^2}$ $\sigma_{h1} = 0.379$

$\sigma_{h2} := \sqrt{(dd2 \cdot \sigma_d)^2 + \left(dPDOF2 \cdot \sigma_{PDOF} \cdot \frac{\pi}{180}\right)^2 + \left(d\phi 2 \cdot \sigma_{\phi 2} \cdot \frac{\pi}{180}\right)^2}$ $\sigma_{h2} = 0.16$

$k1 := 1.5530$ $k2 := 1.5529$

$\delta k := 0.1$

$\sigma_k := \frac{\delta k}{StdErr}$ $\sigma_k = 0.051$

$\delta 1 := 1 + \frac{h1^2}{k1^2}$ $\delta 1 = 1.67$ $\delta 2 := 1 + \frac{h2^2}{k2^2}$ $\delta 2 = 1.031$

$\gamma 1 := \frac{1}{\delta 1}$ $\gamma 1 = 0.599$ $\gamma 2 := \frac{1}{\delta 2}$ $\gamma 2 = 0.97$

$dk1 := -2 \cdot \frac{h1^2}{k1^3}$ $dk1 = -0.863$ $dk2 := -2 \cdot \frac{h2^2}{k2^3}$ $dk2 = -0.04$

$dh1 := 2 \cdot \frac{h1}{k1^2}$ $dh1 = -1.054$ $dh2 := 2 \cdot \frac{h2}{k2^2}$ $dh2 = -0.227$

$\sigma_{\delta 1} := \sqrt{(dk1 \cdot \sigma_k)^2 + (dh1 \cdot \sigma_{h1})^2}$ $\sigma_{\delta 2} := \sqrt{(dk2 \cdot \sigma_k)^2 + (dh2 \cdot \sigma_{h2})^2}$

$\sigma_{\delta 1} = 0.402$ $\sigma_{\delta 2} = 0.036$

Mass

$m1 := 2031$ $m2 := 2136$

$\delta m := 50$

$\sigma_m := \frac{\delta m}{StdErr}$ $\sigma_m = 25.51$

Coefficient of Restitution

$ep := 0.6$

$\delta ep := 0.0$

$\sigma_{ep} := \frac{\delta ep}{StdErr}$ $\sigma_{ep} = 0$

Nominal Mean DeltaV and Variance

$\Delta v1 := \sqrt{\frac{2 \cdot m2 \cdot (EC1 + EC2) \cdot (1 + ep)}{m1 \cdot (m1 \cdot \delta 2 + m2 \cdot \delta 1) \cdot (1 - ep)}}$ $\Delta v2 := \Delta v1 \cdot \frac{m1}{m2}$

$\Delta v1 = 6.553$ $\Delta v2 = 6.231$

$$dm1 := \frac{\left[(-m2)\cdot(EC1+EC2)\cdot\frac{1+ep}{m1^2\cdot(m1\cdot\delta2+m2\cdot\delta1)\cdot(1-ep)} - m2(EC1+EC2)\cdot\frac{1+ep}{m1\cdot(m1\cdot\delta2+m2\cdot\delta1)^2\cdot(1-ep)}\cdot\delta2\right]}{\left[\frac{2\cdot m2(EC1+EC2)\cdot(1+ep)}{m1\cdot(m1\cdot\delta2+m2\cdot\delta1)\cdot(1-ep)}\right]^{\frac{1}{2}}}$$

$$dm1 = -1.632\times 10^{-3}$$

$$dm2 := \frac{\left[(EC1+EC2)\cdot\frac{1+ep}{m1\cdot(m1\cdot\delta2+m2\cdot\delta1)\cdot(1-ep)} - m2(EC1+EC2)\cdot\frac{1+ep}{m1\cdot(m1\cdot\delta2+m2\cdot\delta1)^2\cdot(1-ep)}\cdot\delta1\right]}{\left[\frac{2\cdot m2(EC1+EC2)\cdot(1+ep)}{m1\cdot(m1\cdot\delta2+m2\cdot\delta1)\cdot(1-ep)}\right]^{\frac{1}{2}}}$$

$$dm2 = 4.19\times 10^{-4}$$

$$dEC1 := \frac{m2\frac{1+ep}{m1\cdot(m1\cdot\delta2+m2\cdot\delta1)\cdot(1-ep)}}{\left[\frac{2\cdot m2(EC1+EC2)\cdot(1+ep)}{m1\cdot(m1\cdot\delta2+m2\cdot\delta1)\cdot(1-ep)}\right]^{\frac{1}{2}}}$$

$$dEC1 = 3.837\times 10^{-5}$$

$$dEC2 := \frac{m2\frac{1+ep}{m1\cdot(m1\cdot\delta2+m2\cdot\delta1)\cdot(1-ep)}}{\left[\frac{2\cdot m2(EC1+EC2)\cdot(1+ep)}{m1\cdot(m1\cdot\delta2+m2\cdot\delta1)\cdot(1-ep)}\right]^{\frac{1}{2}}}$$

$$dEC2 = 3.837\times 10^{-5}$$

$$d\delta1 := \frac{-\left[m2^2\cdot(EC1+EC2)\cdot\frac{1+ep}{m1\cdot(m1\cdot\delta2+m2\cdot\delta1)^2\cdot(1-ep)}\right]}{\left[\frac{2\cdot m2(EC1+EC2)\cdot(1+ep)}{m1\cdot(m1\cdot\delta2+m2\cdot\delta1)\cdot(1-ep)}\right]^{\frac{1}{2}}}$$

$$d\delta1 = -0.913$$

$$d\delta2 := \frac{-\left[m2(EC1+EC2)\cdot\frac{1+ep}{(m1\cdot\delta2+m2\cdot\delta1)^2\cdot(1-ep)}\right]}{\left[\frac{2\cdot m2(EC1+EC2)\cdot(1+ep)}{m1\cdot(m1\cdot\delta2+m2\cdot\delta1)\cdot(1-ep)}\right]^{\frac{1}{2}}}$$

$$d\delta2 = -0.868$$

$$dep := \frac{\left[m2 \cdot \frac{EC1 + EC2}{m1 \cdot (m1 \cdot \delta 2 + m2 \cdot \delta 1) \cdot (1 - ep)} + m2 \cdot (EC1 + EC2) \cdot \frac{1 + ep}{m1 \cdot (m1 \cdot \delta 2 + m2 \cdot \delta 1) \cdot (1 - ep)^2} \right]}{\left[\frac{2 \cdot m2 \cdot (EC1 + EC2) \cdot (1 + ep)}{m1 \cdot (m1 \cdot \delta 2 + m2 \cdot \delta 1) \cdot (1 - ep)} \right]^{\frac{1}{2}}}$$

$dep = 4.841$

$$\sigma_{\Delta v1} := \sqrt{dm1^2 \cdot \sigma_m^2 + dm2^2 \cdot \sigma_m^2 + dEC1^2 \cdot \sigma_{EC1}^2 + dEC2^2 \cdot \sigma_{EC2}^2 + d\delta 1^2 \cdot \sigma_{\delta 1}^2 + d\delta 2^2 \cdot \sigma_{\delta 2}^2 + dep^2 \cdot \sigma_{ep}^2}$$

$\delta\Delta v1 := \sigma_{\Delta v1} \cdot StdEn$

$\sigma_{\Delta v1} = 0.438$

$\delta\Delta v1 = 0.859$

$dm11 := \frac{\Delta v1}{m2}$ $dm11 = 2.266 \times 10^{-3}$

$dm12 := (-\Delta v1) \cdot \frac{m1}{m2^2}$ $dm12 = -2.155 \times 10^{-3}$

$d1\Delta v1 := \frac{m1}{m2}$ $d1\Delta v1 = 0.951$

$$\sigma_{\Delta v2} := \sqrt{dm11^2 \cdot \sigma_m^2 + dm12^2 \cdot \sigma_m^2 + d1\Delta v1^2 \cdot \sigma_{\Delta v1}^2}$$

$\delta\Delta v2 := \sigma_{\Delta v2} \cdot StdEn$

$\sigma_{\Delta v2} = 0.424$

$\delta\Delta v2 = 0.832$

$RatioDv1 := \frac{\delta\Delta v1}{\Delta v1}$ $RatioDv1 = 17.748\%$ $RatioDv2 := \frac{\delta\Delta v2}{\Delta v2}$ $RatioDv2 = 18.07\%$

Appendix I: Analysis of contributions to overall uncertainty in individual input parameters

These results are derived from the analytical model (Appendix H) using raw input data from RICSAC tests (Appendix D) and discussed in Chapter 5. Results have been arranged so that similar impact configurations are grouped together.

Table I.1: Overall result and uncertainty in Δv_1 and Δv_2

Overall uncertainty generated using 95% confidence limits on parameters as described by Smith & Noga [**108**]

Collision Type	60° Front to side			90° Front to side			10° Front to front		10° Front to rear		
Test number	**1**	**6**	**7**	**8**	**9**	**10**	**11**	**12**	**3**	**4**	**5**
Δv1 (m/s)	5.256	5.196	6.059	6.553	6.652	10.947	9.729	15.949	3.026	6.588	5.903
Δv2 (m/s)	7.881	8.521	13.187	6.231	3.063	5.299	6.101	11.07	4.799	10.284	10.735
Uncertainty Δv1 %	22.853	28.486	28.536	19.088	23.333	22.144	10.728	6.354	14.541	9.723	9.917
Uncertainty Δv2 %	23.098	28.909	29.415	19.388	23.945	22.774	11.55	7.665	15.129	10.553	11.095

Table I.2: Effect of uncertainty in crush measurements δC on Δv_1 and Δv_2 (%)

Collision Type	60° Front to side			90° Front to side			10° Front to front		10° Front to rear		
Test number	**1**	**6**	**7**	**8**	**9**	**10**	**11**	**12**	**3**	**4**	**5**
±0.01 m	1.013	1.057	1.054	0.826	0.947	0.626	0.327	0.27	0.613	0.332	0.417
±0.05 m	5.067	5.285	5.272	4.129	4.735	3.131	1.635	1.349	3.065	1.66	2.084
±0.0762 m	7.723	8.054	8.034	6.293	7.216	4.771	2.494	2.054	4.672	2.531	3.176
±0.10 m	10.135	10.57	10.543	8.259	9.469	6.262	3.269	2.698	6.13	3.32	4.169

Table I.3: Effect of uncertainty in damage length measurements δL on Δv_1 and Δv_2 (%)

Collision Type	60° Front to side			90° Front to side			10° Front to front		10° Front to rear		
Test number	**1**	**6**	**7**	**8**	**9**	**10**	**11**	**12**	**3**	**4**	**5**
±0.01 m	0.21	0.219	0.156	0.182	0.29	0.291	0.437	0.253	0.47	0.355	0.339
±0.05 m	1.03	1.096	0.781	0.909	1.451	1.455	2.185	1.263	2.33	1.776	1.697
±0.10 m	2.07	2.192	1.563	1.818	2.902	2.909	4.37	2.526	4.66	3.552	3.394
±0.15 m	3.1	3.287	2.344	2.727	4.353	4.364	6.55	3.788	6.99	5.328	5.091
±0.1524 m	3.148	3.34	2.382	2.771	4.422	4.434	6.66	3.849	7.104	5.413	5.173
±0.20 m	4.13	4.383	3.126	3.636	5.803	5.818	8.74	5.051	9.32	7.103	6.788

Table I.4: Effect of uncertainty in mass measurements δm on Δv_1 (%)

Collision Type	60° Front to side			90° Front to side			10° Front to front		10° Front to rear		
Test number	**1**	**6**	**7**	**8**	**9**	**10**	**11**	**12**	**3**	**4**	**5**
±10 kg	0.41	0.473	0.642	0.362	0.65	0.647	0.507	0.506	0.426	0.417	0.488
±25 kg	1.02	1.182	1.606	0.905	1.626	1.618	1.267	1.266	1.066	1.044	1.219
±50 kg	2.05	2.363	3.211	1.811	3.252	3.237	2.534	2.532	2.132	2.087	2.438
±100 kg	4.1	4.727	6.423	3.622	6.504	6.473	5.068	5.064	4.263	4.174	4.875

Table I.5: Effect of uncertainty in mass measurements δm on Δv_2 (%)

Collision Type	60° Front to side			90° Front to side			10° Front to front		10° Front to rear		
Test number	**1**	**6**	**7**	**8**	**9**	**10**	**11**	**12**	**3**	**4**	**5**
±10 kg	0.95	1.093	1.565	0.77	1.257	1.245	0.995	0.996	0.938	0.921	1.108
±25 kg	2.38	2.731	3.913	1.925	3.144	3.114	2.487	2.489	2.345	2.302	2.77
±50 kg	4.76	5.463	7.826	3.85	6.287	6.277	4.974	4.978	4.69	4.604	5.54
±100 kg	9.52	10.926	15.652	7.699	12.574	12.455	9.947	9.956	9.38	9.208	11.08

Table I.6: Effect of uncertainty in PDOF measurements $\delta PDOF$ on Δv_1 and Δv_2 (%)

Collision Type	60° Front to side			90° Front to side			10° Front to front		10° Front to rear		
Test number	**1**	**6**	**7**	**8**	**9**	**10**	**11**	**12**	**3**	**4**	**5**
±1°	1.046	1.337	1.342	0.804	1.006	0.99	0.356	0.144	0.521	0.338	0.329
±5°	5.23	6.686	6.708	4.018	5.032	4.949	1.782	0.721	2.604	1.688	1.646
±10°	10.6	13.372	13.416	8.035	10.065	9.898	3.563	1.441	5.209	3.376	3.291
±15°	15.7	20.057	20.124	12.053	15.097	14.847	5.345	2.162	7.813	5.064	4.937
±20°	20.9	26.743	26.832	16.071	20.13	19.796	7.126	2.882	10.417	6.752	6.583
±25°	26.1	33.429	33.54	20.089	25.162	24.745	8.908	3.603	13.022	8.44	8.228

Table I.7: Effect of uncertainty in position of point of application δd on Δv_1 and Δv_2 (%)

Collision Type	60° Front to side			90° Front to side			10° Front to front		10° Front to rear		
Test number	**1**	**6**	**7**	**8**	**9**	**10**	**11**	**12**	**3**	**4**	**5**
±0.01 m	0.14	0.171	0.174	0.165	0.296	0.277	0.084	0.023	0.12	0.089	0.1
±0.05 m	0.7	0.857	0.873	0.824	1.479	1.385	0.42	0.117	0.598	0.446	0.502
±0.0762 m	1.081	1.307	1.33	1.256	2.255	2.111	0.64	0.178	0.911	0.68	0.765
±0.10 m	1.4	1.716	1.747	1.648	2.959	2.771	0.84	0.234	1.196	0.892	1.004
±0.20 m	2.8	3.445	3.508	3.299	5.925	5.55	1.682	0.469	2.394	1.786	2.012

Table I.8: Effect of uncertainty in radii of gyration δk on Δv_1 and Δv_2 (%)

Collision Type	60° Front to side			90° Front to side			10° Front to front		10° Front to rear		
Test number	**1**	**6**	**7**	**8**	**9**	**10**	**11**	**12**	**3**	**4**	**5**
±0.01 m	0.01	0.078	0.077	0.095	0.206	0.173	0.016	0.001	0.034	0.018	0.018
±0.05 m	0.41	0.391	0.387	0.476	1.03	0.863	0.079	0.005	0.168	0.092	0.09
±0.10 m	0.82	0.782	0.774	0.952	2.06	1.727	0.159	0.011	0.336	0.184	0.18
±0.20 m	1.65	1.565	1.549	1.903	4.119	3.454	0.318	0.022	0.67	0.368	0.361

Table I.9: Effect of uncertainty in A stiffness coefficient δA on Δv_1 and Δv_2 (%)

Collision Type	60° Front to side			90° Front to side			10° Front to front		10° Front to rear		
Test number	**1**	**6**	**7**	**8**	**9**	**10**	**11**	**12**	**3**	**4**	**5**
±5%	1.33	1.073	1.061	2.223	2.065	1.256	1.098	0.809	2.419	1.293	1.473
±10%	2.67	2.146	2.122	4.445	4.13	2.511	2.195	1.619	4.839	2.587	2.947
±15%	3.998	3.22	3.184	6.668	6.195	3.767	3.293	2.428	7.258	3.88	4.42
±20%	5.33	4.293	4.245	8.891	8.259	5.022	4.39	3.237	9.678	5.173	5.894

Table I.10: Effect of uncertainty in B stiffness coefficient δB on Δv_1 and Δv_2 (%)

Collision Type	60° Front to side			90° Front to side			10° Front to front		10° Front to rear		
Test number	**1**	**6**	**7**	**8**	**9**	**10**	**11**	**12**	**3**	**4**	**5**
±5%	0.72	1.388	1.314	0.877	0.336	0.636	0.717	0.996	0.657	0.65	0.855
±10%	1.44	2.776	2.682	1.753	0.672	1.272	1.435	1.992	1.314	1.301	1.709
±15%	2.16	4.164	3.942	2.63	1.008	1.909	2.152	2.988	1.971	1.951	2.564
±20%	2.87	5.553	5.257	3.507	1.344	2.545	2.869	3.984	2.628	2.602	3.419

Table I.11: Overall uncertainty in Δv_1 and Δv_2 (Constrained adjustment factor

Overall uncertainty generated using 95% confidence levels described by Smith & Noga [**108**] and adjustment factor limited to 2

Collision Type	60° Front to side		
Test number	**1**	**6**	**7**
Δv1 (m/s)	5.256	5.196	6.059
Δv2 (m/s)	7.881	8.521	13.187
Uncertainty Δv1 %	14.636	14.645	12.742
Uncertainty Δv2 %	15.254	15.451	14.605

Table I.12: Effect of uncertainty in PDOF measurements *δPDOF* on Δv_1 and Δv_2 (%) (Constrained adjustment factor)

Collision Type	60° Front to side		
Test number	**1**	**6**	**7**
±1°	1.046	1.377	1.342
±5°	4.642	6.213	3.844
±10°	6.676	7.568	5.404
±15°	9.108	9.402	7.297
±20°	11.619	11.487	9.323
±25°	14.344	13.71	11.41

Appendix J: Mathcad Monte Carlo Model to Determine Uncertainty in Δ*v* (RICSAC 8)

The Monte Carlo model to determine the uncertainty in DeltaV is developed in Chapter 6.

Monte Carlo Simulation for RICSAC 8

Standard error factor to convert 95% confidence limits to standard deviation:

StdErr := 1.9(

Minimum value for uncertainty [using a small positive value avoids error in Mathcad function rnorm(...)]:

$minE := 1 \cdot 10^{-15}$

Calculation of Crush Energy

Measurement Data

Vehicle 1

$$C1 := \begin{pmatrix} 6.9 \\ 7.34 \\ 7.78 \\ 8.22 \\ 8.66 \\ 9.1 \end{pmatrix}$$

Vehicle 2

$$C2 := \begin{pmatrix} 15.7 \\ 21.1 \\ 23.4 \\ 15 \\ 11.2 \\ 2 \end{pmatrix}$$

δC := 7.62 (7.62cm is equivalent to 3 inches)

$\sigma_c := \frac{\delta C}{StdErr}$ $\sigma_c = 3.888$

Damage Length (L)

L1 := 185.4 L2 := 214.(

δL := 15.24 (15.24cm is equivalent to 6 inches)

$\sigma_L := \frac{\delta L}{StdErr}$ $\sigma_L = 7.776$

Mass

m1 := 203 m2 := 213(

δm := 50

$\sigma_m := \frac{\delta m}{StdErr}$ $\sigma_m = 25.51$

MaxM1 := m1 + δm MaxM2 := m2 + δm

MinM1 := m1 − δm MinM2 := m2 − δm

Coefficient of Restitution

ep := 0.3

δep := 0.05 $\sigma_{ep} := \frac{\delta ep}{StdErr}$ $\sigma_{ep} = 0.026$

Principal Directions of Force (PDOF)
(Base Side: 0=Front, 90=right, 180=rear, 270=left)

BaseSide1 := 0 BaseSide2 := 90

PDOF1 := −20.5 PDOF2 := 69.5

δPDOF := 20

$\sigma_{PDOF} := \frac{\delta PDOF}{StdErr}$ $\sigma_{PDOF} = 10.204$

MaxPDOF1 := PDOF1 + δPDOF MaxPDOF2 := PDOF2 + δPDOF

MinPDOF1 := PDOF1 − δPDOF MinPDOF2 := PDOF2 − δPDOF

δ1 and δ2 data

ϕ1 := −0.98557 ϕ2 := −77.446

d1 := 2.4701 d2 := 0.91163

$\delta d := \frac{10}{100}$

$\sigma_d := \frac{\delta d}{StdErr}$ $\sigma_d = 0.051$

k1 := 1.5530 k2 := 1.5529

δk := 0.1

$\sigma_k := \frac{\delta k}{StdErr}$ $\sigma_k = 0.051$

Stiffness Coefficients

δACoeff := 10%

δBCoeff := 10%

(Permits simultaneous adjustment of both coefficients)

A1 := 623.5 A2 := 250.5

δA1 := δACoeff · A1 δA2 := δACoeff · A2

$\sigma_{A1} := \frac{\delta A1}{StdErr}$ $\sigma_{A1} = 31.811$ $\sigma_{A2} := \frac{\delta A2}{StdErr}$ $\sigma_{A2} = 12.781$

B1 := 23.3 B2 := 34.8

δB1 := δBCoeff · B1 δB2 := δBCoeff · B2

$\sigma_{B1} := \frac{\delta B1}{StdErr}$ $\sigma_{B1} = 1.189$ $\sigma_{B2} := \frac{\delta B2}{StdErr}$ $\sigma_{B2} = 1.776$

MaxA1 := A1 + δA1 MaxA2 := A2 + δA2

MinA1 := A1 − δA1 MinA2 := A2 − δA2

MaxB1 := B1 + δB1 MaxB2 := B2 + δB2

MinB1 := B1 − δB1 MinB2 := B2 − δB2

Energy Range Calculations

Using variation in A & B Coefficients only, ie ignoring crush and PDOF variation

$i := 0..4$

$\alpha_1 := \sum_i \left(C1_i + C1_{i+1}\right)$ $\quad$ $\alpha_2 := \sum_i \left(C2_i + C2_{i+1}\right)$

$\alpha_1 = 80$ $\quad$ $\alpha_2 = 159.1$

$\beta_1 := \sum_i \left[\left(C1_i\right)^2 + C1_i \cdot C1_{i+1} + \left(C1_{i+1}\right)^2\right]$ $\quad$ $\beta_2 := \sum_i \left[\left(C2_i\right)^2 + C2_i \cdot C2_{i+1} + \left(C2_{i+1}\right)^2\right]$

$\beta_1 = 966.05$ $\quad$ $\beta_2 = 4.303 \times 10^3$

$$E1 := 0.01\left[\left(\frac{5 \cdot A1^2}{2 \cdot B1} + \frac{B1 \cdot \beta_1}{6} + \frac{A1 \cdot \alpha_1}{2}\right) \cdot \frac{L1}{5}\right] \qquad E1 = 2.611 \times 10^4$$

$$E2 := 0.01\left[\left(\frac{5 \cdot A2^2}{2 \cdot B2} + \frac{B2 \cdot \beta_2}{6} + \frac{A2 \cdot \alpha_2}{2}\right) \cdot \frac{L2}{5}\right] \qquad E2 = 2.12 \times 10^4$$

$$MaxE1 := 0.01\left[\left[\frac{5 \cdot (A1 + \delta A1)^2}{2 \cdot (B1 + \delta B1)} + \frac{(B1 + \delta B1) \cdot \beta_1}{6} + \frac{(A1 + \delta A1) \cdot \alpha_1}{2}\right] \cdot \frac{L1}{5}\right] \qquad MaxE1 = 2.872 \times 10^4$$

$$MaxE2 := 0.01\left[\left[\frac{5 \cdot (A2 + \delta A2)^2}{2 \cdot (B2 + \delta B2)} + \frac{(B2 + \delta B2) \cdot \beta_2}{6} + \frac{(A2 + \delta A2) \cdot \alpha_2}{2}\right] \cdot \frac{L2}{5}\right] \qquad MaxE2 = 2.332 \times 10^4$$

$$MinE1 := 0.01\left[\left[\frac{5 \cdot (A1 - \delta A1)^2}{2 \cdot (B1 - \delta B1)} + \frac{(B1 - \delta B1) \cdot \beta_1}{6} + \frac{(A1 - \delta A1) \cdot \alpha_1}{2}\right] \cdot \frac{L1}{5}\right] \qquad MinE1 = 2.349 \times 10^4$$

$$MinE2 := 0.01\left[\left[\frac{5 \cdot (A2 - \delta A2)^2}{2 \cdot (B2 - \delta B2)} + \frac{(B2 - \delta B2) \cdot \beta_2}{6} + \frac{(A2 - \delta A2) \cdot \alpha_2}{2}\right] \cdot \frac{L2}{5}\right] \qquad MinE2 = 1.908 \times 10^4$$

$$pRawRangeE1 := \frac{MaxE1 - E1}{E1} \qquad pRawRangeE1 = 10\%$$

$$pRawRangeE2 := \frac{MaxE2 - E2}{E2} \qquad pRawRangeE2 = 10\%$$

Energy Adjustment Calculations

(Ensures that energy adjustment factor never exceeds 2 as per CRASH)

$$CF1 := \min\left[2, 1 + \tan\left[(PDOF1 - BaseSide1)\cdot\frac{\pi}{180}\right]^2\right] \qquad CF1 = 1.14$$

$$CF2 := \min\left[2, 1 + \tan\left[(PDOF2 - BaseSide2)\cdot\frac{\pi}{180}\right]^2\right] \qquad CF2 = 1.14$$

$$MaxCF1 := \max\left[CF1, \min\left[2, 1 + \tan\left[(MinPDOF1 - BaseSide1)\cdot\frac{\pi}{180}\right]^2\right]\right] \qquad MaxCF1 = 1.729$$

$$MaxCF2 := \max\left[CF2, \min\left[2, 1 + \tan\left[(MinPDOF2 - BaseSide2)\cdot\frac{\pi}{180}\right]^2\right]\right] \qquad MaxCF2 = 1.729$$

$$MinCF1 := \min\left[CF1, MaxCF1, \min\left[2, 1 + \tan\left[(MaxPDOF1 - BaseSide1)\cdot\frac{\pi}{180}\right]^2\right]\right] \qquad MinCF1 = 1$$

$$MinCF2 := \min\left[CF2, MaxCF2, \min\left[2, 1 + \tan\left[(MaxPDOF2 - BaseSide2)\cdot\frac{\pi}{180}\right]^2\right]\right] \qquad MinCF2 = 1$$

$EC1 := E1\cdot CF1$ $\qquad$ $EC2 := E2\cdot CF2$

$EC1 = 2.975\times 10^4$ $\qquad$ $EC2 = 2.416\times 10^4$

$MaxEC1 := MaxE1\cdot MaxCF1$ $\qquad$ $MaxEC2 := MaxE2\cdot MaxCF1$

$MinEC1 := MinE1\cdot MinCF1$ $\qquad$ $MinEC2 := MinE2\cdot MinCF2$

$$RangeEC1 := \frac{MaxEC1 - EC1}{EC1} \qquad RangeEC1 = 66.908\%$$

$$RangeEC2 := \frac{MaxEC2 - EC2}{EC2} \qquad RangeEC2 = 66.908\%$$

Position of centroid calculations

Angle ϕ defined so that lateral variation is equal to δd

$$\delta\phi1 := \frac{180}{\pi}\,asin\left(\frac{\delta d}{d1}\right) \qquad \delta\phi1 = 2.32$$

$$\sigma_{\phi1} := \frac{\delta\phi1}{StdErr} \qquad \sigma_{\phi1} = 1.184$$

$$\delta\phi2 := \frac{180}{\pi}\,asin\left(\frac{\delta d}{d2}\right) \qquad \delta\phi2 = 6.298$$

$$\sigma_{\phi2} := \frac{\delta\phi2}{StdErr} \qquad \sigma_{\phi2} = 3.213$$

$$h1 := d1\cdot\sin\left[(PDOF1 + \phi1)\cdot\frac{\pi}{180}\right] \qquad h1 = -0.905$$

$$h2 := d2\cdot\sin\left[(PDOF2 + \phi2)\cdot\frac{\pi}{180}\right] \qquad h2 = -0.126$$

Gamma & Delta calculations

$$\delta1 := 1 + \frac{h1^2}{k1^2} \qquad \delta1 = 1.339$$

$$\gamma1 := \frac{1}{\delta1} \qquad \gamma1 = 0.747$$

$$\delta2 := 1 + \frac{h2^2}{k2^2} \qquad \delta2 = 1.007$$

$$\gamma2 := \frac{1}{\delta2} \qquad \gamma2 = 0.993$$

Mean, Minimum and Maximum Results

Nominal Mean ΔV

$$\Delta v1 := \sqrt{\frac{2 \cdot m2 \cdot (EC1 + EC2) \cdot (1 + ep)}{m1 \cdot (m1 \cdot \delta 2 + m2 \cdot \delta 1) \cdot (1 - ep)}} \qquad \Delta v2 := \Delta v1 \cdot \frac{m1}{m2}$$

$\Delta v1 = 6.553$ $\Delta v2 = 6.231$

Maximum Δv

$$MaxDv1 := \sqrt{\frac{2 \cdot m2 \cdot (MaxEC1 + MaxEC2) \cdot (1 + ep)}{m1 \cdot (m1 \cdot \delta 2 + m2 \cdot \delta 1) \cdot (1 - ep)}} \qquad MaxDv2 := MaxDv1 \cdot \frac{m1}{m2}$$

$MaxDv1 = 8.466$ $MaxDv2 = 8.05$

Minimum Δv

$$MinDv1 := \sqrt{\frac{2 \cdot m2 \cdot (MinEC1 + MinEC2) \cdot (1 + ep)}{m1 \cdot (m1 \cdot \delta 2 + m2 \cdot \delta 1) \cdot (1 - ep)}} \qquad MinDv2 := MinDv1 \cdot \frac{m1}{m2}$$

$MinDv1 = 5.823$ $MinDv2 = 5.537$

Difference and Range

$MaxDiff := MaxDv1 - \Delta v1$ $MaxDiff = 1.913$ $pMaxDiff := \frac{MaxDiff}{\Delta v1}$ $pMaxDiff = 29.193\%$

$MinDiff := \Delta v1 - MinDv1$ $MinDiff = 0.73$ $pMinDiff := \frac{MinDiff}{\Delta v1}$ $pMinDiff = 11.136\%$

Probability Calculations

(Assuming normal distribution of source data)

Number of data points:

Seed(Seed(5)) n := 1000

Function to generate random distribution about mean value v with standard deviation sd truncated to maximum variation of l. Prevents occurrence of values outside range v - sd*l to v + sd*l

RNormLim(n, v, sd, l) :=
- ret ← rnorm(n, v, sd)
- for i ∈ 0..last(ret)
  - e ← ret_i if $ret_i < (v + sd \cdot l) \wedge ret_i > (v - sd \cdot l)$
  - e ← rnd(2·sd·l) + v − sd·l otherwise
  - ret_i ← e
- ret

Function to generate random distribution about mean value v with standard deviation sd truncated at lower end to zero and upper end to 2*v Prevents occurrence of values outside range 0 to 2*v

RNormZero(data, v, sd) :=
- ret ← rnorm(n, v, sd)
- for i ∈ 0..last(ret)
  - e ← ret_i if $ret_i < (2 \cdot v) \wedge ret_i > (0)$
  - e ← rnd(2·v) otherwise
  - ret_i ← e
- ret

Crush Dimensions

$$C11 := \begin{pmatrix} RNormZero(n, C1_0, \sigma_c) \\ RNormZero(n, C1_1, \sigma_c) \\ RNormZero(n, C1_2, \sigma_c) \\ RNormZero(n, C1_3, \sigma_c) \\ RNormZero(n, C1_4, \sigma_c) \\ RNormZero(n, C1_5, \sigma_c) \end{pmatrix}$$

$$C22 := \begin{pmatrix} RNormZero(n, C2_0, \sigma_c) \\ RNormZero(n, C2_1, \sigma_c) \\ RNormZero(n, C2_2, \sigma_c) \\ RNormZero(n, C2_3, \sigma_c) \\ RNormZero(n, C2_4, \sigma_c) \\ RNormZero(n, C2_5, \sigma_c) \end{pmatrix}$$

$$VecL1 := rnorm(n, L1, \sigma_L)$$

$$VecL2 := rnorm(n, L2, \sigma_L)$$

Mass

$Vecm1 := rnorm(n, m1, \sigma_m)$

$maxm1 := max(Vecm1)$ $maxm1 = 2.133 \times 10^3$

$minm1 := min(Vecm1)$ $minm1 = 1.938 \times 10^3$

$Vecm2 := rnorm(n, m2, \sigma_m)$

$maxm2 := max(Vecm2)$ $maxm2 = 2.253 \times 10^3$

$minm2 := min(Vecm2)$ $minm2 = 2.039 \times 10^3$

Stiffness Coefficients

$VecA1 := RNormLim(n, A1, \sigma_{A1}, 1.96)$

$VecB1 := RNormLim(n, B1, \sigma_{B1}, 1.96)$

$VecA2 := RNormLim(n, A2, \sigma_{A2}, 1.96)$

$VecB2 := RNormLim(n, B2, \sigma_{B2}, 1.96)$

$VecA1 := rnorm(n, A1, \sigma_{A1})$

$VecB1 := rnorm(n, B1, \sigma_{B1})$

$VecA2 := rnorm(n, A2, \sigma_{A2})$

$VecB2 := rnorm(n, B2, \sigma_{B2})$

$maxA1 := max(VecA1)$ $maxA1 = 768.712$

$minA1 := min(VecA1)$ $minA1 = 491.828$

$maxB1 := max(VecB1)$ $maxB1 = 27.601$

$minB1 := min(VecB1)$ $minB1 = 18.468$

$maxA2 := max(VecA2)$ $maxA2 = 295.097$

$minA2 := min(VecA2)$ $minA2 = 204.35$

$maxB2 := max(VecB2)$ $maxB2 = 42.645$

$minB2 := min(VecB2)$ $minB2 = 27.977$

Calculation of PDOF

$VecPDOF1 := RNormLim(n, PDOF1, \sigma_{PDOF}, 2)$

$VecPDOF1 := rnorm(n, PDOF1, \sigma_{PDOF})$

$minPDOF1 := min(VecPDOF1)$ $minPDOF1 = -59.385$

$maxPDOF1 := max(VecPDOF1)$ $maxPDOF1 = 16.499$

$VecPDOF2 := RNormLim(n, PDOF2, \sigma_{PDOF}, 1.96)$

$VecPDOF2 := rnorm(n, PDOF2, \sigma_{PDOF})$

$minPDOF2 = min(VecPDOF2)$ $minPDOF2 = 33.699$

$maxPDOF2 = max(VecPDOF2)$ $maxPDOF2 = 113.005$

Energy Adjustment Factor

Standard unlimited adjustment factor calculation

$$VecCF1 := \overrightarrow{\left[1 + \tan\left[(VecPDOF1 - BaseSide1) \cdot \frac{\pi}{180}\right]^2\right]}$$

$$VecCF2 := \overrightarrow{\left[1 + \tan\left[(VecPDOF2 + BaseSide2) \cdot \frac{\pi}{180}\right]^2\right]}$$

Function to provide random adjustment factors limited to a maximum value lim

$$MaxLimCF(pdf, side, lim) := \left| \begin{array}{l} ret \leftarrow \overrightarrow{\left[1 + \tan\left[(pdf - side) \cdot \frac{\pi}{180}\right]^2\right]} \\ \text{for } i \in 0..last(ret) \\ \quad \left| \begin{array}{l} e \leftarrow ret_i \text{ if } ret_i < lim \\ e \leftarrow rnd(1) + 1 \text{ otherwise} \\ ret_i \leftarrow e \end{array} \right. \\ ret \end{array} \right.$$

$VecCF1 := MaxLimCF(VecPDOF1, BaseSide1, 2)$

$minCF1 := min(VecCF1)$ $minCF1 = 1$

$maxCF1 := max(VecCF1)$ $maxCF1 = 3.856$

$VecCF2 := MaxLimCF(VecPDOF2, BaseSide2, 2)$

$minCF2 := min(VecCF2)$ $minCF2 = 1$

$maxCF2 := max(VecCF2)$ $maxCF2 = 3.248$

Moment arm calculations

$Vecd1 := rnorm(n, d1, \sigma_d)$

$mind1 := min(Vecd1)$ $mind1 = 2.291$

$maxd1 := max(Vecd1)$ $maxd1 = 2.66$

$Vec\phi 1 := rnorm(n, \phi 1, \sigma_{\phi 1})$

$min\phi 1 := min(Vec\phi 1)$ $min\phi 1 = -5.934$

$max\phi 1 := max(Vec\phi 1)$ $max\phi 1 = 3.487$

$\overrightarrow{Vech1 := \left[Vecd1 \cdot \sin\left[(VecPDOF1 + Vec\phi 1) \cdot \frac{\pi}{180} \right] \right]}$

$minh1 := min(Vech1)$ $minh1 = -2.208$

$maxh1 := max(Vech1)$ $maxh1 = 0.68$

$Vecd2 := rnorm(n, d2, \sigma_d)$

$mind2 := min(Vecd2)$ $mind2 = 0.721$

$maxd2 := max(Vecd2)$ $maxd2 = 1.095$

$Vec\phi 2 := rnorm(n, \phi 2, \sigma_{\phi 1})$

$min\phi 2 := min(Vec\phi 2)$ $min\phi 2 = -81.823$

$max\phi 2 := max(Vec\phi 2)$ $max\phi 2 = -72.772$

$\overrightarrow{Vech2 := \left[Vecd2 \cdot \sin\left[(VecPDOF2 + Vec\phi 2) \cdot \frac{\pi}{180} \right] \right]}$

$minh2 := min(Vech2)$ $minh2 = -0.649$

$maxh2 := max(Vech2)$ $maxh2 = 0.529$

Gamma & Delta calculations

$Veck1 := rnorm(n, k1, \sigma_k)$

$\overrightarrow{Vec\delta 1 := \left(1 + \frac{Vech1^2}{Veck1^2} \right)}$

$\overrightarrow{Vec\gamma 1 := \frac{1}{Vec\delta 1}}$

$min\gamma 1 := min(Vec\gamma 1)$ $min\gamma 1 = 0.314$

$max\gamma 1 := max(Vec\gamma 1)$ $max\gamma 1 = 1$

$Veck2 := rnorm(n, k2, \sigma_k)$

$\overrightarrow{Vec\delta 2 := \left(1 + \frac{Vech2^2}{Veck2^2} \right)}$

$\overrightarrow{Vec\gamma 2 := \frac{1}{Vec\delta 2}}$

$min\gamma 2 := min(Vec\gamma 2)$ $min\gamma 2 = 0.846$

$max\gamma 2 := max(Vec\gamma 2)$ $max\gamma 2 = 1$

Coefficient of Restitution

$Vece := rnorm(n, ep, \sigma_{ep})$

Calculation of Energy

$i := 0..4$

$$Vec\alpha_1 := \overrightarrow{\sum_i \left(C11_i + C11_{i+1}\right)}$$

$$Vec\beta_1 := \overrightarrow{\sum_i \left[\left(C11_i\right)^2 + C11_i \cdot C11_{i+1} + \left(C11_{i+1}\right)^2\right]}$$

$$VecE1 := \overrightarrow{\left[0.01\left[\left(\frac{5 \cdot VecA1^2}{2 \cdot VecB1} + \frac{VecB1 \cdot Vec\beta_1}{6} + \frac{VecA1 \cdot Vec\alpha_1}{2}\right) \cdot \frac{VecL1}{5}\right]\right]}$$

$$Vec\alpha_2 := \overrightarrow{\sum_i \left(C22_i + C22_{i+1}\right)}$$

$$Vec\beta_2 := \overrightarrow{\sum_i \left[\left(C22_i\right)^2 + C22_i \cdot C22_{i+1} + \left(C22_{i+1}\right)^2\right]}$$

$$VecE2 := \overrightarrow{\left[0.01\left[\left(\frac{5 \cdot VecA2^2}{2 \cdot VecB2} + \frac{VecB2 \cdot Vec\beta_2}{6} + \frac{VecA2 \cdot Vec\alpha_2}{2}\right) \cdot \frac{VecL2}{5}\right]\right]}$$

$dataVecE1 := histogram(100, VecE1)$

$minE1 := min(VecE1)$ $\quad minE1 = 1.57 \times 10^4$

$maxE1 := max(VecE1)$ $\quad maxE1 = 3.931 \times 10^4$

$MeanE1 := mean(VecE1)$ $\quad MeanE1 = 2.64 \times 10^4$

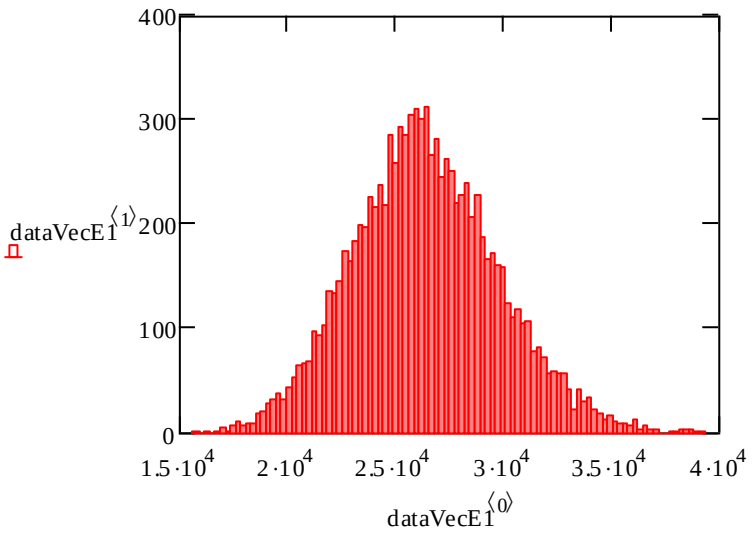

Energy Adjustment

$\overrightarrow{VecEC1} := (VecE1 \cdot VecCF1)$ $\overrightarrow{VecEC2} := (VecE2 \cdot VecCF2)$

dataVecEC1 := histogram(100, VecEC1)

minEC1 := min(VecEC1) minEC1 = 1.587×10^{4}

maxEC1 := max(VecEC1) maxEC1 = 1.03×10^{5}

MeanEC1 := mean(VecEC1) MeanEC1 = 3.16×10^{4}

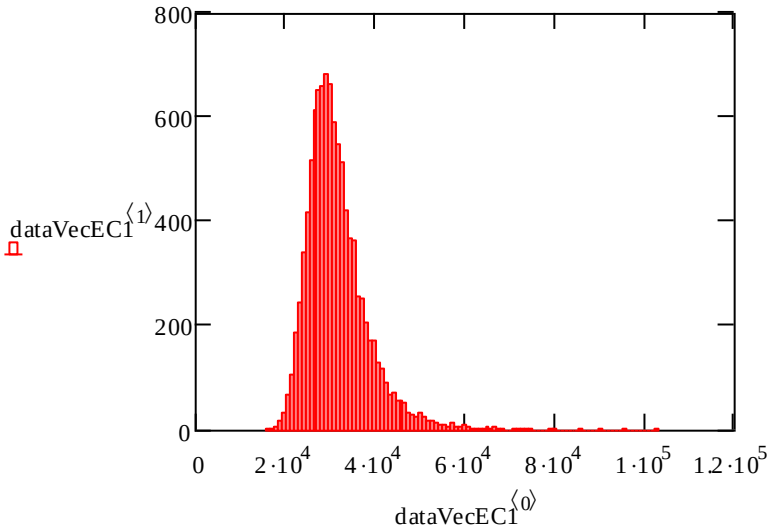

RangeVecEC1 := maxEC1 – MeanEC1 RangeVecEC1 = 7.144×10^{4}

DeviationEC1 := stdev(VecEC1) DeviationEC1 = 6.767×10^{3}

Prob95EC1 := DeviationEC1·1.9(Prob95EC1 = 1.326×10^{4}

Prob99EC1 := DeviationEC1·2.57(Prob99EC1 = 1.743×10^{4}

$pRangeEC1 := \frac{RangeEC1}{MeanEC1}$ $pRangeEC1 = 2.117 \times 10^{-3}\%$

$pProb95EC1 := \frac{Prob95EC1}{MeanEC1}$ pProb95EC1 = 41.964%

$pProb99EC1 := \frac{Prob99EC1}{MeanEC1}$ pProb99EC1 = 55.153%

Probability Results

$$\overrightarrow{Vec\Delta v1} := \sqrt{\frac{2 \cdot Vecm2 \cdot (VecEC1 + VecEC2) \cdot (1 + ep)}{Vecm1 \cdot (Vecm1 \cdot Vec\delta 2 + Vecm2 \cdot Vec\delta 1) \cdot (1 - ep)}} \qquad \overrightarrow{Vec\Delta v2} := \left(Vec\Delta v1 \cdot \frac{Vecm1}{Vecm2} \right)$$

Vehicle 1 Analysis

$data := histogram(100, Vec\Delta v1)$

$min\Delta v1 := min(Vec\Delta v1)$ $min\Delta v1 = 5.356$

$max\Delta v1 := max(Vec\Delta v1)$ $max\Delta v1 = 10.677$

$Mean\Delta v1 := mean(Vec\Delta v1)$ $Mean\Delta v1 = 6.659$

$Range\Delta v1 := max\Delta v1 - Mean\Delta v1$ $Range\Delta v1 = 4.018$ $pRange\Delta v1 := \frac{Range\Delta v1}{Mean\Delta v1}$

$pRange\Delta v1 = 60.333\%$

$Deviation\Delta v1 := Stdev(Vec\Delta v1)$ $Deviation\Delta v1 = 0.431$

$Prob95\Delta v1 := Deviation\Delta v1 \cdot 1.9($ $Prob95\Delta v1 = 0.845$ $pProb95\Delta v1 := \frac{Prob95\Delta v1}{Mean\Delta v1}$

$pProb95\Delta v1 = 12.688\%$

$Prob99\Delta v1 := Deviation\Delta v1 \cdot 2.57($ $Prob99\Delta v1 = 1.11$ $pProb99\Delta v1 := \frac{Prob99\Delta v1}{Mean\Delta v1}$

$pProb99\Delta v1 = 16.676\%$

$Kurtosis1 := kurt(Vec\Delta v1)$ $Kurtosis1 = 1.513$

$Skew1 := skew(Vec\Delta v1)$ $Skew1 = 0.543$

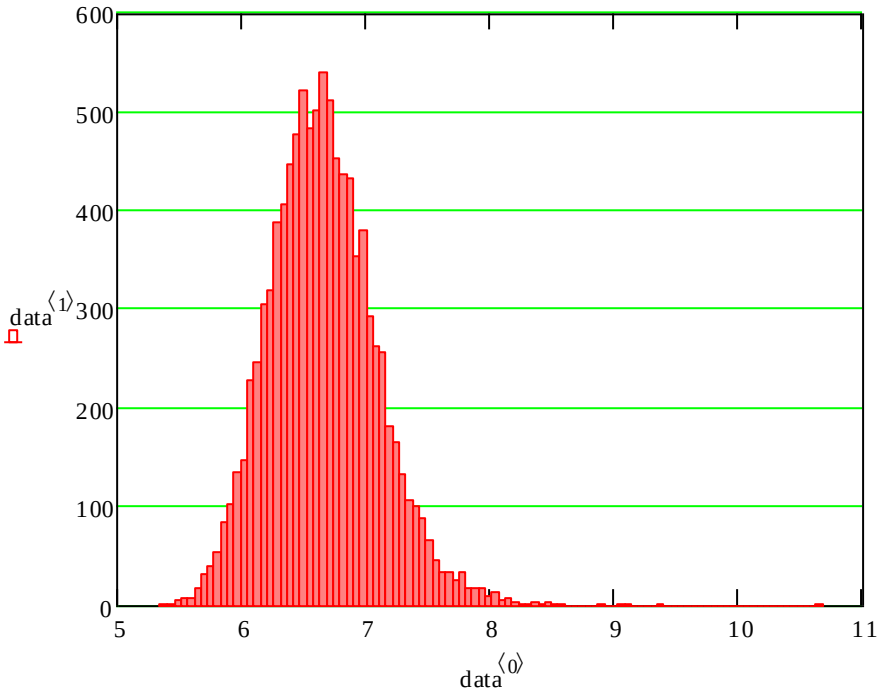

Vehicle 2 Analysis

$data2 := histogram(100, VecΔv2)$

$minΔv2 := min(VecΔv2)$ $minΔv2 = 5.102$

$maxΔv2 := max(VecΔv1)$ $maxΔv2 = 10.677$

$MeanΔv2 := mean(VecΔv1)$ $MeanΔv2 = 6.659$

$RangeΔv2 := maxΔv2 - MeanΔv2$ $RangeΔv2 = 4.018$ $pRangeΔv2 := \frac{RangeΔv2}{MeanΔv2}$

$pRangeΔv2 = 60.333\%$

$DeviationΔv2 := Stdev(VecΔv2)$ $DeviationΔv2 = 0.409$

$Prob95Δv2 := DeviationΔv2 \cdot 1.9($ $Prob95Δv2 = 0.802$ $pProb95Δv2 := \frac{Prob95Δv2}{MeanΔv2}$

$pProb95Δv2 = 12.05\%$

$Prob99Δv2 := DeviationΔv2 \cdot 2.57($ $Prob99Δv2 = 1.055$ $pProb99Δv2 := \frac{Prob99Δv2}{MeanΔv2}$

$pProb99Δv2 = 15.838\%$

$Kurtosis2 := kurt(VecΔv2)$ $Kurtosis2 = 1.194$

$Skew2 := skew(VecΔv2)$ $Skew2 = 0.505$

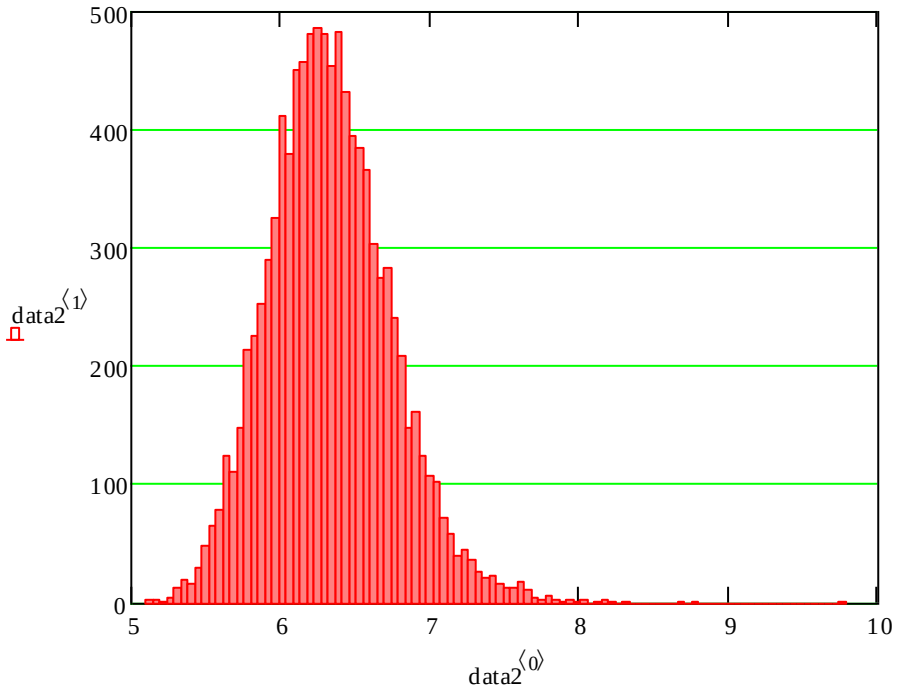

Appendix K: Monte Carlo simulation data and results

Results for head-on into rigid barrier collision. These results are derived from the Monte Carlo model shown in Appendix J and are discussed in Chapter 6.

Table K.1: Nominal values for single vehicle into barrier simulations

Parameter	Vehicle 1	Barrier
C_1 to C_6	0.1, 0.2, 0.4 m	-
L	1.35 m	-
m	1332 kg	10^{20} kg
$PDOF$	0°	0°
d	1.86 m	1 m
ϕ	0°	0°
k	1.426 m	10^{20} m
A	362 N/cm	-
B	48.3 N/cm^2	-

Table K.2: Overall result and uncertainty in Δv_1 and Δv_2

Using 95% confidence limits on parameters as described by Smith & Noga [**108**]

Collision Type	Head-on into barrier		
Test	**0.1 m**	**0.2 m**	**0.4 m**
Δv1 (m/s)	3.871	6.083	10.508
Uncertainty Δv1 %	19.093	13.741	9.976

Table K.3: Effect of uncertainty in crush measurements δC (%)

Collision Type	Head-on into barrier		
Test	**0.1 m**	**0.2 m**	**0.4 m**
±0.01 m	2.427	1.54	0.893
±0.05 m	12.016	7.735	4.408
±0.0762 m	17.453	11.864	6.707
±0.10 m	20.801	15.264	8.808

Table K.4: Effect of uncertainty in damage length measurements *δL* (%)

Collision Type	Head-on into barrier		
Test	**0.1 m**	**0.2 m**	**0.4 m**
±0.01 m	0.368	0.377	0.486
±0.05 m	1.84	1.859	1.856
±0.10 m	3.694	3.691	3.719
±0.15 m	5.569	5.554	5.545
±0.1524 m	5.642	5.624	5.634
±0.20 m	7.47	7.45	7.402

Table K.5: Effect of uncertainty in mass measurements *δm* (%)

Collision Type	Head-on into barrier		
Test	**0.1 m**	**0.2 m**	**0.4 m**
±10 kg	0.377	0.37	0.372
±25 kg	0.933	0.943	0.941
±50 kg	1.877	1.883	1.891
±100 kg	3.724	3.792	3.827

Table K.6: Effect of uncertainty in PDOF measurements *δPDOF* (%)

Collision Type	Head-on into barrier		
Test	**0.1 m**	**0.2 m**	**0.4 m**
±1°	0.008	0.008	0.008
±5°	0.177	0.186	0.185
±10°	0.669	0.672	0.673
±15°	1.265	1.241	1.249
±20°	1.768	1.765	1.756
±25°	2.126	2.089	2.111

Table K.7: Effect of uncertainty in position of point of application *δd* (%)

Collision Type	Head-on into barrier		
Test	**0.1 m**	**0.2 m**	**0.4 m**
±0.01 m	0.002	0.002	0.002
±0.05 m	0.045	0.044	0.045
±0.10 m	0.176	0.178	0.176
±0.20 m	0.704	0.708	0.71

Table K.8: Effect of uncertainty in radii of gyration *δk* (%)

No individual effect on uncertainty due to zero rotation using nominal values.

Table K.9: Effect of uncertainty in A stiffness coefficient *δA* (%)

Collision Type	Head-on into barrier		
Test	**0.1 m**	**0.2 m**	**0.4 m**
±5%	2.133	1.351	0.787
±10%	4.254	2.74	1.566
±15%	6.505	4.084	2.34
±20%	8.657	5.494	3.185

Table K.10: Effect of uncertainty in B stiffness coefficient *δB* (%)

Collision Type	Head-on into barrier		
Test	**0.1 m**	**0.2 m**	**0.4 m**
±5%	0.358	1.144	1.704
±10%	0.716	2.27	3.418
±15%	1.063	3.396	5.132
±20%	1.405	4.495	6.868

Appendix L: Analysis of contributions to overall uncertainty in individual input parameters

These results are derived from the Mathcad model (Appendix K) using raw input data from RICSAC tests (Appendix D). Results have been arranged so that similar impact configurations are grouped together.

Table L.1: Overall result and uncertainty in Δv_1 and Δv_2

Overall uncertainty generated using 95% confidence limits on parameters as described by Smith & Noga [**108**]

Collision Type	60° Front to side			90° Front to side			10° Front to front		10° Front to rear		
Test number	**1**	**6**	**7**	**8**	**9**	**10**	**11**	**12**	**3**	**4**	**5**
Δv1 (m/s)	5.256	5.196	6.059	6.553	6.652	10.947	9.729	15.949	3.026	6.588	5.903
Δv2 (m/s)	7.881	8.521	13.187	6.231	3.063	5.299	6.101	11.07	4.799	10.284	10.735
Uncertainty Δv1 %	26.81	32.806	34.014	12.788	17.359	16.424	10.897	7.025	14.81	10.01	10.517
Uncertainty Δv2 %	26.798	32.847	34.127	12.833	17.256	16.291	10.798	6.916	14.904	10.133	10.702

Table L.2: Effect of uncertainty in crush measurements δC on Δv_1 and Δv_2 (%)

Collision Type	60° Front to side			90° Front to side			10° Front to front		10° Front to rear		
Test number	**1**	**6**	**7**	**8**	**9**	**10**	**11**	**12**	**3**	**4**	**5**
±0.01 m	1.29	1.242	1.248	1.04	1.285	0.811	0.42	0.327	0.823	0.443	0.536
±0.05 m	6.365	6.223	6.249	5.254	6.487	4.101	2.127	1.65	4.044	2.247	2.696
±0.0762 m	9.688	9.39	9.432	7.852	9.782	6.228	3.196	2.511	6.124	3.374	4.082
±0.10 m	12.508	12.276	12.3	10.375	12.725	8.151	4.247	3.309	8.106	4.412	5.408

Table L.3: Effect of uncertainty in damage length measurements δL on Δv_1 and Δv_2 (%)

Collision Type	60° Front to side			90° Front to side			10° Front to front		10° Front to rear		
Test number	**1**	**6**	**7**	**8**	**9**	**10**	**11**	**12**	**3**	**4**	**5**
±0.01 m	0.205	0.22	0.159	0.186	0.297	0.298	0.446	0.258	0.461	0.362	0.335
±0.05 m	1.03	1.093	0.788	0.915	1.463	1.466	2.187	1.271	2.324	1.778	1.678
±0.10 m	2.101	2.183	1.553	1.822	2.913	2.919	4.351	2.526	4.66	3.538	3.409
±0.15 m	3.106	3.307	2.348	2.716	4.334	4.346	6.621	3.779	6.898	5.29	4.032
±0.1524 m	3.153	3.366	2.398	2.777	4.391	4.409	6.706	3.852	7.111	5.386	5.122
±0.20 m	4.135	4.358	3.091	3.605	5.77	5.781	8.708	5.007	9.357	7.106	6.843

Table L.4: Effect of uncertainty in mass measurements δm on Δv_1 (%)

Collision Type	60° Front to side			90° Front to side			10° Front to front		10° Front to rear		
Test number	**1**	**6**	**7**	**8**	**9**	**10**	**11**	**12**	**3**	**4**	**5**
±10 kg	0.408	0.468	0.638	0.363	0.653	0.65	0.501	0.508	0.426	0.417	0.487
±25 kg	1.028	1.202	1.591	0.898	1.643	1.607	1.278	1.256	1.056	1.031	1.288
±50 kg	2.047	2.37	3.202	1.803	3.242	3.226	2.521	2.522	2.124	2.103	2.433
±100 kg	4.097	4.708	6.356	3.579	6.572	6.418	5.054	5.01	4.274	4.169	4.866

Table L.5: Effect of uncertainty in mass measurements δm on Δv_2 (%)

Collision Type	60° Front to side			90° Front to side			10° Front to front		10° Front to rear		
Test number	**1**	**6**	**7**	**8**	**9**	**10**	**11**	**12**	**3**	**4**	**5**
±10 kg	0.537	0.609	0.873	0.391	0.497	0.493	0.431	0.667	0.489	0.485	0.594
±25 kg	1.351	1.544	2.193	0.982	1.264	1.232	1.104	1.09	1.203	1.203	1.496
±50 kg	2.704	3.051	4.456	1.987	2.517	2.484	2.179	2.202	2.451	2.44	2.954
±100 kg	5.367	6.064	8.834	3.928	5.026	4.924	4.307	4.356	4.845	4.855	5.899

Table L.6: Effect of uncertainty in PDOF measurements $\delta PDOF$ on Δv_1 and Δv_2 (%)

Collision Type	60° Front to side			90° Front to side			10° Front to front		10° Front to rear		
Test number	**1**	**6**	**7**	**8**	**9**	**10**	**11**	**12**	**3**	**4**	**5**
±1°	0.906	1.193	1.172	0.39	0.598	0.63	0.351	0.173	0.565	0.37	0.376
±5°	4.573	5.988	5.985	1.947	3.035	3.175	1.761	0.884	2.841	1.83	1.844
±10°	9.527	12.437	12.548	3.867	5.903	6.415	3.515	1.771	5.541	3.564	3.687
±15°	15.193	20.222	20.575	5.735	8.911	9.723	5.241	2.755	7.979	5.216	5.406
±20°	23.325	30.842	30.928	7.599	11.652	13.16	6.992	3.682	10.208	6.761	7.095
±25°	38.489	52.151	58.887	11.008	16.272	18.82	8.638	4.759	12.194	8.094	8.522

Table L.7: Effect of uncertainty in position of point of application δd on Δv_1 and Δv_2 (%)

Collision Type	60° Front to side			90° Front to side			10° Front to front		10° Front to rear		
Test number	**1**	**6**	**7**	**8**	**9**	**10**	**11**	**12**	**3**	**4**	**5**
±0.01 m	0.136	0.144	0.139	0.162	0.294	0.276	0.084	0.025	0.111	0.076	0.073
±0.05 m	0.687	0.722	0.697	0.818	1.477	1.392	0.42	0.133	0.545	0.389	0.367
±0.0762 m	1.063	1.1	1.076	1.249	2.253	2.114	0.647	0.21	0.841	0.59	0.566
±0.10 m	1.363	1.445	1.41	1.64	2.952	2.791	0.86	0.289	1.106	0.775	0.738
±0.20 m	2.718	2.869	2.789	3.26	5.808	5.405	1.751	0.756	2.231	1.585	1.508

Table L.8: Effect of uncertainty in radii of gyration δk on Δv_1 and Δv_2 (%)

Collision Type	60° Front to side			90° Front to side			10° Front to front		10° Front to rear		
Test number	**1**	**6**	**7**	**8**	**9**	**10**	**11**	**12**	**3**	**4**	**5**
±0.01 m	0.083	0.078	0.077	0.095	0.204	0.174	0.016	0.001	0.033	0.019	0.018
±0.05 m	0.412	0.391	0.39	0.482	1.035	0.866	0.08	0.005	0.168	0.092	0.09
±0.10 m	0.826	0.785	0.779	0.958	2.091	1.756	0.16	0.011	0.335	0.185	0.183
±0.20 m	1.693	1.603	1.613	1.961	4.23	3.554	0.335	0.023	0.695	0.383	0.387

Table L.9: Effect of uncertainty in A stiffness coefficient δA on Δv_1 and Δv_2 (%)

Collision Type	60° Front to side			90° Front to side			10° Front to front		10° Front to rear		
Test number	**1**	**6**	**7**	**8**	**9**	**10**	**11**	**12**	**3**	**4**	**5**
±5%	1.328	1.072	1.065	2.244	2.061	1.25	1.086	0.814	2.397	1.282	1.474
±10%	2.647	2.137	2.113	4.451	4.14	2.509	2.202	1.606	4.829	2.587	2.945
±15%	3.997	3.195	3.179	6.623	6.185	3.756	3.236	2.421	7.274	3.874	4.41
±20%	5.325	4.309	4.233	8.867	8.271	5.008	4.411	3.256	9.887	5.231	5.936

Table L.10: Effect of uncertainty in B stiffness coefficient δB on Δv_1 and Δv_2 (%)

Collision Type	60° Front to side			90° Front to side			10° Front to front		10° Front to rear		
Test number	**1**	**6**	**7**	**8**	**9**	**10**	**11**	**12**	**3**	**4**	**5**
±5%	0.726	1.384	1.315	0.881	0.34	0.635	0.715	0.993	0.659	0.651	0.85
±10%	1.445	2.788	2.623	1.773	0.677	1.27	1.436	1.988	1.326	1.294	1.693
±15%	2.168	4.164	3.917	2.648	1.046	1.898	2.139	2.961	2.007	1.931	2.574
±20%	2.875	5.565	5.292	3.58	1.446	2.506	2.84	3.999	2.768	2.599	3.39

Appendix M: Comparison of energy adjustment factors using RICSAC test data

This data is used in Chapter 7 section 7.6 where a new model to determine the pre-impact speeds of vehicles is described and validated using the data shown below.

Table M.1: Pre-adjusted values and angles

	Unadjusted (J)		Impact Angle	Angle α (°)		Angle β (°)	
Test	**Veh1**	**Veh2**	**Ψ (°)**	**Veh1**	**Veh2**	**Veh1**	**Veh2**
1	33877	27287	120	11.3	41.3	30.1	29.9
2	46071	92096	120	11.7	41.7	30.1	29.9
3	11842	15202	100	14.1	4.1	0.0	10.0
4	39225	88067	100	11.1	1.1	0.0	10.0
5	10049	94083	100	11.6	1.6	0.0	10.0
6	14541	38550	120	11.0	41.1	30.0	29.9
7	23600	49562	120	12.7	42.7	30.0	30.0
8	26105	21200	90	19.0	19.0	45.1	44.9
9	15321	7618	90	21.8	21.8	45.0	45.0
10	34493	22242	90	25.3	25.3	45.1	44.9
11	44616	61216	171	2.9	11.9	4.6	4.4
12	155207	148443	171	1.0	8.0	2.5	4.5

Table M.2: Standard energy adjustment factors

	Adjustment Factor $1+\tan^2(\alpha)$		Adjusted Energy (J)	
Test	**Veh1**	**Veh2**	**Veh1**	**Veh2**
1	1.04	1.77	35229	48347
2	1.04	1.79	48047	165203
3	1.06	1.01	12589	15280
4	1.04	1.00	40734	88100
5	1.04	1.00	10473	94156
6	1.04	1.76	15090	67880
7	1.05	1.85	24799	91765
8	1.12	1.12	29201	23714
9	1.16	1.16	17772	8837
10	1.22	1.22	42200	27212
11	1.00	1.04	44730	63935
12	1.00	1.02	155254	151375

Table M.3: Calculated results using standard energy adjustment

	Closing Speed (m/s)			Pre-Impact Speed (m/s)	
Test	**Normal**	**Tangential**	**Total**	**Veh1**	**Veh2**
1	15.2	5.2	16.0	9.2	9.3
2	24.3	8.1	25.6	14.8	14.8
3	8.2	2.1	8.5	8.5	0.0
4	17.3	3.4	17.6	17.6	0.0
5	17.0	3.5	17.3	17.3	0.0
6	16.3	5.6	17.3	10.0	10.0
7	22.9	7.1	24.0	13.9	13.9
8	11.4	5.6	12.6	8.9	9.0
9	11.2	4.8	12.2	8.6	8.6
10	17.5	6.3	18.6	13.1	13.2
11	16.2	-2.1	16.3	8.0	8.4
12	27.1	-1.7	27.1	13.6	13.7

Table M.4: New energy adjustment factor

The new energy adjustment factor is described in Chapter 4. Note that restitution (e_p = 0.3) was applied to tests 8,9 and 10. Adjusted restitution values were calculated using equations (4.30) and (4.28)

	Adjusted restitution		Adjustment Factor $1+\tan(\alpha)\tan(\beta)(1-e_t)/(1-e_n)$		Adjusted Energy (J)	
Test	e_n	e_t	**Veh1**	**Veh2**	**Veh1**	**Veh2**
1	0	0	1.116	1.506	37795	41089
2	0	0	1.120	1.513	51592	139366
3	0	0	1.0	1.013	11842	15394
4	0	0	1.0	1.003	39225	88368
5	0	0	1.000	1.005	10049	94545
6	0	0	1.112	1.502	16172	57886
7	0	0	1.130	1.533	26670	75983
8	0.3605	0.1237	1.474	1.470	38480	31159
9	0.3621	0.1448	1.536	1.536	23537	11702
10	0.3615	0.1703	1.616	1.612	55742	35861
11	0	0	1.004	1.016	44798	62209
12	0	0	1.001	1.011	155326	150079

Table M.5: Calculated results using new energy adjustment

	Closing Speed (m/s)			Pre-Impact Speed (m/s)	
Test	**Normal**	**Tangential**	**Total**	**Veh1**	**Veh2**
1	14.7	5.0	15.6	9.0	9.0
2	23.0	7.6	24.2	14.0	14.0
3	8.1	2.0	8.4	8.4	0.0
4	17.2	3.4	17.6	17.6	0.0
5	17.0	3.5	17.3	17.3	0.0
6	15.5	5.3	16.3	9.4	9.4
7	21.5	6.7	22.5	13.0	13.0
8	13.0	6.4	14.5	10.2	10.3
9	12.9	5.5	14.0	9.9	9.9
10	20.1	7.2	21.3	15.1	15.1
11	16.1	-2.1	16.2	8.0	8.3
12	27.0	-1.7	27.1	13.5	13.6